FILLET AND PJP WELDS

FINAL REPORT

Submitted to

AMERICAN INSTITUTE OF STEEL CONSTRUCTION

September 17, 2021

by

Bo Dowswell, P.E., Ph.D.
ARC International, LLC
Birmingham, AL
bo@arcstructural.com

Clayton Cox
Auburn University
Auburn Alabama
rcc0044@auburn.edu

Mohamed S. Gallow, Ph.D., P.E.
ICC Evaluation Service, LLC
Birmingham, AL
mgallow@icc-es.org

Fouad H. Fouad, Ph.D., P.E.
Civil and Environmental Engineering Department
The University of Alabama at Birmingham
Birmingham, AL
ffouad@uab.edu

TABLE OF CONTENTS

CHAPTER 1
INTRODUCTION

This report addresses several design issues related to the strength of fillet welds and partial-joint penetration (PJP) welds.

PROBLEM STATEMENT

Both the AISC *Specification* (AISC, 2016) and AWS D1.1 *Structural Welding Code* (AWS, 2015) permit a 50% directional strength increase for fillet welds loaded perpendicular to the weld axis. This strength increase was established experimentally; however, theoretical analyses using various methods result in smaller transverse-to-longitudinal weld strength ratios.

Of the available experimental data on fillet weld strength, the overwhelming majority is based on short welds. For end-loaded fillet welds with a length greater than 100 times the weld size, AISC *Specification* Section J2.2b(d) considers the detrimental effect by requiring the calculations to use a reduced weld length. This solution addresses the effect of non-uniform relative axial deformation of the connecting elements; however, any potential length effects for shorter welds are not addressed in the *Specification*.

For PJP welds subjected to tension normal to the weld axis, AISC *Specification* Section J2.4(a) specifies a nominal stress equal to 60% of the weld metal strength. Theoretically, the rupture stress at the effective throat is equal to 100% of the weld metal strength. The basis of the 0.6 factor is ambiguous and recent experimental tests have shown that it may be too conservative. According to the Commentary to *Specification* Section J2.4, "The factor of 0.6 on F_{EXX} for the tensile strength of PJP groove welds has been used since the early 1960s to compensate for factors such as the notch effect of the unfused area of the joint and uncertain quality in the root of the weld due to the difficulty in performing nondestructive evaluation. It does not imply that the tensile failure mode is by shear stress on the effective throat, as in fillet welds."

For a large test program on fillet welded specimens by Preece (1968) and Higgins and Preece (1969), all specimens ruptured in the weld metal "even when the mechanical properties of the weld metal exceeded those of the base metal by a substantial amount." Based on this, the strength of fillet welds is calculated using a critical section in the weld metal coinciding with the theoretical effective throat. Calculations for the fusion zone strengths along the weld legs are not required in either the AISC *Specification* or AWS D1.1. Although basic theoretical calculations indicate that the strength of fillet welds with matching filler metals are not controlled by fusion zone rupture, the fusion zone could potentially control the strength of PJP welds. Factors that can potentially result in higher strength in the heat affected zone (HAZ) are constraint from the adjacent base metal and increased material strength caused by the rapid cooling after welding.

AISC *Steel Construction Manual* (AISC, 2017) Tables 8-4 through 8-11 are used to calculate the strength of eccentrically-loaded weld groups. The tables were developed using the instantaneous center of rotation (ICR) method with 70 ksi weld metal strength. For other weld metal strengths,

Table 8-3 provides electrode strength coefficients, C_1, that are used with Tables 8-4 through 8-11. The values for C_1 are dependent on the filler metal strength; however, they are not proportional to the weld metal tensile strength ratio when $F_{EXX} \geq 80$ ksi. This results in a significant strength reduction for higher-strength welds, which is not required in either the AISC *Specification* or AWS D1.1.

OBJECTIVES

The objectives of this research are:

1. Develop a rational explanation of the directional strength increase for fillet welds.
2. Determine if length has a significant effect on the strength of fillet welds.
3. Investigate the effect of loading angle on the strength of PJP welds.
4. Investigate the fusion zone strength of PJP welds.
5. Investigate the background of electrode strength coefficient, C_1, in *Manual* Table 8-3. Determine the accuracy of C_1 and propose new design values if necessary.

SCOPE

To meet the objectives of this research project, the available literature was reviewed, failure theories were used to derive theoretical equations, and experimental specimens with both fillet and PJP welds were tested.

CHAPTER 2
LITERATURE REVIEW

CODES AND SPECIFICATIONS

AISC *Specification* (AISC, 2016)

The strength of welded joints is defined by Equation J2-3 in AISC *Specification* Section J2.4(a). For each condition, the weld metal nominal stresses, F_{nw}, are listed in Table J2.5 along with the corresponding values for ϕ (LRFD) and Ω (ASD).

$$R_n = F_{nw}A_{we} \qquad (\textit{Spec.}\ \text{Eq. J2-3})$$

For PJP welds, $F_{nw} = 0.60F_{EXX}$, with $\phi = 0.75$ and $\Omega = 2.00$ for shear loading and $\phi = 0.80$ and $\Omega = 1.88$ for tension loading normal to the weld axis. The effective area, A_{we}, of groove welds is defined in Section J2.1a as the length times the effective throat, E. The effective throat is based on the welding process, the welding position and the groove type according to Table J2.1. For example, for FCAW in the flat (F) or horizontal (H) position with a 45° bevel groove, the effective throat is equal to the groove depth, S.

The weld metal nominal stress can be calculated using Equation J2-5, with $\phi = 0.75$ and $\Omega = 2.00$ from Table J2.5. This can be written with Equations 2.1 and 2.2, where the directional strength increase factor, k_{ds}, is calculated separately. The effective area, A_{we}, of fillet welds is defined in Section J2.2a as the effective length times the effective throat, E. The effective throat is the shortest distance from the root to the face of the diagrammatic weld.

$$F_{nw} = 0.6F_{EXX}\left(1.0 + 0.50\sin^{1.5}\theta\right) \qquad (\textit{Spec.}\ \text{Eq. J2-5})$$

$$F_{nw} = 0.6F_{EXX}k_{ds} \qquad (2.1)$$

$$k_{ds} = 1.0 + 0.50\sin^{1.5}\theta \qquad (2.2)$$

where

A_{we} = effective area of the weld, in.^{2}
E = effective throat of the weld, in.
F_{EXX} = filler metal classification strength, ksi
F_{nw} = nominal stress of the weld metal, ksi
k_{ds} = directional strength increase factor
w = fillet weld leg size, in.
w_1 = size of fillet weld Leg 1, in.
w_2 = size of fillet weld Leg 2, in.

θ = angle between the line of action of the required force and the weld longitudinal axis as shown in Figure 2.1, degrees

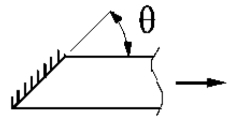

Fig. 2.1. Loading angle for fillet welds.

For equal-leg fillet welds, the effective throat is

$$E = \frac{w}{\sqrt{2}} \tag{2.3}$$

For non-equal-leg fillet welds, the effective throat is

$$E = \frac{w_1 w_2}{\sqrt{w_1^2 + w_2^2}} \tag{2.4}$$

Design requirements for fillet welds with high l/w ratios are in AISC *Specification* Section J2.2b(d). When $l/w \le 100$, the effective length is equal to the actual length. For end-loaded fillet welds with $l/w > 100$, the effective length is calculated with Equation J2-1. For end-loaded fillet welds with $l/w > 300$, the effective length is $180w$.

$$\beta = 1.2 - 0.002\left(\frac{l}{w}\right) \le 1.0 \qquad \text{(}\textit{Spec.}\text{ Eq. J2-1)}$$

where
l = actual length of end-loaded weld, in.
w = weld leg size, in.

AWS D1.1 (2015)

The requirements for PJP and fillet weld strengths in AWS D1.1 (2015) are similar to the ASD portions of the AISC *Specification*. Equations 2.5 through 2.10 are required to calculate the strengths of weld groups according to the Instantaneous Center of Rotation (ICR) method according to AWS D1.1 Section 2.6.4.3.

$$F_{vi} = 0.3F_{EXX}\left(1.0 + 0.50\sin^{1.5}\theta\right)F(\rho) \tag{2.5}$$

$$F(\rho) = \left[\rho\left(1.9 - 0.9\rho\right)\right]^{0.3} \tag{2.6}$$

$$\rho = \frac{\Delta_i}{\Delta_m} \tag{2.7}$$

$$\Delta_m = 0.209w\left(\theta + 6\right)^{-0.32} \tag{2.8}$$

$$\Delta_u = 1.087w\left(\theta + 6\right)^{-0.65} < 0.17w \tag{2.9}$$

$$\Delta_i = \Delta_u \frac{r_i}{r_{crit}} \tag{2.10}$$

where

- F_{vi} = allowable stress of the weld metal, ksi
- r_{crit} = distance from the instantaneous center of rotation to the weld element with the minimum Δ_u/r_i ratio, in.
- r_i = distance from the instantaneous center of rotation to element i, in.
- Δ_m = deformation of weld element at maximum stress, in.
- Δ_u = deformation of weld element at ultimate stress (rupture), in.
- Δ_i = deformation of weld element at intermediate stress levels, in.

These equations were developed by Lesik and Kennedy (1990), except that their polynomial function for $F(\rho)$ was replaced by the simpler empirical approximation according to Equation 2.6. Also, an upper limit of $0.17w$ was added to the original equation for Δ_u, resulting in Equation 2.9.

CSA (2014)

The Canadian Standard CSA (2014) specifies Equation 2.11 for the strength of linear concentrically-loaded fillet weld groups. Equation 2.12 defines M_w, which is a coefficient that accounts for any differences in the weld deformation capacity that are caused by their orientation. In the case of a single fillet weld, $M_w = 1.0$.

$$R_n = 0.67F_{EXX}\left(1.0 + 0.50\sin^{1.5}\theta\right)A_{we}M_w \tag{2.11}$$

$$M_w = \frac{0.85 + \theta_1/600}{0.85 + \theta_2/600} \tag{2.12}$$

where

- ϕ = 0.67
- θ_1 = angle between the line of action of the required force and the weld longitudinal axis for the weld segment under consideration, degrees
- θ_2 = angle between the line of action of the required force and the weld longitudinal axis for the weld segment in the group that is nearest to 90°

Eurocode 3 (CEN, 2005)
The Eurocode 3 (CEN, 2005) directional method is applicable to both fillet and PJP welds. Both Equation 2.13 and 2.14 must be satisfied.

$$\sqrt{\sigma_T^2 + 3\left(\tau_T^2 + \tau_L^2\right)} \leq \frac{F_{EXX}}{\beta_w \gamma_{M2}} \tag{2.13}$$

$$\sigma_T \leq \frac{0.9 F_{EXX}}{\gamma_{M2}} \tag{2.14}$$

For the simplified method, which is applicable only to fillet welds, the available stress at the theoretical effective throat is calculated with Equation 2.15.

$$F_{nw} \leq \frac{F_{EXX}}{\sqrt{3}\,\beta_w \gamma_{M2}} \tag{2.15}$$

where

β_w = correlation factor (0.80 for S235 steel, 0.85 for S275 steel, 0.90 for S355 steel and 1.0 for S420 and S460 steel)
γ_{M2} = partial safety factor, =1.25
σ_T = normal stress perpendicular to the plane of the throat, ksi.
τ_L = shear stress in the plane of the throat, parallel to the weld axis, ksi.
τ_T = shear stress in the plane of the throat, perpendicular to the weld axis, ksi.

The Eurocode 3 design requirements for fillet welds with high l/w ratios are similar to those in AISC *Specification* Section J2.2b(d), except the effective throat is used instead of the weld leg size. For lap joints longer than 150E, Equation 2.16 is applicable.

$$\beta = 1.2 - \frac{0.2l}{150E} \leq 1.0 \tag{2.16}$$

AIJ (2012)
The Architectural Institute of Japan (AIJ, 2012) specifies Equation 2.17 for the strength of fillet welds. Equations 2.18 and 2.18 are applicable to longitudinal and transverse PJP welds, respectively. Because Equation 2.19 is based on the tensile strength of the base metal, it is valid only when matching or overmatching weld metal is used.

$$F_{nw} = \frac{F_{EXX}}{\sqrt{3}}\left(1.0 + 0.40 \sin\theta\right) \tag{2.17}$$

$$F_{nw} = \frac{F_{EXX}}{\sqrt{3}} \tag{2.18}$$

$$F_{nw} = F_u \tag{2.19}$$

where

F_u = specified minimum tensile stress of the weaker base metal joined, ksi

FILLET WELDS

ABW (1931)

ABW (1931) reported a comprehensive series of experimental tests on many different configurations for both fillet and groove welds. The specified tensile strength of the weld metal was 56 ksi; however, the actual tensile strength was not reported. The average shear rupture strength on the throat of the concentrically-loaded fillet weld specimens was 42.5 ksi and the average strength of butt welds in tension was 49.6 ksi. A conclusion from the tests on joints with combined longitudinal and transverse welds is that failure of the transverse welds always precludes failure of the longitudinal welds at loads that are less than the sum of the independent strengths.

AWS (1937)

The early research on fillet welded connections was primarily concerned with the elastic stress distributions, both along the weld length and in the weld cross section. The available research on fillet-welded joints prior to 1937, consisting of 150 references, was summarized in AWS (1937). The research shows highly nonlinear stresses along the length and in the weld cross section, even for the simplest configurations.

Spraragen and Claussen (1942)

Spraragen and Claussen (1942) reviewed 77 references on fillet welds that were published between 1932 and 1939. For longitudinally-loaded fillet welds, the rupture stress at the throat is between 0.64 and 0.84 times the uniaxial tensile strength. Although longitudinally-loaded fillet welds had high elastic stress concentrations at the end, it was shown that the rupture strength of short welds (l/w between 1.4 and 19), is unaffected by the weld length.

Tests on double-lap specimens with transversely-loaded fillet welds showed that the specimens with tensile loads were approximately 20% higher than for compression-loaded specimens. Also, several research projects showed that the rupture strength of transversely-loaded T-joints varies between 75% and 100% of the strength of double-lap specimens. This effect was caused by the constraint provided by the transverse contact force at the faying surfaces of the double-lap as well as the friction resulting from these forces. A gapped T-joint designed by Kist (1936) to eliminate the transverse force that causes friction at the faying surfaces had only 64% of the strength of a double-lap specimen with similar welds. It was concluded that the rupture stress at the throat of transversely-loaded fillet welds was slightly higher than the uniaxial tensile strength measured with all-weld-metal coupons.

Vreedenburgh (1954)

Vreedenburgh (1954) continued the work of Kist (1936) with supplementary tests and analyses. Although Kist assumed the rupture plane was always defined by the theoretical throat, Vreedenburgh found out that the rupture planes were not always coincident with the theoretical throat. Additionally, Vreedenburgh found that the experimental behavior was not compatible with any of the available failure theories. Because of this, an empirical solution was adopted. As shown in Figure 2.2, the shear strength of the weld was assumed to be 0.75 times the weld metal uniaxial tensile strength, σ_t. For transversely-loaded equal-leg welds, the weld throat is oriented 45° from the load and the strength is $0.84\sigma_t$. Based on this approach, the ratio of the transverse fillet weld strength to longitudinal fillet weld strength is 0.84/0.75 = 1.12. Also, according to Figure 2.2, welds subjected to compression at the effective throat are 70% stronger than welds subjected to tension at the effective throat.

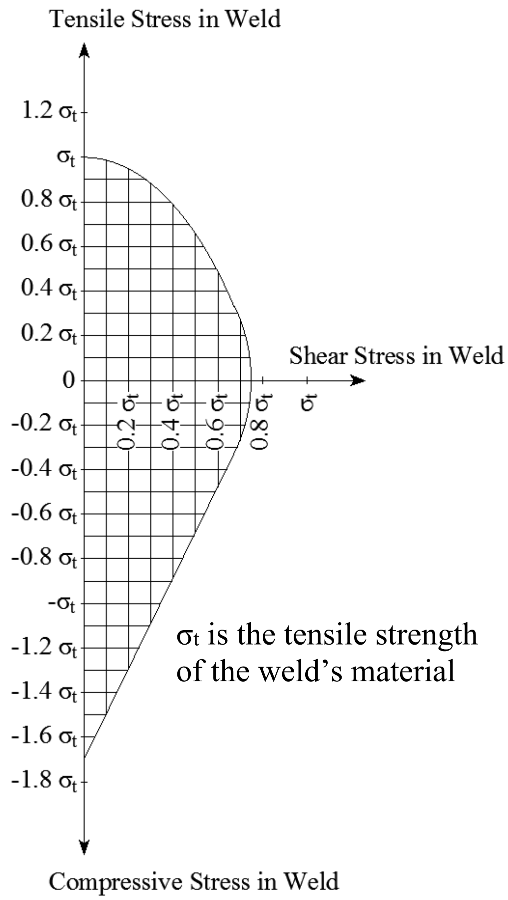

Fig. 2.2. Fillet weld critical limiting stress according to Vreedenburgh (1954).

Archer et al. (1964)

Archer et al. (1964) compared different failure theories with experimental results to determine which one best represents the actual strength of fillet welds. The failure theories included maximum principal stress, maximum shear stress and von-Mises. The comparisons also included calculations that considered the moments at the weld legs that were caused by the small eccentricity between the load and the resisting force; however, the results were more accurate when these moments were neglected. The authors determined that the maximum shear stress method, while neglecting the moment in the weld, provides the best fit. The predicted orientation angle of the rupture plane compared well with the experimental results. Nevertheless, the calculated weld strength using maximum shear stress slightly underestimated the experimental strength that was determined using double-lap specimens with longitudinal welds.

Douwen and Witteveen (1966)

Douwen and Witteveen (1966) recommended combining the normal and shear stresses on the theoretical effective throat using von Mises equation. Because von Mises yield criterion was found to be conservative, the resulting effective stress was multiplied by a correlation factor, β, that is dependent on the base metal strength. The authors recommended $\beta = 0.7$ for St 37 steel and 0.85 for St 51 steel. Both the International Institute of Welding (IIW, 1976) and Eurocode 3 (CEN, 2005) adopted this approach later.

Swannell (1968)
To obtain a uniform shear distribution along the weld length, Swannell (1968) subjected circular fillet weld groups to torsional moments. The weld metal uniaxial tensile strength was 64.4 ksi and the mean rupture stress at the throat was 57.0 ksi, resulting in an average shear strength equal to 88.5% of the tensile strength.

Preece (1968), Higgins and Preece (1969)
Preece (1968) and Higgins and Preece (1969) documented 168 tests on double-lap specimens with either longitudinal or transverse fillet welds. The variables were weld size (¼, ⅜ and ½-in.), electrode strength (60, 70, 90 and 110 ksi), weld length (1.5, 2, 3 and 4 in.) and base metal (ASTM A36, A441 and A514).

The experimental rupture stress increased slightly with length, however, the increase of 3% was deemed negligible. All specimens ruptured in the weld metal "even when the mechanical properties of the weld metal exceeded those of the base metal by a substantial amount." The transverse welds averaged 1.57 and 1.44 times stronger than longitudinal welds for 70 and 110 ksi electrodes, respectively.

For the ¼-in. fillet welds, the average measured weld size was 20% greater than the specified size. For the ⅜ and ½-in. fillet welds, the average measured weld sizes were 13 and 5% greater than the specified sizes, respectively.

Ligtenburg (1968), Strating (1971)
Ligtenburg (1968) compiled the data from a series of experiments where fillet-welded joints were tested in nine different countries. The specimens were double- and single-lap joints with longitudinal, transverse and combined longitudinal/transverse welds. Only the SMAW welding process was used, but the weld sizes and plate material properties varied.

Strating (1971) tested 38 different specimens with three duplicates each for a total of 114 tests. The specimens were similar to Lightenburg's double-lap specimens; however, the FCAW, GMAW and SAW processes were used instead of SMAW. Both self-shielded and gas-shielded (CO_2) FCAW was used. The GMAW shielding gases were CO_2 and Argon/CO_2/O_2.

The authors recommended that the weld rupture strength calculations should be based on the average tensile stress of the base metal and the weld metal. A linear regression analysis showed that the strength of longitudinally- and transversely-loaded welds can be predicted with Equations L1 and L2, respectively. A conclusion from the tests on joints with combined longitudinal and transverse welds is that failure of the transverse welds always precludes failure of the longitudinal welds at loads that are less than the sum of the independent strengths.

$$R_n = 0.83 F_{EXX} A_{we} \tag{2.20}$$

$$R_n = 1.33F_{EXX}A_{we} \tag{2.21}$$

Butler and Kulak (1971)

Butler and Kulak (1971) measured the load-deformation of fillet welds in double-lap joints. 60 ksi electrodes were specified to deposit ¼ in. fillet welds at angles of 0°, 30°, 60° and 90° from the loading direction. The authors found that the strength and ductility is dependent on the loading direction and developed empirical equations 2.22 through 2.26 to describe the load-deformation behavior of the specific welds that were tested. These equations are plotted in Figure 2.3 for θ = 0°, 30°, 60° and 90°. Equation 2.23 results in k_{ds} = 15.8/10.9 = 1.45 when θ = 90°.

$$R = R_u\left(1-e^{-\mu\Delta}\right)^{\lambda} \tag{2.22}$$

$$R_u = \frac{10+\theta}{0.92+0.0603\theta} \tag{2.23}$$

$$\Delta_u = 0.225\left(\theta+5\right)^{-0.47} \tag{2.24}$$

$$\mu = 75e^{0.0114\theta} \tag{2.25}$$

$$\lambda = 0.4e^{0.0146\theta} \tag{2.26}$$

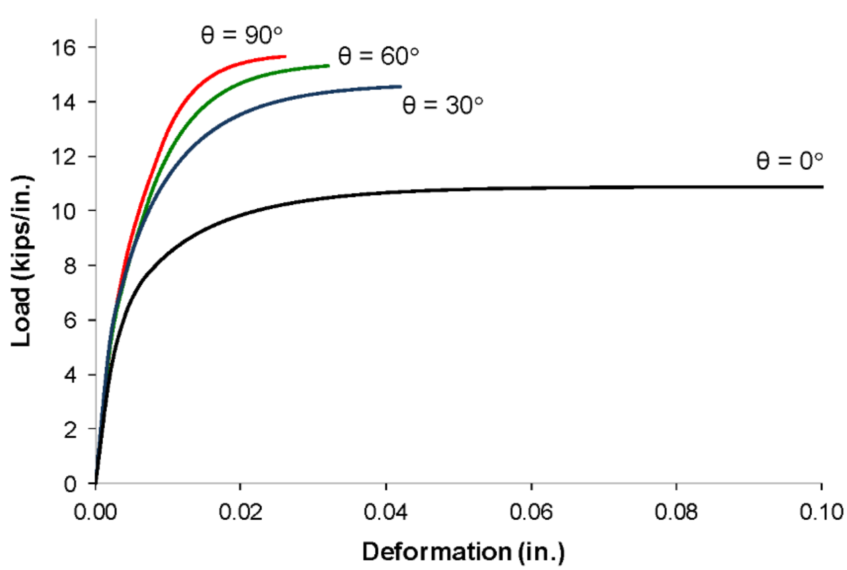

Fig. 2.3. Load-deformation curves for ¼ in. E60 fillet welds.

Kato and Morita (1974)

Kato and Morita (1974) calculated the strength of transverse fillet welds using the theory of elasticity and determined that the rupture plane is 22.5° from the loading direction. Based on this critical rupture plane, they developed a directional strength factor of

$$k_{ds} = \frac{1.0 - \pi/4}{\sin^2(22.5°)} \qquad (2.27)$$
$$= 1.46$$

The authors compared their theoretical findings with experimental and finite element results, which verified the rupture plane orientation. Although the stress distribution along the critical section was shown to be non-uniform, the proposed equations were reasonably accurate.

Higgs (1981), Biggs et al. (1981)

Based on cruciform specimens loaded in both directions as shown in Figure 2.4, Higgs (1981) and Biggs et al. (1981) recommended a circular interaction between the normal stresses and shear stresses on the critical section of fillet welds. Figure 2.5 shows that the orientation of the critical section varies with the load ratio, f_y/f_x. The stress interaction on the critical section is shown in Figure 2.6. Figure 2.7 shows the interaction between x- and y-direction loads, f_x and f_y, respectively. It is interesting to note that f_y increases with an increase in f_x up to approximately f_x/f_y.= 0.6.

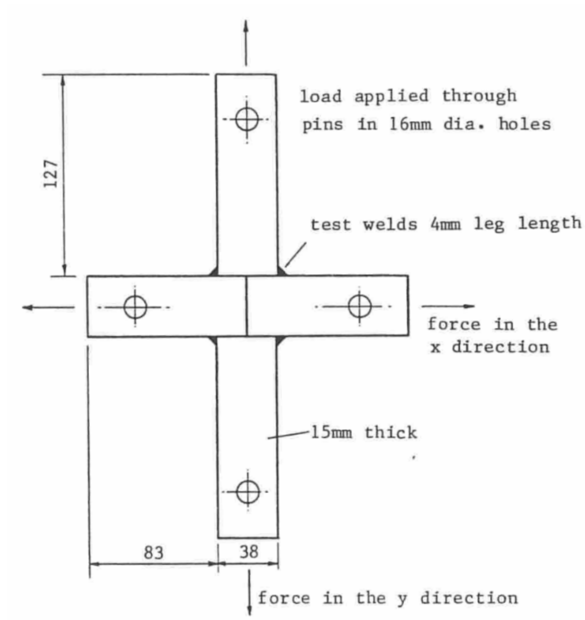

Fig. 2.4. Experimental specimens tested by Higgs. (1981).
(from Biggs et al., 1981)

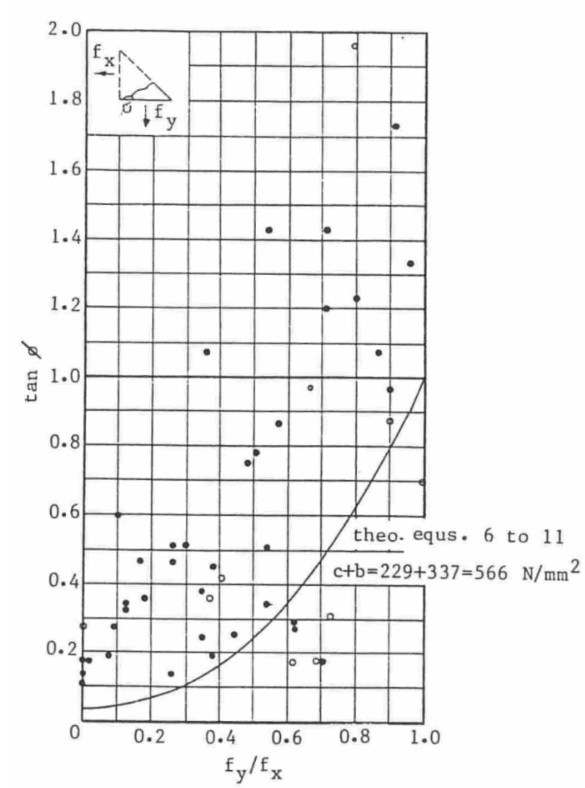

Fig. 2.5. Orientation of the critical section versus the load ratio, f_x/f_y.
(from Biggs et al., 1981)

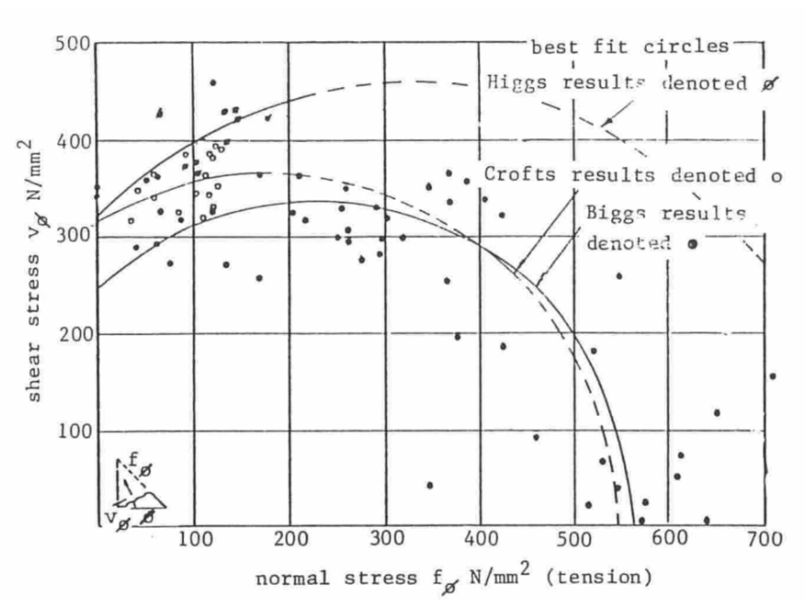

Fig. 2.6. Stress interaction on the critical section.
(from Biggs et al., 1981)

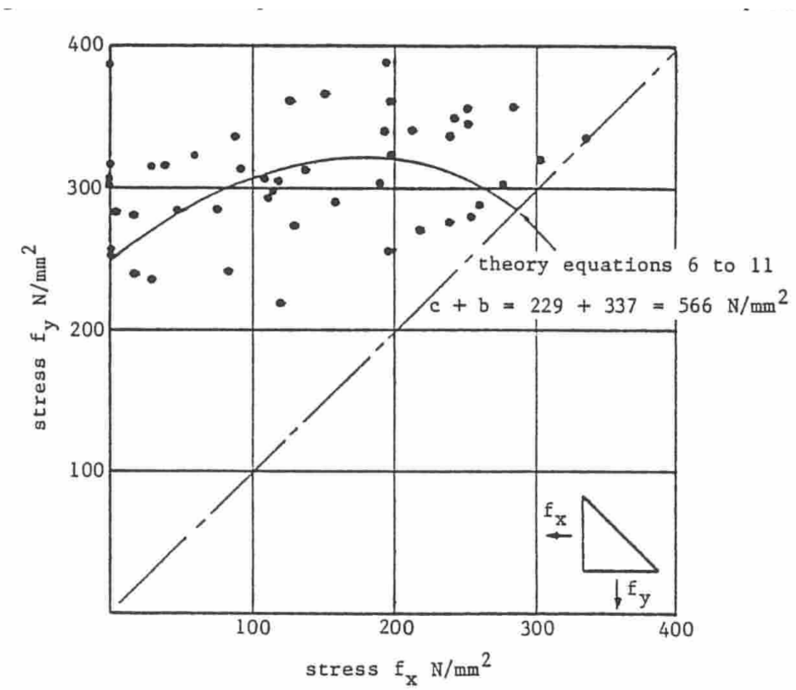

Fig. 2.7. Interaction between x- and y-direction loads.
(from Biggs et al., 1981)

Kamtekar (1982), Kamtekar (1987)
Based on von Mises yield criterion, Kamtekar (1982) derived equations to calculate the strength of longitudinally- and transversely-loaded fillet welds. The same theory was used by Kamtekar (1987) to derive equation 2.28 for the full range of loading angles (0° < θ < 90°). The theory predicts that transverse welds rupture along the leg (fusion zone) at a 41% higher load than longitudinal welds.

$$k_{ds} = \sqrt{2 - \cos^2 \theta} \qquad (2.28)$$

Pham (1983)
Pham (1983) documented a series of 36 tests on transversely-loaded T-joints connected with fillet welds using the FCAW and SAW welding processes. Macro-etches showed that the theoretical throat increased by 30% for FCAW welds and 50% for SAW welds with a coefficient of variation of 0.20 for both processes. Many of the welds ruptured along the fusion zone; however, the experimental loads exceeded the expected strengths due to oversized welds and overstrength weld metals.

Neis (1985)
Neis (1985) used plasticity theory to derive the ultimate strength and maximum displacement of fillet welds. Although several simplifying assumptions were required, limited comparisons with

experimental results showed "an acceptable fit." The ultimate (rupture) force and deformation is calculated with Equations 2.29 and 2.30 respectively.

$$R_u = \sigma_{tu} w L \sqrt{\frac{1+15\sin^2\alpha_d}{6\left(1+7\sin^2\alpha_d\right)}} \tag{2.29}$$

$$\delta_u = \varepsilon_u \sqrt{\frac{3}{2\left(1+7\sin^2\alpha_d\right)}} \tag{2.30}$$

The complete load-deformation curve can be plotted with Equations 2.31 through 2.33.

$$R_i = R_u \frac{f_i}{f_u} \tag{2.31}$$

$$f_i = 1 - \frac{e^{-25\delta_i} + e^{-75\delta_i}}{2} \tag{2.32}$$

$$f_u = 1 - \frac{e^{-25\delta_u} + e^{-75\delta_u}}{2} \tag{2.33}$$

where

- R_i = strength at deformation Δ_i, kips
- α_d = angle between the weld longitudinal axis and the weld displacement direction
- δ_i = Δ_i/w
- δ_u = Δ_u/w
- ε_u = uniaxial engineering tensile rupture strain
- σ_{tu} = true tensile rupture stress, ksi
- σ_{uw} = uniaxial engineering tensile rupture stress, ksi

As a conservative estimate, the authors noted that the true tensile rupture stress can be calculated with Equation 2.34.

$$\sigma_{tu} = \sigma_u \left(1+0.75\varepsilon_u\right) \tag{2.34}$$

Equation 2.35 provides an approximate value of the angle between the weld longitudinal axis and the weld displacement direction.

$$\tan\alpha_d = \frac{\tan\theta}{4} \tag{2.35}$$

Kennedy and Kriviak (1985)

Kennedy and Kriviak (1985) discussed Butler and Kulak (1971) Equation 2.22, plotting it as an interaction curve, along with the available experimental data. This led to the surprising conclusion that the strength of a longitudinally-loaded fillet weld increases when a transverse load is added as shown in Figure 2.8. The authors developed Equation 2.36, which provides a more conservative estimate of fillet weld strength compared to Equation 2.22. Equation 2.36 results in k_{ds} = 1.42 when θ = 90°.

$$1.2\left(\frac{V_T}{V_u}\right)^2 - \frac{V_T}{V_u} + \frac{V_L}{V_u} = 1.0 \tag{2.36}$$

where

V_L = longitudinal load, kips

V_T = transverse load, kips

V_u = weld strength at θ = 0°, kips

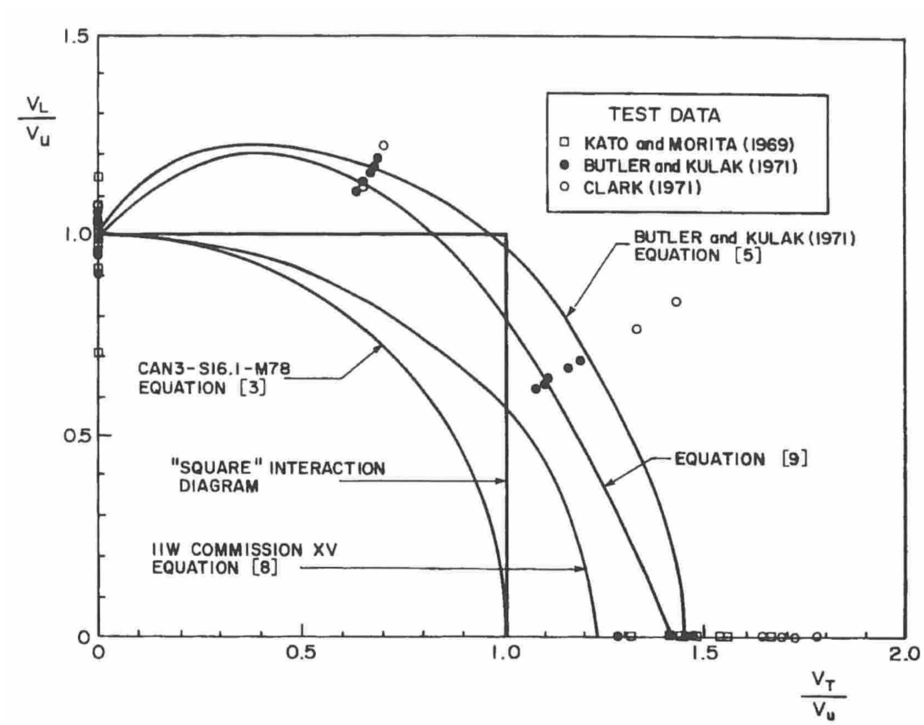

Fig. 2.8. Interaction of longitudinal and transverse fillet welds.
(from Kennedy and Kriviak, 1985)

Faltus (1986)

Early attempts by International Institute of Welding (IIW) committees to develop an accurate design equation resulted in Equation 2.37, which was originally proposed by Van der Eb in 1952. This equation was later adopted by the International Organization for Standardization (ISO).

$$\sqrt{\sigma_T^2 + 1.8\left(\tau_T^2 + \tau_L^2\right)} = F_{EXX} \tag{2.37}$$

Equation 2.37 results in a shear rupture stress of $0.745F_{EXX}$ when $\theta = 0°$ and $k_{ds} = 1.13$ when $\theta = 90°$. In 1974, the 1.8 constant was changed to 3, which results in von Mises equation. Because this increased the conservative error compared to the experimental results, the stress was reduced by a correlation factor, β_w, which had values of 0.70 or 0.85 depending on the steel grade. Also, a limit was added to ensure that the normal stress was not greater than the weld metal tensile strength. This resulted in Equations 2.38 and 2.39, which is the basis for the equations in Eurocode 3.

$$\beta_w \sqrt{\sigma_T^2 + 3\left(\tau_T^2 + \tau_L^2\right)} \le F_{EXX} \tag{2.38}$$

$$\sigma_T \le F_{EXX} \tag{2.39}$$

McClellan (1989)
McClellan (1989) tested 96 double-lap specimens with either longitudinal or transverse fillet welds. The joints were fabricated using the FCAW process with either CO_2 or 75% argon/25% CO_2 shielding gasses. The specified weld sizes were either ¼ or ⅜ in. and the specified electrode strengths were either 70 or 100 ksi. By evaluating the rupture surfaces and macro-etches, the author concluded that the penetration depth was similar to that of a weld deposited with the SMAW process. The rupture surface for the transverse welds was oriented at approximately 22.5° from the load direction. The transverse welds averaged 1.51 and 1.39 times stronger than longitudinal welds for 70 and 100 ksi electrodes, respectively.

Miazga and Kennedy (1989), Lesik and Kennedy (1990), Kennedy et al. (1990)
Miazga and Kennedy (1989) developed an analytical model to predict the fillet weld strength in double-lap joints as a function of the loading direction. The model includes a variable failure plane angle and restraining conditions at the weld root. They validated their model by testing 42 specimens with varying load angles from 0 to 90° in 15° increments. The fracture was ductile for the cases of longitudinal loading. For transverse loading, the fracture transitioned from brittle at the weld root where the crack initiated to ductile fracture at the crack termination. The area of the rupture surface is

$$A_\theta = \frac{wL\sin\left(45°\right)}{\sin\left(45° + \alpha\right)} \tag{2.40}$$

Where α is the angle between the loading direction and the rupture surface as shown in Figure 2.9. The normal stress on the rupture surface is

$$\sigma = \frac{P\sin\theta}{A_\theta}\left(\sin\alpha + a\cos\alpha\right) \tag{2.41}$$

The shear stress on the rupture surface is

$$\tau = \frac{P}{A_\theta}\sqrt{(\sin\theta\cos\alpha + a\sin\theta\sin\alpha)^2 + \cos^2\theta} \tag{2.42}$$

Where a is a portion of P that defines the transverse force on the weld cross section that is required for equilibrium of the weld free body diagram as shown in Figure 2.9. Due to the nonlinear stresses at the weld cross section, the authors were unable to determine an accurate equation to define a; however, the experimental results showed that a constant value of 0.345 is applicable for θ between 45° and 90°. For smaller values of θ, a could not be determined due to the scattered test results.

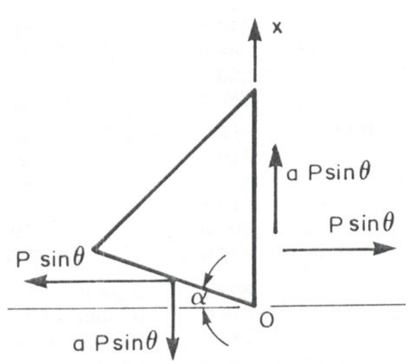

Fig. 2.9. Weld free body diagram.
(from Miazga and Kennedy, 1989)

Among the failure theories considered by Miazga and Kennedy (1986), which included von-Mises, maximum normal stress and maximum shear stress (Tresca), the Tresca theory was determined to be the most accurate in determining the ultimate weld strength and rupture plane orientation, α. Setting dτ/dα = 0, results in Equation 2.43.

$$\tan(45° + \alpha) = \frac{(\cos\alpha - a\sin\alpha)^2 + \cot^2\theta}{(\cos\alpha - a\sin\alpha)(\sin\alpha + a\cos\alpha)} \tag{2.43}$$

The weld strength, P_θ, at a loading angle θ is calculated by setting the maximum shear stress equal to the ultimate shear strength, τ_u. Combining Equations 2.40 and 2.42 results in Equation 2.44.

$$P_\theta = \frac{\tau_u wL\sin(45°)}{\sin(45° + \alpha)\sqrt{(\sin\theta\cos\alpha - a\sin\theta\sin\alpha)^2 + \cos^2\theta}} \tag{2.44}$$

Based on the six experimental specimens with longitudinal fillet welds, τ_u can be estimated as 0.764 of the electrode tensile strength. For a = 0.345, α = 13.0°, which results in k_{ds} = 1.32 when θ = 90°. The effect of constraint in the plane of the rupture surface was considered by multiplying

Equation 2.44 by a semi-empirical constraint factor, k, which is calculated with Equation 2.45. This results in k_{ds} = 1.50 when θ = 90° and an experimental-to-calculated strength ratio of 1.004 with a standard deviation of 0.088. A plot of $k \times P_\theta$ and the experimental results are shown in Figure 2.10.

$$k = 1 + 0.141 \sin\theta \tag{2.45}$$

The weld strength is determined by calculating the rupture angle with Equation 2.43, substituting this value into Equation 2.44 and multiplying by Equation 2.45. In an effort to simplify the design process, Lesik and Kennedy (1990) developed Equation 2.2 by fitting the curve in Figure 2.10. Equation 2.2 is slightly conservative, with a maximum error of 1.5% at θ = 45°.

For lap-joints in compression, the transverse force is not available. Miazga and Kennedy (1989) noted that the welds for these joints can be designed with a = 0, which results in α = 22.5° and k_{ds} = 1.34 when θ = 90°. For this condition, the experimental-to-calculated strength ratio is 0.928 with a standard deviation of 0.065 when compared to the experimental results of Swannell and Skewes (1979). This approach was also recommended for T-joints in both tension and compression. In an effort to simplify the design process, Kennedy et al. (1990) developed Equation 2.46 by fitting a curve developed using Equations 2.43, 2.44 and 2.45 with a = 0.

$$k_{ds} = 1.0 + 0.34 \sin^{1.5}\theta \tag{2.46}$$

For the E48014 electrodes in the Miazga and Kennedy (1989) research, the specified uniaxial tensile strength was 480 MPa and the measured strength was 538 MPa resulting in an overstrength factor of 1.12. Lesik and Kennedy (1988) and Lesik and Kennedy (1990) summarized the electrode strength statistics for four previous projects found in the literature with a total of 672 weld metal tensile tests. For these tests, the average overstrength factor, σ_u/F_{EXX}, was 1.12 with a coefficient of variation of 0.077.

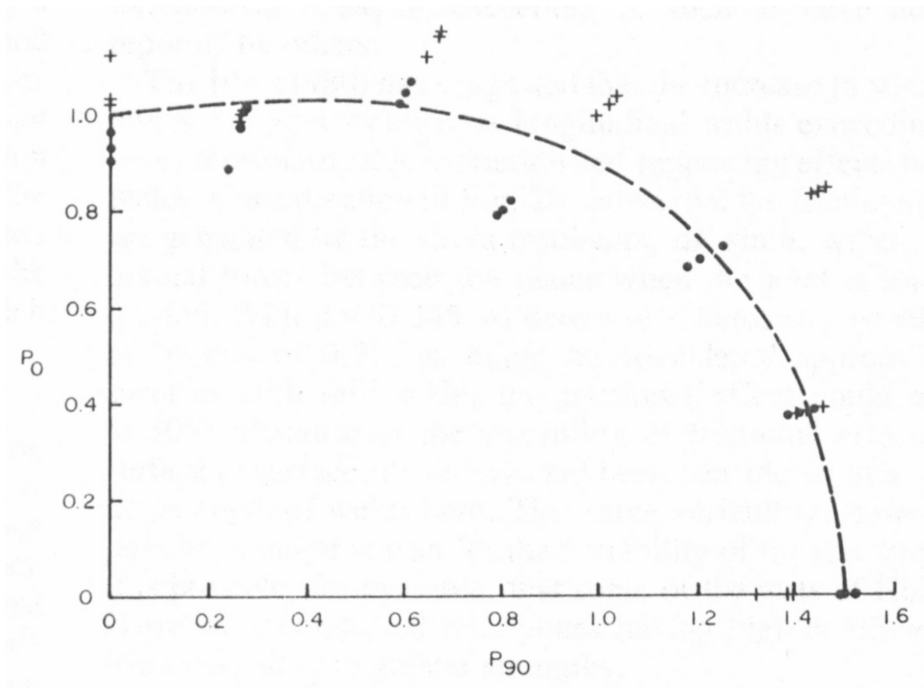

Fig. 2.10. Plot of $k \times P_\theta$ compared to the experimental results.
(from Miazga and Kennedy, 1989)

Chan and Ogle (1992)
Chan and Ogle (1992) tested a 12.5 mm flat plate that was cut to the geometry of a large transversely-loaded double-lap splice connection. The simulated fillet welds had 100 mm leg sizes. When loaded to 82% of the rupture load, strain gages showed that inelastic stress redistribution resulted in a near constant von Mises stress along planes oriented at both 0° and 22.5° from the load. After significant plastic flow approximately along the 22.5° plane, a crack formed at the root and grew to about 22 mm long in the direction of the plastic band.

Bowman and Quinn (1994)
Bowman and Quinn (1994) experimentally examined the strength and deformation of fillet welds in double-lap joints for three different weld leg sizes (¼, ⅜, and ½ in.), weld orientations (longitudinal and transverse), and three root gap configurations (0, 1⁄16, and ⅛ in.). Root gaps were fabricated by using spacer bars between the plates to represent distortions or inadequate fitup of plates. Eighteen specimens were prepared using 70 ksi SMAW welds with A572 Grade 50 plates.

The strength ratio between the transverse and longitudinal weld was between 1.3 and 1.7 for specimens with no gaps and 1.2 and 1.4 for gapped specimens. For the same specified weld size, the strength of the gapped specimens did not decrease significantly from non-gapped specimens because of the relatively higher weld penetration in the first, along with the weld flow in the gap.

Iwankiw (1997)
Based on equilibrium on the theoretical effective throat (defined with α = 45°), Iwankiw (1997) derived Equation 2.47 which produces results within 10% of Equation 2.2. Equation 2.47 results in k_{ds} = 1.41 when θ = 90°.

$$k_{ds} = \sqrt{\frac{2}{1+\cos^2\theta}} \tag{2.47}$$

Mellor et al. (1999)
Using experimental results from the literature and the results of finite element models, Mellor et al. (1999) simplified an empirical equation that predicts the strength of fillet welds, resulting in Equation 2.48.

$$R_n = K_{at}F_cE_pL \tag{2.48}$$

Where E_p is the actual weld throat defined as the penetration depth plus the effective throat according to AISC *Specification* Section J2.2a. F_c is the rupture stress that considers the effect of base metal dilution. The authors developed Equation 2.49 as a simplified expression for F_c.

$$F_c = 0.6F_{EXX} + 0.4F_u \tag{2.49}$$

Where F_u is the tensile strength of the base metal. K_{at} is an empirical coefficient, which can be calculated with Equation 2.50 for transversely-loaded double-lap fillet weld joints.

$$K_{at} = 0.079 + 1.931\frac{E}{E_p} - 1.084\left(\frac{E}{E_p}\right)^2 \tag{2.50}$$

The authors found that, for transversely-loaded fillet welds, double-lap joints are stronger than T-joints. The higher loads were believed to be caused by friction at the faying surfaces in the lap joints, higher stress concentrations in the T-joint, and higher rigidity of the T-joint. Based on the experimental and theoretical results, the range of K_{at} was 0.93-1.04 and 0.82-0.98 for double-lap and T-joints, respectively.

Ng et al. (2002), Ng et al. (2004)
Ng et al. (2002) tested 102 transversely-loaded fillet weld specimens in double-lap and cruciform T-joints. Both the SMAW and FCAW processes were used in the fabrication. The specified weld size for the cruciform specimens was ¼ in. For the lapped specimens, two weld sizes were considered: ¼ in. and ½ in.

The calculated mean strength, using the measured rupture surface area, was approximately the same for both welding processes. However, the penetration for the FCAW specimens was much higher than for the SMAW specimens, resulting in higher rupture strengths for the FCAW specimens. The measured rupture surface width for the SMAW welds was similar to the theoretical effective throat dimension. The measured rupture surface width of the FCAW welds was about 1.5 to 2 times the theoretical effective throat dimension.

The tests showed that the rupture stress decreased nonlinearly with an increase in weld size. The average rupture stress for the lapped specimens was 13% higher than that of the cruciform specimens. Also, the lapped specimens were approximately 3.8 times as ductile as the cruciform specimens. Most of the specimens failed by ductile shear rupture at, or near, the weld shear leg ($\alpha = 0^o$). The test-to-predicted strength ratio ranged from 1.28 to 2.57 compared to the AISC *Specification* equations.

Deng et al. (2003)
Deng et al. (2003) investigated the strength of fillet welds in double-lap joints fabricated with both the SMAW and FCAW processes. The welds were subjected to three loading angles: $\theta = 0°$, 45° and 90°. A reliability analysis showed that the AISC *Specification* equations are applicable to welds fabricated with both SMAW and FCAW processes. The FCAW process resulted in higher root penetration than the SMAW process; therefore, the calculations are more conservative for FCAW welds. The average experimental strength for the FCAW specimens was approximately 50% higher than that of SMAW specimens. However, the mean rupture stress calculated with the measured rupture surface area was approximately the same for both welding processes.

Li et al. (2007)
Li et al. (2007) tested 12 transversely-loaded fillet weld specimens in cruciform T-joints. The specimens were welded with the FCAW process. The tests showed that lap-joints are between 0 and 30% stronger than T-joints. A reliability analysis was performed on transversely-loaded fillet welds using 1160 experimental data points from previous and current research. This indicated that, for lap-joints, the safety index is 4.5 and for T-joints, the safety index is 4.3. The authors analyzed 1,706 measurements on weld leg or throat dimensions from 12 research projects and determined that the average measured-to-specified ratio, ρ_G, is 1.08 with a coefficient of variation of 0.142. For the weld uniaxial metal tensile strength, 716 specimens from eight research projects showed that the average measured-to-specified ratio, ρ_{M1}, is 1.13 with a coefficient of variation of 0.080.

Based on the results of 304 specimens from eight research projects, the shear-to-tensile strength ratio of 0.60 in the AISC *Specification* equations is conservative. The average measured-to-specified ratio, ρ_{M2}, is 1.29 with a coefficient of variation of 0.130. This is identical to an average $\tau_u/\sigma_{uw} = 0.774$.

Gomez et al. (2008) and Kanvinde et al. (2009)
The strength in fillet-welded cruciform T-joints was determined theoretically and experimentally, while changing different parameters. The FCAW process was used with two electrodes: E70T-7 (non-toughness rated) and E70T7-K2 (toughness rated), two root notch lengths (plate thickness): 1.25 and 2.5 in., and two weld sizes: ½ and ⁵⁄₁₆ in. The experimental program consisted of eight combinations with three specimens each.

The root notch length had an insignificant effect on the weld strength and ductility. Generally, the calculated strength according to the AISC *Specification* was accurate compared to the experimental results. The ductility of the specimens with E70T7-K2 weld material was almost twice that of the specimens with E70T-7 weld. From the experimental results, the rupture angle of the weld, measured from the tension face, ranged from 20º to 80º. The photomicrograph of the fracture surface showed that the crack was initiated horizontally at the weld root for about 0.06 in. (1.5 mm) as a ductile tension fracture (crack opening fracture mode) then transitioned to the measured fracture angle as a brittle shear fracture.

The authors were able to predict the weld strength using fracture mechanics and finite element models. From the experimental results, a 2D plain-strain model was created to simulate the test specimens. The weld root was modeled as a half circle of 0.004 in. radius, which is acceptable because the anticipated crack tip blunting in the weld root at fracture is about 0.01 in. The size of the elements around the notch tip was 0.002 in. The FEA model was validated and calibrated by comparing the load-deformation curve of the weld with the curves obtained from testing. The critical fracture toughness of the weld root was calculated by integrating the stresses and strains within the 20 mesh contours around the crack tip. This value was used to determine the fracture load of other specimens of the same weld size, yet with different root notch lengths. The specimens were loaded gradually until the fracture toughness of the zone around the crack tip reached the previously calculated critical fracture toughness. This was considered the weld rupture strength. It was found that the strength and fracture ductility of pre-cracked welds are not dependent on the crack length, if it is above 1 in. This can be supported by the fact that the weld yields and exceeds its plastic limit prior to its failure. Smaller root notch lengths (less than 1 in.) were claimed to have higher ductility, but same strength.

Lu et al. (2015)
Both transverse and longitudinal fillet welds were studied by Lu et al. (2015). The objective was to develop a unified shear strength definition for fillet welds that account for the actual stress distribution and rupture plane. Finite element results and the traction stress approach were used to determine the critical fracture plane and the stress concentrations along the weld line of longitudinal fillet welds. The results were verified with 128 experimental tests.

The authors found that the weld strength can be determined from the membrane term and that the bending term can be neglected. Accordingly, the shear stress on the rupture plane of a transverse fillet weld is calculated with Equation 2.51.

$$\tau_T = \frac{P}{EL}\frac{\sqrt{2}}{4}\left[1+\sin(2\alpha)+\cos(2\alpha)\right] \tag{2.51}$$

Where α is the angle between the loading direction and the rupture plane. Setting $d\tau_T/d\alpha = 0$, results in $\alpha = 22.5°$. Substituting this into Equation 2.51 results in Equation 2.52. According to Equation 2.52, $k_{ds} = 1.48$.

$$\begin{aligned}\tau_T &= \frac{P}{EL}\frac{2+\sqrt{2}}{4} \\ &= 0.854\frac{P}{EL}\end{aligned} \tag{2.52}$$

Lu and Dong (2020)
Based on the shear stresses on the rupture plane, Lu and Dong (2020) derived Equation 2.53.

$$P_\theta = \frac{\tau_u wL}{(\sin\alpha + \cos\alpha)\sqrt{(\sin\theta\cos\alpha)^2 + \cos^2\theta}} \tag{2.53}$$

For transversely-loaded welds, the transverse compression force, *a*, that was originally included in the Miazga and Kennedy (1989) derivations, was used to develop Equation 2.54.

$$P_\theta = \frac{\tau_u wL}{(\sin\alpha + \cos\alpha)(\cos\alpha - a\sin\alpha)} \tag{2.54}$$

Setting $d\tau_u/d\alpha = 0$, results the critical angle between the loading direction and the rupture surface according to Equation 2.55.

$$\tan 2\theta = \frac{1-a}{1+a} \tag{2.55}$$

The authors showed that the theoretical value for *a* is approximately 0.3, which results in $\alpha = 14.2°$ and $k_{ds} = 1.30$. For $a = 0$, the directional strength increase factor is calculated using Equation 2.56 with $\alpha = 22.5°$, which results in $k_{ds} = 1.17$.

$$k_{ds} = \frac{4}{\sqrt{2}\left(1 + \sin 2\alpha + \cos 2\alpha\right)} \tag{2.56}$$

Luo et al. (2020a)
Luo et al. (2020a) evaluated the limit loads of welded T-joints using both slip-line theory and finite element models. Three different weld types were evaluated: 1. Double fillet welds, 2. PJP double-bevel groove welds with 45° groove angles, 3. Combined fillet/PJP welds. The calculations showed that transverse fillet welds are 41% stronger than longitudinal fillet welds. For longitudinal welds, the theoretical rupture surface angles coincided with the orientation of the effective throat as defined in AISC *Specification* Section J2.2a. According to their theory, the rupture surface angle for transverse fillet welds is 0° from the loading direction.

Luo et al. (2020b)
Luo et al. (2020b) studied the effect of loading angle on both fillet welds and PJP welds using 17 experimental specimens and 21 finite element models. T-joints were used for the fillet welds and both T- and butt-joints were studied for the PJP welds. The PJP welds had double-bevel grooves with a 45% penetration ratio and 45° groove angles. The specimens were fabricated with a 5 mm specified effective throat using the GMAW process with CO_2 shielding.

The research showed that the directional strength increase for fillet welds in equation 2.2 is non-conservative. The strength of fillet welds can be calculated with Equation 2.57, which has a mean test-to-predicted ratio of 1.00 and a standard deviation of 0.036.

$$k_{ds} = 1.0 + 0.34 \sin^{1.5} \theta \tag{2.57}$$

PARTIAL JOINT PENETRATION (PJP) WELDS

Satoh et al. (1974)
Satoh et al. (1974) tested welded T-joints with PJP double-bevel groove welds with several variables including the groove angle, the preparation depth and the size of the reinforcing fillet weld. Matching weld metal was used for all specimens. For the case without reinforcing fillet welds, the nominal stress on the effective throat as defined in AISC *Specification* Section J2.2a can be calculated with Equation 2.58.

$$F_{pjp} = F_{EXX}\sqrt{\frac{1}{3}+\sin^2\theta_p} \qquad (2.58)$$

Where θ_p is the groove angle measured from the load direction. The specimens ruptured either in the weld metal, in the fusion zone perpendicular to the load, or a combined path forming a bilinear crack through the PJP fusion zone and the fillet weld metal. Based on these ruptures in the fusion zone, the authors recommended that the tensile stress on the fusion zone perpendicular to the load should not exceed the base metal tensile strength.

Lawrence and Cox (1976)
Lawrence and Cox (1976) tested CJP butt-welded plates of A514 steel with matching electrodes and intentional defects of varying length at the center of the weld thickness. Based on a limit analysis of a cracked plate, they determined that reasonable upper- and lower-bound predictions could be based on the von Mises and Tresca criteria, respectively. This results in weld rupture stresses on the net weld cross section between 1.00 and $2/\sqrt{3} = 1.15$ times F_{EXX}.

Popov and Stephen (1977)
Popov and Stephen (1977) tested column splice details with butt-welded flanges subjected to static tension and reversible cyclic loading. The specimens were fabricated using W14x320 ($t_f = 2.09$) shapes of A572 Grade 50 material with matching (70 ksi) filler metal. The welds "were made using NR311 Inner-Shield welding." For one specimen, the flanges had CJP welds. The six remaining specimens were fabricated with PJP single-bevel groove welds with a 45° groove angle, with specified weld sizes of ⅜, ¾ and 1 in. The weld rupture stresses increased with decreasing weld sizes, resulting in strength increases of 6% for a 49% penetration ratio, 28% for a 38% penetration ratio and 40% for a 23% penetration ratio. The authors noted that the specimens with PJP welds exhibited "very little ductility."

Similar column splice specimens with penetration ratios between ¼ and ¾ were subjected to cyclic axial and flexural loads by Yabe et al. (1994). The results showed that the deformation capacity increases with the penetration ratio.

Gagnon and Kennedy (1989)
Gagnon and Kennedy (1989) tested 75 PJP groove weld specimens with five penetration ratios, *p* (20, 40, 60, 80 and 100%), and two steel strengths. The effect of eccentricity was studied by using both single specimens and paired specimens oriented back-to-back. The specimens had two plates that were welded together with single-bevel butt welds, which had a preparation defined by a 45° groove angle in one of the plates.

The specimens ruptured at or near the fusion zone of the plate with the square preparation. The rupture stresses for all specimens were similar to or greater than the measured uniaxial tensile stress of the weld metal. Table 2.1 shows the effect of the penetration ratio on the rupture stress, where the rupture stress decreases with increasing penetration. This effect, which is caused by the transverse constraint of the weld metal by the base metal, can be calculated with Equation 2.59.

$$F_c = F_{EXX}\left(1.55 - 1.16p + 0.61p^2\right) \tag{2.59}$$

where

p = penetration ratio

Table 2.1. Average experimental rupture stresses for each penetration ratio.

p	20%	40%	60%	80%	100%
σ_e/σ_{uw}	1.33	1.18	1.13	1.08	1.00

σ_e = experimental rupture stress, ksi
σ_{uw} = measured weld metal uniaxial tensile stress, ksi

Khurshid et al. (2015)

Khurshid et al. (2015) tested CJP and PJP butt welded joints in high-strength steel plates with specified tensile strengths of 750 and 980 MPa. Both matching and undermatching filler metals were used, and specimens with overmatching filler metal were tested for the lower-strength base metal. The CJP preparations were double-V grooves and the PJP welds had single-V grooves. The PJP welds had a 67% penetration ratio and both weld types had a 90° groove angle. All CJP specimens ruptured in the base metal. Rupture in the PJP specimens started at the root and propagated along the fusion zone. The deformation capacity of the CJP specimens was several times that of the PJP specimens. The ductility of overmatching PJP welds was slightly lower than matching welds, but the deformation capacity of the undermatching welds was significantly higher (25% to 53%). The available design strengths were compared to the experimental rupture loads, showing actual safety factors between 2.1 and 3.0 for the AWS D1.1 allowable strength equations.

Ran et al. (2019)

Ran et al. (2019) tested 108 butt-welded high-strength CJP specimens with mismatched tensile strength ratios between 0.696 and 1.27. The results indicated a slight increase in the rupture load (between 4 and 10%) for undermatching welds when the weld length increased from 25 mm to 100 mm. This behavior is caused by the transverse restraint in the width and thickness directions provided by the adjacent plates, which are stressed to a lower portion of the strength. The authors noted that the weld metal yields at a load equal to $(2/\sqrt{3})^{n+1}$ times the yield stress, where n is the strain-hardening exponent. This results in a yield load of 1.18 times the uniaxial yield load. Similar behavior can be expected in both matched and mismatched PJP joints.

Luo et al. (2020a)

Luo et al. (2020a) evaluated the limit loads of welded T-joints using both slip-line theory and finite element models. Three different weld types were evaluated: 1. Double fillet welds, 2. PJP double-bevel groove welds with a 45° groove angle, 3. Combined fillet/PJP welds. The calculations showed that transverse PJP welds are 183% stronger than longitudinal PJP welds. For longitudinal welds, the theoretical rupture surface angles coincided with the orientation of the effective throat as defined in AISC *Specification* Section J2.2a. According to the theory, the rupture surface angle for transverse PJP welds is 36° from the loading direction.

Luo et al. (2020b)
Luo et al. (2020b) studied the effect of loading angle on both fillet welds and PJP welds using 17 experimental specimens and 21 finite element models. T-joints were used for the fillet welds and both T- and butt-joints were studied for the PJP welds. The PJP welds had double-bevel grooves with a 45% penetration ratio and 45° groove angles. The specimens were fabricated with a 5 mm specified effective throat using the GMAW process with CO_2 shielding.

The research showed that the AISC *Specification* equations for PJP welds are over-conservative for $\theta > 0$. Due to the effects of transverse constraint and weld reinforcement (measured dimensions were not reported), the strength of the PJP T-joints were 1.23 times the strength of the butt-joints. The authors proposed Equation 2.60 for PJP T-joints, which has a mean test-to-calculated ratio of 1.00 and a standard deviation of 0.014.

$$k_{ds} = 1.0 + 0.629\theta + 0.068\theta^2 \tag{2.60}$$

They also proposed Equation 2.61 for PJP Butt-joints, which has a mean test-to-calculated ratio of 0.995 and a standard deviation of 0.038.

$$k_{ds} = 1.0 + 0.035\theta + 0.295\theta^2 \tag{2.61}$$

Reynolds et al. (2020)
Reynolds et al. (2020) tested six PJP welds in T-joints with single-bevel 45° groove angles and specified effective throats of ⅞ and 1¾ in. 1- and 2-in. thick A572 Grade 50 plates were welded in the Flat position with FCAW-G 70 ksi matching electrodes. Three specimens were loaded longitudinally and three were loaded transversely. Additionally, 15 specimens with combined PJP/fillet welds were loaded transversely.

All strength calculations used the measured weld geometries and material properties. The longitudinally-loaded specimens ruptured in the weld metal at loads that were accurately predicted with the AISC *Specification* equations. The mean rupture load for the transversely-loaded PJP specimens was 30% higher than the strength calculated with the AISC *Specification* equations. The authors noted that the rupture strength is most accurately predicted using the base metal tensile strength and the fusion zone area at the transverse plate (which is identical to the effective weld area) according to Equation 2.62.

$$R_n = F_u A_{we} \tag{2.62}$$

The mean rupture load for the combined PJP/fillet specimens was 21% higher than the strength calculated with the AISC *Specification* equations. These specimens ruptured along a roughly bilinear path forming a crack near the PJP fusion zone at the transverse plate and projecting diagonally through the weld metal. This rupture pattern, which is similar to that described by Satoh et al. (1974), is shown in Figure 2.11. The authors noted that the reinforcing fillet welds provided no significant increase in strength for the geometries tested and they recommended that the strength is best calculated by neglecting the reinforcing fillet. However, they noted that this may not be the case where overmatching electrodes are used.

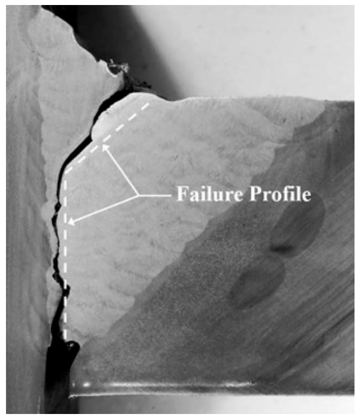

Fig. 2.11. Rupture plane from Reynolds et al. (2020).

HIGH-STRENGTH WELDS

Collin and Johansson (2005)

Collin and Johansson (2005) tested 27 longitudinally- and transversely-loaded fillet welds in high-strength steel joints. The measured uniaxial weld metal tensile strengths were 548 and 758 MPa. The authors noted that the Eurocode 3 (CEN, 2005) directional method is over-conservative for transverse fillet welds. They recommended Equation 2.63, which compared well with the experimental rupture loads and results in k_{ds} = 1.41 when θ = 90°.

$$\sqrt{\sigma_T^2 + 2\tau_T^2 + 3\tau_L^2} \leq F_{EXX} \quad (2.63)$$

Kuhlmann et al. (2008)

Kuhlmann et al. (2008) tested both longitudinally- and transversely-loaded fillet welds as well as PJP welds in high-strength steel joints. Compared to the Eurocode 3 (CEN, 2005) directional method, the authors proposed a less conservative value of β_w = 0.85 for S460 steel. For the longitudinally-loaded fillet welds, the shear rupture stress was accurately calculated with Equation 2.13.

Rasche and Kuhlmann (2009)

Rasche and Kuhlmann (2009) studied both the strength and ductility of fillet-welded connections in high strength steel using experimental and numerical analyses. The weld electrode was selected to match the base metal in the first part of the study. The objective was to determine a more accurate correlation factor, β_w, for use in Eurocode 3 (CEN, 2005). The authors recommended β_w = 0.79 for longitudinal fillet welds connecting S460M steel, instead of 1.0 as specified in Eurocode 3.

In investigating different filler metals, overmatching electrodes increased the strength. For tests with S690Q base metals, changing the filler metal from 690 MPa specified strength to 890 MPa increased the weld resistance by 9%; however, the ductility was reduced by almost 50%. Consequently, they concluded that the strength is controlled by the filler metal rather than the base metal.

Bjork et al. (2012)

Bjork et al. (2012) tested 28 fillet welded high-strength steel joints loaded either in the transverse or longitudinal directions. Additionally, six specimens with both longitudinal and transverse welds were tested. The GMAW process was used and the measured uniaxial weld metal tensile strengths were 690, 915 and 1,245 MPa. Both double-lap and cruciform T-joints were tested.

Most of the specimens with transversely-loaded T-joints ruptured along the HAZ or fusion zone and generally, the remaining specimens ruptured in the weld metal. The longitudinally-loaded welds ruptured approximately along the theoretical effective throat, which is defined at a rupture angle of 45°. For the transversely-loaded specimens that ruptured in the weld metal, the rupture angles were approximately 20° from the load direction.

The strength of the longitudinally-loaded specimens with $l/E \leq 50$ was accurately predicted with the Eurocode equations. For the specimens with $50 < l/E \leq 150$ the strength was approximately 15% less than for the shorter welds.

Bjork et al. (2014)
Bjork et al. (2014) tested three high-strength linear fillet welds subjected only to in-plane moments. Two electrodes were specified with 980 MPa (140 ksi) strength, but different elongation values: 14% and 19%. The specimen with 19% elongation reached the plastic strength according to AISC *Specification* Equation J2-5, including the directional strength factor (M_n = $0.90F_{EXX}EL^2/4$). However, both specimens with 14% elongation reached only the elastic strength according to AISC *Specification* Equation J2-5, including the directional strength factor ($M_n = 0.90F_{EXX}EL^2/6$).

Sun et al. (2019)
Sun et al. (2019) tested 44 transversely-loaded fillet welds in high-strength double-lap joints and T-joints. The GMAW process was used and the measured uniaxial weld metal tensile strengths were 627, 727, 771 and 956 MPa. The rupture angles were approximately 20° (13° to 24°) from the load direction for all weld sizes and electrode grades. The average ductility of double-lap joints was similar to that of T-joints. The test-to-predicted ratios were between 1.68 and 2.52 with an average of 2.01 for the Eurocode equations. For the AISC equations, the test-to-predicted ratios were between 1.08 and 1.61 with an average of 1.29.

Of the two joint types, the measured rupture surface area was larger for the T-joints. Due to the penetration and the low rupture surface angle, much of the rupture area for the T-joints was in the HAZ rather than the weld metal. In high-strength welds, metallurgical softening causes the HAZ to be weaker than the base metal. This may explain why, although the measured rupture surface was larger at the T-joints, the rupture load for both joint types was approximately the same. Another factor that was discussed by the authors is the presence of friction at the faying surfaces of the lap-joints which cannot exist in the T-joints.

LONG FILLET WELDS

Although the tests summarized by Spraragen and Claussen (1942) showed that longitudinally-loaded fillet welds had high elastic stress concentrations at the end, it was shown that the rupture strength of short welds (*l*/*w* between 1.4 and 19), is unaffected by the weld length. The fillet weld tests by Higgins and Preece (1969), where the weld length varied from 1.5 to 4 in. (*l*/*w* between 6 and 16) showed that the experimental rupture stress increased slightly with length, however, the increase of 3% was deemed negligible and subsequent longitudinally-loaded tests had 2-in. long welds. Based on experimental testing by Biggs et al. (1981) on relatively short welds and comparisons with research from the literature, the authors concluded that the strength of long welds "are comparable with those for short welds."

Rosenthal and Levray (1939) tested ten longitudinally-loaded double-lap fillet weld joints. SMAW electrodes with a measured uniaxial tensile strength, σ_{uw}, of 57 ksi were used to connect plates with varying weld lengths. The normalized shear rupture stress, τ_u/σ_{uw}, is plotted against the normalized length, *l*/*E*, in Figure 2.12. The data follows a trend of reduced strength with increasing length.

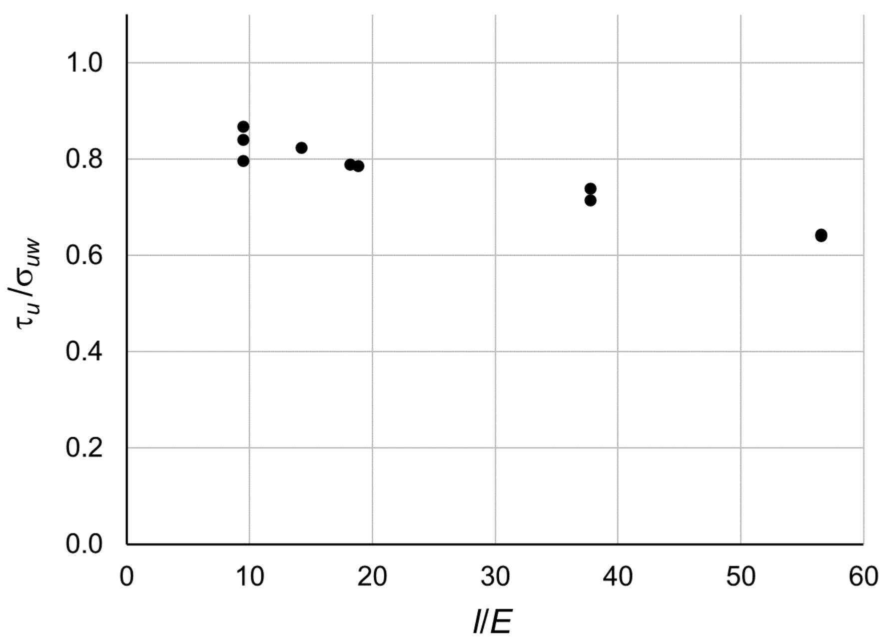

Fig. 2.12. Normalized rupture stress versus normalized length for the longitudinal fillet welds tested by Rosenthal and Levray (1939) .

Longitudinally-loaded fillet welds in lap joints have an uneven stress distribution along the weld, potentially causing an unzipping of the connection if the ends rupture. At low loads, when the welds are elastic, the stress distribution along the weld axis is nonuniform with the peak stresses at the weld ends as shown in Figure 2.13. This effect is caused by differential axial deformation of the connected elements. Equations were developed by Troelsch (1932) and Mocanu and Buga (1970) to describe this phenomenon in the elastic range. The stress concentrations are dependent on the axial stiffness of each connected element, the shear stiffness of the welds and the weld length. At higher loads, inelastic weld deformation allows stress redistribution, causing more uniform stresses.

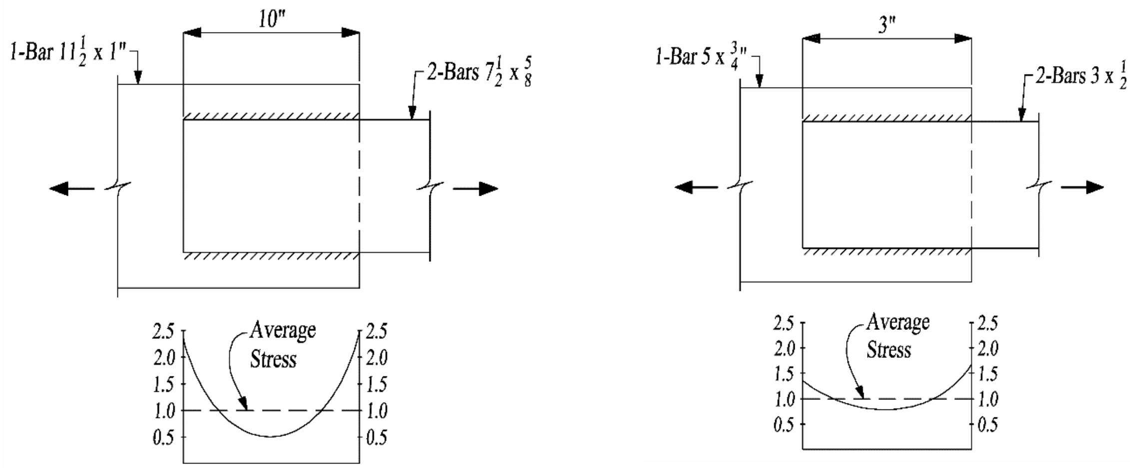

Fig. 2.13. Experimental stress distribution for end loaded fillet welds. (Redrawn from Moon, 1948).

Khanna (1969) studied long fillet welds theoretically and experimentally, with an emphasis on the ultimate strength. For three longitudinally-welded lap-joints with l/w = 75 (l = 17 in., w = 0.225 in.), the strengths were 3% lower than similar specimens with l/w = 4 (l = 1 in., w = 0.25 in.). However, this slight reduction was attributed to the nonuniform weld size along the length rather than the nonuniform stresses.

Feder (1994) used experimental results and inelastic finite element models to show that the inelastic weld deformations allowed stress redistribution, resulting in a more uniform stress distribution along the weld axis at the rupture load. Experiments by Blackwood (1930, 1931) showed that the plastic deformation of short welds is adequate to allow stress redistribution, so the welds are evenly stressed.

Bjork et al. (2012) tested 12 longitudinally-loaded double-lap fillet weld joints. GMAW electrodes with measured uniaxial tensile strengths, σ_u, of 100, 133 and 181 ksi were used to connect plates with varying weld lengths. The normalized shear rupture stress, τ_u/σ_{uw}, is plotted against the normalized length, l/E, in Figure 2.14. The authors noted that, generally, the rupture strength of the specimens with $l/E \leq 50$ was accurately predicted with the Eurocode equations. For the specimens with $50 < l/E \leq 150$ the strength was approximately 15% less than for the shorter welds.

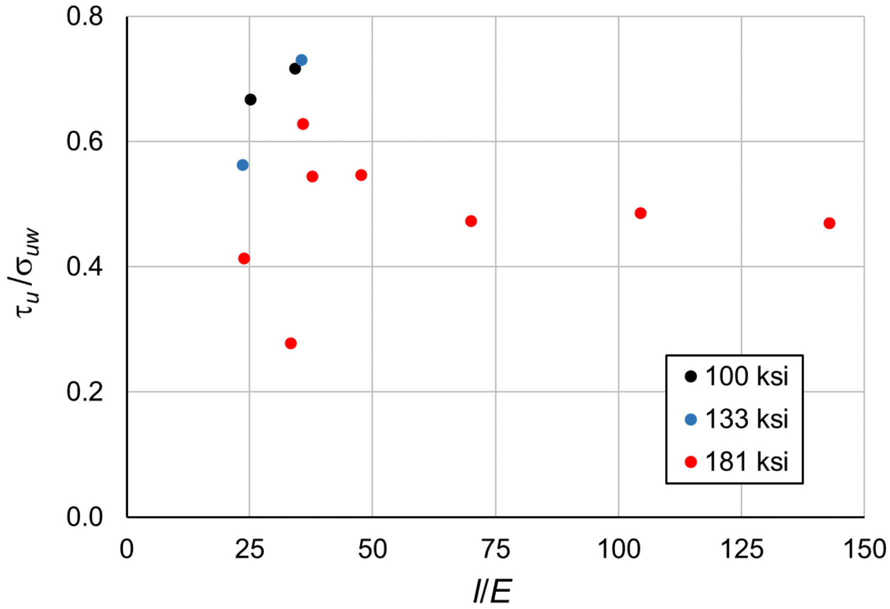

Fig. 2.14. Normalized rupture stress versus normalized length for the longitudinal fillet welds tested by Bjork et al. (2012).

SHEAR-TO-TENSILE STRENGTH RATIO

According to Brockenbrough and Johnston (1974), the shear rupture strength of structural steel "ranges from 2/3 to 3/4 of the tensile strength." Gaines (1987) noted that a shear-to-tensile strength ratio of 0.75 has been approved for the design of welds in steel Naval ships. Lesik and Kennedy (1988) and Lesik and Kennedy (1990) summarized the weld shear strength data for four previous projects found in the literature with a total of 126 tests on longitudinally-loaded fillet weld joints. They calculated an average shear-to-tensile strength ratio, τ_u/σ_{uw}, of 0.749 with a coefficient of variation of 0.121. Melchers (1999) noted that, for the reliability analysis of longitudinal fillet welds, the ratio of shear strength to tensile strength is 0.84 with a standard deviation of 0.09 and a coefficient of variation of 0.10.

Table 2.2 summarizes the various shear-to-tensile strength ratios discussed in Chapter 2. For the specification provisions, the ratio ranges from 0.577 to 0.75. Generally, these values are conservative compared to the experimental results, which range from 0.64 to 0.885.

Table 2.2. Shear-to-tensile strength ratios, τ_u/σ_{uw}.

Reference	τ_u/σ_{uw}	Source	Comments
AISC *Specification* (AISC, 2016)	0.60	Specification	
AWS D1.1 (2015)	0.60	Specification	
Canadian Standard CSA (2014)	0.67	Specification	
Eurocode 3 (CEN, 2005)	0.722	Specification	β_w = 0.80
Eurocode 3 (CEN, 2005)	0.679	Specification	β_w = 0.85
Eurocode 3 (CEN, 2005)	0.642	Specification	β_w = 0.90
Eurocode 3 (CEN, 2005)	0.577	Specification	β_w = 1.0
AIJ (2012)	0.577	Specification	
Naval Ships	0.75	Specification	Gaines (1987)
International Institute of Welding (IIW)	0.745	Specification	Van der Eb (1952)
Spraragen and Claussen (1942)	0.64-0.84	Experimental	
Vreedenburgh (1954)	0.75	Experimental	
Swannell (1968)	0.885	Experimental	
Ligtenburg (1968), Strating (1971)	0.83	Experimental	
Brockenbrough and Johnston (1974)	0.67-0.75	Experimental	
Lesik and Kennedy (1988, 1990)	0.749	Experimental	
Miazga and Kennedy (1989)	0.764	Experimental	
Melchers (1999)	0.84	Experimental	
Li et al. (2007)	0.774	Experimental	
τ_u = measured weld metal shear rupture stress σ_{uw} = measured weld metal uniaxial tensile stress			

Krumpen and Jordan (1984) developed equations to estimate the shear strength of weld metal as a function of the tensile strength by curve fitting experimental results from the literature with filler metal classification strengths between 60 and 140 ksi. Equations 2.64 and 2.66 were developed for SMAW and GWAM electrodes, respectively. These equations were divided by the tensile strength, σ_{uw}, resulting in the shear-to-tensile strength ratios according to Equations 2.65 and 2.67.

$$\tau_u = 1.8\sigma_{uw}^{0.80} \tag{2.64}$$

$$\frac{\tau_u}{\sigma_{uw}} = \frac{1.8}{\sigma_{uw}^{0.20}} \tag{2.65}$$

$$\tau_u = 2.5\sigma_{uw}^{0.75} \tag{2.66}$$

$$\frac{\tau_u}{\sigma_{uw}} = \frac{2.5}{\sigma_{uw}^{0.25}} \tag{2.67}$$

These equations were used to calculate the shear-to-tensile strength ratios in Table 2.3. Comparisons between Table 2.2 and 2.3 indicate that all of the specification ratios in Table 2.2 are over-conservative. Although the Eurocode 3 values are conservative by approximately 1.15 to 1.30, the general trend is captured, where the strength ratio reduces with increasing tensile strength.

Table 2.3. Shear-to-tensile strength ratios calculated with the Krumpen and Jordan (1984) Equations.

F_{EXX} ksi	τ_u/σ_{uw}	
	SMAW	**GMAW**
60	0.794	0.898
70	0.770	0.864
80	0.749	0.836
90	0.732	0.812
100	0.717	0.791
110	0.703	0.772

DIRECTIONAL STRENGTH INCREASE FOR FILLET WELDS

An increase in the load angle, θ, for fillet welds results in a nonlinear strength increase and a decrease in ductility. Based on 18 experimental tests with loading angles of 0°, 30°, 60° and 90°, Clark (1971) showed that the transversely-loaded welds were approximately 70% stronger than the longitudinally-loaded welds. Gaines (1987) noted that a transverse-to-longitudinal strength ratio of 1.44 has been approved for the design of fillet welds in steel Naval ships.

Table 2.4 summarizes the transverse-to-longitudinal strength ratios found in the literature. The experimental values are between 1.12 and 1.70. The theoretical ratios range from 1.30 to 1.48, with a ratio of 1.50 for the semi-empirical equation developed by Miazga and Kennedy (1989). For the various specifications reviewed, the ratios are between 1.13 and 1.50.

Table 2.4. Fillet weld transverse-to-longitudinal strength ratios, k_{ds}, for θ = 90°.

Reference	k_{ds}	Source	Comments
AISC *Specification* (AISC, 2016)	1.50	Specification	
AWS D1.1 (2015)	1.50	Specification	
Canadian Standard CSA (2014)	1.50	Specification	
Eurocode 3 (CEN, 2005)	1.22	Specification	Directional Method
AIJ (2012)	1.40	Specification	
Naval Ships	1.44	Specification	Gaines (1987)
International Institute of Welding (IIW)	1.13	Specification	Van der Eb (1952)
Vreedenburgh (1954)	1.12	Experimental	
Archer et al. (1959)	1.56	Experimental	
Preece (1968)	1.57	Experimental	F_{EXX} = 70 ksi
Preece (1968)	1.44	Experimental	F_{EXX} = 110 ksi
Ligtenburg (1968), Strating (1971)	1.60	Experimental	
Butler and Kulak (1971)	1.45	Experimental	
Clark (1971)	1.70	Experimental	
Kato and Morita (1974)	1.46	Experimental	
Kamtekar (1982), Kamtekar (1987)	1.41	Theoretical	
Kennedy and Kriviak (1985)	1.42	Experimental	
Neis (1985)	1.41	Theoretical	
McClellan (1989)	1.51	Experimental	F_{EXX} = 70 ksi
McClellan (1989)	1.39	Experimental	F_{EXX} = 100 ksi
Miazga and Kennedy (1989)	1.50	Semi-empirical	
Bowman and Quinn (1994)	1.20-1.70	Experimental	
Iwankiw (1997)	1.41	Theoretical	
Collin and Johansson (2005)	1.41	Semi-empirical	
Lu et al. (2015)	1.48	Theoretical	
Lu and Dong (2020)	1.30	Theoretical	
Luo et al. (2020a)	1.41	Theoretical	
Luo et al. (2020b)	1.34	Experimental	

FUSION ZONE STRENGTH

Several research projects, including Preece (1968), tested experimental specimens with over-matched weld metal, showing that rupture typically occurs in the weld metal, including the specimens where the weld metal strength exceeded the base metal strength by a substantial amount. Because of this, an evaluation of the strength of fusion zones is not required by the AISC *Specification*.

Rupture at the fusion zone has been reported in experimental specimens for both fillet and PJP welds. Under some conditions, such as single-bevel PJP welds, fusion zone rupture can be expected because the theoretical effective throat coincides with one of the fusion zones. In this case, the theoretical calculations are correct and provide an accurate estimate of the joint strength. However, unexpected fusion zone ruptures, where rupture occurs along a surface that does not coincide with the theoretical effective throat, have also occurred in tests. Unexpected fusion zone ruptures have been documented in only in a small portion of the experimental specimens.

High-Strength Steel

According to Bjork et al. (2018), high-strength base metals, which were defined as materials with $F_y \geq 500$ MPa (72.5 ksi), are more prone to rupture at the fusion zones than lower-strength steels. According to the authors, "due to softening and other metallurgical effects," the fusion zones "may be weaker than the adjacent base material."

Ginn et al. (2011) tested 20 double-lap longitudinal fillet weld specimens. The joints were fabricated using the GMAW process with high-strength inner plates ($F_y = 460$ MPa, $F_u = 720$ MPa) and standard-grade outer plates. The electrodes were selected to match the high-strength plates. The variables were weld size (6, 8 and 10 mm), weld length (50, 85 and 120 mm) and base metal thickness. The specimens ruptured either in the weld metal or along the fusion zone of the high-strength plate. Generally, the specimens that failed in the fusion zone had lower experimental rupture stresses.

Most of the transversely-loaded fillet welded high-strength steel joints tested by Bjork et al. (2012), ruptured along the fusion zone. Generally, the remaining specimens, including the longitudinally-loaded welds, ruptured in the weld metal. For the transversely-loaded specimens that ruptured in the weld metal, the rupture angles were approximately 20° from the load direction.

Tuominen et al. (2018) tested transversely-loaded T-joints with single-sided fillet welds and PJP single-bevel groove welds. There were no fusion zone ruptures for the specimens with base metal yield stresses equal to 400 MPa. However, for the 13 specimens fabricated with S960 material, which had a measured yield stress of 1041 MPa, a measured rupture stress of 1210 MPa and a measured weld metal tensile stress of 980 MPa, three specimens ruptured at the fusion zone, three specimens ruptured in the weld metal and the remaining specimens failed in the base material.

Due to the penetration and the low rupture surface angle, much of the rupture area for the transversely-loaded fillet welded T-joints tested by Sun et al. (2019) was in the HAZ rather than the weld metal. The authors noted that metallurgical softening may have reduced the rupture stresses for these joints.

Fillet Welds

Ales (1990) reported a fusion zone rupture at the top portion of a single-plate shear connection, where double fillet welds were used to connect the plate to the supporting rectangular HSS column.

The fusion zone rupture of a transversely-loaded double fillet weld specimen was documented by Dubina and Stratan (2002). Due to excessive convexity, the shortest distance from the root to the face was along the fusion zone; therefore, this rupture plane would be predicted if the actual weld profile were used in the analysis.

Zhao and Hancock (1995) tested nine specimens with transversely-loaded fillet welds connecting cold-formed rectangular HSS shapes to end plates in T-joints. Eight of the specimens ruptured in the base metal and one failed at the fusion zone of the HSS wall. The experimental rupture strength of the specimen that failed along the fusion zone was only 86% of the average experimental strength of the remaining specimens.

PJP Welds

For the PJP groove weld specimens tested by Gagnon and Kennedy (1989), the primary rupture location was at or near the fusion zone of the plate with the square preparation. The rupture stresses for all specimens were similar to or greater than the measured uniaxial tensile stress of the weld metal.

CHAPTER 3
EXPERIMENTAL PROGRAM

To meet the objectives of this research project, experimental specimens with both fillet and PJP welds were tested. Three different base metal strengths and three different weld metal strengths were specified. A total of 71 specimens were tested, including 18 transverse fillet weld specimens, 15 longitudinal fillet weld specimens, 17 transverse PJP weld specimens, 15 transverse PJP weld specimens and 6 skewed PJP weld specimens. The specimen shop drawings are in Appendix A. All specimens were shop welded using the Flux-Core Arc Welding (FCAW) process with CO2 gas shielding. Welding Procedure Specifications (WPS) for each filler metal classification strength are in Appendix C.

SPECIMEN GEOMETRY

Transverse Fillet Weld Specimens

Compared to lap joints, Ng et al. (2002) reported slightly lower strength and significantly lower ductility for cruciform joints. Therefore, the transverse fillet weld specimens in this project are of the cruciform configuration as shown in Figure 3.1. The specimen variables are listed in Table 3.1. All runoff tabs were removed before testing.

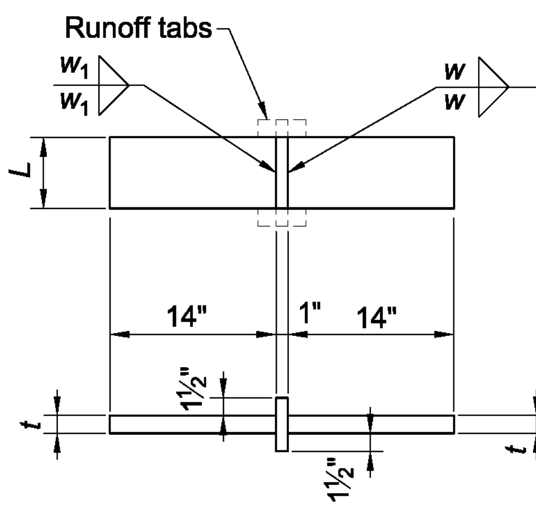

Fig. 3.1. Transverse fillet weld specimens.

Table 3.1. Transverse Fillet Weld Specimen Details.						
Spec. No.	F_{EXX} ksi	F_y ksi	w in.	w_1 in.	t in.	L in.
FT1	70	36	¼	5⁄16	1	2
FT2	70	36	¼	5⁄16	1	4
FT3	70	36	¼	5⁄16	1	6
FT4	70	36	⅜	½	1¼	2
FT5	70	36	⅜	½	1¼	4
FT6	70	36	⅜	½	1¼	6
FT7	70	36	½	⅝	1¾	2
FT8	70	36	½	⅝	1¾	4
FT9	70	36	½	⅝	1¾	6
FT10	80	65	¼	5⁄16	1	6
FT11	80	70	⅜	½	1½	6
FT12	80	70	½	⅝	2	4
FT13	100	65	¼	5⁄16	1¼	2
FT14	100	65	¼	5⁄16	1¼	6
FT15	100	70	⅜	½	1¾	2
FT16	100	70	⅜	½	1¾	6
FT17	100	70	½	⅝	2	2
FT18	100	70	½	⅝	2	4

F_{EXX} = filler metal classification strength (specified minimum uniaxial tensile strength)
F_y = specified minimum yield strength of the plates

Longitudinal Fillet Weld Specimens

The longitudinal fillet weld specimens are shown in Figure 3.2, and the variables are listed in Table 3.2. The specimens were partially saw-cut at both the specimen mid-length and the runoff tabs, resulting in continuous weld lengths, *L*. These partial-depth cuts encompassed the entire weld, including the penetration.

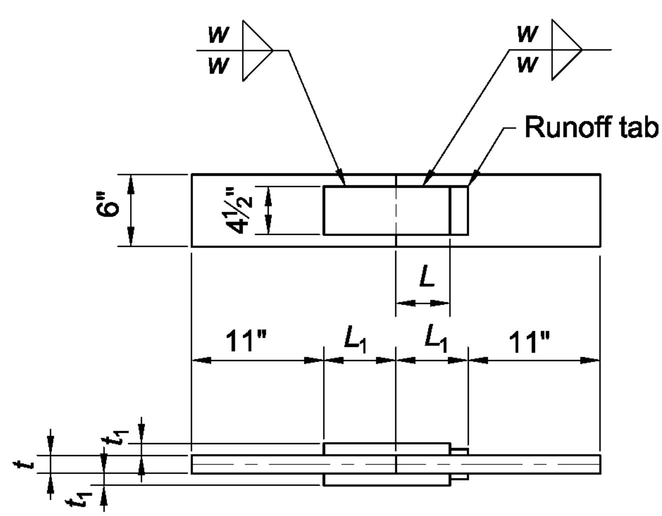

Fig. 3.2. Longitudinal fillet weld specimens.

Table 3.2. Longitudinal Fillet Weld Specimen Details.							
Spec. No.	F_{EXX} ksi	F_y ksi	w in.	t in.	t_1 in.	L in.	L_1 in.
FL1	70	36	¼	1	¾	2	3
FL2	70	36	¼	1	¾	4	5
FL3	70	36	¼	1½	1	6	8
FL4	70	36	⅜	1	¾	2	3
FL5	70	36	⅜	1½	1	4	5
FL6	70	36	⅜	1½	1	6	8
FL7	70	36	½	1	¾	2	3
FL8	70	36	½	1½	1	4	5
FL9	80	70	¼	1½	1	6	8
FL10	80	70	⅜	1½	1	4	5
FL11	100	65	¼	1	¾	2	3
FL12	100	70	¼	1½	1	6	8
FL13	100	65	⅜	1	¾	2	3
FL14	100	70	⅜	1½	1	4	5
FL15	100	65	½	1	¾	2	3

F_{EXX} = filler metal classification strength (specified minimum uniaxial tensile strength)
F_y = specified minimum yield strength of the plates

Transverse PJP Weld Specimens

The transverse PJP weld specimens were fabricated using butt joints with double-bevel groove preparations according to prequalified joint designation B-P5. The specimen details are shown in Figure 3.3, with the variables listed in Table 3.3. All runoff tabs were removed before testing.

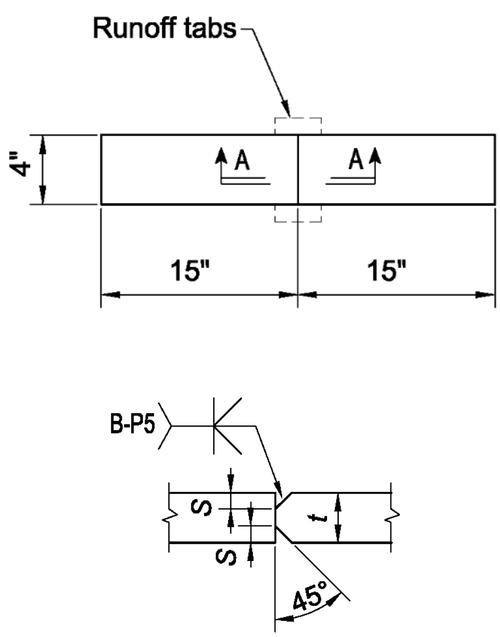

Section A-A

Fig. 3.3. Transverse PJP weld specimens.

Table 3.3. Transverse PJP Specimen Details.					
Spec. No.	**F_{EXX} ksi**	**F_y ksi**	**S in.**	**t in.**	**% Fused**
PT1	70	36	¼	¾	67
PT2	70	36	⅜	1	75
PT3	70	36	5⁄16	1½	42
PT4	70	36	⅜	1½	50
PT5	70	36	½	1½	67
PT6	70	36	½	2	50
PT7	70	65	¼	¾	67
PT8	70	70	⅜	1½	50
PT9	80	36	¼	¾	67
PT10	80	36	⅜	1½	50
PT11	80	36	½	1½	67
PT12	80	65	¼	¾	67
PT13	80	70	⅜	1½	50
PT14	100	36	¼	¾	67
PT15	100	36	⅜	1½	50
PT16	100	65	¼	¾	67
PT17	100	70	⅜	1½	50

F_{EXX} = filler metal classification strength (specified minimum uniaxial tensile strength)
F_y = specified minimum yield strength of the plates
S = specified weld preparation groove depth for each weld
% Fused = theoretical value based on the specified geometry = (100%)($2S/t$)

Longitudinal PJP Weld Specimens

The longitudinal PJP weld specimens were fabricated using both corner and T-joints with groove preparations according to prequalified joint designations C-P5 and T-P5, respectively. The specimen details are shown in Figure 3.4, with the variables listed in Table 3.4. The specimens were partially saw-cut at both the specimen mid-length and the runoff tabs, resulting in 4-in. long continuous welds. These partial-depth cuts encompassed the entire weld, including the penetration.

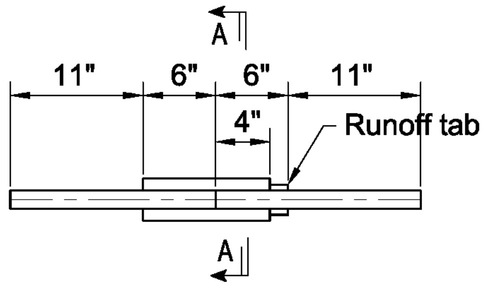

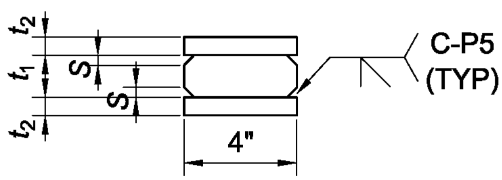

Section A-A (Joint Type B)

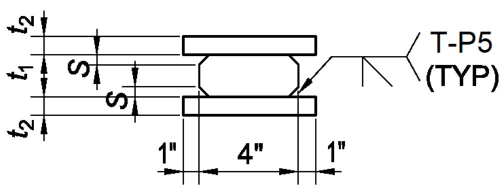

Section A-A (Joint Type T)

Fig. 3.4. Longitudinal PJP weld specimens.

Table 3.4. Longitudinal PJP Specimen Details.

Spec. No.	F_{EXX} ksi	F_y ksi	S in.	t_1 in.	t_2 in.	Joint Type
PL1	70	36	¼	1½	¾	B
PL2	70	36	5⁄16	2	1	B
PL3	70	36	⅜	2½	1¼	B
PL4	70	36	7⁄16	2½	1¼	B
PL5	80	36	¼	2	1	B
PL6	80	36	⅜	2½	1¼	B
PL7	100	36	¼	2	1	B
PL8	100	36	5⁄16	2½	1¼	B
PL9	80	65/70	¼	2 (70 ksi)	1 (65 ksi)	B
PL10	80	65/70	⅜	2 (70 ksi)	1 (65 ksi)	B
PL11	100	65/70	¼	2 (70 ksi)	1 (65 ksi)	B
PL12	100	65/70	5⁄16	2 (70 ksi)	1 (65 ksi)	B
PL13	70	36	⅜	2½	1	T
PL14	80	36	⅜	2½	1	T
PL15	100	36	5⁄16	2½	1	T

F_{EXX} = filler metal classification strength (specified minimum uniaxial tensile strength)
F_y = specified minimum yield strength of the plates

Skewed PJP Weld Specimens

The skewed PJP weld specimens were fabricated using butt joints with double-bevel groove preparations according to prequalified joint designation B-P5. The specimen details are shown in Figure 3.5, with the variables listed in Table 3.5. Specimens PS3 and PS6 were specified with a ½ in. groove depth; however, the measured depth of 7⁄16 in. is listed in Table 3.5. All runoff tabs were removed before testing.

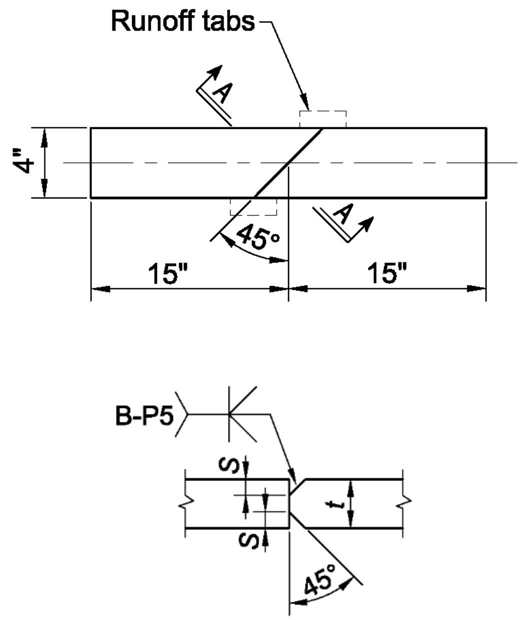

Section A-A

Fig. 3.5. Skewed PJP weld specimens.

Table 3.5. Skewed PJP Specimen Details.

Spec. No.	F_{EXX} ksi	F_y ksi	S in.	t in.	% Fused
PS1	70	36	¼	¾	67
PS2	70	36	⅜	1½	50
PS3	70	36	7⁄16	1½	67
PS4	100	36	¼	¾	67
PS5	100	36	⅜	1½	50
PS6	100	36	7⁄16	1½	67

F_{EXX} = filler metal classification strength (specified minimum uniaxial tensile strength)
F_y = specified minimum yield strength of the plates

PROCEDURE

The specimens were tested on a 600 kip Tinius Olsen universal testing machine at a load rate of 20 to 30 kips per minute. A loaded test specimen is shown in Figure 3.6.

Fig. 3.6. Test setup.

Pre-Test Measurements

The weld lengths were measured for each weld. Dimensions of each fillet weld leg were measured at multiple locations along the weld length. As shown in Figures 3.7a and 3.7b, w_L is the measurement parallel to the faying surface and w_T is the measurement perpendicular to the faying surface. For PJP welds, the reinforcement, x, was measured at multiple locations along the weld length. This dimension is shown in Figure 3.7c. The specimen measurements are listed in Appendix G.

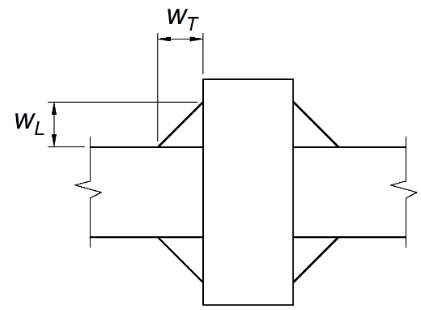

a. Transverse fillet welds

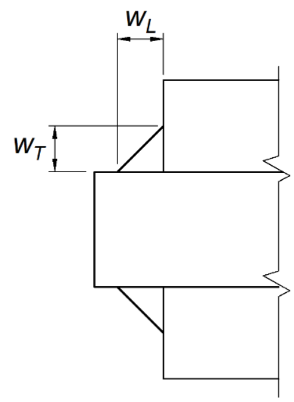

b. Longitudinal fillet welds

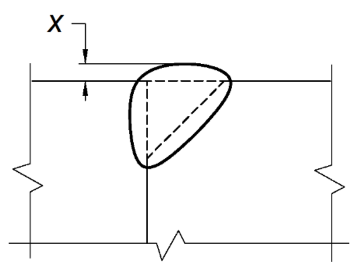

c. Partial penetration welds

Fig. 3.7. Pre-test weld size measurements.

Post-Test Measurements and Preparation

Figure 3.8 shows the specimens after testing. The length of the rupture surface, L_r, was measured for all specimens and the rupture width, E_r, was measured at multiple locations along the weld length. The rupture angles, γ, were measured from the faying surface as shown in Figure 3.9. Typically, the rupture surfaces were irregular and varied along the length; therefore, the rupture angles were measured at multiple locations along the length. The specimen measurements are listed in Appendix G. Specimens FL5, FL14, PL2, PL4, PL8, PL13, PL14 and PL15 were selected for cross-sectional macro etching. For these specimens, the weld dimensions that were measured manually were verified with digital measurements. The specimens were sectioned with a band saw, as shown in Figure 3.10. Photographs of the specimens, including the etched cross sections, are in Appendix F.

Fig. 3.8. Specimens after testing.

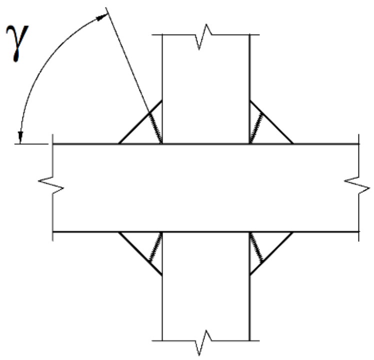

a. Transverse fillet welds

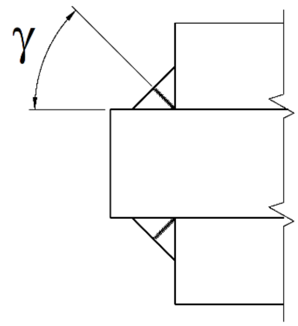

b. Longitudinal fillet welds

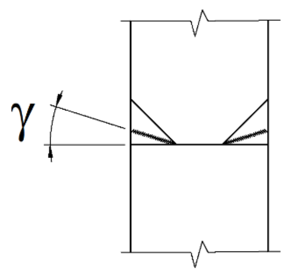

c. Transverse PJP welds

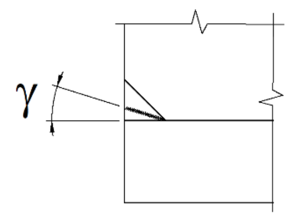

d. Longitudinal and skewed PJP welds

Fig. 3.9. Post-test rupture angle measurements.

Fig. 3.10. Sectioning a specimen for etching.

RESULTS

Material Properties

Mill Test Reports (MTR) for the plates are in Appendix B. For each material grade and thickness, the measured yield and ultimate stresses from the MTRs are listed in Table 3.6. All of the values met the requirements in the corresponding ASTM standard. An ancillary test on the 2 in. A709 HPS 70WF3 plate revealed upper yield and ultimate stresses that were approximately 3% less than the values reported in the MTR.

Table 3.6. Measured tensile properties from the mill test reports.

ASTM Grade	t in.	Specified Minimum		Measured	
		F_y ksi	F_u ksi	σ_{yb} ksi	σ_{ub} ksi
A36	0.75	36	58	44.0	72.0
A36	1	36	58	48.5	77.0
A36	1.25	36	58	42.2	70.5
A36	1.5	36	58	44.5	71.9
A36	1.75	36	58	37.2	66.9
A36	2	36	58	42.1	70.5
A36	2.5	36	58	42.0	72.0
A572 Grade 65	0.75	65	80	72.5	94.0
A572 Grade 65	1	65	80	74.2	94.1
A572 Grade 65	1.25	65	80	70.5	91.5
A709 HPS 70W T3[a]	1.5	70	85	82.0	99.0
A709 HPS 70W F3[a]	1.75	70	85	80.0	93.0
A709 HPS 70W F3[a]	2	70	85	82.0	95.0

[a]Quenched and tempered

Mill Test Reports (MTR) for each filler metal classification strength are in Appendix D. All-weld-metal tension tests, according to ASTM A370 (ASTM, 2017), were used to measure the weld metal strength. Tension coupons were machined from standard groove-welded test plates. Three test plates for each weld classification were manufactured according to AWS A5.20. Plate dimensions are shown in Figure 3.11. The same figure shows the location, where the tensile coupons were cut. Tension coupons were prepared according to AWS B4.0 (AWS, 2016) and shaped for the tension test as shown in Figure 3.12. All-weld-metal test reports are in Appendix E and the mean measured tensile strengths are listed in Table 3.7.

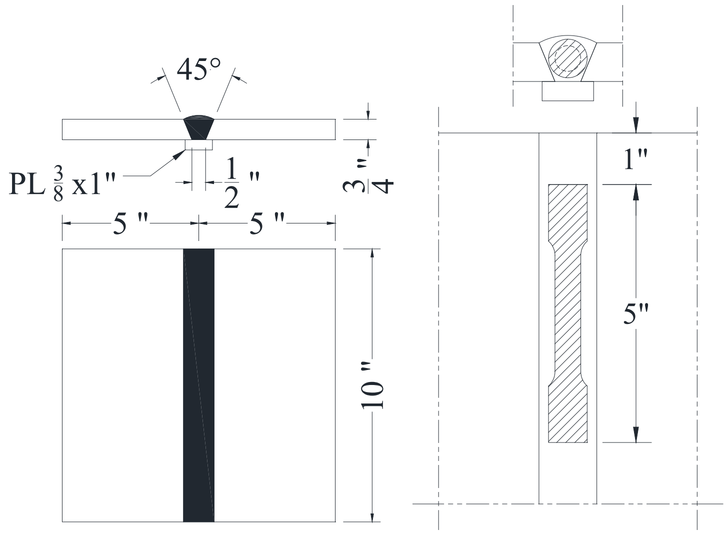

Fig. 3.11. Groove-welded test plates for all-weld-metal tension tests.

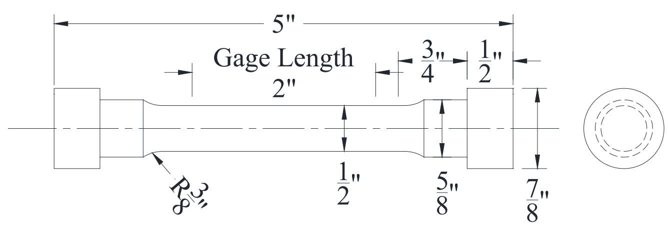

Fig. 3.12. Tensile specimen geometry for all-weld-metal tension tests.

Table 3.7. Average tensile test results.

Classification	σ_{uw} ksi	Elongation %	Reduction in Area %
E71T	75.8	31.0	69.3
E81T1	80.8	29.3	70.0
E101T1	100	23.3	60.0

σ_{uw} = experimental uniaxial tensile rupture stress based on all-weld-metal specimens, ksi

Rupture Surfaces

Typically, the rupture surfaces were irregular, with rupture angles that varied along the length. Generally, the specimens ruptured in the weld metal. The section on Fusion Zone Rupture discusses several specimens that ruptured along the fusion zone, either partially or completely.

Weld Strength

The experimental rupture loads for the specimens are listed in Appendix G. Table 3.8 shows the average P_e/P_n, P_e/P_c and f_r/σ_{uw} ratios for the longitudinal fillet weld specimens, where P_e is the experimental rupture load, P_n is the nominal strength calculated with the AISC *Specification* equations, P_c is the strength calculated with the measured weld size and the measured weld metal tensile strength, f_r is the rupture stress calculated with the measured rupture surface area and σ_{uw} is the experimental uniaxial tensile rupture stress based on all-weld-metal specimens. Table 3.9 shows the average values for the P_e/P_n, P_e/P_c and f_r/σ_{uw} ratios for the transverse fillet weld specimens.

Table 3.8. Strength ratios for longitudinal fillet welds.

F_{EXX} ksi	P_e / P_n		P_e / P_c		f_r / σ_{uw}	
	Average	Standard Deviation	Average	Standard Deviation	Average	Standard Deviation
70	2.09	0.266	1.66	0.160	0.857	0.0448
80	1.95	0.0988	1.83	0.112	0.978	0.0610
100	1.44	0.153	1.24	0.0906	0.769	0.119
All Specimens	1.85	0.366	1.54	0.260	0.844	0.103

Table 3.9. Strength ratios for transverse fillet welds.

F_{EXX} ksi	P_e / P_n		P_e / P_c		f_r / σ_{uw}	
	Average	Standard Deviation	Average	Standard Deviation	Average	Standard Deviation
70	1.84	0.306	1.51	0.175	0.888	0.100
80	1.53	0.189	1.42	0.103	0.980	0.0418
100	1.24	0.102	1.06	0.0730	0.857	0.0770
All Specimens	1.59	0.360	1.34	0.245	0.893	0.0946

Tables 3.10, 3.11 and 3.12 show the average values for the P_e/P_n, P_e/P_c and f_r/σ_{uw} ratios for the longitudinal, transverse and skewed PJP weld specimens, respectively. P_c was calculated with an effective throat equal to the groove depth with no consideration of the reinforcement.

Table 3.10. Strength ratios for longitudinal PJP welds.

F_{EXX} ksi	P_e / P_n		P_e / P_c		f_r / σ_{uw}	
	Average	Standard Deviation	Average	Standard Deviation	Average	Standard Deviation
70	1.48	0.153	1.36	0.142	0.762	0.0704
80	1.18	0.277	1.17	0.274	0.776	0.106
100	1.23	0.122	1.23	0.122	0.730	0.0620
All Specimens	1.31	0.234	1.26	0.205	0.756	0.0831

Table 3.11. Strength ratios for transverse PJP welds.

F_{EXX} ksi	P_e / P_n		P_e / P_c		f_r / σ_{uw}	
	Average	Standard Deviation	Average	Standard Deviation	Average	Standard Deviation
70	2.33	0.362	2.15	0.334	1.28	0.156
80	1.71	0.225	1.69	0.223	1.56	0.182
100	1.56	0.123	1.56	0.123	1.17	0.130
All Specimens	1.97	0.446	1.88	0.372	1.34	0.219

Table 3.12. Strength ratios for skewed PJP welds.						
F_{EXX} ksi	**P_e / P_n**		**P_e / P_c**		**f_r /σ_{uw}**	
	Average	**Standard Deviation**	**Average**	**Standard Deviation**	**Average**	**Standard Deviation**
70	1.62	0.149	1.50	0.138	1.02	0.0723
100	1.16	0.0112	1.16	0.0112	0.94	0.0236
All Specimens	1.39	0.255	1.33	0.196	0.98	0.0689

CHAPTER 4
ANALYSIS AND DISCUSSION

ELECTRODE STRENGTH COEFFICIENT

Instantaneous Center of Rotation Method

Butler et al (1972) developed the Instantaneous Center of Rotation (ICR) method based on the empirical load-deformation curves from Butler and Kulak (1971), who tested linear fillet welds at angles of 0°, 30°, 60° and 90° from the loading direction. The tests by Butler and Kulak (1971) as well as the tests on eccentrically-loaded weld groups by Butler et al. (1972) used 60 ksi electrodes and ¼ in. fillet welds. According to Butler et al (1972), "Because E60 and E70 electrodes have specified ultimate elongations nearly the same, it is felt that these results could be applied to connections made using E70 electrodes by proper consideration of the increase in electrode strength. The method could be used for fillet welds made from electrodes other than E60 and E70 by ascertaining the load-deformation response for these welds."

The ICR equations in AWS D1.1 Section 2.6.4.3 were primarily developed by Lesik and Kennedy (1990). Lesik and Kennedy (1990) used linear regression to develop the load-deformation curves with the data from Miazga and Kennedy (1989), who tested 70 ksi fillet welds with varying load angles from 0 to 90° in 15° increments.

Because the ICR method is iterative, considerable design effort is required to calculate the strength of a weld group using this method. AISC *Manual* Tables 8-4 through 8-11 provide a simpler, non-iterative design method by listing the appropriate ICR coefficients for several different weld group geometries.

Background of the Electrode Strength Coefficient

The values in AISC *Manual* Tables 8-4 through 8-11 were calculated using F_{EXX} = 70 ksi. The strength of weld groups with other weld metal strengths can be calculated by adjusting the table coefficients by the electrode strength coefficient, C_1 in *Manual* Table 8-3.

The 6th Edition AISC *Manual* was the first to provide information on eccentrically-loaded weld groups. The elastic method was used to develop design tables with 60 ksi weld metal strength. The weld group strengths for other weld metal strengths were calculated with the weld metal strength ratio, F_{EXX}/60 ksi. The 7th Edition *Manual* used elastic design with 70 ksi welds; therefore, the weld group strength for other weld metal strengths was calculated with the weld metal strength ratio, F_{EXX}/70 ksi.

The 8th Edition *Manual* was the first to publish design tables that were based on the ICR method. The development of these tables, which were also published in the 9th Edition *Manual*, was discussed by Tide (1980). The table coefficients were calculated with 70 ksi weld metal and C_1 was used to calculate the weld group strength for other weld metal strengths, where $C_1 = F_{EXX}$/70 ksi.

For the 1st Edition LRFD *Manual* and the 13th Edition combined ASD/LRFD *Manual*, as well as all later editions, the tables were based on the ICR method with 70 ksi weld metal. However, the value of C_1 included a reduction factor equal to either 0.90 (for 80 and 90 ksi welds) or 0.85 (for 100 and 110 ksi welds). These values are shown in Table 4.1.

Table 4.1. Electrode strength coefficient, C_1.

F_{EXX}	60	70	80	90	100	110
C_1	0.857	1.00	1.03	1.16	1.21	1.34
$\frac{F_{EXX}}{70\,\text{ksi}}$	0.857	1.00	1.14	1.29	1.43	1.57
$\frac{C_1}{\left(\frac{F_{EXX}}{70\,\text{ksi}}\right)}$	1.00	1.00	0.90	0.90	0.85	0.85

The background of these reduction factors is ambiguous, and communication with members of past Manual Committees (Thornton, 2020; Tide, 2020) revealed no further information. It is believed that these reductions are recommended in the *Manual* because higher-strength welds are less ductile than E60 and E70 welds. Sufficient ductility of the critical weld segment within the weld group is required for load redistribution without rupture of the critical weld. The lower ductility of high-strength welds combined with the lack of research on eccentrically-loaded high-strength weld groups likely resulted in the 0.90 and 0.85 reduction factors recommended in the *Manual*. Similar factors are not required for designing higher strength welds using the AISC *Specification* or AWS D1.1.

Ductility of High-Strength Welds

To investigate the accuracy of the current electrode strength coefficients, the ductility of high-strength welds will be evaluated. Because transverse fillet welds have much less deformation capacity than longitudinal fillet welds, the ductility of transverse high-strength welds are the primary concern. In weld groups with both longitudinal and transverse welds, the longitudinal weld strength will be limited by the ductility of the transverse weld. According to Equation 2.9, the normalized rupture deformations for longitudinal and transverse welds are Δ_u/w = 0.17 and Δ_u/w = 0.056, respectively.

Figure 4.1 shows a plot of the weld metal tensile strength versus the normalized rupture deformation, Δ_u/w, of fillet welds. The data are from the 93 experimental tests on high-strength longitudinally- and transversely-loaded fillet welds by Collin and Johansson (2005), Bjork et al. (2012) and Sun et al. (2019). The red x data points represent transverse welds and the blue hollow circles represent longitudinal welds. The red and blue vertical dashed lines represent the AWS normalized rupture deformations for longitudinal and transverse welds, respectively. It can be observed that, for tensile strengths less than 120 ksi, the AWS equations provide conservative estimates of the normalized rupture deformations.

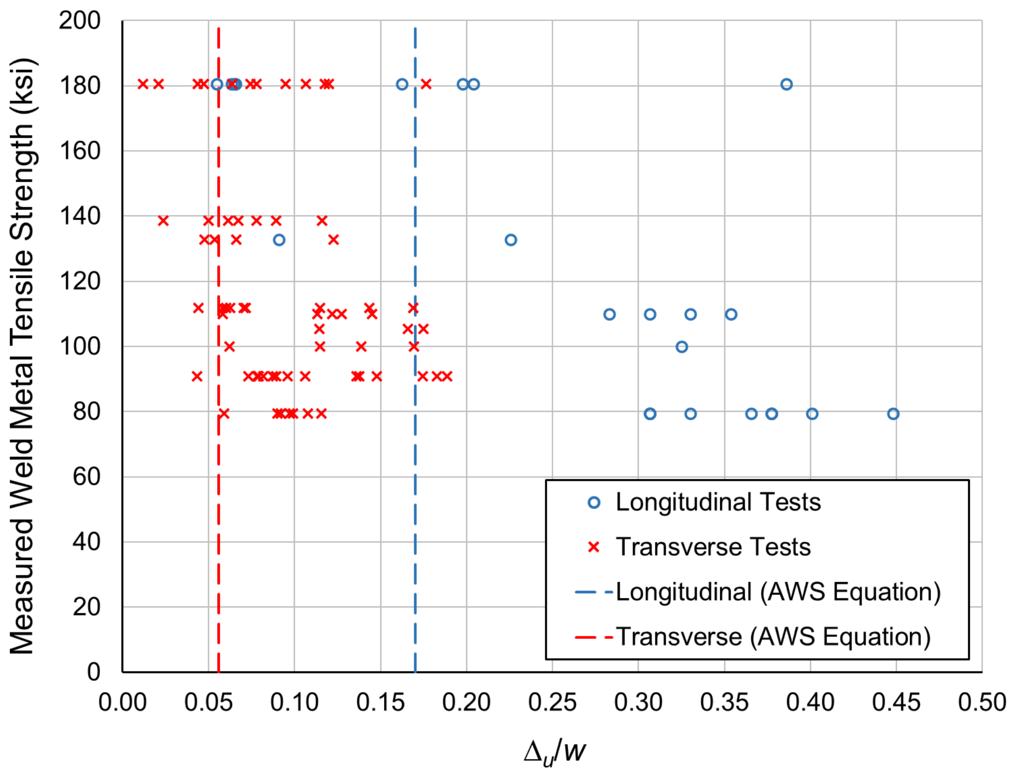

Fig. 4.1. Weld metal tensile strength versus normalized rupture deformation.

The average normalized deformations from this data are listed in Table 4.2. The data for 60 ksi welds from Butler and Kulak (1971) are also listed. A comparison of the rupture deformations shows that, for longitudinal welds, the rupture deformation of high-strength welds is 68% of that of 60 ksi welds; however, the rupture deformation of transverse welds is independent of strength. Because the shape of the load-deformation curves for high-strength welds is similar to that of 60 ksi welds, high-strength longitudinal welds in weld groups will reach a higher proportion of their rupture load compared to 60 ksi welds. The average transverse-to-longitudinal normalized deformation ratio for lap joints is 0.103/0.284 = 0.363, which is similar to the value calculated with AWS D1.1 Equation AWS-5: 0.056/0.17 = 0.33.

Table 4.2. Average normalized deformation.

Joint Type	**F_{EXX} = 60 ksi (Butler and Kulak, 1971)**	**High Strength Steel ($F_{EXX} \approx$ 80 to 180 ksi)**	
	Average Δ_u/w	**Number of specimens**	**Average Δ_u/w**
Longitudinal	0.420	26	0.284
Transverse (Total)	--	67	0.0966
Transverse lap-joints	0.104	36	0.103
Transverse T-joints	--	31	0.0889

Load-Deformation Curves

An evaluation of the load-deformation curves can provide further information on the behavior of high-strength fillet welds. The equations developed by Neis (1985) explicitly compensate for the effect of reduced weld metal ductility on the behavior.

The elongation requirements for carbon and low-alloy steels for SMAW, GMAW, FCAW and SAW welding processes from AWS A5.1 (AWS, 2012), A5.5 (AWS, 2014), A5.17 (AWS, 2019), A5.18 (AWS, 2017), A5.20 (AWS, 2015), A5.23 (AWS, 2011), A5.28 (AWS, 2020) and A5.29 (AWS, 1998) are summarized in Table 4.3. Generally, weld metals exceed these requirements. For example, the average elongation measurements for the all-weld-metal tensile tests in Table 3.7 of this report are approximately 40 to 50% higher that the required minimum values in Table 4.3. Therefore, the values in Table 4.4 are considered appropriate lower-bounds for analyses with the Neis (1985) equations. The strength ratios, σ_{tu}/F_{EXX}, in Table 4.4 are between 1.11 and 1.17. These values are similar to the constraint factor by Miazga and Kennedy (1989), which is 1.14 when θ = 90°.

Table 4.3. Minimum elongation for all-weld-metal tension tests, percent.

F_{EXX} ksi	Welding Process			
	SMAW	GMAW	FCAW	SAW
60	17 to 22	--	22	22
70	17 to 25	19 to 24	20 to 22	22
80	17 to 24	17 to 24	19	20
90	17 to 24	16 to 18	16 to 17	17
100	16 to 20	16	15 to 18	16
110	15 to 20	15	15	15
120	11 to 18	14 to 15	14	14

Table 4.4. Variables for Neis (1985) equations.

F_{EXX} ksi	ε_u	σ_{tu} ksi	σ_{tu}/F_{EXX}
70	0.22	81.6	1.17
80	0.19	91.4	1.14
90	0.17	101	1.12
100	0.16	112	1.12
110	0.15	122	1.11
120	0.14	133	1.11

The Butler and Kulak (1971) curves were scaled up from 60 ksi to 70 ksi and plotted in Figures 4.2 and 4.3 for longitudinal and transverse welds, respectively. These normalized load versus normalized deformation curves are for 70 ksi electrodes. The figures also include the AWS and Neis (1985) equations. The curves show that the Neis curves provide a close approximation of the shape of the empirical curves of Butler and Kulak, while also resulting in rupture loads that are similar to the AWS curves. Also, the Neis equations explicitly compensate for the effect of reduced weld metal ductility on the behavior. Therefore, the Neis curves will be used as a baseline to project the behavior of higher-strength weld metals.

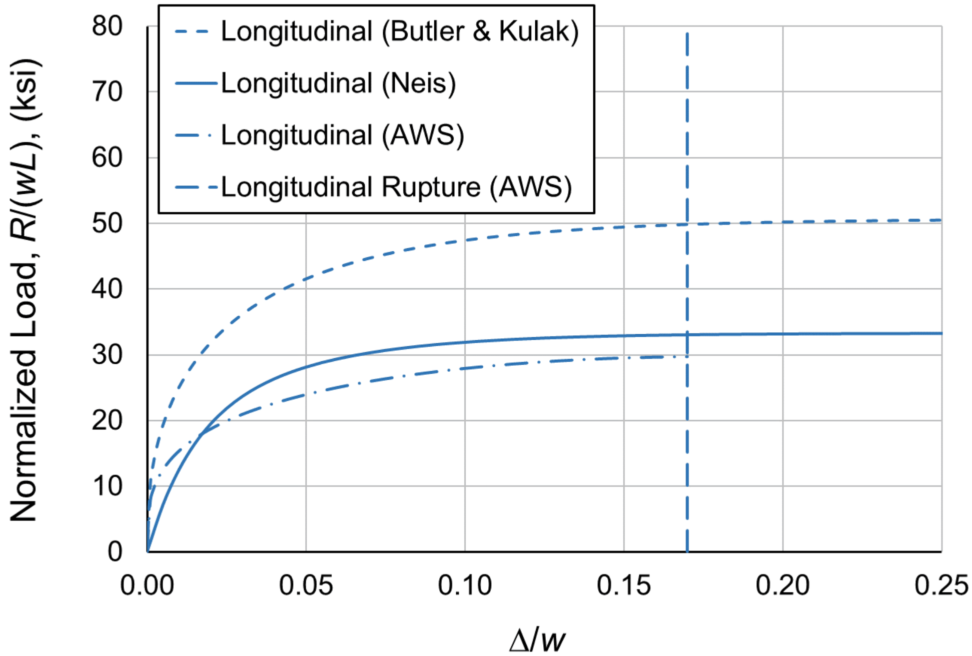

Fig. 4.2. Normalized load versus normalized deformation for 70 ksi longitudinal fillet welds.

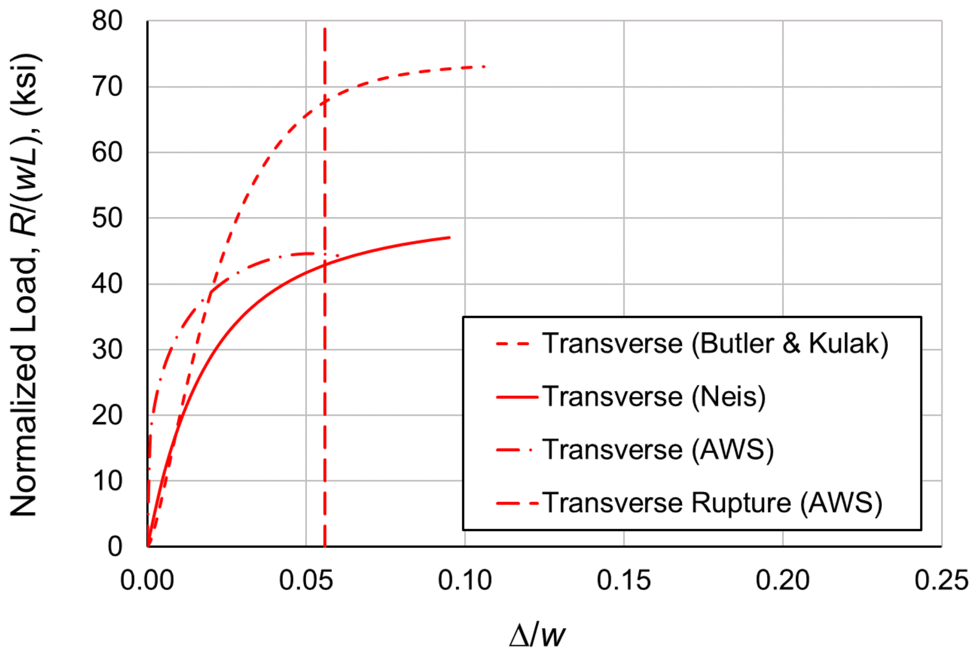

Fig. 4.3. Normalized load versus normalized deformation for 70 ksi transverse fillet welds.

For both the AWS and Neis (1985) equations, the normalized load versus normalized deformation curves are plotted in Figures 4.4 and 4.5 for 70 ksi and 120 ksi electrodes, respectively. Generally, the AWS curves are higher than the Neis curves for transverse welds and lower than the Neis curves for longitudinal welds. Because the AWS equations predict a similar, but more conservative, proportion of the longitudinal strength at the transverse rupture load, it can be concluded that the AWS curves are conservative for both 70 ksi and 120 ksi electrodes.

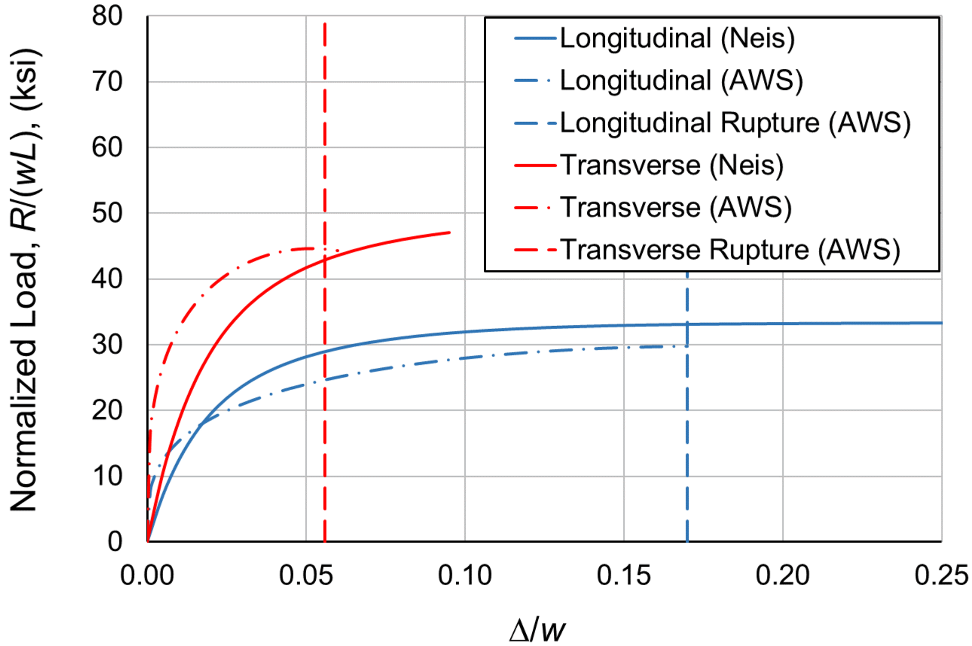

Fig. 4.4. Normalized load versus normalized deformation for 70 ksi fillet welds.

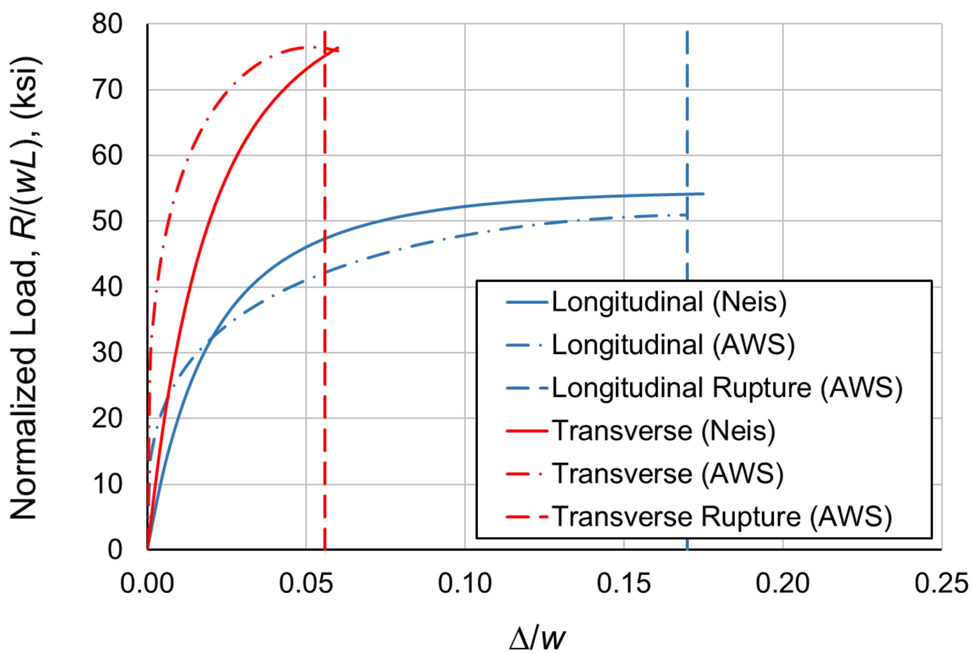

Fig. 4.5. Normalized load versus normalized deformation for 120 ksi fillet welds.

Recommendations

Based on the experimental rupture deformations and the load-deformation curves, it was concluded that the electrode strength coefficient, C_1 in *Manual* Table 8-3 can be based on the direct ratio, F_{EXX}/70 ksi, when $F_{EXX} \leq 120$ ksi.

EFFECT OF LENGTH ON THE STRENGTH OF FILLET WELDS

The literature review showed that, for relatively short welds, the weld length has no significant effect on the strength. Because longer welds in longitudinally-loaded fillet welded lap joints have an uneven stress distribution along the weld, differential axial deformation of the connected elements can cause a significant reduction in the weld strength.

Figure 4.6 shows the results of the longitudinally-loaded welds tested in this project, where the normalized rupture stresses, τ_u/σ_{uw}, are plotted against the normalized lengths, L_r/E_r. Fillet and PJP welds are represented by the hollow triangles and the x data points, respectively. The different colors represent the different weld metal strengths. For each data set, the clear trend is that the weld strength increases with length.

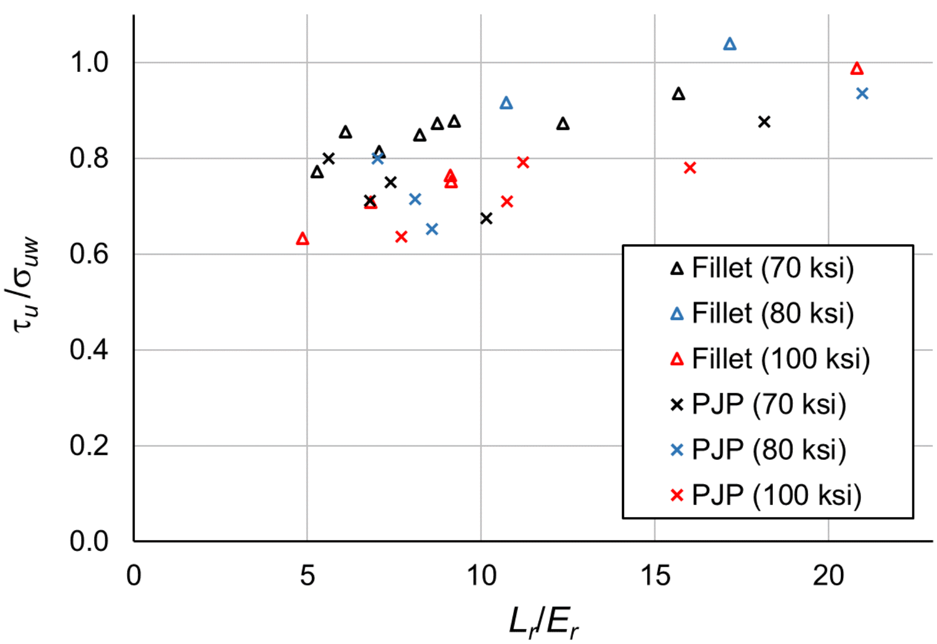

Fig. 4.6. Normalized rupture stress versus normalized length for longitudinal welds.

Although the experimental results reported in Figure 4.6 show that the weld strength increases with length, these results are applicable only to relatively short welds. For longer welds in longitudinally-loaded fillet welded lap joints, the differential axial deformation of the connected elements can cause a significant reduction in the weld strength. The stress concentrations will decrease when the welds begin to yield, but for long joints, the inelastic deformation will not be adequate to allow the weld to be uniformly stressed along its length. In this section, a reduction factor will be derived using the deformations defined by Equations 2.8 and 2.9.

At full strength, Equation 2.8 results in a deformation of 0.12w for longitudinally-loaded fillet welds. The rupture deformation according to Equation 2.9 is 0.17w. Therefore, the remaining deformation capacity of a fully-loaded weld is

$$\Delta_a = \Delta_u - \Delta_m = 0.17w - 0.12w = 0.05w \tag{4.1}$$

It is assumed that the weld segment at one end of the connecting element will deform $0.12w$ and the other end will deform $0.17w$, resulting in a relative displacement of $0.05w$. For uniform loading along the weld, the relative displacement of the connection elements between the weld ends is

$$\Delta = \frac{Pl}{2E_c}\left(\frac{1}{A_1} - \frac{1}{A_2}\right) \tag{4.2}$$

where

A_1 = sectional area of the smallest connecting element, in.^{2}
A_2 = sectional area of the largest connecting element, in.^{2}
E_c = modulus of elasticity of the connecting elements
P = axial force, kips

For double-lap joints, the total area of the outer plates is used for A_1 or A_2.

Setting Δ equal to Δ_a and solving for w results in the critical fillet weld size

$$w = \frac{10Pl}{E_c}\left(\frac{1}{A_1} - \frac{1}{A_2}\right) \tag{4.3}$$

Because the connecting elements are assumed to be elastic, the minimum area is $A_1 = P/F_y$. Substituting this into Equation 4.3 and solving for the critical length ratio, l/w, as a function of the area ratio, A_2/A_1, results in Equation 4.4.

$$\frac{l}{w} = \frac{E_c}{10F_y\left(1 - \frac{1}{A_2/A_1}\right)} \tag{4.4}$$

The critical length ratio, can be expressed with Equation 4.5, where k_2 is dependent solely on the area ratio as shown in Table 4.5.

$$\frac{l}{w} = k_2\frac{E_c}{F_y} \tag{4.5}$$

Table 4.5. Length coefficients for various area ratios.	
A_2/A_1	**k_2**
1.5	0.30
2.0	0.20
2.5	0.17
3.0	0.15
3.5	0.14
4.0	0.13
∞	0.10

A reasonable worst-case area ratio is 2.5, resulting in the following recommended revisions for AISC *Specification* Section J2.2b(d):

When $F_{EXX} \leq 120$ ksi, the effective length of fillet welds is

(1) For end-loaded fillet welds with a length up to $0.17E_cw/F_y$, it is permitted to take the effective length equal to the actual length.

(2) When the length of the end-loaded fillet weld exceeds $0.17E_cw/F_y$, the effective length shall be determined by multiplying the actual length by the reduction factor, β, determined as:

$$\beta = 1.2 - \frac{l}{w}\frac{F_y}{E_c} \tag{4.6}$$

where
l = length of a single weld in the loading direction, in.
w = weld leg size, in.

(3) When the length of the weld exceeds $0.51E_cw/F_y$, the effective length shall be taken as $0.31E_cw/F_y$

FUSION ZONE STRENGTH

Specimen Fusion Zone Ruptures

All of the longitudinal fillet weld specimens ruptured in the weld metal. This was expected because all of these specimens had σ_{ub}/σ_{uw} ratios between 0.940 and 1.17.

Generally, the longitudinal PJP weld specimens, which had σ_{ub}/σ_{uw} ratios between 0.770 and 1.17, ruptured in the weld metal. Only Weld 4 in Specimen PL4 ruptured at the fusion zone of the outside plate as shown in Figures 4.7a and b. The measured tensile stresses were 70.5 ksi for the outer plates and 75.8 ksi for the weld metal. However, the primary cause of the fusion zone rupture was the weld geometry. The average reinforcement of this weld, shown in Figure 4.7c, was 0.049 in. according to the pre-test measurements. This reinforcement created a condition where, based on digital measurements from the etched section, the shortest distance from the root to the face was along the fusion zone. In this case, the rupture strength was unaffected by the change in rupture location.

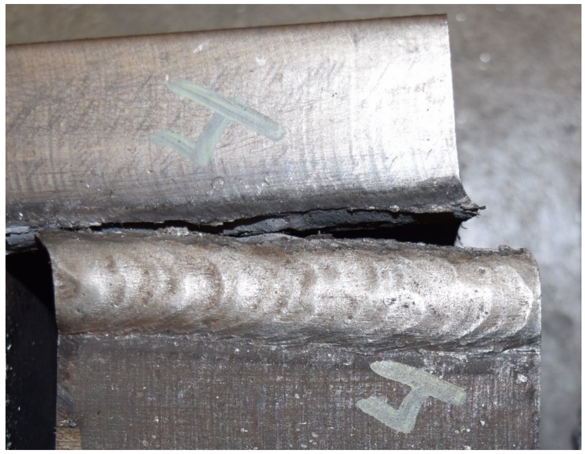

a. Ruptured specimen.

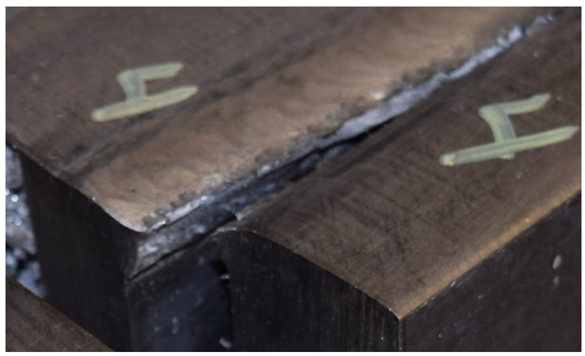

b. Ruptured specimen.

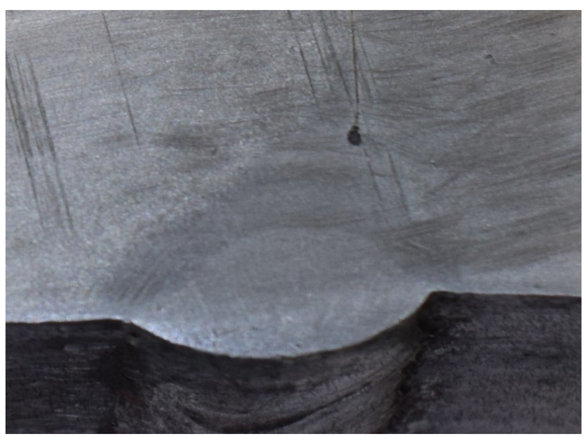

c. Etched section.

Fig. 4.7. Specimen PL4 Weld 4.

In all but four specimens, the transverse fillet welds ruptured completely in the weld metal. These specimens had σ_{ub}/σ_{uw} ratios between 0.719 and 1.31. Specimen PT1 had a mixed rupture surface in both the weld and fusion zone as shown in Figure 4.8. The measured tensile stresses were 72.0 ksi for the plates and 75.8 ksi for the weld metal. Specimen PT7 ruptured at the fusion zone of the non-prepared plate as shown in Figure 4.9. This was unexpected because the specimen had undermatching weld metal with measured tensile stresses of 94.0 ksi for the plates and 75.8 ksi for the weld metal. For Specimen PT14, the bottom weld ruptured in the weld metal; however, the top rupture surface primarily followed the fusion zone in the non-prepared plate as shown in Figure 4.10. This specimen had overmatching weld metal with measured tensile stresses of 72.0 ksi for the plates and 100 ksi for the weld metal. Specimen PT16 ruptured at the fusion zone in the non-prepared plate as shown in Figure 4.11. The measured tensile stresses were 94.0 ksi for the plates and 100 ksi for the weld metal.

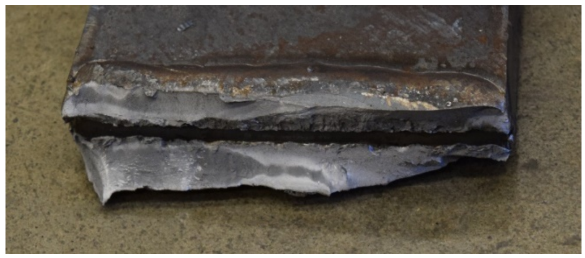

Fig. 4.8. Specimen PT1.

Fig. 4.9. Specimen PT7.

Fig. 4.10. Specimen PT14.

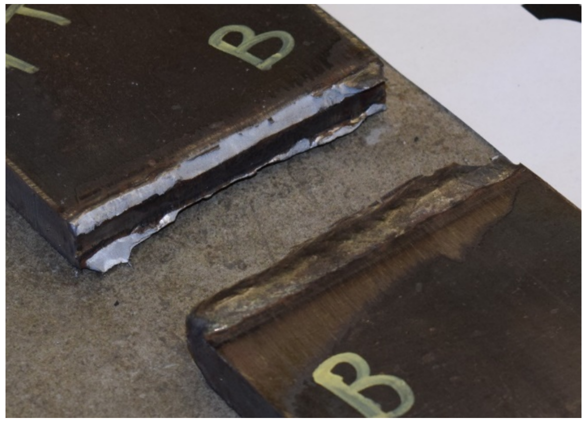

Fig. 4.11. Specimen PT16.

\

Six of the transverse fillet weld specimens ruptured partially of completely in the fusion zone. Generally, for the specimens that ruptured in the weld metal, the rupture angles, γ, were between 50° and 80°. The specimens that ruptured at the fusion zone had rupture angles greater than 80°. These specimens had σ_{ub}/σ_{uw} ratios between 0.883 and 1.23. For Specimen FT1, the fusion zone at the bottom weld ruptured as shown in Figure 4.12. For Specimen FT2, the fusion zone at the top weld ruptured as shown in Figure 4.13. For these Specimens, the measured tensile stresses were 77.0 ksi for the plates and 75.8 ksi for the weld metal. As shown in Figure 4.14, fusion zone rupture in the bottom weld occurred in Specimen FT4, which had measured tensile stresses of 70.5 ksi for the plate and 75.8 ksi for the weld metal. Figure 4.15 shows the fusion zone rupture in the top weld and partially at the bottom weld of Specimen FT8. For this specimen, the measured tensile stresses were 66.9 ksi for the plate and 75.8 ksi for the weld metal. A fusion zone rupture also occurred in the bottom weld of Specimen FT9, which had measured tensile stresses of 66.9 ksi for the plate and 75.8 ksi for the weld metal. The fusion zones of both the top and bottom welds of Specimen FT11 ruptured. The measured tensile stresses were 99.0 ksi for the plate and 80.8 ksi for the weld metal.

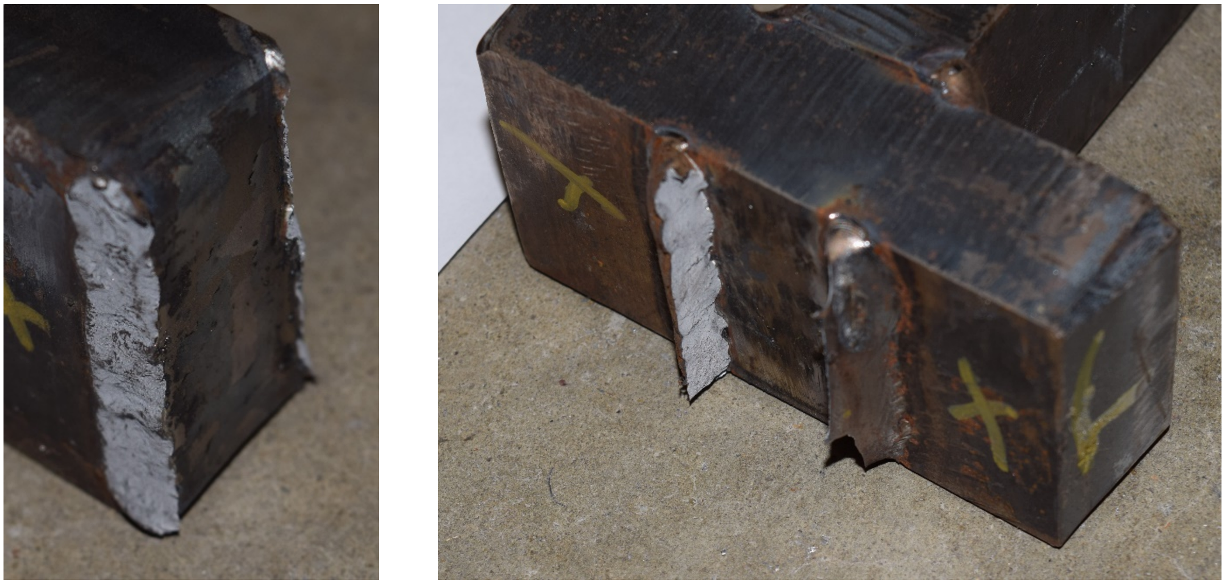

Fig. 4.12. Specimen FT1.

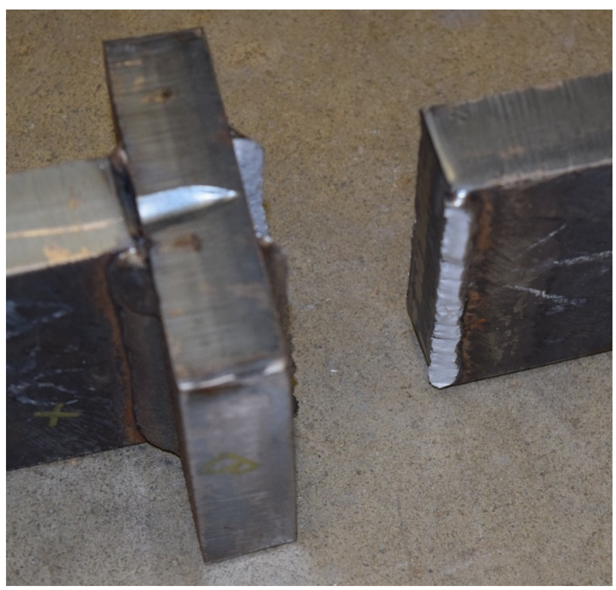

Fig. 4.13. Specimen FT2.

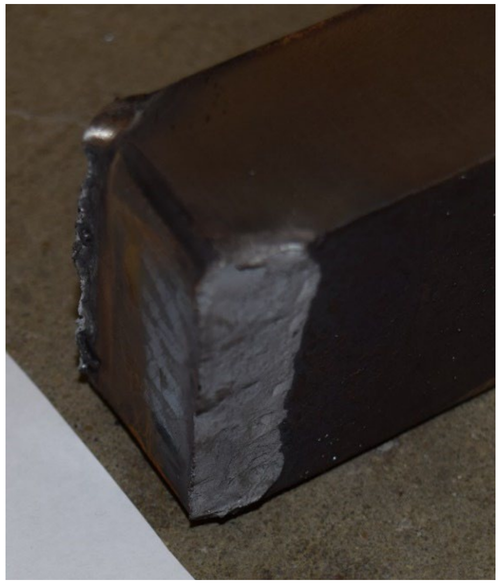

Fig. 4.14. Specimen FT4.

Fig. 4.15. Specimen FT8.

Design Methods

Due to intermixing of the weld metal with the base metal, several researchers have suggested using various proportions of the base metal strength, F_u, and the weld metal strength, F_{EXX}, in the design of welded joints. In a previous section of this report, the experimental results were compared to the strengths calculated with the measured weld metal strength, σ_{uw}. In this section, the experimental results for the specimen groups that ruptured at or near the fusion zone are compared to the strengths calculated with both the average and minimum of the measured weld metal strength and the measured base metal strength, σ_{ub}. σ_{ua} is the average of σ_{uw} and σ_{ub}. σ_{um} is the minimum of σ_{uw} and σ_{ub}. For the specimens that were fabricated from plates with different tensile strengths, the tensile strength of the plate that was the most likely to rupture in the fusion zone was used in the calculations.

Tables 4.6a and 4.6b show the average values for the P_e/P_n, P_e/P_c and f_r/σ_u ratios for the longitudinal PJP weld specimens using σ_{ua} and σ_{um}, respectively. P_c was calculated with an effective throat equal to the groove depth with no consideration of the reinforcement. Because the inner and outer plates had different measured tensile stresses, the calculations were based on σ_{ub} of the outer plates.

Table 4.6a. Strength ratios for longitudinal PJP welds using σ_{ua}.

F_{EXX} ksi	P_e / P_n		P_e / P_c		f_r / σ_{ua}	
	Average	Standard Deviation	Average	Standard Deviation	Average	Standard Deviation
70	1.62	0.168	1.38	0.125	0.775	0.0751
80	1.28	0.385	1.17	0.319	0.762	0.0989
100	1.44	0.216	1.34	0.171	0.793	0.0267
All Specimens	1.46	0.300	1.30	0.235	0.777	0.0744

Table 4.6b. Strength ratios for longitudinal PJP welds using σ_{um}.

F_{EXX} ksi	P_e / P_n		P_e / P_c		f_r / σ_{um}	
	Average	Standard Deviation	Average	Standard Deviation	Average	Standard Deviation
70	1.78	0.185	1.42	0.118	0.793	0.0797
80	1.45	0.518	1.24	0.317	0.812	0.1020
100	1.79	0.439	1.49	0.268	0.875	0.0398
All Specimens	1.68	0.424	1.38	0.262	0.824	0.0856

Tables 4.7a and 4.7b show the average values for the P_e/P_n, P_e/P_c and f_r/σ_u ratios for the transverse PJP weld specimens using σ_{ua} and σ_{um}, respectively. P_c was calculated with an effective throat equal to the groove depth with no consideration of the reinforcement.

Table 4.7a. Strength ratios for transverse PJP welds using σ_{ua}.

F_{EXX} ksi	P_e / P_n		P_e / P_c		f_r / σ_{ua}	
	Average	Standard Deviation	Average	Standard Deviation	Average	Standard Deviation
70	2.44	0.385	2.11	0.334	1.26	0.153
80	1.86	0.274	1.69	0.223	1.56	0.209
100	1.85	0.212	1.71	0.123	1.27	0.125
All Specimens	2.13	0.432	1.89	0.372	1.35	0.213

Table 4.7b. Strength ratios for transverse PJP welds using σ_{um}.						
F_{EXX} ksi	P_e / P_n		P_e / P_c		f_r /σ_{um}	
	Average	Standard Deviation	Average	Standard Deviation	Average	Standard Deviation
70	2.68	0.421	2.22	0.325	1.33	0.164
80	2.09	0.389	1.82	0.245	1.67	0.216
100	2.30	0.463	1.90	0.333	1.41	0.189
All Specimens	2.42	0.495	2.03	0.358	1.45	0.240

Tables 4.8a and 4.8b show the average values for the P_e/P_n, P_e/P_c and f_r/σ_u ratios for the transverse fillet weld specimens using σ_{ua} and σ_{um}, respectively. Because the transverse and longitudinal plates had different measured tensile stresses, the calculations were based on σ_{ub} of the longitudinal plates.

Table 4.8a. Strength ratios for transverse fillet welds using σ_{ua}.						
F_{EXX} ksi	P_e / P_n		P_e / P_c		f_r /σ_{ua}	
	Average	Standard Deviation	Average	Standard Deviation	Average	Standard Deviation
70	2.01	0.334	1.55	0.144	0.916	0.114
80	1.50	0.201	1.30	0.0912	0.895	0.0299
100	1.35	0.121	1.10	0.0724	0.887	0.0772
All Specimens	1.71	0.404	1.36	0.234	0.903	0.0938

Table 4.8b. Strength ratios for transverse fillet welds using σ_{um}.						
F_{EXX} ksi	P_e / P_n		P_e / P_c		f_r /σ_{um}	
	Average	Standard Deviation	Average	Standard Deviation	Average	Standard Deviation
70	2.22	0.369	1.60	0.125	0.951	0.133
80	1.53	0.189	1.42	0.103	0.980	0.0418
100	1.49	0.149	1.14	0.0725	0.920	0.0776
All Specimens	1.86	0.459	1.42	0.234	0.946	0.107

Discussion

For longitudinal PJP welds, the f_r/σ_{ua} ratio for all specimens in Table 4.6a is 0.777 with a standard deviation of 0.0744. This indicates a more accurate solution compared to the 0.756 ratio in Table 3.10, which has a standard deviation of 0.0831. This is caused primarily by the strength of the specimens with overmatching weld metal.

Similar conclusions can be drawn by comparing the ratios in Table 4.7a to those in Table 3.11 for transverse PJP welds. In this case, the values in Table 4.7 show a more uniform level of conservatism, which is caused by the reduction in the calculated strength of the specimens with overmatching weld metal.

Because the fillet welded specimens were fabricated with more closely matched weld metals, comparisons between the strength ratios of Tables 4.8 and 3.9 reveal only slight differences. However, both the P_e/P_c and f_r/σ_{ua} ratios are more uniform, with lower standard deviations.

SHEAR-TO-TENSILE STRENGTH RATIO

Table 4.9 lists the average shear-to-tensile strength ratios, τ_u/σ_{uw}, for each weld strength tested in this report. These values include the results for all longitudinally-loaded fillet and PJP weld specimens. Generally, these FCAW values are between the SMAW and GMAW values in Table 2.3, which were calculated with the equations developed by Krumpen and Jordan (1984). The data also agrees reasonably-well with the statistical analysis by Lesik and Kennedy (1988) and Lesik and Kennedy (1990), who calculated an average shear-to-tensile strength ratio, τ_u/σ_{uw}, of 0.749 with a coefficient of variation of 0.121.

Table 4.9. Shear-to-tensile strength ratios.

F_{EXX} ksi	τ_u/σ_{uw}	
	Average	Standard Deviation
70	0.820	0.0725
80	0.843	0.134
100	0.752	0.0996
All Specimens	0.803	0.104

Both the current experimental results and the results discussed in the literature review show that a reasonable design value for F_{nw}/F_{EXX} is 0.70. Although a reliability analysis is required before implementing the increase from 0.60 to 0.70, the current and proposed test-to-predicted ratios, P_e/P_c, are shown in Tables 4.10 and 4.11 for longitudinal fillet welds and longitudinal PJP welds, respectively. Because the effective throat is along the fusion zone of the PJP welds, Table 4.12 provides the strength ratios calculated with $\tau_u/\sigma_{ua} = 0.70$ and $\tau_u/\sigma_{um} = 0.70$, where σ_{ua} and σ_{um} are defined in the section on fusion zone strength.

Table 4.10. Strength ratios for longitudinal fillet welds.

F_{EXX} ksi	P_e / P_c (τ_u/σ_{uw} = 0.60)		P_e / P_c (τ_u/σ_{uw} = 0.70)	
	Average	Standard Deviation	Average	Standard Deviation
70	1.66	0.160	1.42	0.137
80	1.83	0.112	1.57	0.0962
100	1.24	0.0906	1.06	0.0777
All Specimens	1.54	0.260	1.32	0.222

Table 4.11. Strength ratios for longitudinal PJP welds.

F_{EXX} ksi	P_e / P_c (τ_u/σ_{uw} = 0.60)		P_e / P_c (τ_u/σ_{uw} = 0.70)	
	Average	Standard Deviation	Average	Standard Deviation
70	1.36	0.142	1.17	0.121
80	1.17	0.274	1.01	0.235
100	1.23	0.122	1.05	0.105
All Specimens	1.26	0.205	1.08	0.176

Table 4.12. Strength ratios for longitudinal PJP welds.				
F_{EXX} ksi	**P_e / P_c (τ_u/σ_{ua} = 0.70)**		**P_e / P_c (τ_u/σ_{um} = 0.70)**	
	Average	**Standard Deviation**	**Average**	**Standard Deviation**
70	1.19	0.107	1.21	0.101
80	1.00	0.273	1.06	0.272
100	1.15	0.147	1.28	0.229
All Specimens	1.12	0.201	1.19	0.225

DIRECTIONAL STRENGTH INCREASE FOR FILLET WELDS

An increase in the load angle, θ, for fillet welds results in a nonlinear strength increase and a decrease in ductility. AISC *Specification* Equation J2-5 is plotted for θ = 0°, 30°, 60° and 90° in Figure 4.16. Figure 4.17 shows an equivalent interaction curve for the AISC nominal weld strength based on vector components at θ = 0° and θ = 90°. The curve shows that if a weld is loaded to its rupture strength in longitudinal shear, it can sustain an additional load in the transverse direction of up to 45% of the transverse shear strength without rupture. This is supported by the experimental data reported by Biggs et al. (1981).

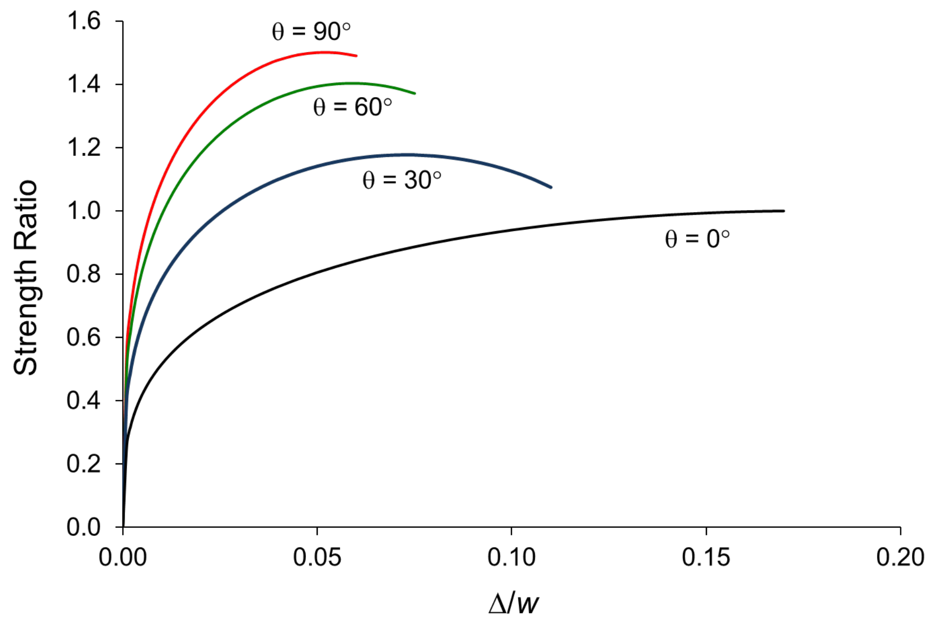

Fig. 4.16. AISC strength ratio versus normalized deformation for fillet welds.

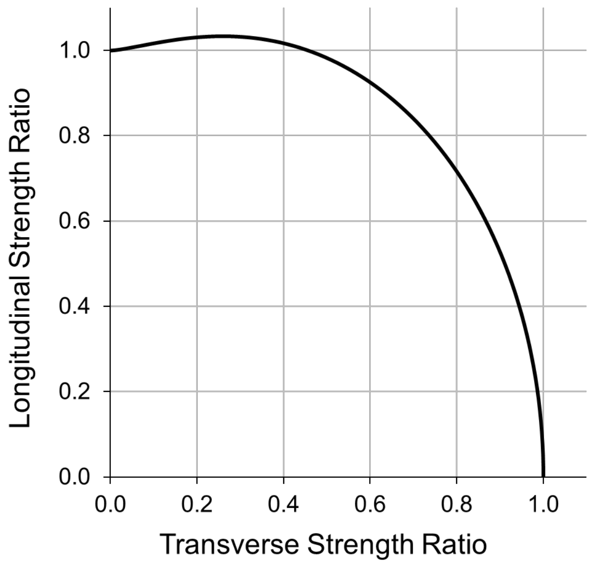

Fig. 4.17. Interaction between longitudinal and transverse loading.

Table 2.4 summarizes the transverse-to-longitudinal strength ratios found in the literature. The experimental values are between 1.12 and 1.70. The theoretical ratios range from 1.30 to 1.48, with a ratio of 1.50 for the semi-empirical equation developed by Miazga and Kennedy (1989). For the various specifications reviewed, the ratios are between 1.13 and 1.50. The P_e/P_c ratios in Tables 3.8 and 3.9 indicate that, for the experimental results in this report, the average transverse-to-longitudinal strength ratio is (1.34)(1.50)/(1.54) = 1.30.

Although the plastic flow strength has been used for some limit analysis models, most of the theoretical models for fillet weld strength were developed using failure theories that were intended to predict first yield (maximum principal stress, maximum shear stress, von-Mises effective stress). Clearly, there are difficulties in attempting to predict rupture with these failure criteria.

The AISC *Specification* defines the effective throat as the shortest distance from the root to the face of the diagrammatic weld. However, theoretical calculations and measurements of experimental rupture plane orientations have shown that the rupture angle, α, decreases as the loading angle, θ, increases. The experimental rupture angles were approximately 45º when $\theta = 0°$ and 22.5º when $\theta = 90°$. This increases the rupture plane width from $0.707w$ when $\alpha = 45°$ to $0.765w$ when $\alpha = 22.5°$. Also, the state of stress at the rupture plane changes from simple shear when $\theta = 0°$ to combined shear and tension when $\theta = 90°$.

In Appendix H, three different failure theories were considered in the derivations for the strength of skewed fillet welds: von-Mises, maximum normal stress and maximum shear stress (Tresca). For each model, the surface where maximum stresses are generated was determined for both longitudinal and transverse loading. The location of maximum stress is not necessarily located in the plane of minimum throat. It was determined that the rupture load is highly-dependent on the perpendicular force, F, which is defined as $a \times P$, as shown in Figure 4.18. This strength dependence on a may explain the discrepancies in the experimental research and the reason lap joints generally perform better than T-joints (Ng et al., 2002).

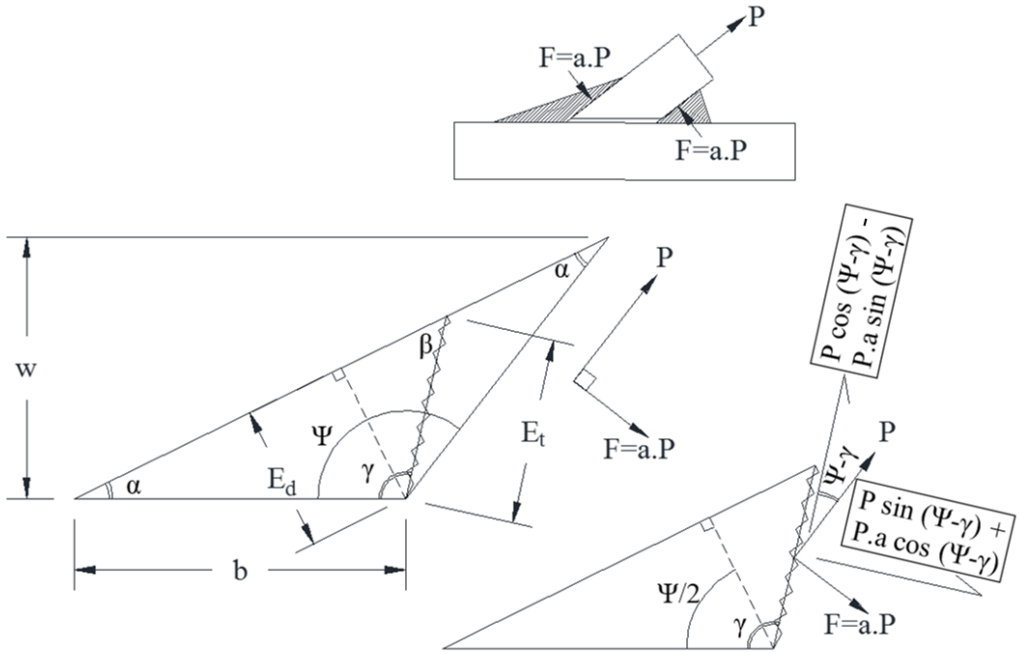

Fig. 4.18. Skewed T-Joint with double fillet welds.

The Tresca criterion was determined to be the most accurate failure theory to predict the rupture strength of welds. The directional strength increase factor, k_{ds}, was plotted using the theoretical equation that was developed using the Tresca criterion. Equation 4.7 was developed by curve fitting these data points. Both the theoretical data points and the curve-fit equation are plotted in Figure 4.19.

$$k_{ds} = 1.17 + 0.508a - 0.266a^2 \tag{4.7}$$

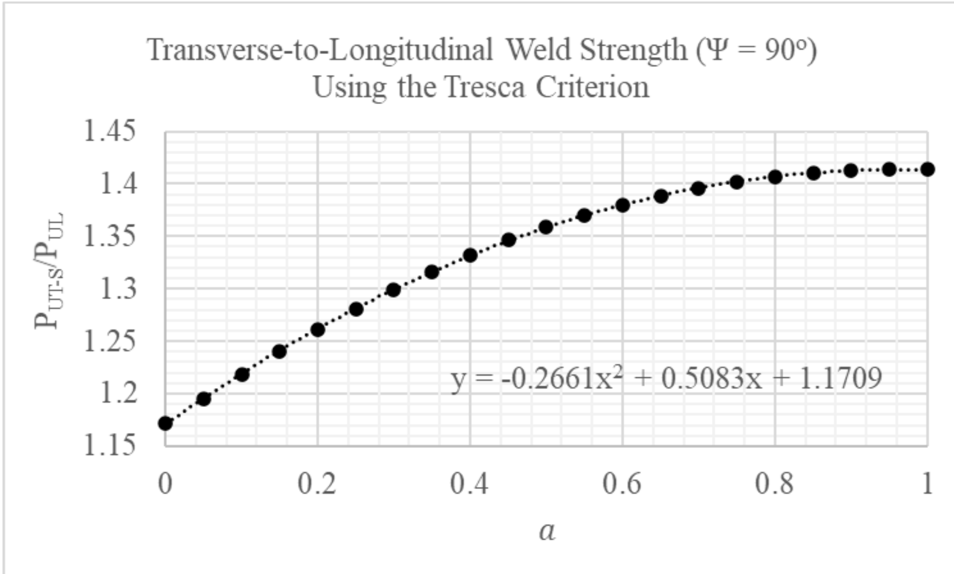

Fig. 4.19. Transverse-to-longitudinal strength ratio using the Tresca criterion.

Based on experimental results for lap joints, Miazga and Kennedy (1989) showed that a constant value of 0.345 is applicable for θ between 45º and 90º. Lu and Dong (2020) showed that the theoretical value for a is approximately 0.3. Gallow (2019) determined that a = 0.21 provided the most accurate solution compared to his experimental tests on lap joints. Table 4.13 shows the recommended values of a with the corresponding values for k_{ds}, which were calculated with Equation 4.7.

Table 4.13. k_{ds} from Equation 4.7.

a	k_{ds}
0	1.17
0.21	1.27
0.3	1.30
0.345	1.31
1	1.41

For k_{ds} = 1.30, the directional strength increase can be calculated with Equation 4.8. Equation 4.9 is proposed for calculating the nominal weld metal stress for fillet welds, F_{nw}.

$$k_{ds} = 1.0 + 0.30 \sin^{1.5} \theta \tag{4.8}$$

$$F_{nw} = 0.7 F_{EXX} \left(1.0 + 0.30 \sin^{1.5} \theta\right) \tag{4.9}$$

Table 4.14 shows the average values of the P_e/P_c ratios for the transverse fillet weld specimens using Equation 4.9. To consider the base metal strength, ratios are shown for $F_{nw} = 0.910\sigma_{uw}$ as well as $F_{nw} = 0.910\sigma_{ua}$ and $F_{nw} = 0.910\sigma_{um}$. For transverse welds, Equation 4.9 produces similar results compared to AISC *Specification* Equation J2-5; therefore, the values in Table 4.14 are similar to those in Tables 3.9, 4.8a and 4.8b.

Table 4.14. Strength ratios for transverse fillet welds using Equation 4.9.						
F_{EXX} ksi	P_e / P_c (F_{nw} = 0.910σ_{uw})		P_e / P_c (F_{nw} = 0.910σ_{ua})		P_e / P_c (F_{nw} = 0.910σ_{um})	
	Average	Standard Deviation	Average	Standard Deviation	Average	Standard Deviation
70	1.49	0.173	1.53	0.143	1.59	0.124
80	1.41	0.102	1.29	0.0902	1.41	0.102
100	1.05	0.0722	1.08	0.0716	1.12	0.0717
All Specimens	1.33	0.243	1.34	0.232	1.40	0.232

The average P_e/P_c ratio in Table 4.14 for $F_{nw} = 0.910\sigma_{ua}$ is 1.34 with a standard deviation of 0.232. These values are similar to those in Table 4.10 for longitudinal fillet welds with $\tau_u/\sigma_{uw} = 0.70$, which had an average of 1.32 and a standard deviation of 0.222. Therefore, it is concluded that Equation 4.9 provides a uniform reliability level for all fillet weld specimens documented in this report.

Similar to the proposals by Van der Eb (Faltus, 1986) and Collin and Johansson (2005), a design equation for fillet welds was developed by modifying von Mises criterion according to Equation 4.10. This equation results in $k_{ds} = 1.29$ when $\theta = 90°$.

$$\sqrt{0.8\sigma^2 + 1.6\tau_T^2 + 2\tau_L^2} \leq F_{EXX} \tag{4.10}$$

STRENGTH OF TRANSVERSE PJP WELDS

In the AISC *Specification*, the transverse-to-longitudinal strength ratio for PJP welds is 1.00. Both the Eurocode 3 (CEN, 2005) and Architectural Institute of Japan (AIJ, 2012) equations result in a transverse-to-longitudinal strength ratio of $\sqrt{3} = 1.73$. Because the strength ratios, P_e/P_c, in Table 3.11 are over-conservative, this section will study the effect of designing transverse PJP welds with $F_{nw} = F_{EXX}$ in lieu of the AISC *Specification* value of $F_{nw} = 0.60F_{EXX}$. If $0.6\sigma_{uw}$ is replaced by $1.0\sigma_{uw}$, the P_e/P_c ratios in Table 4.15 replace the values shown in Table 3.11. In both cases, P_c was calculated with an effective throat equal to the groove depth with no consideration of the reinforcement. Because the effective throat is along the fusion zone, the strength ratios calculated with σ_{ua} and σ_{um} are also listed in Table 4.15. The most accurate results are for the strengths calculated with $F_{nw} = 1.0\sigma_{ua}$.

Table 4.15. Strength ratios for transverse PJP welds using $F_{nw} = 1.0\sigma_u$.

F_{EXX} ksi	P_e / P_c ($F_{nw} = 1.00\sigma_{uw}$)		P_e / P_c ($F_{nw} = 1.00\sigma_{ua}$)		P_e / P_c ($F_{nw} = 1.00\sigma_{um}$)	
	Average	Standard Deviation	Average	Standard Deviation	Average	Standard Deviation
70	1.29	0.201	1.27	0.193	1.33	0.195
80	1.02	0.134	1.01	0.146	1.09	0.147
100	0.94	0.0741	1.02	0.114	1.14	0.200
All Specimens	1.13	0.223	1.14	0.206	1.22	0.215

OTHER COMMENTS

PJP Weld Geometry
The etched PJP specimens showed that, generally, the welds had a significant unfused distance at the root. This is shown in Figures 4.20 and 4.21 for Specimens PL2 and PL15, respectively. These distances, measured digitally, were typically between 1⁄16 and 3⁄16 in. for the etched PJP specimens.

Longitudinal PJP Specimens PL13, PL14 and PL15 were fabricated with T-joints and the remaining specimens were fabricated with corner joints. For the T-joints, the average measured rupture surface width, E_r, was 1.32 times the depth of preparation, S. This was much larger than for the corner joints, where E_r averaged 0.970 times S. However, the results indicated that the normalized rupture stress calculated with the measured rupture surface area, f_r / σ_{uw}, was similar for all specimens. Therefore, the T-joints were significantly stronger than the corner joints due to the larger effective throat dimensions. The larger effective throats were caused by the differences in reinforcement geometries for each joint type. The average reinforcement was $0.675S$ and $0.121S$ for the T-joints and corner joints, respectively. The reinforcement geometries for corner and T-joints are shown in Figures 4.20 and 4.21, respectively.

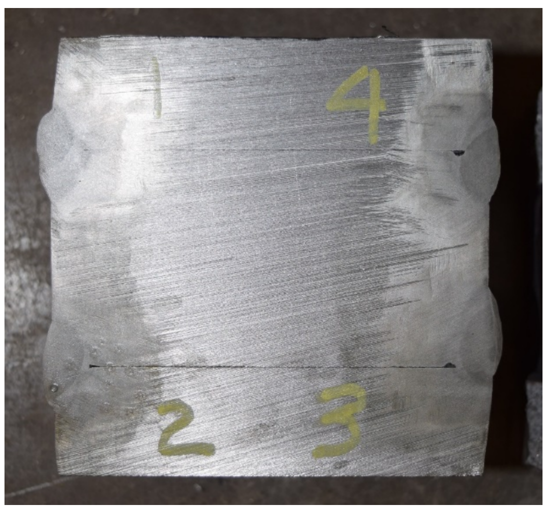

Fig. 4.20. Specimen PL2 (etched).

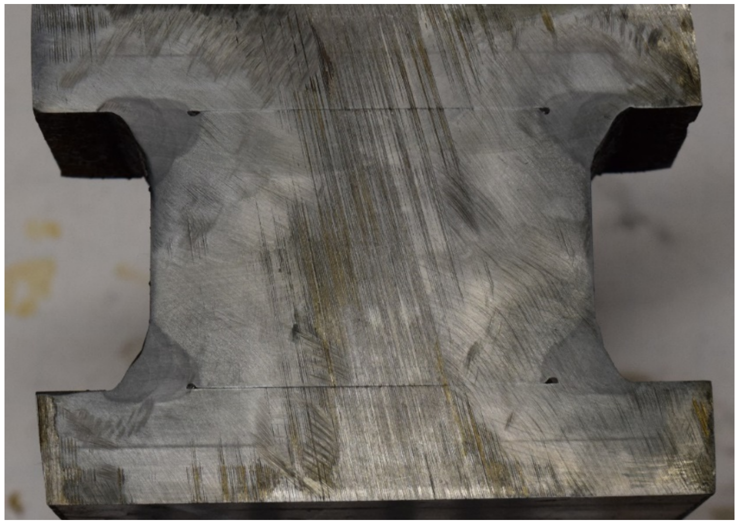

Fig. 4.21. Specimen PL15 (etched).

The rupture surface widths for the transverse PJP specimens with F_{EXX} = 70 ksi were as expected, with an average value of 1.01 times the depth of preparation, *S*. However, for the specimens with F_{EXX} = 80 and 100 ksi, the rupture surface widths averaged only 0.733*S*. This difference was primarily caused by differences in the reinforcement dimensions, which averaged 0.217*S* for the 70 ksi specimens and only 0.0599*S* for the 80 and 100 ksi specimens.

Fillet Weld Geometry

For the fillet weld specimens, the etched sections revealed the expected weld profiles, including appropriate penetration as shown for Specimen FL5 in Figure 4.22. Because the longitudinal specimens had approximately 45° rupture angles, which coincides with the effective throat, the penetration depth can be estimated by subtracting the effective throat based on the measured weld dimensions from the measured rupture surface width. Based on this, the penetration depth varied from approximately – 1⁄16 in. to + 1⁄16 in., with average values between – 0.0332 in. and + 0.0621 in. for each specimen. Most of the negative values were for the 100 ksi specimens and the larger positive values were for the 70 ksi specimens.

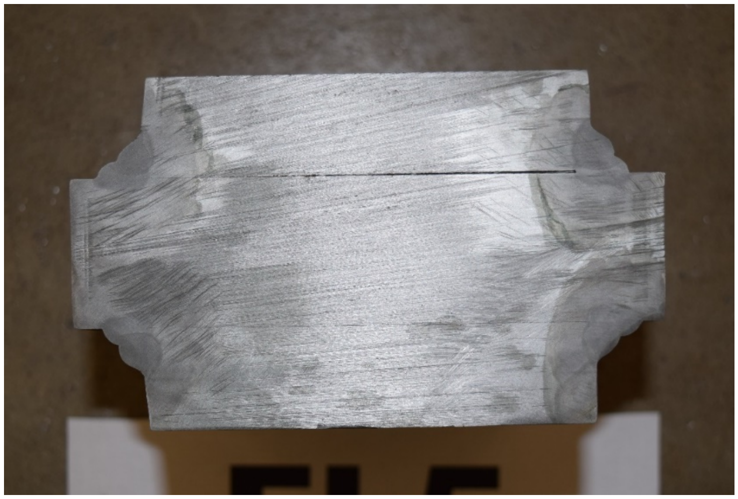

Fig. 4.22. Specimen FL5 (etched).

Generally, the measured fillet weld leg dimensions, w_m, were larger than the specified weld sizes, w. For the 33 fillet weld specimens, the measured-to-specified leg ratio, $\rho_G = w_m/w$, averaged 1.16 with a coefficient of variation (COV) of 0.101. However, as with the previous research by Li et al. (2007), ρ_G decreases with increasing weld size according to Table 4.16. ρ_G was also calculated with the effective throat ratio, based on the measured unequal leg dimensions, with almost identical results.

Table 4.16. Fillet weld measured-to-specified leg ratios.

w	$\rho_G = w_m/w$	COV
¼	1.23	0.0802
⅜	1.19	0.0581
½	1.02	0.0542
All Specimens	1.16	0.101

Design of Skewed PJP Welds

Similar to the proposals by Van der Eb (Faltus, 1986) and Collin and Johansson (2005), a design equation for skewed PJP welds was developed by modifying von Mises criterion according to Equation 4.11. Equation 4.11 is conservative compared to the experimental rupture stresses of the skewed PJP specimens, with an average experimental-to-calculated ratio of 1.31 and a standard deviation of 0.0728.

$$\sqrt{\sigma^2 + 2\tau^2} \leq F_w \qquad (4.11)$$

where

F_u = specified minimum tensile strength of the base metal, ksi

F_w = F_{EXX} for joints with matching and undermatching weld metal, ksi

= $(F_{EXX} + F_u)/2$ for joints with overmatching weld metal, ksi

σ = normal stress perpendicular to the plane of the throat, ksi.

τ = shear stress in the plane of the throat, ksi.

CHAPTER 5
SUMMARY AND CONCLUSIONS

SUMMARY

This report addressed several design issues related to the strength of fillet welds and PJP welds. To meet the objectives of this research project, the available literature was reviewed, failure theories were used to derive theoretical equations, and a total of 71 experimental specimens with both fillet and PJP welds were tested. The objectives of this project included an evaluation of:

1. The directional strength increase factor for fillet welds
2. The effect of length on the strength of fillet welds
3. The strength of PJP welds subjected to tension normal to the weld axis
4. The fusion zone strength of PJP welds
5. Electrode strength coefficient, C_1, in AISC *Manual* Table 8-3

DESIGN RECOMMENDATIONS

Equation 4.9 provides a uniform reliability level for all fillet weld specimens documented in this report. Compared to AISC *Specification* Equation J2-5, Equation 4.9 results in a 1% strength increase for transversely-loaded welds and a 17% increase for longitudinally-loaded welds. For short fillet welds, the proposed shear strength of $0.7F_{EXX}$ is conservative, which results in a margin to accommodate the strength variations for joints with low l/w ratios. For longer welds in longitudinally-loaded fillet-welded lap joints, a revised design method was proposed that explicitly considers the effects of yield stress and modulus of elasticity on the weld strength.

PJP welds can be designed using Equation 4.11. Compared to AISC *Specification* Equation J2-3 with $F_{nw} = 0.60F_{EXX}$, Equation 4.11 results in a 67% strength increase for transversely-loaded welds and a 18% increase for longitudinally-loaded welds.

For fillet and PJP joints with matching electrodes, calculation of the fusion zone strength is not required. For fillet and PJP joints with overmatching electrodes, the fusion zone strength can be calculated with the average of the base metal strength, F_u, and the weld metal strength, F_{EXX}.

Based on the experimental rupture deformations and the load-deformation curves, it was concluded that the electrode strength coefficient, C_1 in *Manual* Table 8-3 can be based on the direct ratio, $F_{EXX}/70$ ksi, when $F_{EXX} \leq 120$ ksi.

FUTURE RESEARCH

The recommendations in this report should be verified with a reliability analysis that includes the data in this report as well as the extensive data for both fillet and PJP welds in the existing literature. A complete analysis would include longitudinal, transverse and skewed fillet welds, as well as joints that combine longitudinal and transverse fillet welds. It would also be beneficial to study the reliability of eccentrically-loaded fillet weld joints. For PJP welds, both longitudinal and transverse welds should be evaluated. Where adequate test results are available, high-strength welds should be included in the analysis.

SYMBOLS

A_1 = sectional area of the smallest connecting element, in.^{2}
A_2 = sectional area of the largest connecting element, in.^{2}
A_{we} = effective area of the weld, in.^{2}
C_1 = electrode strength coefficient
E = effective throat of the weld, in.
E_c = modulus of elasticity of the connecting elements, ksi
E_p = actual weld throat defined as the penetration depth plus the effective throat according to AISC *Specification* Section J2.2a, in.
E_r = experimental rupture surface width, in.
F_c = rupture stress that considers the effect of base metal dilution, ksi
F_{EXX} = filler metal classification strength (specified minimum uniaxial tensile strength), ksi
F_{nw} = nominal stress of the weld metal, ksi
F_u = specified minimum tensile strength of the base metal, ksi
F_{vi} = allowable stress of the weld metal, ksi
F_w = F_{EXX} for joints with matching and undermatching weld metal, ksi
= $(F_{EXX} + F_u)/2$ for joints with overmatching weld metal, ksi
F_y = specified minimum yield strength, ksi
K_{at} = empirical coefficient for transversely-loaded double-lap fillet weld joints
L = weld length, in.
L_r = experimental rupture surface length, in.
M_w = coefficient that accounts for differences in the weld deformation capacity.
P = axial force, kips
P_e = experimental rupture load, kips
P_n = nominal strength calculated with the AISC *Specification* equations, kips
P_c = strength calculated with the measured weld size and the measured weld metal tensile strength, kips
R_i = strength at deformation Δ_i, kips
S = PJP weld preparation groove depth, in.
V_L = longitudinal load, kips
V_T = transverse load, kips
V_u = weld strength at $\theta = 0°$, kips
a = the portion of P that defines the transverse force on the weld cross section
f_r = experimental rupture stress calculated with the measured rupture surface area, ksi
k = constraint factor
k_2 = length coefficient
k_{ds} = directional strength increase factor
l = length of a single weld in the loading direction, in.
n = strain-hardening exponent
p = penetration ratio
r_{crit} = distance from the instantaneous center of rotation to the weld element with the minimum Δ_u/r_i ratio, in.
r_i = distance from the instantaneous center of rotation to element i, in.
t = thickness, in.

w = fillet weld leg size, in.
w_1 = size of fillet weld Leg 1, in.
w_2 = size of fillet weld Leg 2, in.
w_L = measured leg dimension parallel to the faying surface, in.
w_T = measured leg dimension perpendicular to the faying surface, in.
x = measured reinforcement dimension for PJP welds, in.
α = angle between the loading direction and the rupture plane, degrees
α_d = angle between the weld longitudinal axis and the weld displacement direction
β_w = correlation factor
Δ = relative displacement of connecting elements between weld ends, in.
Δ_a = remaining deformation capacity of a weld element at maximum strength, in.
Δ_m = deformation of weld element at maximum stress, in.
Δ_u = deformation of weld element at ultimate stress (rupture), in.
Δ_i = deformation of weld element at intermediate stress levels, in.
δ_i = Δ_i/w
δ_u = Δ_u/w
ε_u = uniaxial engineering tensile rupture strain
γ = experimental angle from the faying surface to the rupture surface, degrees
γ_{M2} = partial safety factor
σ = normal stress perpendicular to the plane of the throat, ksi
σ_e = experimental rupture stress, ksi
σ_T = normal stress perpendicular to the plane of the throat, ksi.
σ_{tu} = true tensile rupture stress, ksi
σ_{ua} = average of σ_{uw} and σ_{ub}, ksi
σ_{ub} = experimental tensile stress of the base metal, ksi
σ_{um} = minimum of σ_{uw} and σ_{ub}, ksi
σ_{uw} = experimental uniaxial tensile rupture stress of the weld metal, ksi
τ = shear stress in the plane of the throat, ksi.
τ_L = shear stress in the plane of the throat, parallel to the weld axis, ksi.
τ_T = shear stress in the plane of the throat, perpendicular to the weld axis, ksi
τ_u = shear rupture stress, ksi
θ = angle between the line of action of the required force and the weld longitudinal axis, degrees
θ_1 = angle between the line of action of the required force and the weld longitudinal axis for the weld segment under consideration, degrees
θ_2 = angle between the line of action of the required force and the weld longitudinal axis for the weld segment in the group that is nearest to 90°
θ_p = groove angle measured from the load direction, degrees

REFERENCES

ABW (1931), *Report of Structural Steel Welding Committee*, American Bureau of Welding, American Welding Society.

AIJ (2012), *Recommendations for Design of Connections in Steel Structures*, The Architectural Institute of Japan.

AISC (2017), *Steel Construction Manual*, Fifteenth Edition, May, American Institute of Steel Construction, Chicago, IL.

AISC (2016), *Specification for Structural Steel Buildings*, ANSI/AISC 360-10, July 7, American Institute of Steel Construction, Chicago, IL.

Ales, J.M. (1990), *The Design of Shear Tabs Welded to Tubular Columns*, Master's Thesis, The University of Wisconsin at Milwaukee, December.

Archer, F.E., Fischer, H.K. and Kitchen, E.M. (1959), "Fillet Welds Subjected to Bending and Shear," *Civil Engineering and Public Works Review*, Vol. 54, pp. 455-458.

Archer, F.E., Fischer, H.K. and Kitchen, E.M. (1964), *The Strength of Fillet Welds*, University of New South Wales.

ASTM (2017), *Standard Test Methods and Definitions for Mechanical Testing of Steel Products*, ASTM A370-17, ASTM International, West Conshohocken, PA.

AWS (2020), *Specification for Low-Alloy Steel Electrodes and Rods for Gas Shielded Arc Welding*, AWS A5.28/A5.28M, American Welding Society, Miami, FL.

AWS (2019), *Specification for Carbon Steel Electrodes and Fluxes for Submerged Arc Welding*, AWS A5.17/A5.17M, American Welding Society, Miami, FL.

AWS (2017), *Specification for Carbon Steel Electrodes and Rods for Gas Shielded Arc Welding*, AWS A5.18/A5.18M, American Welding Society, Miami, FL.

AWS (2016), *Standard Methods for Mechanical Testing of Welds*, AWS B4.0:2016, American Welding Society, Miami, FL.

AWS (2015), *Structural Welding Code-Steel*, AWS D1.1:2015, American Welding Society, Miami, FL.

AWS (2015), *Specification for Carbon Steel Electrodes for Flux Cored Arc Welding*, AWS A5.20/A5.20M, American Welding Society, Miami, FL.

AWS (2014), *Specification for Low-Alloy Steel Electrodes for Shielded Metal Arc Welding*, AWS A5.5/A5.5M, American Welding Society, Miami, FL.

AWS (2012), *Specification for Carbon Steel Electrodes for Shielded Metal Arc Welding*, AWS A5.1/A5.1M, American Welding Society, Miami, FL.

AWS (2011), *Specification for Low-Alloy Steel Electrodes and Fluxes for Submerged Arc Welding*, AWS A5.23/A5.23M, American Welding Society, Miami, FL.

AWS (1998), *Specification for Low-Alloy Steel Electrodes for Flux Cored Arc Welding*, AWS A5.29/A5.29M, American Welding Society, Miami, FL.

AWS (1937), "Stress Distribution in Fillet Welds," *Welding Research Supplement*, May, American Welding Society, Miami, FL.

Biggs, M.S., Crofts, M.R., Higgs, J.D. Martin, L.H. and Tzogius, A. (1981), "Failure of Fillet Weld Connections Subject to Static Loading," *Joints in Structural Steelwork, Proceedings of the Conference held at Teeside Polytechnic*, Pentech Press, London, England.

Bjork, T., Ahola, A. and Tuominen, N. (2018), "On the Design of Fillet Welds Made of Ultra-High-Strength Steel," *Welding in the World*, Vol. 62.

Bjork, T., Penttila, T. and Nykanen, T. (2014), "Rotation Capacity of Fillet Weld Joints Made of High-Strength Steel," *Welding in the World*, Vol. 58.

Bjork, T., Toivonen, J. and Nykanen, T. (2012), "Capacity of Fillet Welded Joints Made of Ultra High-Strength Steel," *Welding in the World*, Vol. 56.

Blackwood, R.R. (1931), "Strength of Fillet Welds in Structural Mild Steel II," *Commonwealth Engineer*, Vol. 18, No. 3, pp. 89-97.

Blackwood, R.R. (1930), "Strength of Fillet Welds in Structural Mild Steel," *Commonwealth Engineer*, Vol. 18, No. 2, pp. 50-55.

Bowman, M.D. and Quinn, B.P. (1994), "Examination of Fillet Weld Strength," *Engineering Journal*, American Institute of Steel Construction, Vol. 31, No. 3, pp. 98-108.

Brockenbrough, R.L. and Johnston, B.G. (1974), *Steel Design Manual*, United States Steel Corporation.

Butler, L.J., and Kulak, G.L. (1971), "Strength of Fillet Welds as a Function of Direction of Load," *Welding Research Supplement*, pp. 231-234.

Butler, L.J., Pal, S. and Kulak, G.L. (1972), "Eccentrically Loaded Welded Connections," *Journal of the Structural Division*, American Society of Civil Engineers, Vol. 98, No. ST5, May.

CEN (2005), *Eurocode 3: Design of Steel Structures—Part 1–8: Design of Joints*, EN 1993-1-8. Brussels, Belgium.

Chan, S.W.K. and Ogle, M.H. (1992), "Elastic-Plastic Behavior of a Simulated Transverse Fillet-Welded Lap Joint Subjected to In-Plane Tensile Loading," *Low Cycle Fatigue and Elasto-Plastic Behavior of Materials-3*, Elsevier Applied Science.

Clark, P.J. (1971), "Basis of Design for Fillet-Welded Joints Under Static Loading," Conference on Welding Product Design, Cambridge, England.

Collin, P.P. and Johansson, P.B. (2005), "Design of Welds in High Strength Steel," Proceedings of the Fourth European Conference on Steel and Composite Structures.

CSA (2014), *Design of Steel Structures*, S16-14, Canadian Standards Association, Toronto, Canada.

Deng, K.L., Grondin, G.Y. and Driver, R.G. (2003), *Effect of Loading Angle on the Behavior of Fillet Welds*, Structural Engineering Report No. 251, University of Alberta, June.

Dieter, G.E. and Bacon, D.J. (1986), *Mechanical Metallurgy*, McGraw-hill.

Douwen, A.A.V. and Witteveen, J. (1966), "Proposed Modification of the ISO Formula for the Calculation of Welded Joints," *Lastechniek*, Vol. 32, No. 6.

Dubina, D. and Stratan, A. (2002), "Behavior of Welded Connections of Moment Resisting Frames Beam-to-Column Joints," *Engineering Structures*, Vol. 24.

Faltus, F. (1988), *Joints with Fillet Welds*, Elsevier.

Feder, D.K. (1994), "Recommendations for the Design of Long Fillet Welds," *Welding in the World*, Vol. 33, No. 5.

Gagnon, D.P. and Kennedy, D.J.L. (1989), "Behavior and Ultimate Tensile Strength of Partial Joint Penetration Groove Welds," *Canadian Journal of Civil Engineering*, Vol. 16.

Gaines, E. (1987), "Reduced Fillet Weld Sizes for Naval Ships," *Journal of Ship Production*, Vol. 3, No. 4, pp. 247-255.

Gallow, M.S. (2019), *Behavior of Fillet Welds in Skewed Joints*, Ph.D. Dissertation, The University of Alabama at Birmingham.

Ginn, M., Pate, M. and Wilkinson, T. (2011), "Fillet Weld Connections to High Strength Steel," *Advances in Steel and Aluminum Structures*, Research Publishing.

Gomez, I.R., Kwan, Y.K. Kanvinde, A.M. and Grondin, G.Y. (2008), *Strength and Ductility of Welded Joints Subjected to Out-of-Plane Bending*, Draft Report, American Institute of Steel Construction, June.

Higgins, T.R. and Preece, F.R. (1969), "Proposed Working Stresses for Fillet Welds," *Engineering Journal*, American Institute of Steel Construction, January.

Higgs, J.D. (1981), "A Failure Criterion for Fillet Welds," Ph.D Dissertation, The University of Aston.

IIW (1976), *Design Rules for Arc-Welded Connections in Steel Submitted to Static Loads*, International Institute of Welding.

Iwankiw, N.R. (1997), "Rational Basis for Increased Fillet Weld Strength," *Engineering Journal*, Second Quarter, American Institute of Steel Construction.

Kamtekar, A.G. (1987), "The Strength of Inclined Fillet Welds," *Journal of Constructional Steel Research*, Vol. 7.

Kamtekar, A.G. (1982), "A New Analysis of the Strength of Some Simple Fillet Welded Connections," *Journal of Constructional Steel Research*, Vol. 2, No. 2.

Kanvinde, A.M., Gomez, I.R., Roberts, M., Fell, B.V. and Grondin, G.Y. (2009), "Strength and Ductility of Fillet Welds with Transverse Root Notch," *Journal of Constructional Steel Research*, Vol. 65, No. 4, pp. 948-958.

Kato, B. and Morita, K. (1974), "Strength of Transverse Fillet Welded Joints," *Welding Journal*, Vol. 53, No. 2, pp. 59s-64s.

Kennedy, D.J.L. and Kriviak, G.J. (1985), "The Strength of Fillet Welds Under Longitudinal and Transverse Shear: A Paradox," *Canadian Journal of Civil Engineering*, Vol. 12, pp. 226-231.

Kennedy, D.J.L., Miazga, G.S. and Lesik, D.F. (1990), "Discussion of Fillet Weld Shear Strength," *Welding Journal*, May.

Khanna, C.K. (1969), *Strength of Long Fillet Welds*, Master's Thesis, Nova Scotia Technical College.

Khurshid, M., Barsoum, Z. and Barsoum, I. (2015), "Load Carrying Capacities of Butt Welded Joints in High Strength Steels," *Journal of Engineering Materials and Technology*, Vol. 137, October.

Kist, N.C. (1936), "Berechnung der Schweissnähte unter Berücksichtigung konstanter Gestaltänderungsenergie," Vorbereich 2. Kongress Int. Ver. für Brückenbau und Hochbau.

Krumpen, R.P. and Jordan, C.R. (1984), *Updating of Fillet Weld Strength Parameters for*

Commercial Shipbuilding, Report No. SSC-323, Ship Structure Committee, April.

Kuhlmann, U., Gunther, H.P. and Rasche, C. (2008), "High-Strength Steel Fillet Welded Connections," *Steel Construction*, Issue 1.

Lawrence, F.V. and Cox, E.P. (1976), "Influence of Inadequate Joint Penetration on Tensile Behavior of A514 Steel Welds," *Welding Research Supplement*, May.

Lesik D.F, and Kennedy, D.J.L. (1990), "Ultimate Strength of Fillet Welded Connections Loaded in Plane," *Canadian Journal of Civil Engineering*, Vol. 17, No 1, pp. 55-67.

Lesik, D.F. and Kennedy, D.J.L. (1988), *Ultimate Strength of Eccentrically Loaded Fillet Welded Connections*, Structural Engineering Report 159, University of Alberta, May.

Li, C., Grondin, G.Y. and Driver, R.G. (2007), *Reliability Analysis of Concentrically Loaded Fillet Welds*, Structural Engineering Report No. 271, University of Alberta, October.

Ligtenburg, F.K. (1968), *International Test Series-Final Report*, IIW Document XV-242-68, International Institute of Welding.

Lu, H. and Dong, P. (2020), "An Analytical Shear Strength Model for Load-Carying Fillet-Welded Connections Incorporating Nonlinear Effects," *Journal of Structural Engineering*, Vol. 146, No. 3.

Lu, H., Dong, P. and Boppudi. S. (2015), "Strength Analysis of Fillet Welds Under Longitudinal and Transverse Shear Conditions," *Marine Structures*, Vol. 43, pp. 87-106.

Luo, P., Asada, H. and Tanaka, T. (2020a), "Limit Analysis for Partial-Joint-Penetration Weld T-Joints with Arbitrary Loading Angles," *Engineering Structures*, Vol. 213.

Luo, P., Asada, H., Uang, C.M., and Tanaka, T. (2020b), "Directionality Effect on Strength of Partial-Joint Penetration Groove Weld Joints," *Journal of Structural Engineering*, Vol. 146, No. 4.

McClellan, R.W. (1989), "Evaluation of Fillet Weld Shear Strength of FCAW Electrodes," *Welding Journal*, August.

Melchers, R.E. (1999), *Structural Reliability Analysis and Prediction*, Second Edition, John Wiley & Sons.

Mellor, B.G., Rainey, R.C.T. and Kirk, N.E. (1999), "The Static Strength of End and T Fillet Weld Connections," *Materials & Design*, Vol. 20, No. 4, pp. 193-205.

Miazga, G.S., and Kennedy, D.J.L. (1989), "Behavior of Fillet Welds as a Function of the Angle of Loading," *Canadian Journal of Civil Engineering*, Vol. 16, No. 4, pp. 583-599.

Miazga, G.S., and Kennedy, D.J.L. (1986), *Behavior of Fillet Welds as a Function of the Angle of Loading*, Structural Engineering Report No. 133, University of Alberta, March.

Mocanu, D. and Buga, M. (1970), “Stress Distribution Along Side Fillet Welds and in the Plates of Lap Joints,” *Experimental Stress Analysis*, The Institution of Mechanical Engineers, Paper 42.

Moon, A.R. (1948), *The Design of Welded Steel Structures*, Isaac Pitman and Sons.

Neis, V.V. (1985), “New Constitutive Law for Equal Leg Fillet Welds,” *Journal of Structural Engineering*, Vol. 111, No. 8.

Ng, A.K.F., Driver, R.G. and Grondin, G.Y. (2004), “Behavior of Transverse Fillet Welds: Parametric and Reliability Analysis,” *Engineering Journal*, Second Quarter, American Institute of Steel Construction.

Ng, A.K.F., Driver, R.G. and Grondin, G.Y. (2002), *Behavior of Transverse Fillet Welds*, Structural Engineering Report No. 245, The University of Alberta, October.

Pham, L. (1983), “Co-ordinated Testing of Fillet Welds Part 1-Cruciform Specimens-AWRA Contract 94, AWRA Document P6-35-82,” *Australian Welding Research*, December.

Popov, E.P. and Stephen, R.M. (1977), “Tensile Capacity of Partial Penetration Groove Welds,” *Journal of the Structural Division*, Vol. 103, No. ST9, September.

Preece, F.R. (1968), *AWS-AISC Fillet Weld Study: Longitudinal and Transverse Shear Tests*, Testing Engineers Incorporated, AISC Research Report RR-731, May 31.

Ran, M.M., Sun, F.F., Li, G.Q., Kanvinde, A., Wang, Y.B. and Xiao, R. (2019), “Experimental Study on the Behavior of Mismatched Butt Joints of High-Strength Steel,” *Journal of Constructional Steel Research*, Vol. 153.

Rasche, C. and Kuhlmann, U. (2009), "Investigations on Longitudinal Fillet Welded Lap Joints of HSS," Nordic Steel Construction Conference, Malmö, Sweden, September.

Reynolds, M., Huynh, Q., Rafezy, B.and Uang, C.M. (2020), “Strength of Partial-Joint-Penetration Groove Welds as Affected by Root Opening, Reinforcing and Loading Direction,” *Journal of Structural Engineering*, Vol. 146, No. 8.

Rosenthal, D. and Levray, P. (1939), *The Welding Journal*, Vol. 18, No. 4.

Satoh, K., Seo, K., Higuchi, G. and Yatagai, T. (1974), “Experimental Study on the Mechanical Behavior and the Tensile Strength of Partial Penetration Groove Welded Joint,” *Transactions of the Japan Welding Society*, Vol. 5, No. 2, September.

Spraragen, W. and Claussen, G.E. (1942), “Static Tests of Fillet and Plug Welds-A Review of Literature from 1932 to January 1, 1940,” *Welding Research Supplement*, American Welding Society, April.

Strating, J. (1971), *The Strength of Fillet Welds Made by Automatic and Semi-Automatic Welding Processes*, Stevin Laboratory Report 6-71-6-HL 13, Delft University of Technology, March.

Sun, F.F., Ran, M.M. and Wang, Y.B. (2019), “Mechanical Behavior of Transverse Fillet Welded Joints of High Strength Steel Using Digital Image Correlation Techniques,” *Journal of Constructional Steel Research*, Vol. 162.

Swannell, P. and Skewes, I.C. (1979), “The Design of Welded Brackets Loaded In-Plane: Elastic and Ultimate Load Techniques-AWRA Report P6-8-77,” *Australian Welding Research*, January.

Swannell, P. (1968), “Deformation of Longitudinal Fillet Welds Subjected to a Uniform Shearing Intensity,” *British Welding Journal*, March.

Thornton, W.A. (2020), Personal Communication.

Tide, R.H.R. (2020), Personal Communication.

Tide, R.H.R. (1980), “Eccentrically Loaded Weld Groups-AISC Design Tables,” *Engineering Journal*, Fourth Quarter, American Institute of Steel Construction.

Tousignant, K. and Packer, J.A. (2017), "Numerical Investigation of Fillet Welds in HSS-to-Rigid End-Plate Connections," *Journal of Structural Engineering*, Vol. 143, No. 12.

Troelsch, H.W. (1932), “Distribution of Shear in Welded Connections,” *Proceedings of the American Society of Civil Engineers*, November.

Tuominen, N., Bjork, T. and Ahola, A. (2018), “Effect of Bending Moment on Capacity of Fillet Weld,” *Tubular Structures XVI*, Taylor and Francis.

Vreedenburgh, C.G.J. (1954), "New Principles for the Calculation of Welded Joints," *Welding Journal*, Vol. 33, pp. 743-751.

Wheatley, J.M. and Baker, R.G. (1962), "Mechanical Properties of a Mild Steel Weld Metal Deposited by the Metal-Arc Process," *British Welding Journal*, Vol. 9.

Zhao, X.L. and Hancock, G.J. (1995), “Butt Welds and Transverse Fillet Welds in Thin Cold-Formed RHS Members,” *Journal of Structural Engineering*, Vol. 121, No. 11.

Yabe, Y., Sakamoto, S. and Yakushiji, K. (1994), “Structural Behavior of Steel Columns with Partial-Penetration Welded Joints,” *Welding in the World*, Vol. 33, No. 5.

APPENDIX A

SPECIMEN SHOP DRAWINGS

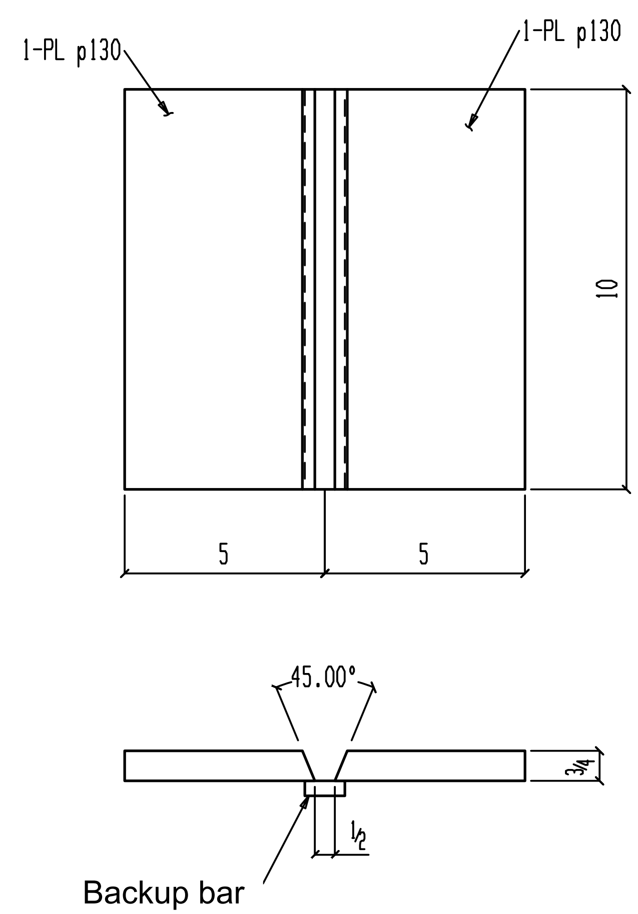

3 MISCS AT1

USE E70XX ELECTRODES

BILL OF MATERIAL

Heat Number	PC MARK	QTY TOTAL	DESCRIPTION	LENGTH		STEEL GRADE	REMARKS
	AT1	3	MISC				
8502026	AT1	3	PL3/4x4 3/4	0	10	A36	
8502026	p130	3	PL3/4x4 3/4	0	10	A36	

BATCH 1

PROJECT	AISC RESEARCH PROJECT	
DN. BY:TMR	DATE: 4-10-18	PAINT: NO PAINT

REVISIONS			PRINT RECORD	
NO.	DATE	DESCRIPTION	DATE	USE
1				FOR FAB
2				
3				
4				
5				
6				
7				
8				

COOPER STEEL
CONSTRUCTION OFFICE
1919 HAYES ST. NASHVILLE TN, 37203
OFFICE: 615-321-5222
FAX: 615-321-3030
AISC CERTIFIED FABRICATOR AND ERECTOR

DRAWING NO: AT1 ORDER NO:2874

RIDDLE STRUCTURAL DETAILING LLC.
7573 MERCER RD
(731) 444-4464
(731) 779-3771
BROWNSVILLE, TENNESSEE 38012

BILL OF MATERIAL

Heat Number	PC MARK	QTY TOTAL	DESCRIPTION	LENGTH		STEEL GRADE	REMARKS
	AT2	3	MISC				
8502026	AT2	3	PL3/4x4 3/4	0	10	A36	
8502026	p130	3	PL3/4x4 3/4	0	10	A36	

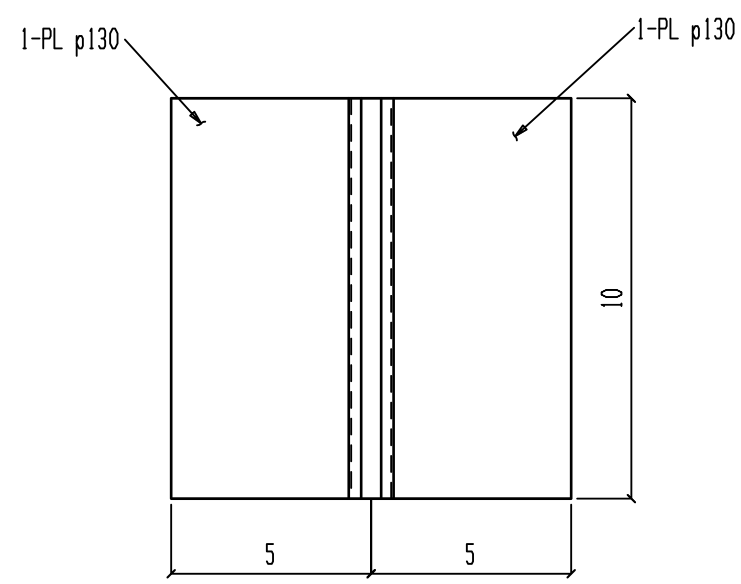

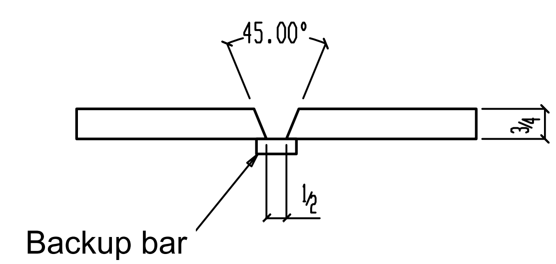

3 MISCS AT2

USE E80XX ELECTRODES

BATCH 1

PROJECT	AISC RESEARCH PROJECT	
DN. BY:TMR	DATE: 4-10-18	PAINT: NO PAINT

REVISIONS			PRINT RECORD	
NO.	DATE	DESCRIPTION	DATE	USE
1				FOR FAB
2				
3				
4				
5				
6				
7				
8				

COOPER STEEL
CONSTRUCTION OFFICE
1919 HAYES ST. NASHVILLE TN, 37203
OFFICE: 615-321-5222
FAX: 615-321-3030
AISC CERTIFIED FABRICATOR AND ERECTOR

DRAWING NO: AT2 ORDER NO:2874

RIDDLE STRUCTURAL DETAILING LLC.
7573 MERCER RD (731) 444-4464 (731) 779-3771
BROWNSVILLE, TENNESSEE 38012

BILL OF MATERIAL

Heat Number	PC MARK	QTY TOTAL	DESCRIPTION	LENGTH		STEEL GRADE	REMARKS
	AT3	3	MISC				
8502026	AT3	3	PL¾x4¾	0	10	A36	
8502026	p130	3	PL¾x4¾	0	10	A36	

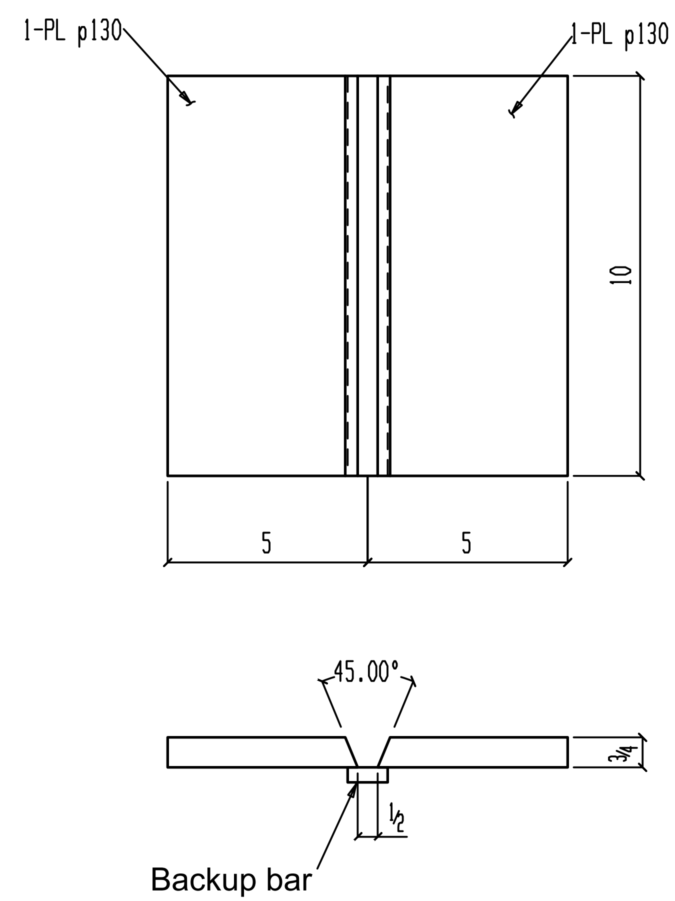

3 MISCS AT3

USE E100XX ELECTRODES

BATCH 1

PROJECT	AISC RESEARCH PROJECT		
DN. BY:TMR	DATE: 4-10-18	PAINT: NO PAINT	

REVISIONS			PRINT RECORD	
NO.	DATE	DESCRIPTION	DATE	USE
1				FOR FAB
2				
3				
4				
5				
6				
7				
8				

COOPER STEEL
CONSTRUCTION OFFICE
1919 HAYES ST. NASHVILLE TN, 37203
OFFICE: 615-321-5222
FAX: 615-321-3030

AISC CERTIFIED FABRICATOR AND ERECTOR

DRAWING NO: AT3 ORDER NO:2874

RIDDLE STRUCTURAL DETAILING LLC.
7573 MERCER RD (731) 444-4464 (731) 779-3771
BROWNSVILLE, TENNESSEE 38012

BILL OF MATERIAL

Heat Number	PC MARK	QTY TOTAL	DESCRIPTION	LENGTH		STEEL GRADE	REMARKS
8502026	BM1	ONE	PL. 3/4 x 5	0	10	A36	
D5715	BM2	1	PL. 1 x 5	0	10	A36	
7506515	BM3	1	PL. 1 1/4 x 5	0	10	A36	
8501452	BM4	1	PL. 1 1/2 x 5	0	10	A36	
7506393	BM5	1	PL. 1 3/4 X 5	0	10	A36	
6502038	BM6	1	PL. 2 x 5	0	10	A36	
8500710	BM7	1	PL. 2 1/2 x 5	0	10	A36	
W7H748	BM8	1	PL. 3/4 x 5	0	10	A572-65	
B7X6627	BM9	1	PL. 1 x 5	0	10	A572-65	
W7H748	BM10	1	PL. 1 1/4 x 5	0	10	A572-65	
7507549	BM11	1	PL. 1 1/2 x 5	0	10	A572-65	
D2044	BM12	1	PL. 1 3/4 x 5	0	10	A572-65	
D2290	BM13	1	PL. 2 x 5	0	10	A572-65	

BATCH 1

PROJECT	AISC RESEARCH PROJECT	
DN. BY:TMR	DATE: 4-10-18	PAINT: NO PAINT

REVISIONS			PRINT RECORD	
NO.	DATE	DESCRIPTION	DATE	USE
1				FOR FAB
2				
3				
4				
5				
6				
7				
8				

COOPER STEEL
CONSTRUCTION OFFICE
1919 HAYES ST. NASHVILLE TN, 37203
OFFICE: 615-321-5222
FAX: 615-321-3030

AISC CERTIFIED FABRICATOR AND ERECTOR

DRAWING NO: BM1 ORDER NO:2874

RIDDLE STRUCTURAL DETAILING LLC.
7573 MERCER RD (731) 444-4464 (731) 779-3771
BROWNSVILLE, TENNESSEE 38012

BILL OF MATERIAL

Heat Number	PC MARK	QTY TOTAL	DESCRIPTION	LENGTH		STEEL GRADE	REMARKS
	FL1	ONE	MISC				
8502026	p49	2	PL¾x4½	0	5	A36	
D5715	p5	2	PL1x6	1	2	A36	

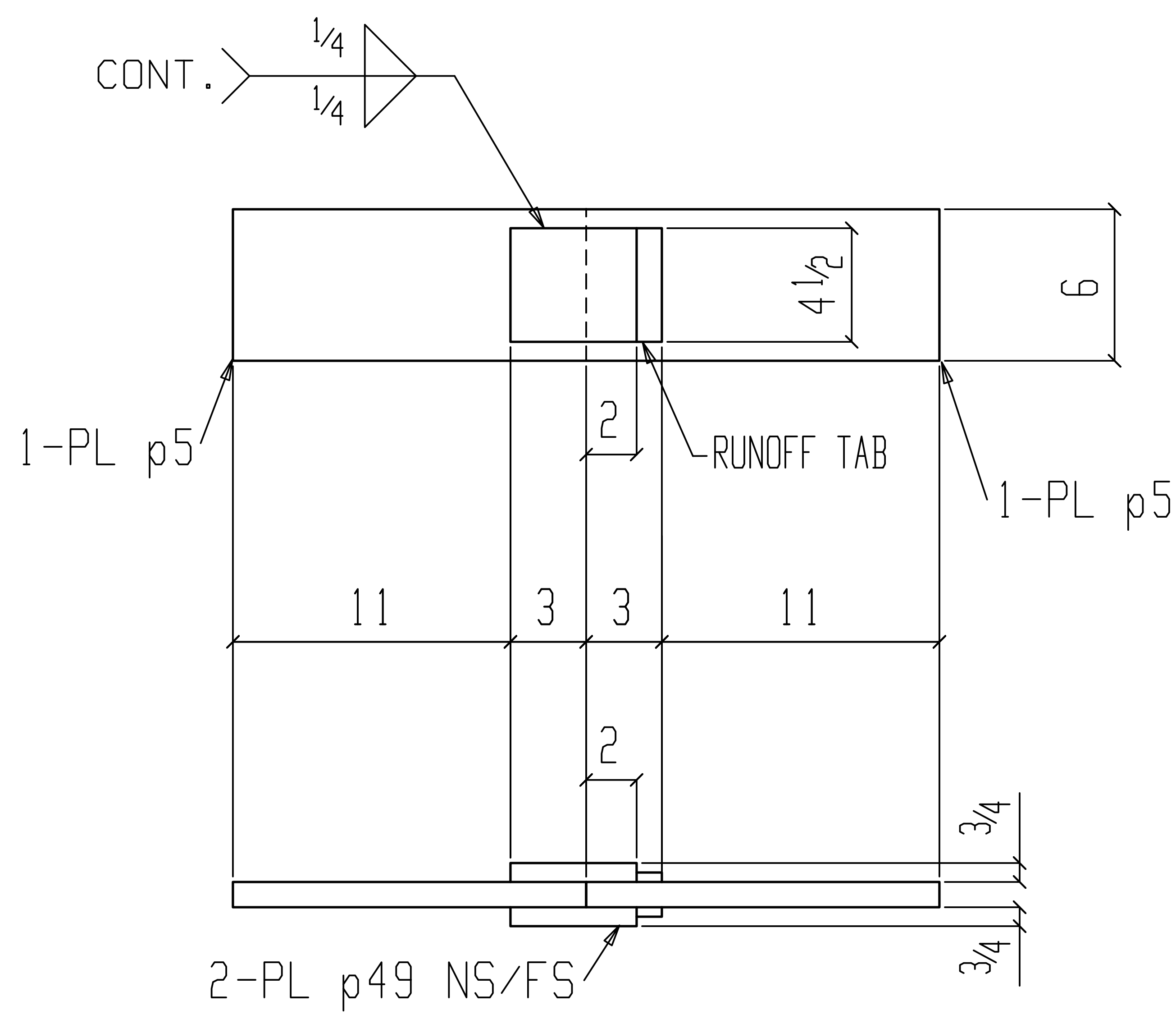

ONE MISC FL1

USE E70XX ELECTRODES

BATCH 1

PROJECT	AISC RESEARCH PROJECT	
DN. BY:TMR	DATE: 4-10-18	PAINT: NO PAINT

REVISIONS			PRINT RECORD	
NO.	DATE	DESCRIPTION	DATE	USE
1				FOR FAB
2				
3				
4				
5				
6				
7				
8				

RIDDLE STRUCTURAL DETAILING LLC.
7573 MERCER RD
(731) 444-4464
(731) 779-3771
BROWNSVILLE, TENNESSEE 38012

COOPER STEEL
CONSTRUCTION OFFICE
1919 HAYES ST. NASHVILLE TN, 37203
OFFICE: 615-321-5222
FAX: 615-321-3030
AISC CERTIFIED FABRICATOR AND ERECTOR

DRAWING NO: FL1 | ORDER NO:2874

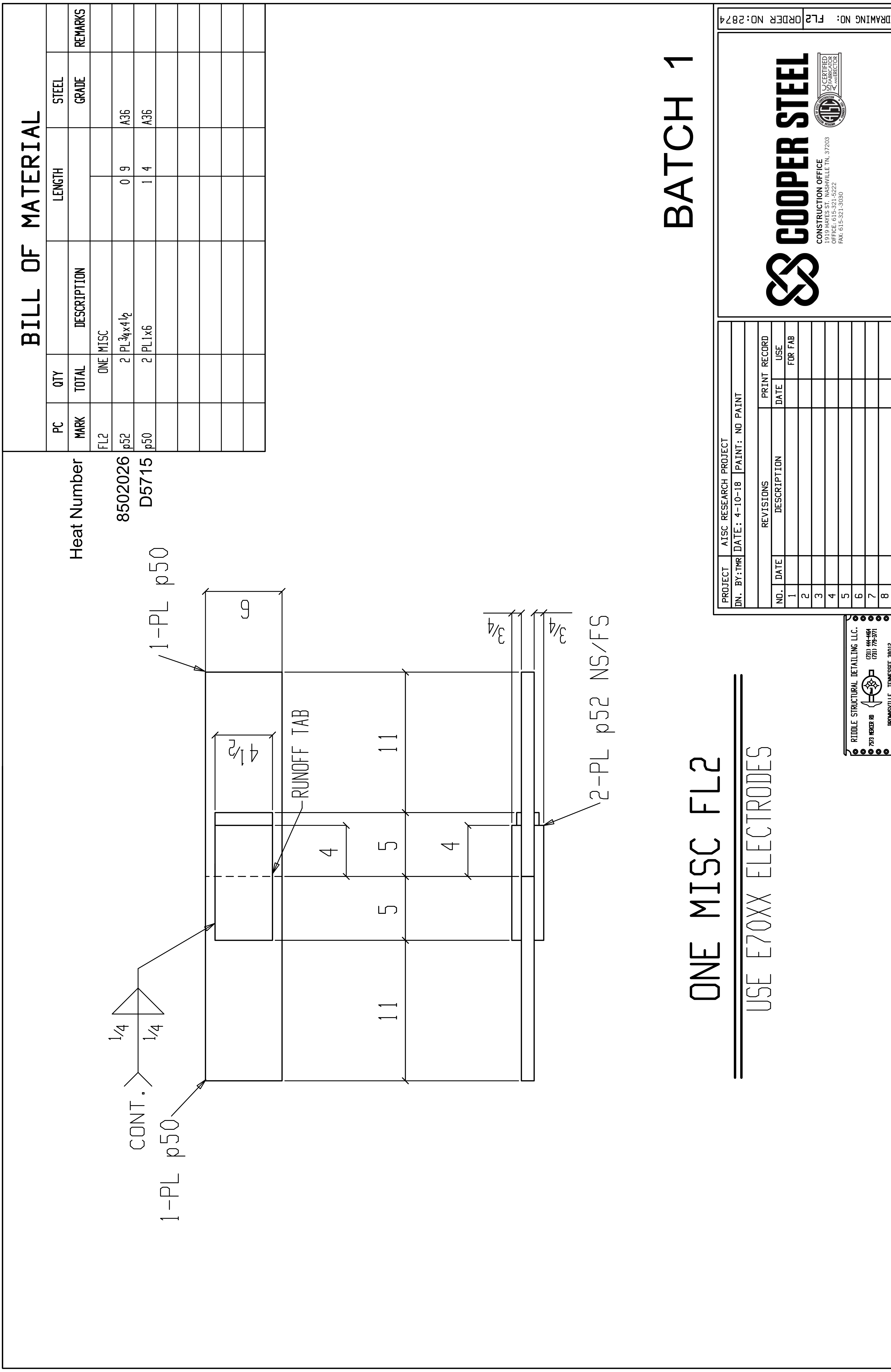

Heat Number	PC MARK	QTY TOTAL	DESCRIPTION	LENGTH		STEEL GRADE	REMARKS
	FL2	ONE	MISC				
8502026	p52	2	PL¾x4½	0	9	A36	
D5715	p50	2	PL1x6	1	4	A36	

BILL OF MATERIAL

PC MARK	QTY TOTAL	DESCRIPTION	LENGTH		STEEL GRADE	REMARKS	Heat Number
FL3	ONE	MISC					
p57	2	PL1x4½	1	2	A36		D5715
p54	2	PL1½x6	1	7	A36		8501452

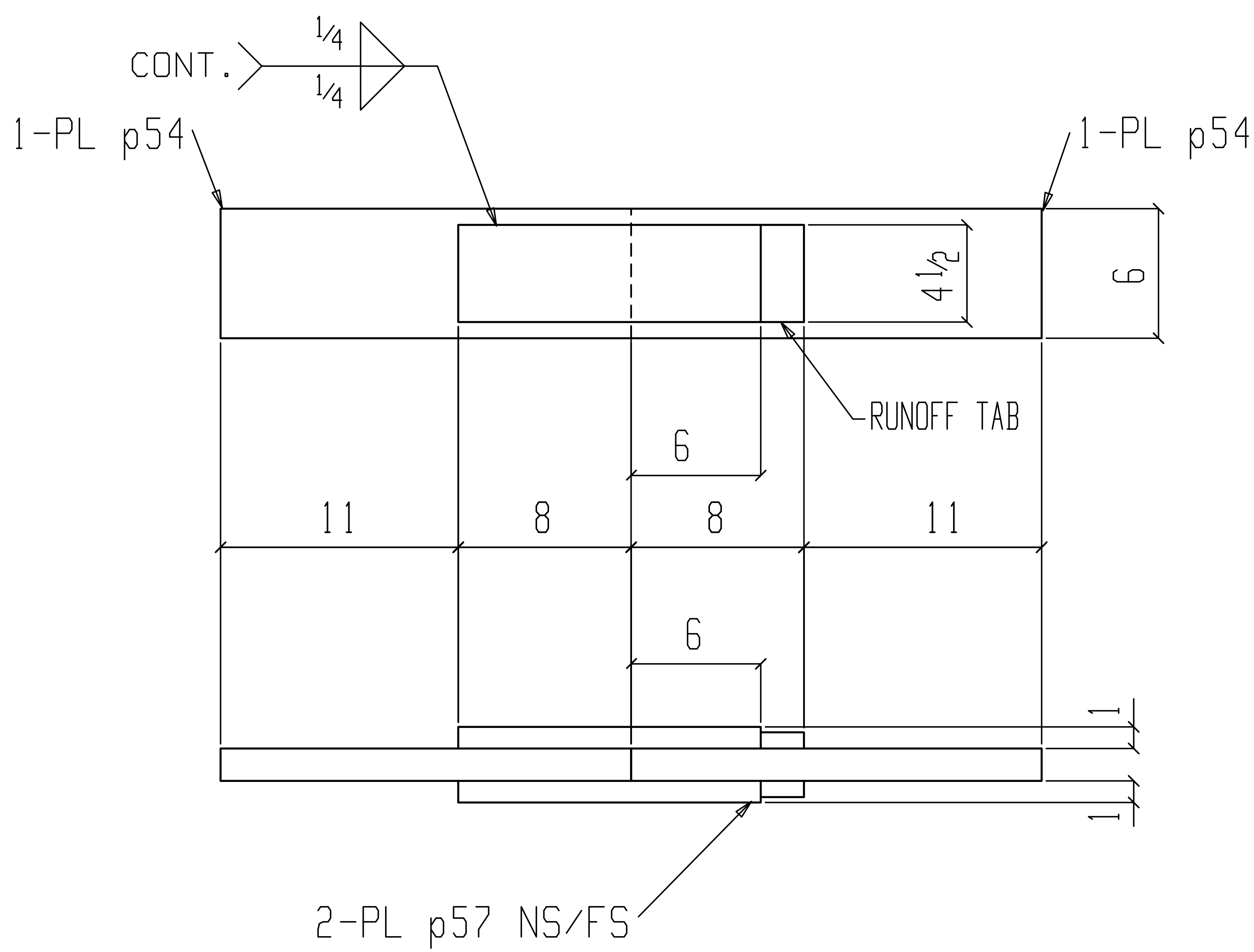

ONE MISC FL3

USE E70XX ELECTRODES

BATCH 1

PROJECT	AISC RESEARCH PROJECT	
DN. BY:TMR	DATE: 4-10-18	PAINT: NO PAINT

REVISIONS			PRINT RECORD	
NO.	DATE	DESCRIPTION	DATE	USE
1				FOR FAB
2				
3				
4				
5				
6				
7				
8				

COOPER STEEL
CONSTRUCTION OFFICE
1919 HAYES ST. NASHVILLE TN, 37203
OFFICE: 615-321-5222
FAX: 615-321-3030

AISC CERTIFIED FABRICATOR AND ERECTOR

DRAWING NO: FL3 ORDER NO:2874

RIDDLE STRUCTURAL DETAILING LLC.
7573 MERCER RD
(731) 444-4464
(731) 779-3771
BROWNSVILLE, TENNESSEE 38012

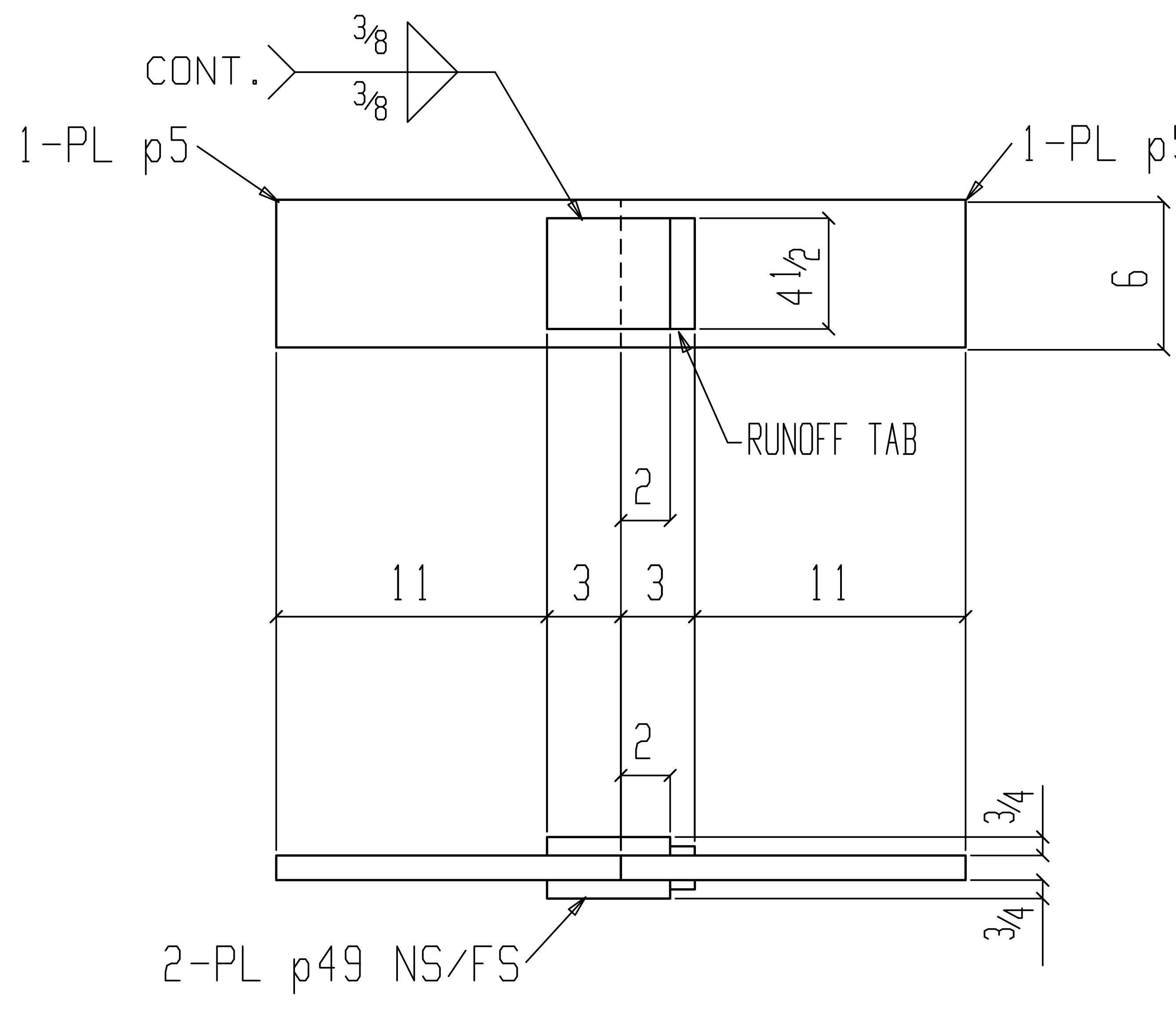

BILL OF MATERIAL

Heat Number	PC MARK	QTY TOTAL	DESCRIPTION	LENGTH		STEEL GRADE	REMARKS
	FL4	ONE	MISC				
8502026	p49	2	PL3/4x4 1/2	0	5	A36	
D5715	p5	2	PL1x6	1	2	A36	

BATCH 1

ONE MISC FL4

USE E70XX ELECTRODES

RIDDLE STRUCTURAL DETAILING LLC.
7573 MERCER RD (731) 444-4464 (731) 779-3771
BROWNSVILLE, TENNESSEE 38012

PROJECT	AISC RESEARCH PROJECT	
DN. BY:TMR	DATE: 4-10-18	PAINT: NO PAINT

REVISIONS			PRINT RECORD	
NO.	DATE	DESCRIPTION	DATE	USE
1				FOR FAB
2				
3				
4				
5				
6				
7				
8				

COOPER STEEL
CONSTRUCTION OFFICE
1919 HAYES ST. NASHVILLE TN, 37203
OFFICE: 615-321-5222
FAX: 615-321-3030
AISC CERTIFIED FABRICATOR AND ERECTOR

DRAWING NO: FL4 ORDER NO:2874

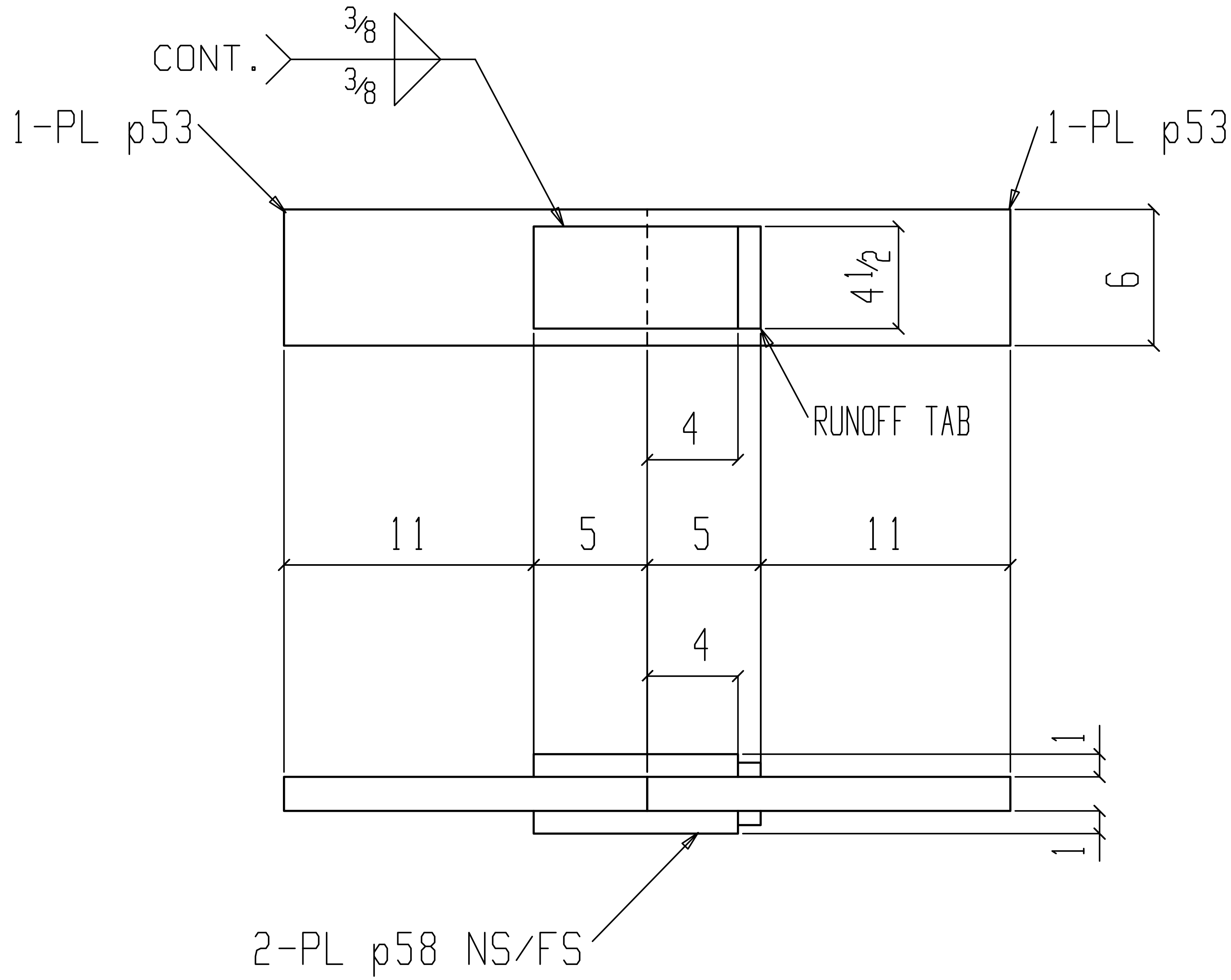

BILL OF MATERIAL

Heat Number	PC MARK	QTY TOTAL	DESCRIPTION	LENGTH		STEEL GRADE	REMARKS
	FL5	ONE	MISC				
D5715	p58	2	PL1x4½	0	9	A36	
8501452	p53	2	PL1½x6	1	4	A36	

BATCH 1

ONE MISC FL5

USE E70XX ELECTRODES

RIDDLE STRUCTURAL DETAILING LLC.
7573 MERCER RD
(731) 444-4464
(731) 779-3771
BROWNSVILLE, TENNESSEE 38012

PROJECT	AISC RESEARCH PROJECT	
DN. BY:TMR	DATE: 4-10-18	PAINT: NO PAINT

REVISIONS			PRINT RECORD	
NO.	DATE	DESCRIPTION	DATE	USE
1				FOR FAB
2				
3				
4				
5				
6				
7				
8				

COOPER STEEL
CONSTRUCTION OFFICE
1919 HAYES ST. NASHVILLE TN, 37203
OFFICE: 615-321-5222
FAX: 615-321-3030
AISC CERTIFIED FABRICATOR AND ERECTOR

DRAWING NO: FL5 ORDER NO:2874

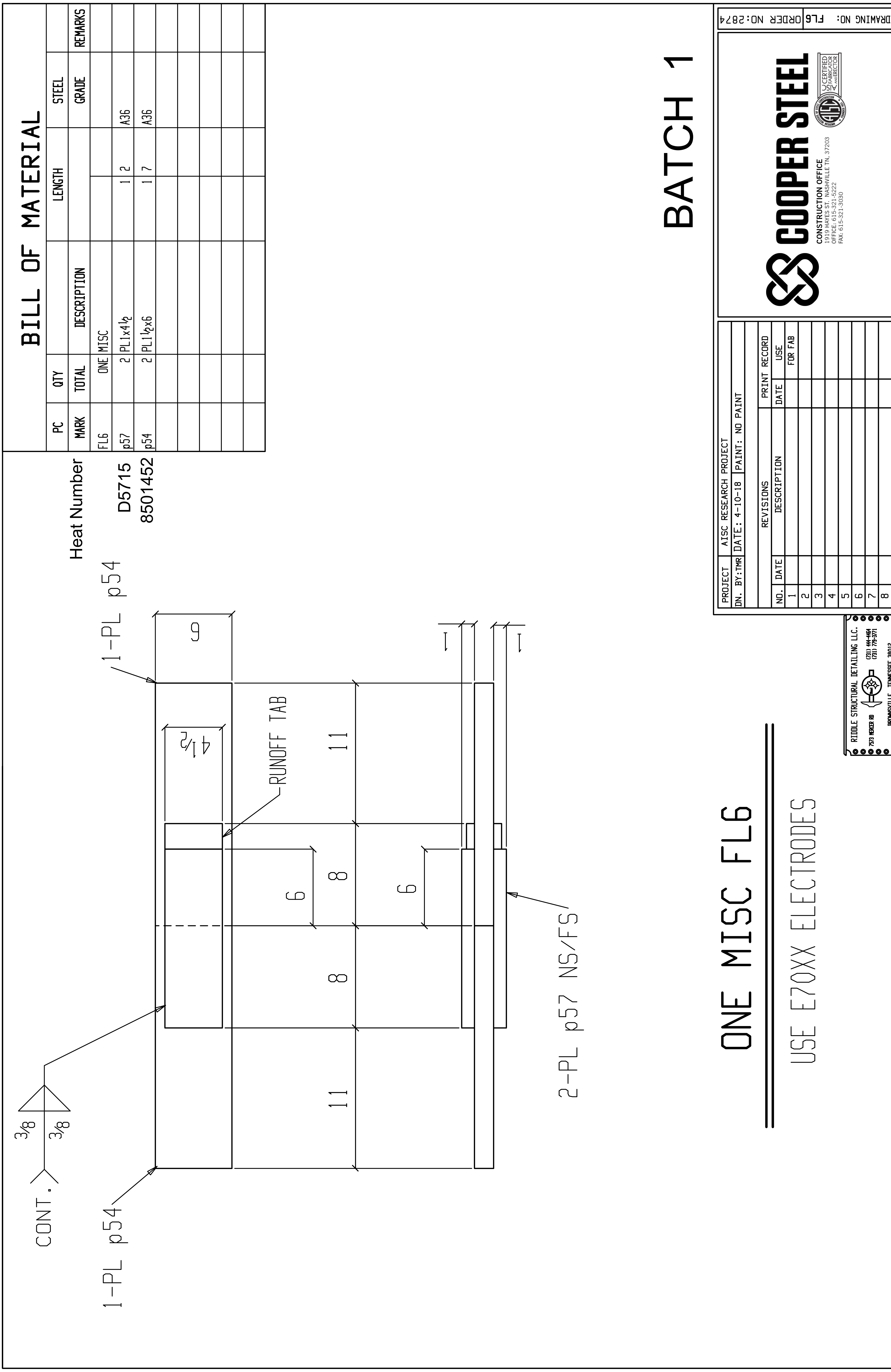
BILL OF MATERIAL
PC MARK | QTY TOTAL | DESCRIPTION | LENGTH | STEEL GRADE | REMARKS
FL6 | ONE | MISC
p57 | 2 | PL1x4½ | 1 2 | A36
p54 | 2 | PL1½x6 | 1 7 | A36
Heat Number
D5715
8501452
BATCH 1
DRAWING NO: FL6 ORDER NO:2874
COOPER STEEL
CONSTRUCTION OFFICE
1919 HAYES ST. NASHVILLE TN. 37203
OFFICE: 615-321-5222
FAX: 615-321-3030
CERTIFIED FABRICATOR and ERECTOR
PROJECT AISC RESEARCH PROJECT
DN. BY:TMR DATE: 4-10-18 PAINT: NO PAINT
REVISIONS
NO. DATE DESCRIPTION
1 2 3 4 5 6 7 8
PRINT RECORD
DATE USE
FOR FAB
RIDDLE STRUCTURAL DETAILING LLC.
7573 MERCER RD
BROWNSVILLE, TENNESSEE 38012
1-PL p54
6
4½
RUNOFF TAB
11
8
6
8
6
11
2-PL p57 NS/FS
3/8
3/8
CONT.
1-PL p54
ONE MISC FL6
USE E70XX ELECTRODES

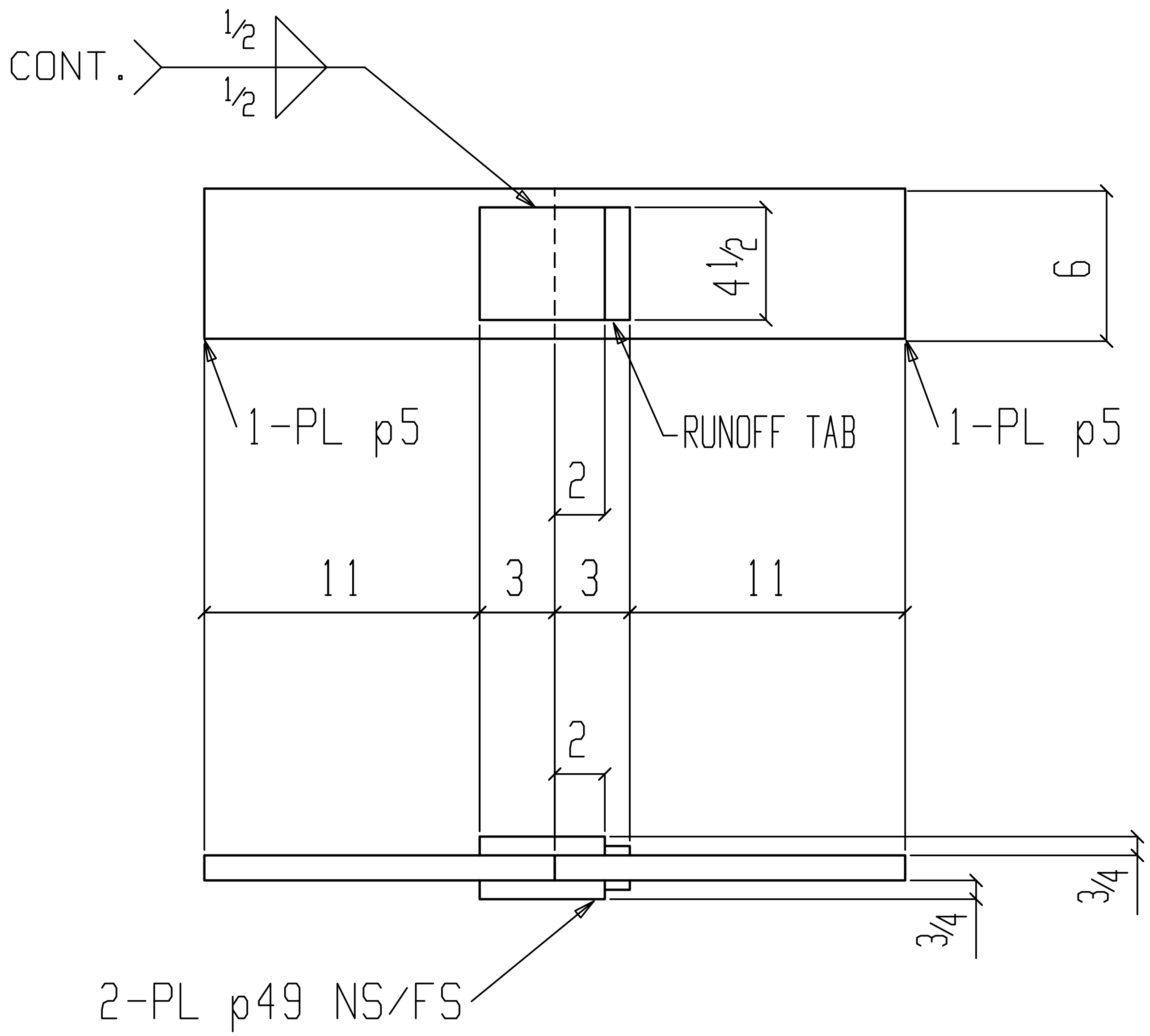

BILL OF MATERIAL

Heat Number	PC MARK	QTY TOTAL	DESCRIPTION	LENGTH		STEEL GRADE	REMARKS
	FL7	ONE	MISC				
8502026	p49	2	PL3/4x4 1/2	0	5	A36	
D5715	p5	2	PL1x6	1	2	A36	

BATCH 1

ONE MISC FL7

USE E70XX ELECTRODES

PROJECT	AISC RESEARCH PROJECT	
DN. BY:TMR	DATE: 4-10-18	PAINT: NO PAINT

REVISIONS			PRINT RECORD	
NO.	DATE	DESCRIPTION	DATE	USE
1				FOR FAB
2				
3				
4				
5				
6				
7				
8				

RIDDLE STRUCTURAL DETAILING LLC.
7573 MERCER RD (731) 444-4464 (731) 779-3771
BROWNSVILLE, TENNESSEE 38012

COOPER STEEL
CONSTRUCTION OFFICE
1919 HAYES ST. NASHVILLE TN, 37203
OFFICE: 615-321-5222
FAX: 615-321-3030
AISC CERTIFIED FABRICATOR AND ERECTOR

DRAWING NO: FL7 ORDER NO:2874

BILL OF MATERIAL

PC MARK	QTY TOTAL	DESCRIPTION	LENGTH		STEEL GRADE	REMARKS	Heat Number
FL8	ONE	MISC					
p58	2	PL1x4½	0	9	A36		D5715
p53	2	PL1½x6	1	4	A36		8501452

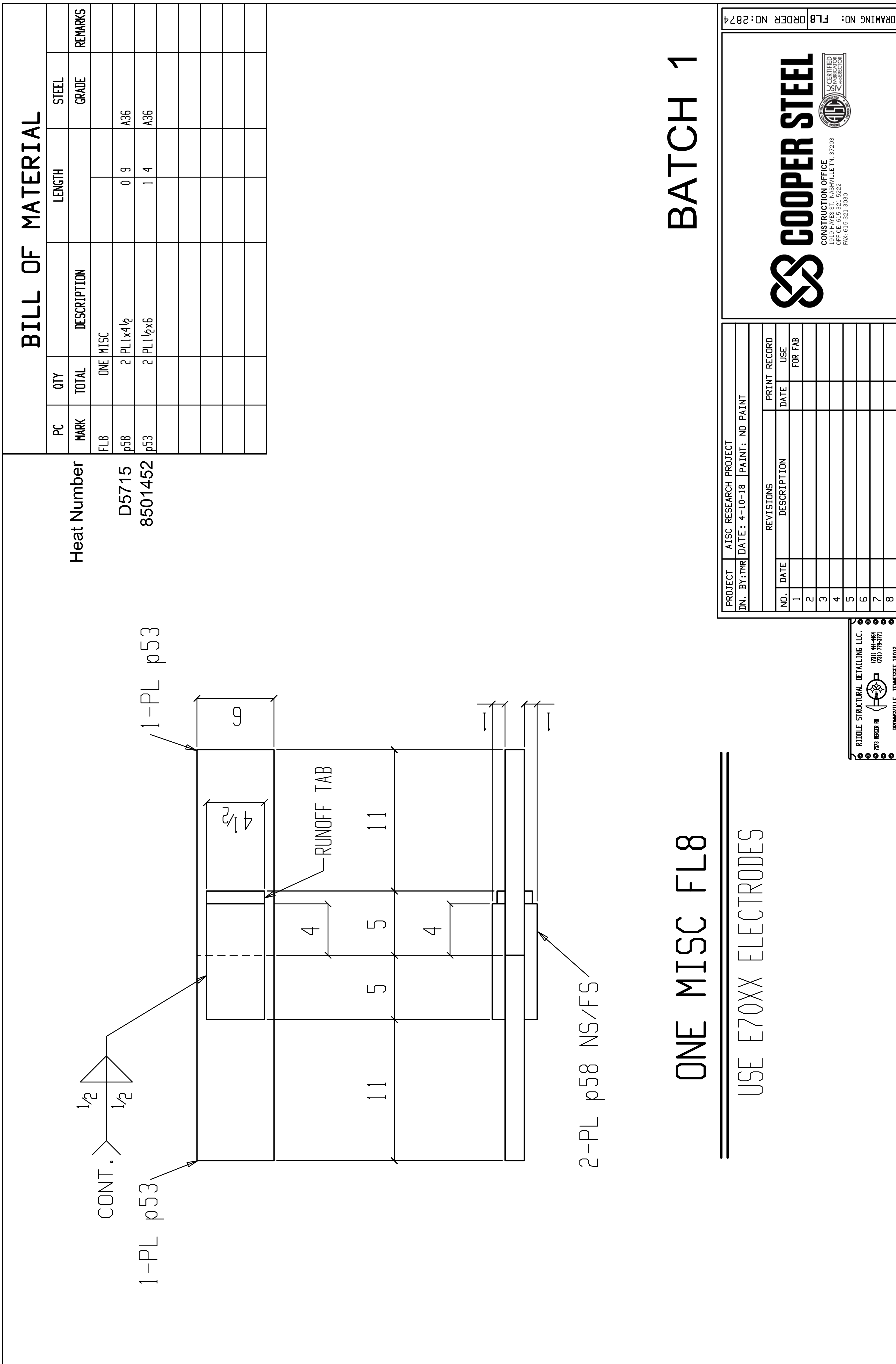

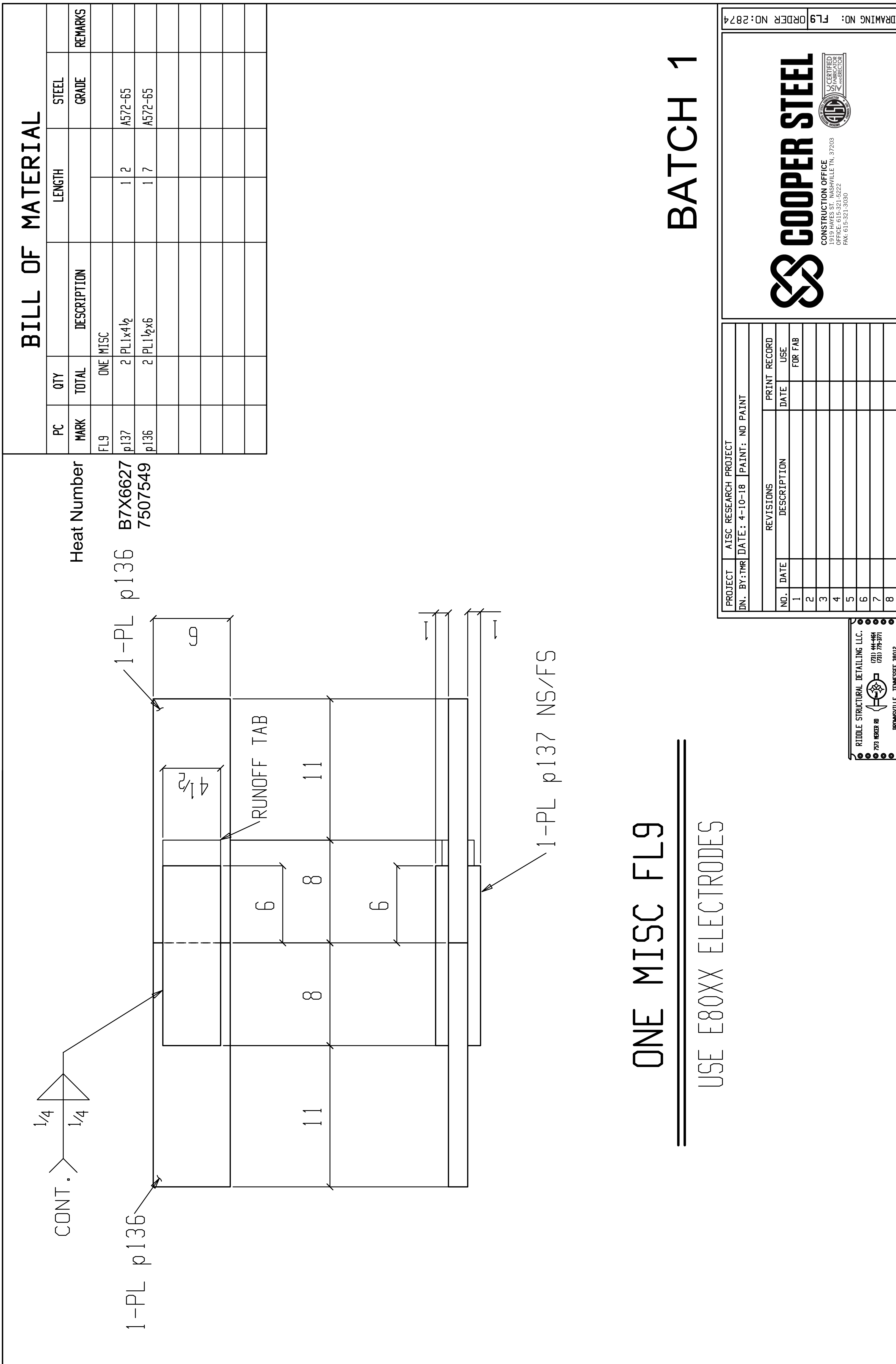
BILL OF MATERIAL
PC MARK | QTY TOTAL | DESCRIPTION | LENGTH | STEEL GRADE | REMARKS
FL9 | ONE | MISC
p137 | 2 | PL1x4½ | 1 2 | A572-65
p136 | 2 | PL1½x6 | 1 7 | A572-65
Heat Number
p136 B7X6627
7507549
1-PL p136
9
4½
RUNOFF TAB
11
8
6
8
6
11
1
1
1-PL p137 NS/FS
CONT.
1/4
1/4
1-PL p136
ONE MISC FL9
USE E80XX ELECTRODES
BATCH 1
DRAWING NO: FL9 ORDER NO:2874
COOPER STEEL
CONSTRUCTION OFFICE
1919 HAYES ST. NASHVILLE TN. 37203
OFFICE: 615-321-5222
FAX: 615-321-3030
CERTIFIED FABRICATOR and ERECTOR
PROJECT AISC RESEARCH PROJECT
DN. BY:TMR DATE: 4-10-18 PAINT: NO PAINT
REVISIONS
PRINT RECORD
NO. DATE DESCRIPTION DATE USE
FOR FAB
1
2
3
4
5
6
7
8
RIDDLE STRUCTURAL DETAILING LLC.
7573 MERCER RD
BROWNSVILLE, TENNESSEE 38012

BILL OF MATERIAL

Heat Number	PC MARK	QTY TOTAL	DESCRIPTION	LENGTH		STEEL GRADE	REMARKS
	FL10	ONE	MISC				
B7X6627	p139	2	PL1x4½	0	9	A572-65	
7507549	p138	2	PL1½x6	1	4	A572-65	

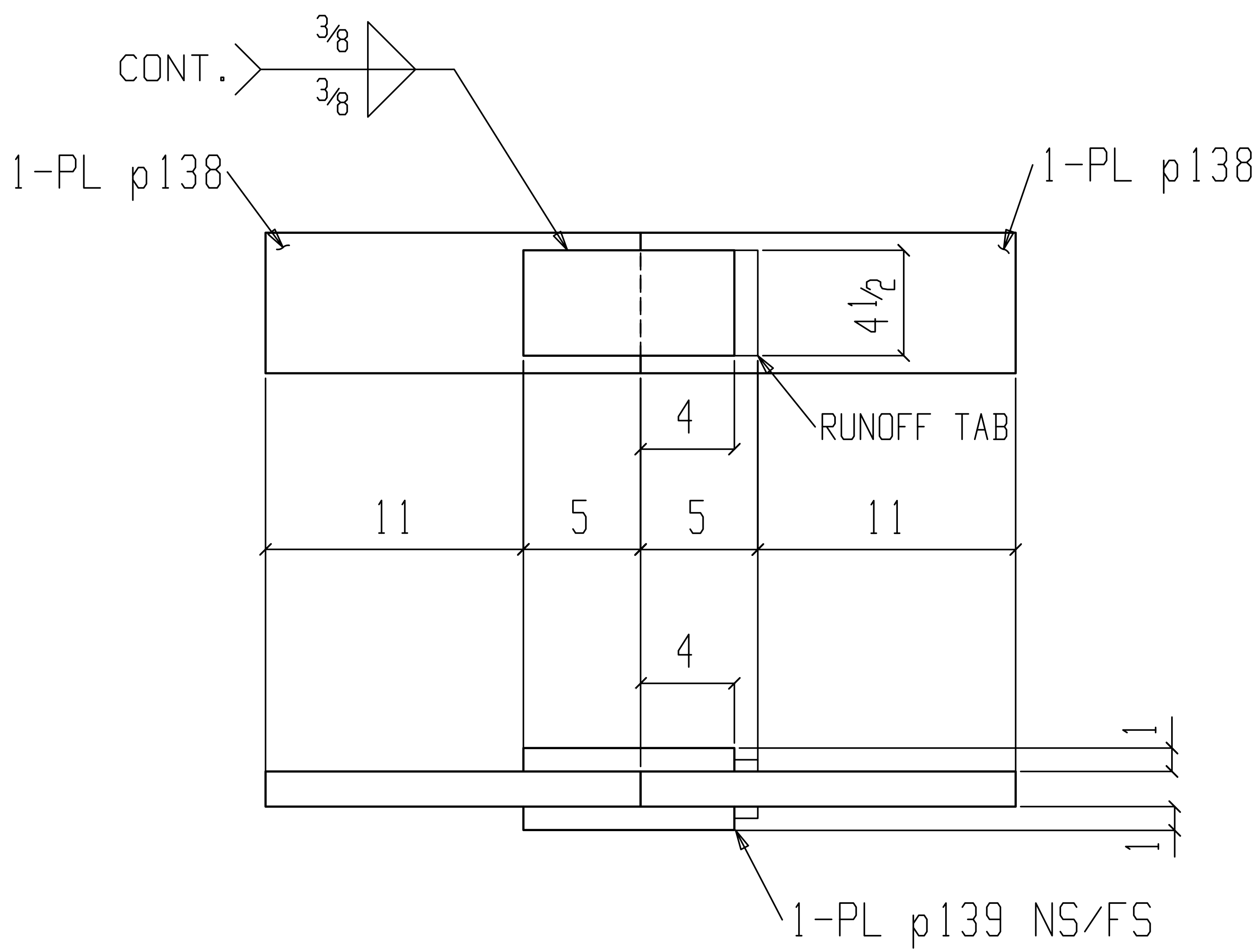

ONE MISC FL10

USE E80XX ELECTRODES

BATCH 1

PROJECT AISC RESEARCH PROJECT
DN. BY:TMR DATE: 4-10-18 PAINT: NO PAINT

NO.	DATE	REVISIONS DESCRIPTION	PRINT RECORD DATE	USE
1				FOR FAB
2				
3				
4				
5				
6				
7				
8				

RIDDLE STRUCTURAL DETAILING LLC.
7573 MERCER RD (731) 444-4464 (731) 779-3771
BROWNSVILLE, TENNESSEE 38012

COOPER STEEL
CONSTRUCTION OFFICE
1919 HAYES ST. NASHVILLE TN, 37203
OFFICE: 615-321-5222
FAX: 615-321-3030
AISC CERTIFIED FABRICATOR and ERECTOR

DRAWING NO: FL10 ORDER NO:2874

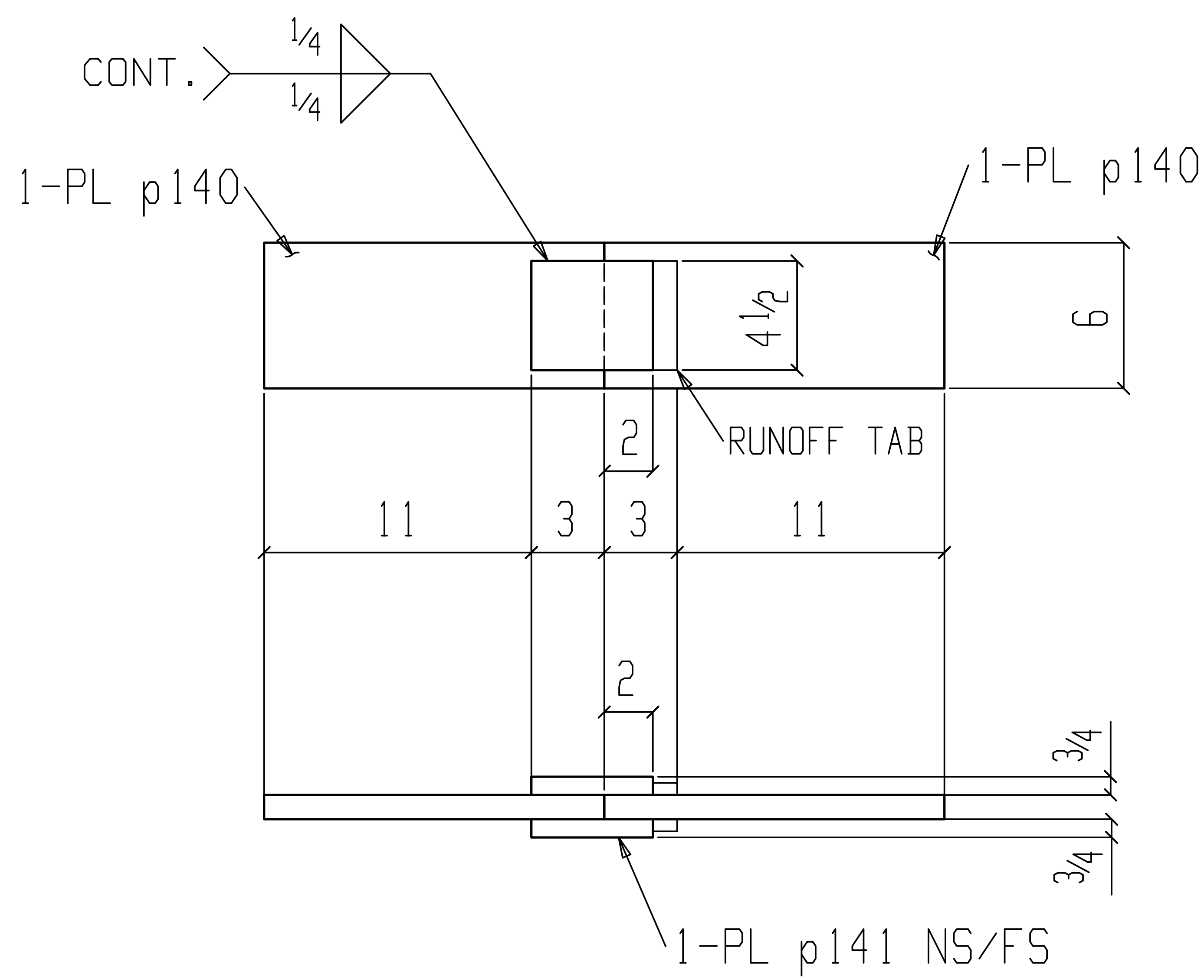

ONE MISC FL11

USE E100XX ELECTRODES

BILL OF MATERIAL

Heat Number	PC MARK	QTY TOTAL	DESCRIPTION	LENGTH		STEEL GRADE	REMARKS
	FL11	ONE	MISC				
W7H748	p141	2	PL¾x4½	0	5	A572-65	
B7X6627	p140	2	PL1x6	1	2	A572-65	

BATCH 1

PROJECT	AISC RESEARCH PROJECT	
DN. BY:TMR	DATE: 4-10-18	PAINT: NO PAINT

REVISIONS			PRINT RECORD	
NO.	DATE	DESCRIPTION	DATE	USE
1				FOR FAB
2				
3				
4				
5				
6				
7				
8				

RIDDLE STRUCTURAL DETAILING LLC.
7573 MERCER RD (731) 444-4464 (731) 779-3771
BROWNSVILLE, TENNESSEE 38012

COOPER STEEL
CONSTRUCTION OFFICE
1919 HAYES ST. NASHVILLE TN, 37203
OFFICE: 615-321-5222
FAX: 615-321-3030
AISC CERTIFIED FABRICATOR AND ERECTOR

DRAWING NO: FL11 ORDER NO:2874

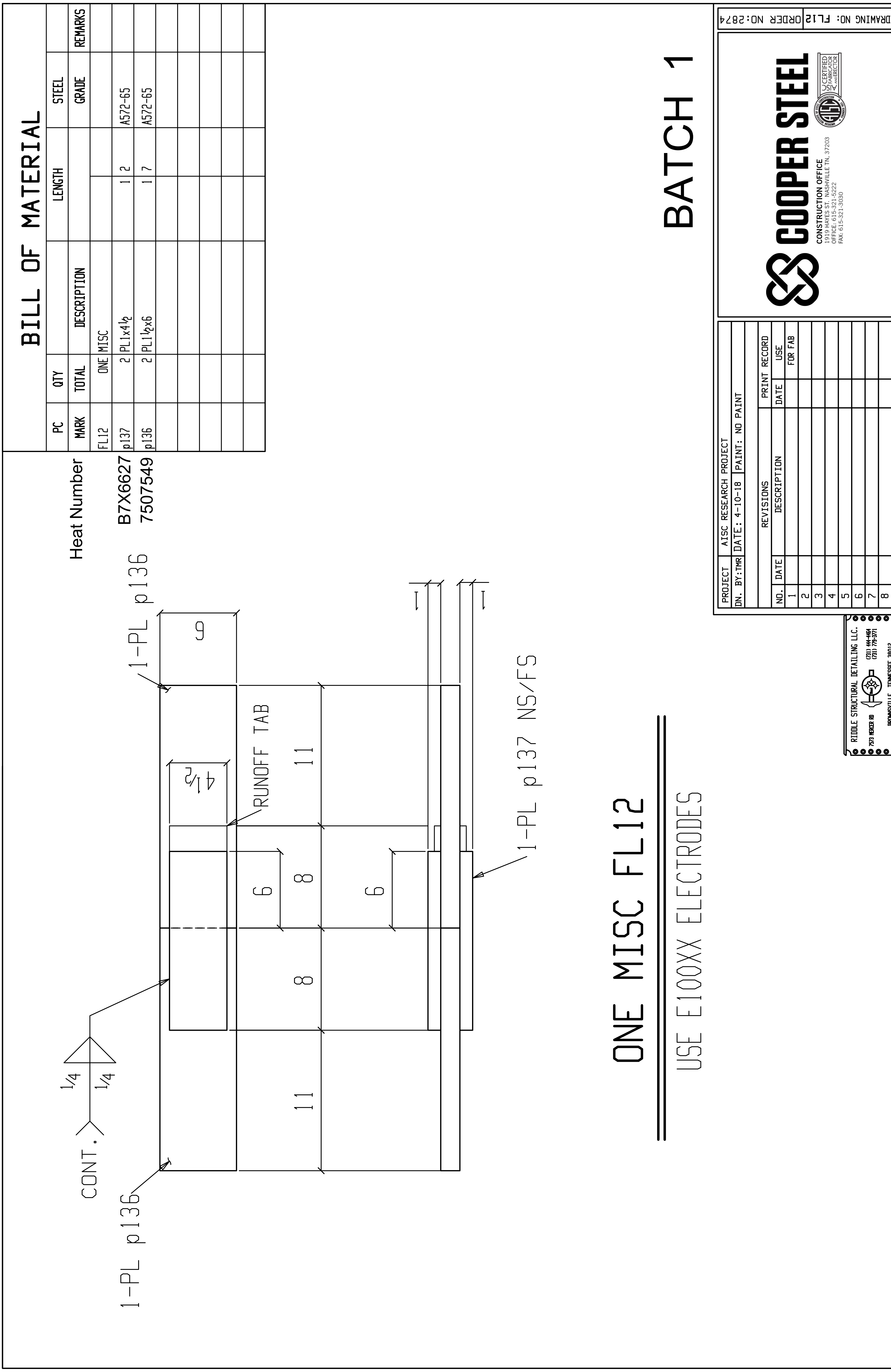
BILL OF MATERIAL
PC MARK | QTY TOTAL | DESCRIPTION | LENGTH | STEEL GRADE | REMARKS
FL12 | ONE | MISC
p137 | 2 | PL1x4½ | 1 2 | A572-65
p136 | 2 | PL1½x6 | 1 7 | A572-65
Heat Number
B7X6627
7507549
BATCH 1
DRAWING NO: FL12 ORDER NO:2874
COOPER STEEL
CONSTRUCTION OFFICE
1919 HAYES ST. NASHVILLE TN, 37203
OFFICE: 615-321-5222
FAX: 615-321-3030
CERTIFIED FABRICATOR and ERECTOR
PROJECT AISC RESEARCH PROJECT
DN. BY:TMR DATE: 4-10-18 PAINT: NO PAINT
REVISIONS
PRINT RECORD
NO. DATE DESCRIPTION DATE USE
FOR FAB
1
2
3
4
5
6
7
8
RIDDLE STRUCTURAL DETAILING LLC.
7573 MERCER RD
BROWNSVILLE, TENNESSEE 38012
1-PL p136
9
RUNOFF TAB
4½
11
6
8
8
11
1-PL p137 NS/FS
1/4
1/4
CONT.
1-PL p136
ONE MISC FL12
USE E100XX ELECTRODES

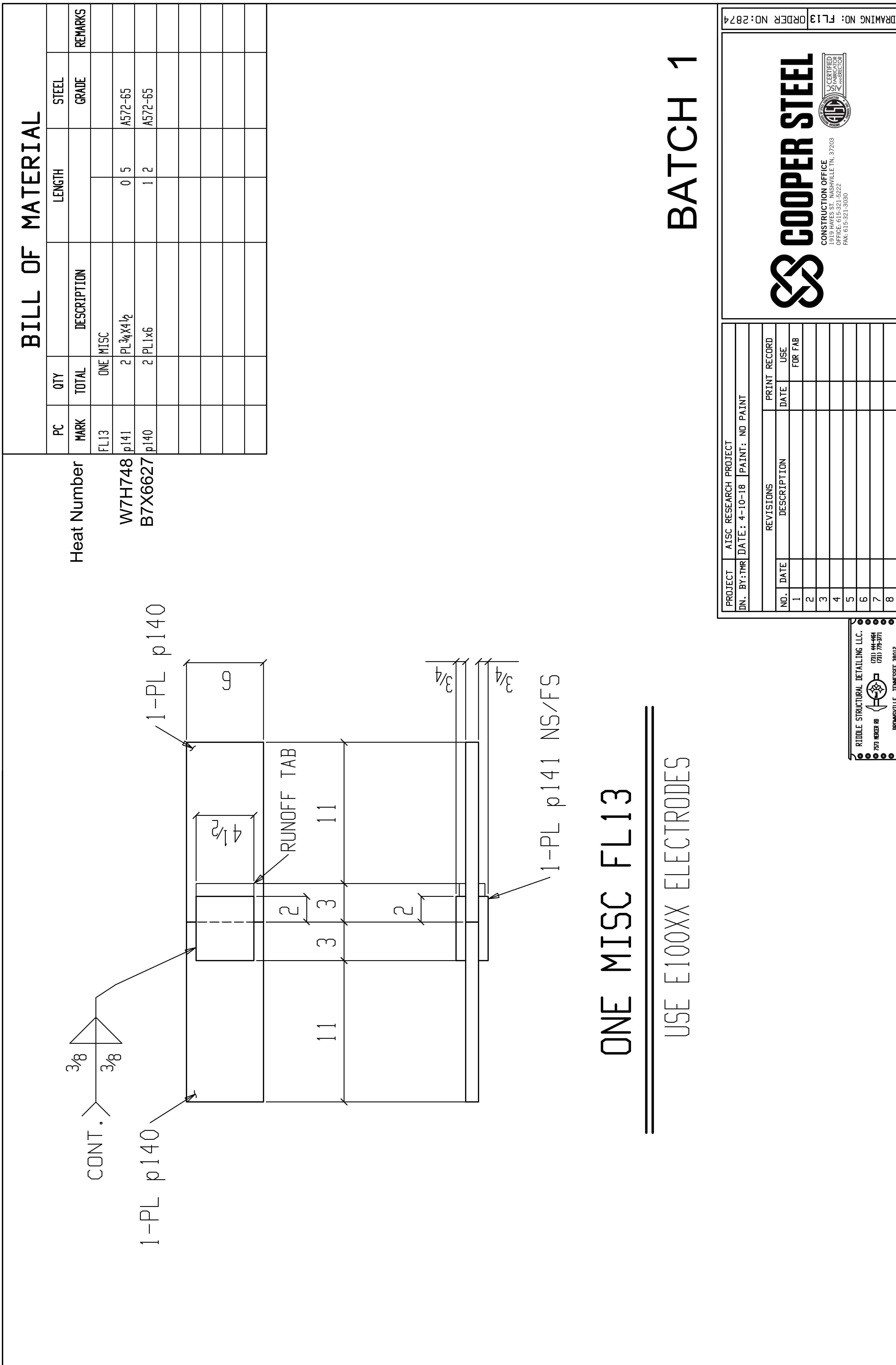
BILL OF MATERIAL
PC MARK | QTY TOTAL | DESCRIPTION | LENGTH | STEEL GRADE | REMARKS
FL13 | ONE | MISC
p141 | 2 | PL3/4X41/2 | 0 5 | A572-65
p140 | 2 | PL1x6 | 1 2 | A572-65
Heat Number
W7H748
B7X6627
BATCH 1
1-PL p140
6
3/4
3/4
41/2
RUNOFF TAB
11
3
3
2
2
11
3/8
3/8
CONT.
1-PL p140
1-PL p141 NS/FS
ONE MISC FL13
USE E100XX ELECTRODES
DRAWING NO: FL13 ORDER NO:2874
COOPER STEEL
CONSTRUCTION OFFICE
1919 HAYES ST. NASHVILLE TN. 37203
OFFICE: 615-321-5222
FAX: 615-321-3030
CERTIFIED FABRICATOR and ERECTOR
PROJECT AISC RESEARCH PROJECT
DN. BY:TMR DATE: 4-10-18 PAINT: NO PAINT
REVISIONS
NO. DATE DESCRIPTION
PRINT RECORD
DATE USE
FOR FAB
1
2
3
4
5
6
7
8
RIDDLE STRUCTURAL DETAILING LLC.
7573 MERCER RD
BROWNSVILLE, TENNESSEE 38012
(731) 444-4464
(731) 779-3771

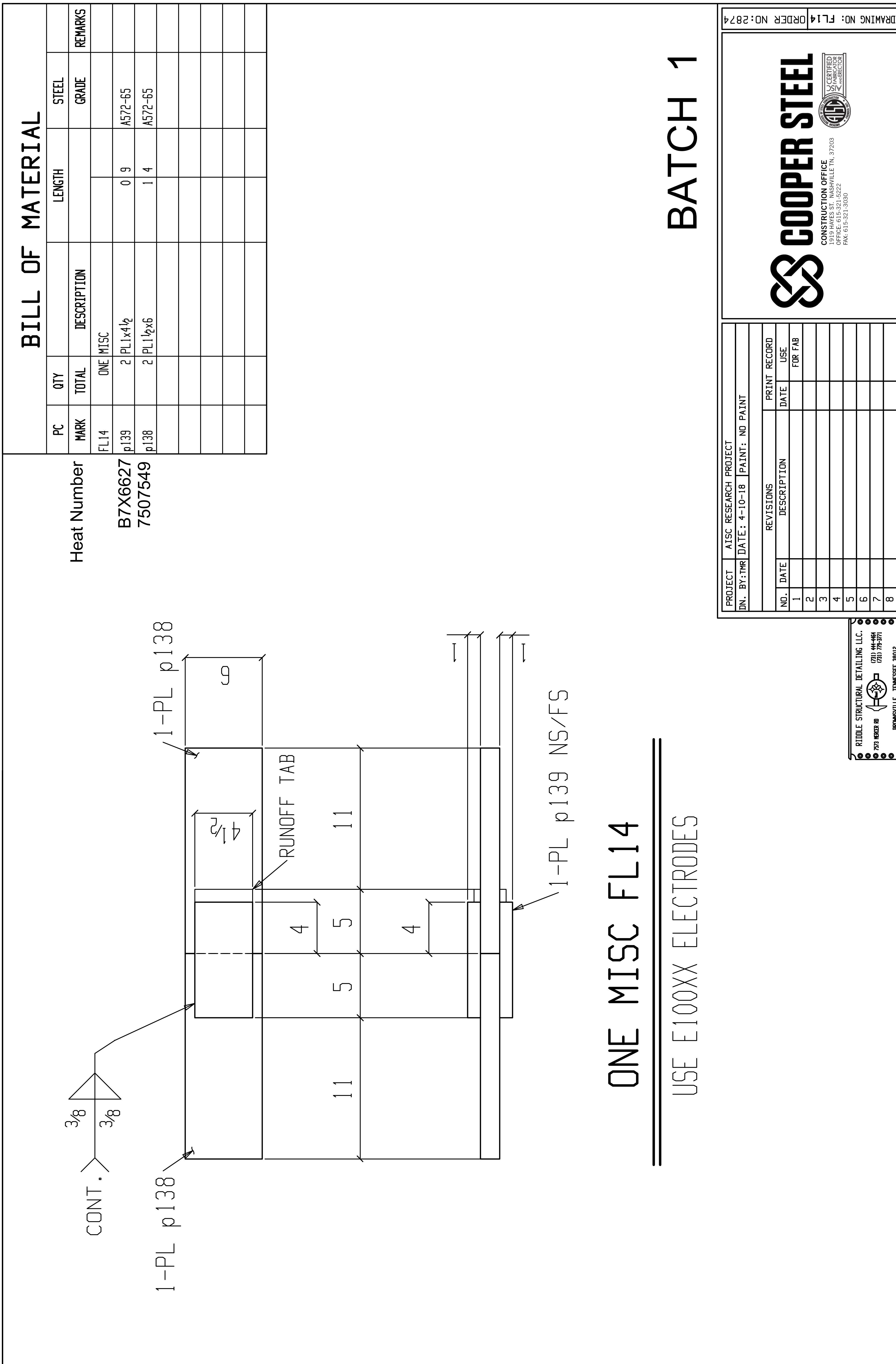
BILL OF MATERIAL
PC MARK | QTY TOTAL | DESCRIPTION | LENGTH | STEEL GRADE | REMARKS
FL14 | ONE | MISC
p139 | 2 | PL1x4½ | 0 9 | A572-65
p138 | 2 | PL1½x6 | 1 4 | A572-65
Heat Number
B7X6627
7507549
BATCH 1
DRAWING NO: FL14 ORDER NO:2874
COOPER STEEL
CONSTRUCTION OFFICE
1919 HAYES ST. NASHVILLE TN. 37203
OFFICE: 615-321-5222
FAX: 615-321-3030
CERTIFIED FABRICATOR and ERECTOR
PROJECT AISC RESEARCH PROJECT
DN. BY:TMR DATE: 4-10-18 PAINT: NO PAINT
REVISIONS
NO. DATE DESCRIPTION
1 2 3 4 5 6 7 8
PRINT RECORD
DATE USE
FOR FAB
RIDDLE STRUCTURAL DETAILING LLC.
7573 MERCER RD
BROWNSVILLE, TENNESSEE 38012
1-PL p138
6
4½
RUNOFF TAB
11
4
5
5
4
11
1-PL p139 NS/FS
1-PL p138
CONT.
3/8
3/8
ONE MISC FL14
USE E100XX ELECTRODES

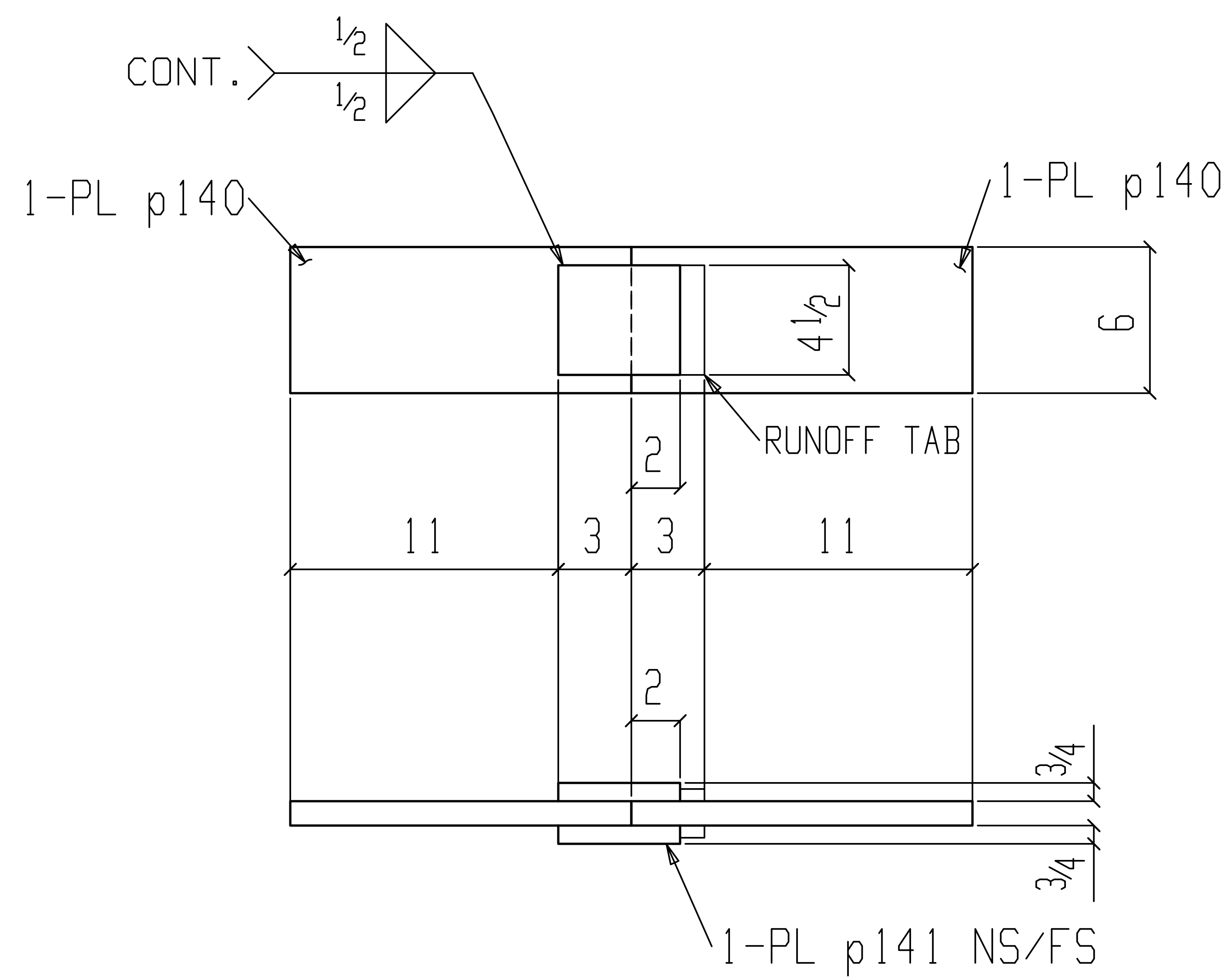

ONE MISC FL15

USE E100XX ELECTRODES

BILL OF MATERIAL

Heat Number	PC MARK	QTY TOTAL	DESCRIPTION	LENGTH		STEEL GRADE	REMARKS
	FL15	ONE	MISC				
W7H748	p141	2	PL3/4X4 1/2	0	5	A572-65	
B7X6627	p140	2	PL1x6	1	2	A572-65	

BATCH 1

PROJECT	AISC RESEARCH PROJECT	
DN. BY:TMR	DATE: 4-10-18	PAINT: NO PAINT

REVISIONS			PRINT RECORD	
NO.	DATE	DESCRIPTION	DATE	USE
1				FOR FAB
2				
3				
4				
5				
6				
7				
8				

COOPER STEEL
CONSTRUCTION OFFICE
1919 HAYES ST. NASHVILLE TN, 37203
OFFICE: 615-321-5222
FAX: 615-321-3030

AISC CERTIFIED FABRICATOR AND ERECTOR

DRAWING NO: FL15 ORDER NO:2874

RIDDLE STRUCTURAL DETAILING LLC.
7573 MERCER RD (731) 444-4464 (731) 779-3771
BROWNSVILLE, TENNESSEE 38012

BILL OF MATERIAL

Heat Number	PC MARK	QTY TOTAL	DESCRIPTION	LENGTH		STEEL GRADE	REMARKS
	FT1	ONE	MISC				
D5715	p1	2	PL1x2	1	2	A36	
D5715	p3	1	PL1x2	0	4	A36	

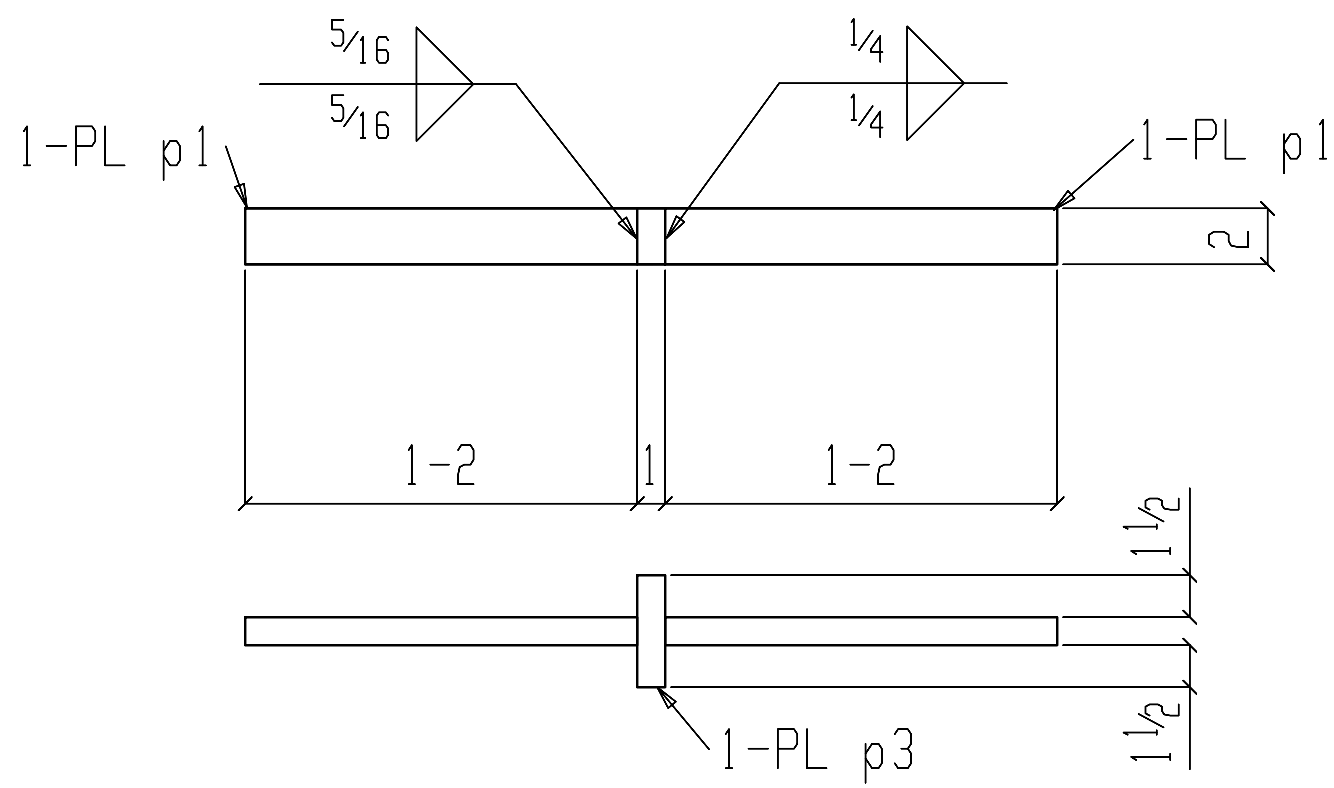

ONE MISC FT1

USE E70XX ELECTRODES

BATCH 1

PROJECT	AISC RESEARCH PROJECT	
DN. BY:TMR	DATE: 4-10-18	PAINT: NO PAINT

REVISIONS			PRINT RECORD	
NO.	DATE	DESCRIPTION	DATE	USE
1				FOR FAB
2				
3				
4				
5				
6				
7				
8				

RIDDLE STRUCTURAL DETAILING LLC.
7573 MERCER RD (731) 444-4464 (731) 779-3771
BROWNSVILLE, TENNESSEE 38012

COOPER STEEL
CONSTRUCTION OFFICE
1919 HAYES ST. NASHVILLE TN, 37203
OFFICE: 615-321-5222
FAX: 615-321-3030
AISC CERTIFIED FABRICATOR AND ERECTOR

DRAWING NO: FT1 ORDER NO:2874

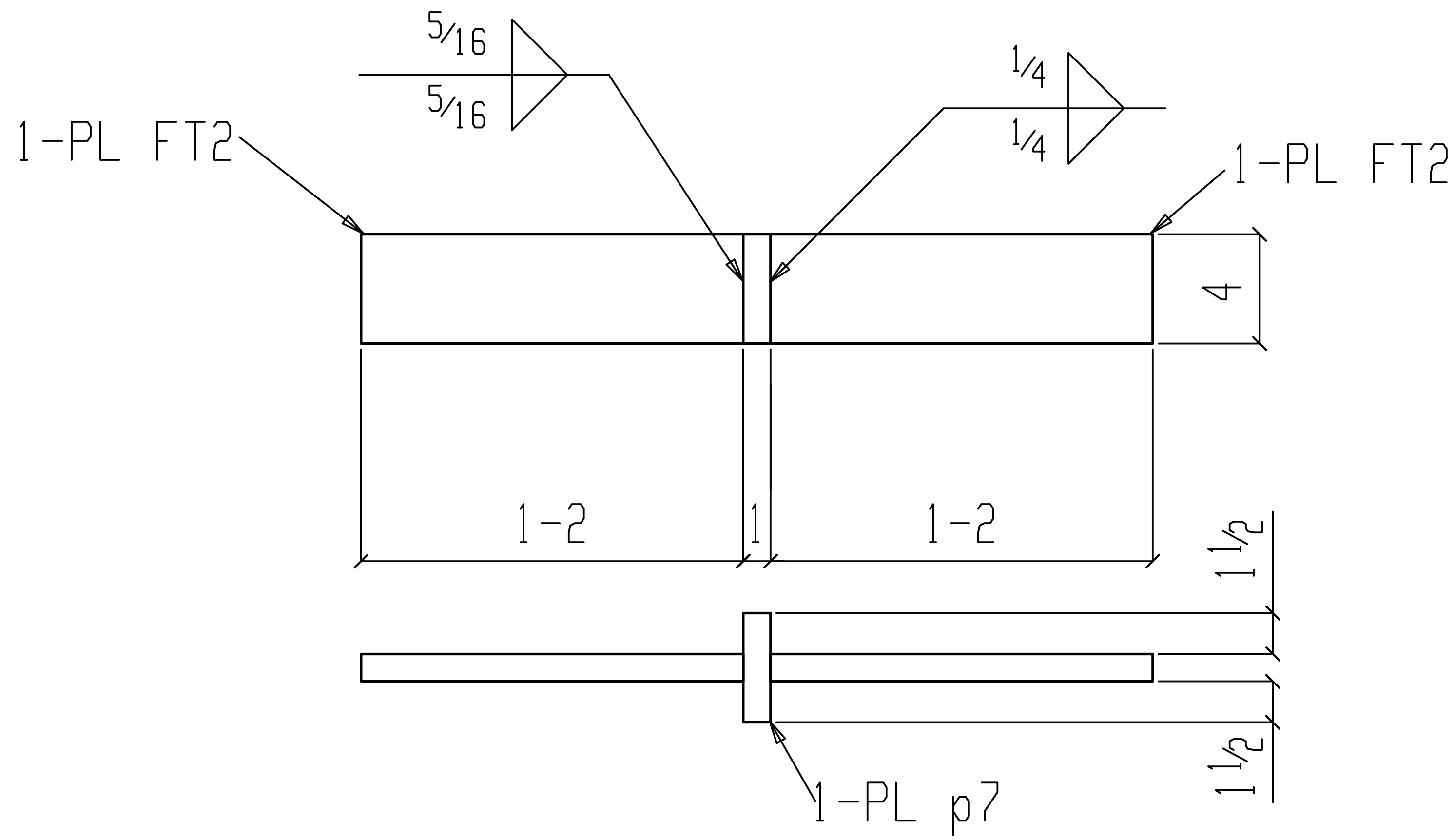

ONE MISC FT2

USE E70XX ELECTRODES

BILL OF MATERIAL

Heat Number	PC MARK	QTY TOTAL	DESCRIPTION	LENGTH		STEEL GRADE	REMARKS
	FT2	ONE	MISC				
D5715	FT2	2	PL1x4	1	2	A36	
D5715	p7	1	PL1x4	0	4	A36	

BATCH 1

PROJECT	AISC RESEARCH PROJECT			
DN. BY:TMR	DATE: 4-10-18	PAINT: NO PAINT		
REVISIONS			PRINT RECORD	
NO.	DATE	DESCRIPTION	DATE	USE
1				FOR FAB
2				
3				
4				
5				
6				
7				
8				

COOPER STEEL
CONSTRUCTION OFFICE
1919 HAYES ST. NASHVILLE TN, 37203
OFFICE: 615-321-5222
FAX: 615-321-3030
AISC CERTIFIED FABRICATOR AND ERECTOR

DRAWING NO: FT2 ORDER NO:2874

RIDDLE STRUCTURAL DETAILING LLC.
7573 MERCER RD
(731) 444-4464
(731) 779-3771
BROWNSVILLE, TENNESSEE 38012

BILL OF MATERIAL

Heat Number	PC MARK	QTY TOTAL	DESCRIPTION	LENGTH		STEEL GRADE	REMARKS
	FT3	ONE	MISC				
D5715	p5	2	PL1x6	1	2	A36	
D5715	p8	1	PL1x4	0	6	A36	

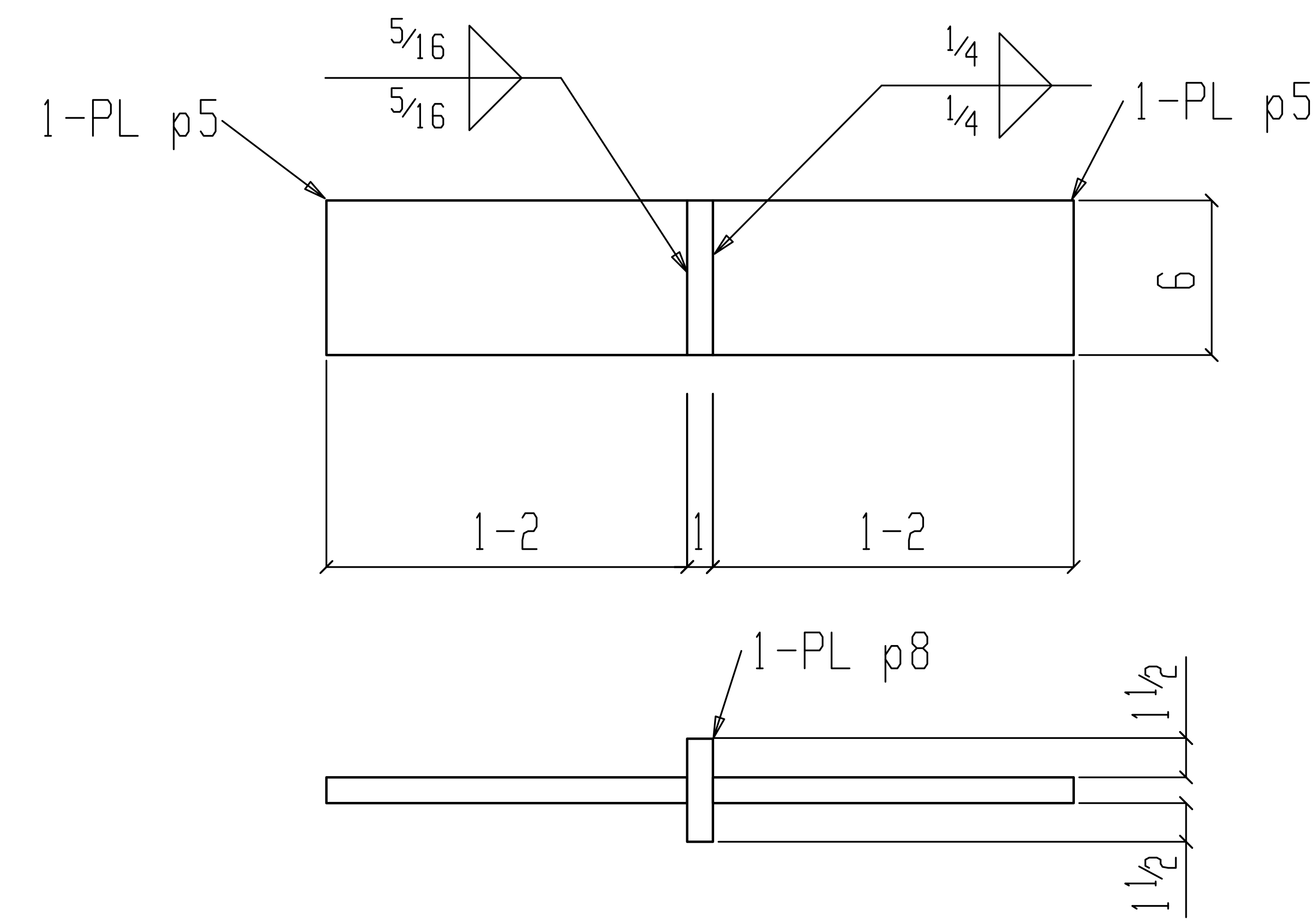

ONE MISC FT3

USE E70XX ELECTRODES

BATCH 1

RIDDLE STRUCTURAL DETAILING LLC.
7573 MERCER RD
(731) 444-4464
(731) 779-3771
BROWNSVILLE, TENNESSEE 38012

PROJECT	AISC RESEARCH PROJECT	
DN. BY:TMR	DATE: 4-10-18	PAINT: NO PAINT

REVISIONS			PRINT RECORD	
NO.	DATE	DESCRIPTION	DATE	USE
1				FOR FAB
2				
3				
4				
5				
6				
7				
8				

COOPER STEEL
CONSTRUCTION OFFICE
1919 HAYES ST. NASHVILLE TN, 37203
OFFICE: 615-321-5222
FAX: 615-321-3030
AISC CERTIFIED FABRICATOR AND ERECTOR

DRAWING NO: FT3 ORDER NO:2874

BILL OF MATERIAL

Heat Number	PC MARK	QTY TOTAL	DESCRIPTION	LENGTH		STEEL GRADE	REMARKS
	FT4	ONE	MISC				
7506515	p9	2	PL1¼x2	1	2	A36	
D5715	p15	1	PL1x2	0	4¼	A36	

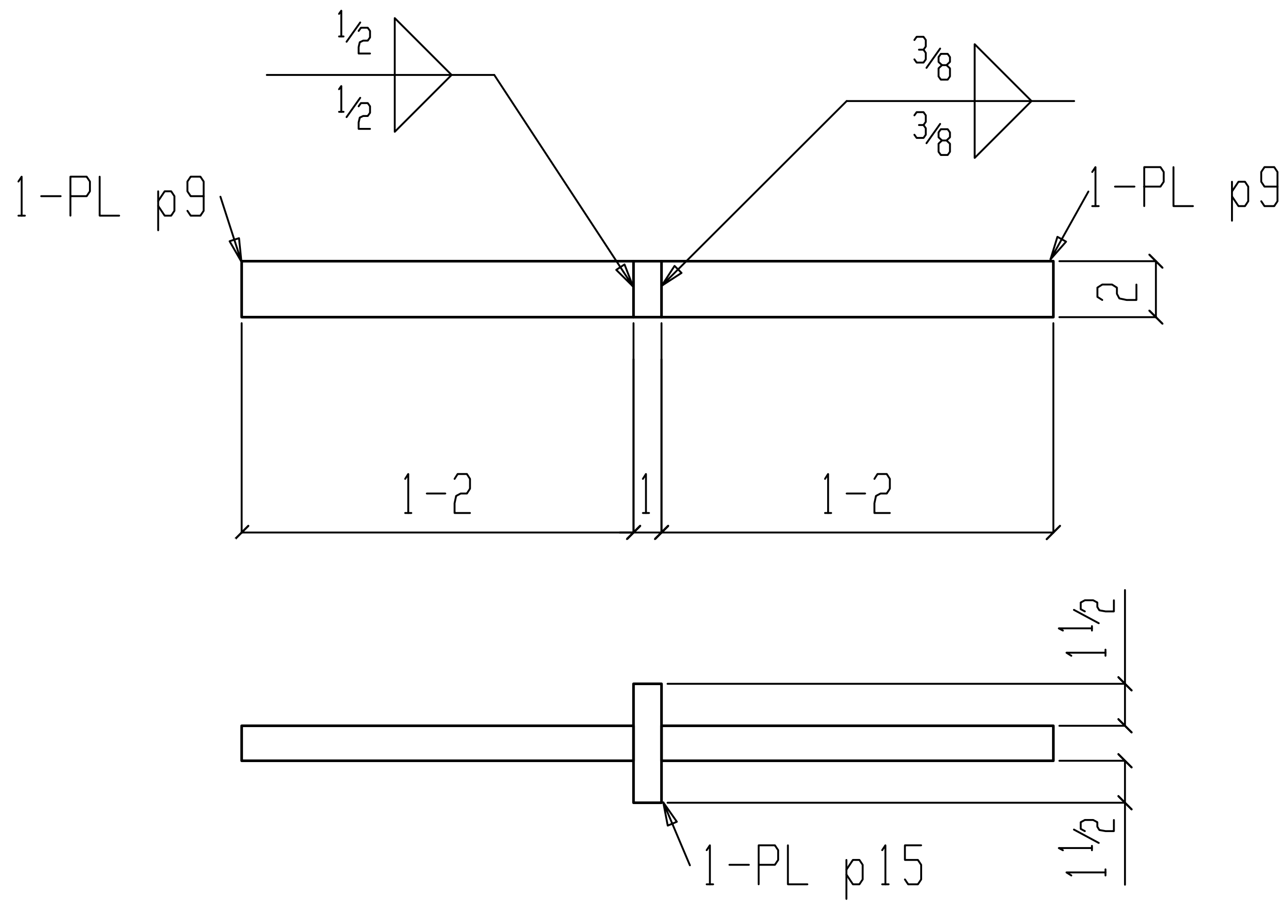

ONE MISC FT4

USE E70XX ELECTRODES

BATCH 1

PROJECT	AISC RESEARCH PROJECT	
DN. BY:TMR	DATE: 4-10-18	PAINT: NO PAINT

REVISIONS			PRINT RECORD	
NO.	DATE	DESCRIPTION	DATE	USE
1				FOR FAB
2				
3				
4				
5				
6				
7				
8				

RIDDLE STRUCTURAL DETAILING LLC.
7573 MERCER RD (731) 444-4464 (731) 779-3771
BROWNSVILLE, TENNESSEE 38012

COOPER STEEL
CONSTRUCTION OFFICE
1919 HAYES ST. NASHVILLE TN, 37203
OFFICE: 615-321-5222
FAX: 615-321-3030
AISC CERTIFIED FABRICATOR AND ERECTOR

DRAWING NO: FT4 ORDER NO:2874

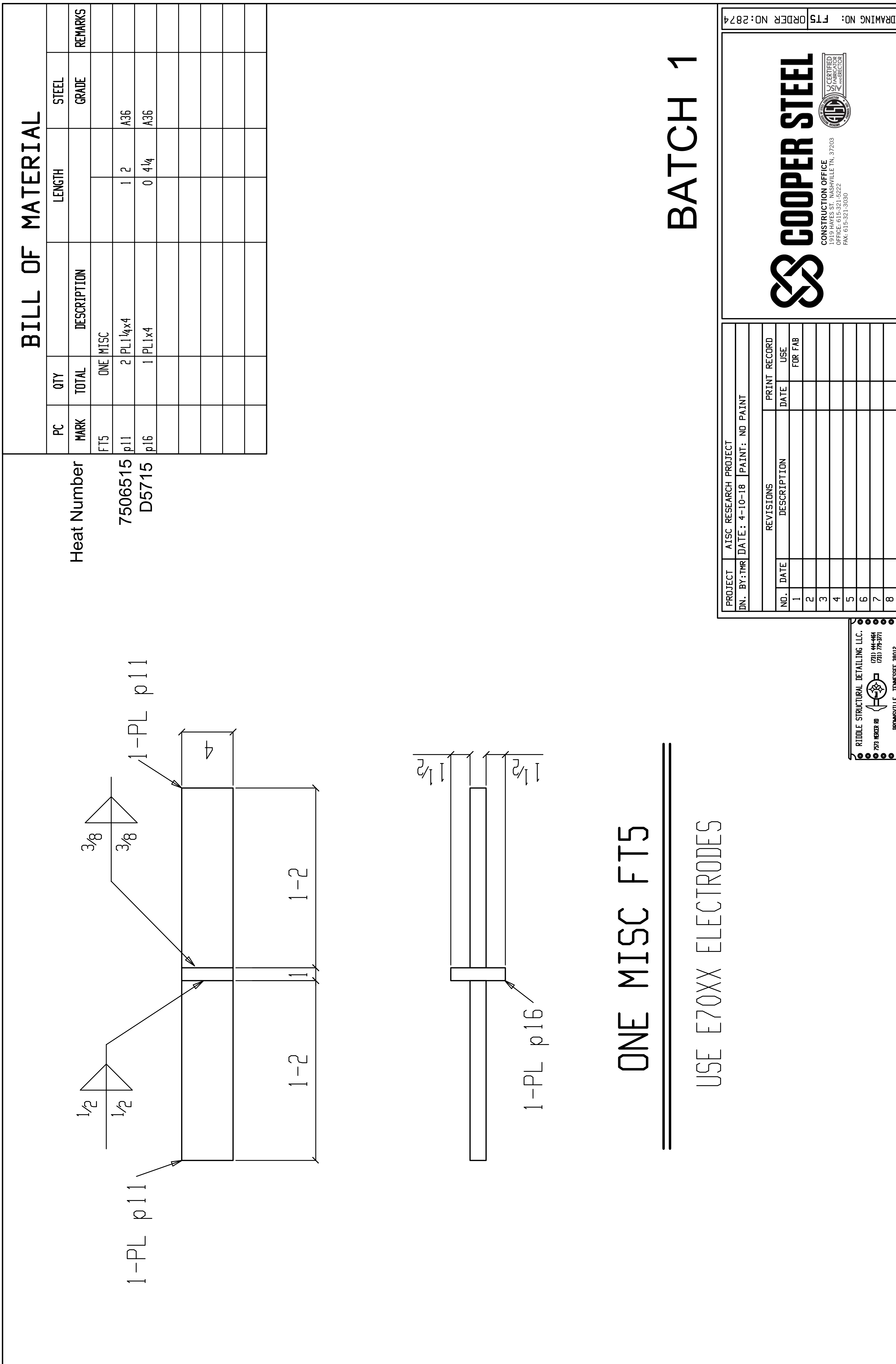
BILL OF MATERIAL
PC MARK | QTY TOTAL | DESCRIPTION | LENGTH | STEEL GRADE | REMARKS
FT5 | ONE | MISC
p11 | 2 | PL1¼x4 | 1 2 | A36
p16 | 1 | PL1x4 | 0 4¼ | A36
Heat Number
7506515
D5715
BATCH 1
DRAWING NO: FT5 ORDER NO:2874
COOPER STEEL
CONSTRUCTION OFFICE
1919 HAYES ST. NASHVILLE TN. 37203
OFFICE: 615-321-5222
FAX: 615-321-3030
CERTIFIED FABRICATOR and ERECTOR
PROJECT AISC RESEARCH PROJECT
DN. BY:TMR DATE: 4-10-18 PAINT: NO PAINT
REVISIONS
PRINT RECORD
NO. DATE DESCRIPTION
DATE USE
FOR FAB
1 2 3 4 5 6 7 8
RIDDLE STRUCTURAL DETAILING LLC.
7573 MERCER RD
(731) 444-4464
(731) 779-3771
BROWNSVILLE, TENNESSEE 38012
1-PL p11
4
3/8
3/8
1-2
1
1-2
1/2
1/2
1-PL p11
1½
1½
1-PL p16
ONE MISC FT5
USE E70XX ELECTRODES

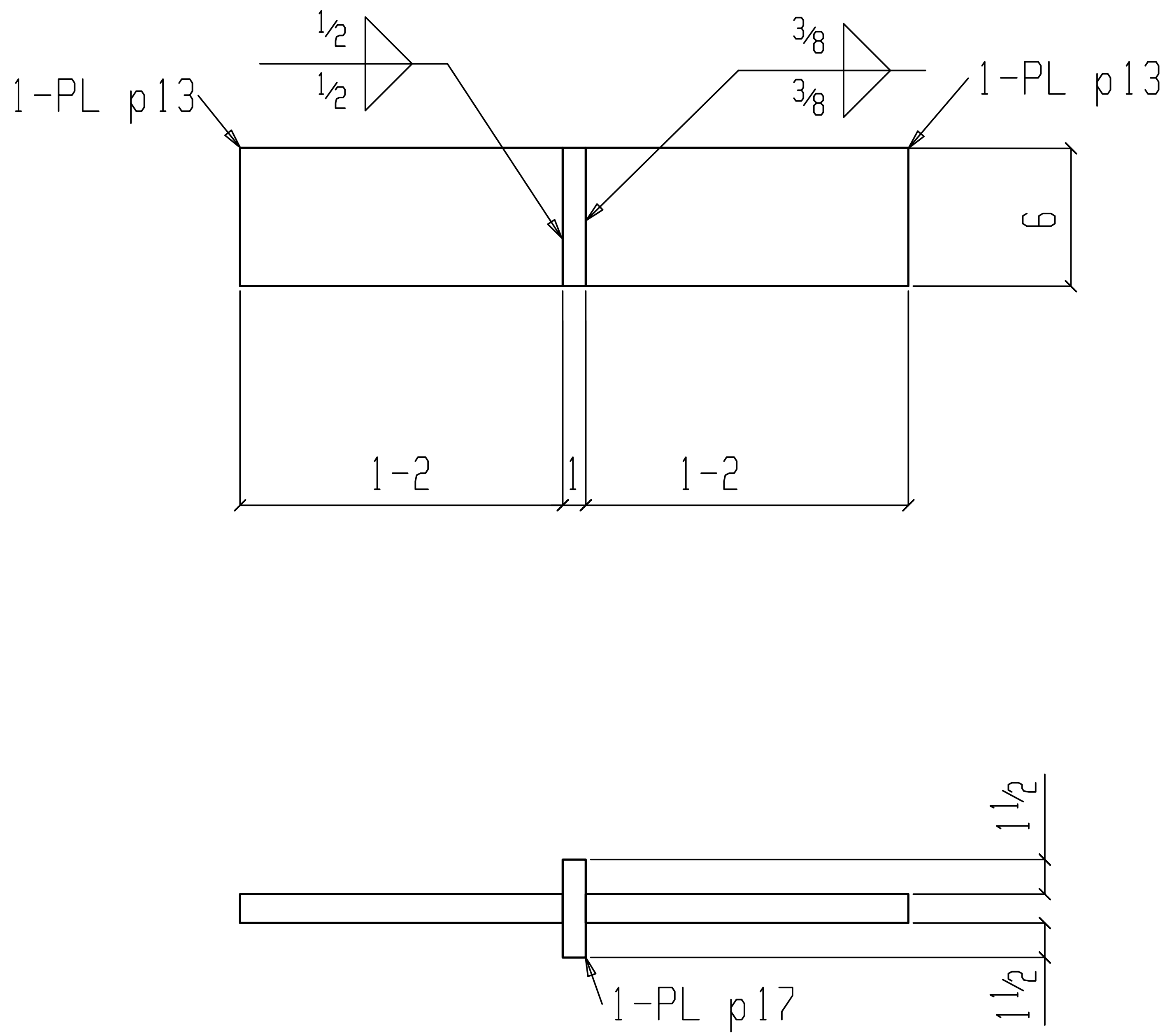

BILL OF MATERIAL

Heat Number	PC MARK	QTY TOTAL	DESCRIPTION	LENGTH		STEEL GRADE	REMARKS
	FT6	ONE	MISC				
7506515	p13	2	PL1¼x6	1	2	A36	
D5715	p17	1	PL1x4¼	0	6	A36	

BATCH 1

ONE MISC FT6

USE E70XX ELECTRODES

PROJECT	AISC RESEARCH PROJECT			
DN. BY:TMR	DATE: 4-10-18	PAINT: NO PAINT		
REVISIONS			PRINT RECORD	
NO.	DATE	DESCRIPTION	DATE	USE
1				FOR FAB
2				
3				
4				
5				
6				
7				
8				

COOPER STEEL
CONSTRUCTION OFFICE
1919 HAYES ST. NASHVILLE TN, 37203
OFFICE: 615-321-5222
FAX: 615-321-3030

AISC CERTIFIED FABRICATOR AND ERECTOR

DRAWING NO: FT6 ORDER NO:2874

RIDDLE STRUCTURAL DETAILING LLC.
7573 MERCER RD
(731) 444-4464
(731) 779-3771
BROWNSVILLE, TENNESSEE 38012

BILL OF MATERIAL

Heat Number	PC MARK	QTY TOTAL	DESCRIPTION	LENGTH		STEEL GRADE	REMARKS
	FT7	ONE	MISC				
7506393	p18	2	PL1¾x2	1	2	A36	
D5715	p20	1	PL1x2	0	4¾	A36	

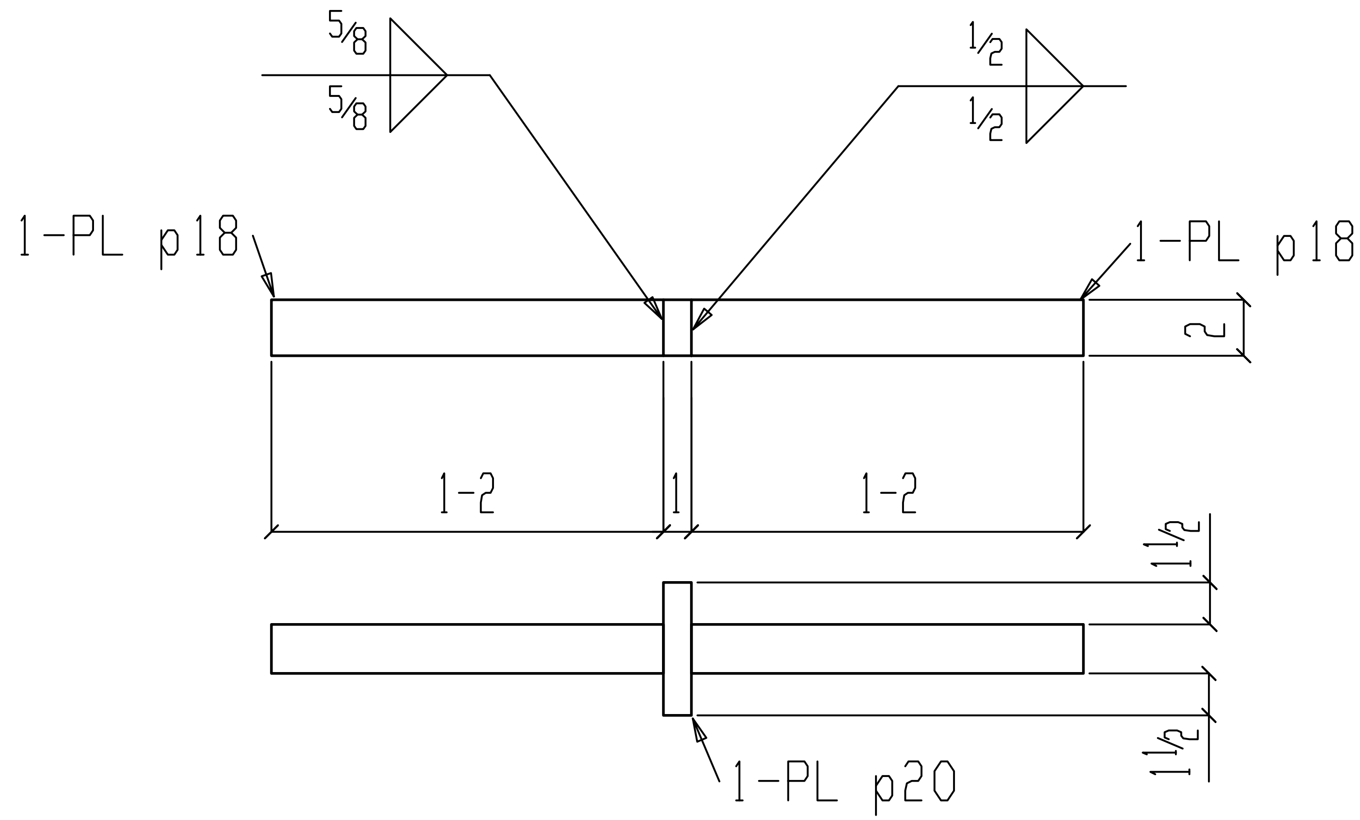

ONE MISC FT7

USE E70XX ELECTRODES

BATCH 1

PROJECT	AISC RESEARCH PROJECT	
DN. BY:TMR	DATE: 4-10-18	PAINT: NO PAINT

REVISIONS			PRINT RECORD	
NO.	DATE	DESCRIPTION	DATE	USE
1				FOR FAB
2				
3				
4				
5				
6				
7				
8				

COOPER STEEL
CONSTRUCTION OFFICE
1919 HAYES ST. NASHVILLE TN, 37203
OFFICE: 615-321-5222
FAX: 615-321-3030
AISC CERTIFIED FABRICATOR AND ERECTOR

DRAWING NO: FT7 ORDER NO:2874

RIDDLE STRUCTURAL DETAILING LLC.
7573 MERCER RD (731) 444-4464 (731) 779-3771
BROWNSVILLE, TENNESSEE 38012

BILL OF MATERIAL

Heat Number	PC MARK	QTY TOTAL	DESCRIPTION	LENGTH		STEEL GRADE	REMARKS
	FT8	ONE	MISC				
7506393	p21	2	PL1¾x4	1	2	A36	
D5715	p22	1	PL1x4	0	4¾	A36	

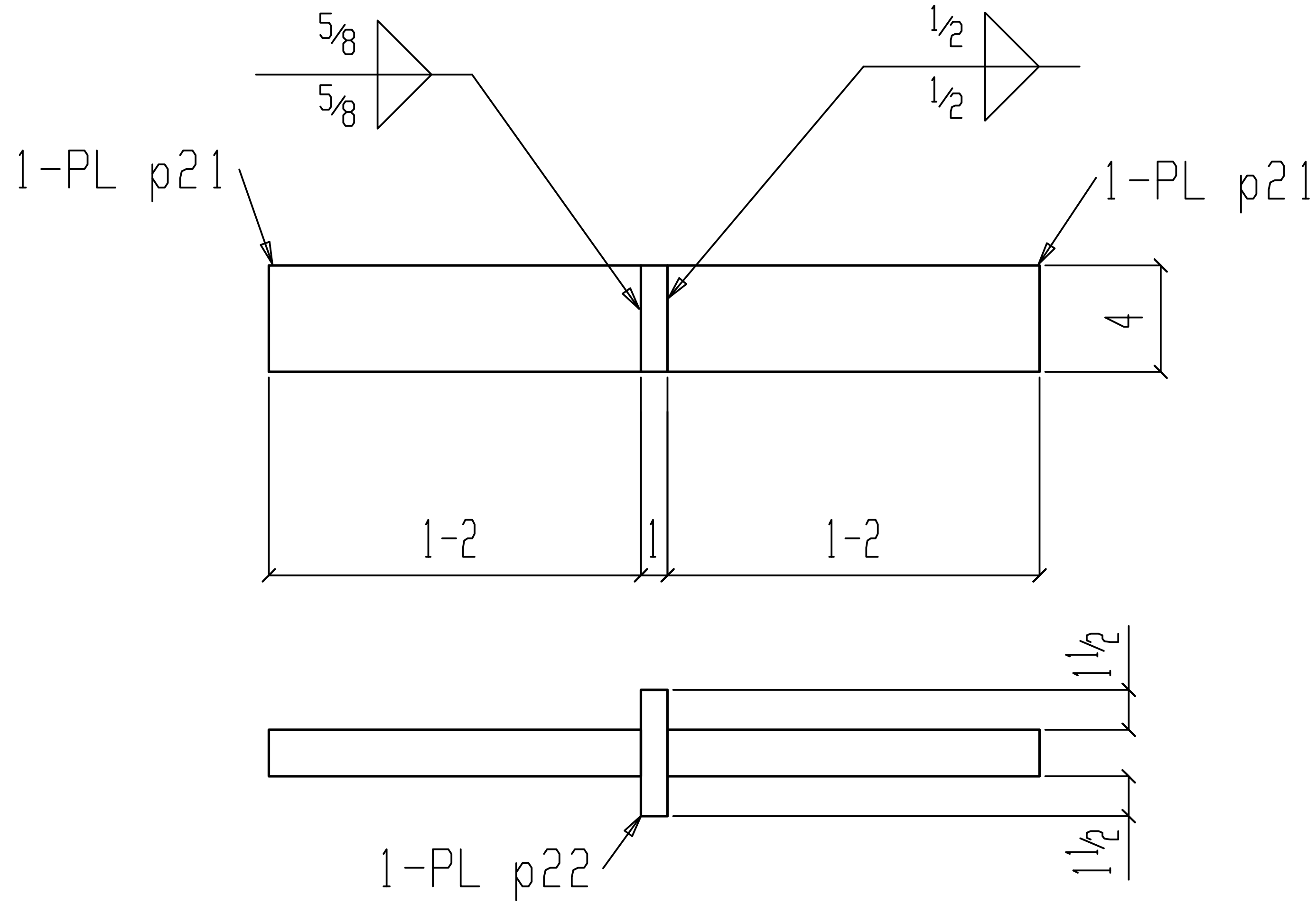

ONE MISC FT8

USE E70XX ELECTRODES

BATCH 1

PROJECT	AISC RESEARCH PROJECT	
DN. BY:TMR	DATE: 4-10-18	PAINT: NO PAINT

REVISIONS			PRINT RECORD	
NO.	DATE	DESCRIPTION	DATE	USE
1				FOR FAB
2				
3				
4				
5				
6				
7				
8				

RIDDLE STRUCTURAL DETAILING LLC.
7573 MERCER RD (731) 444-4464 (731) 779-3771
BROWNSVILLE, TENNESSEE 38012

COOPER STEEL
CONSTRUCTION OFFICE
1919 HAYES ST. NASHVILLE TN, 37203
OFFICE: 615-321-5222
FAX: 615-321-3030
AISC CERTIFIED FABRICATOR AND ERECTOR

DRAWING NO: FT8 ORDER NO:2874

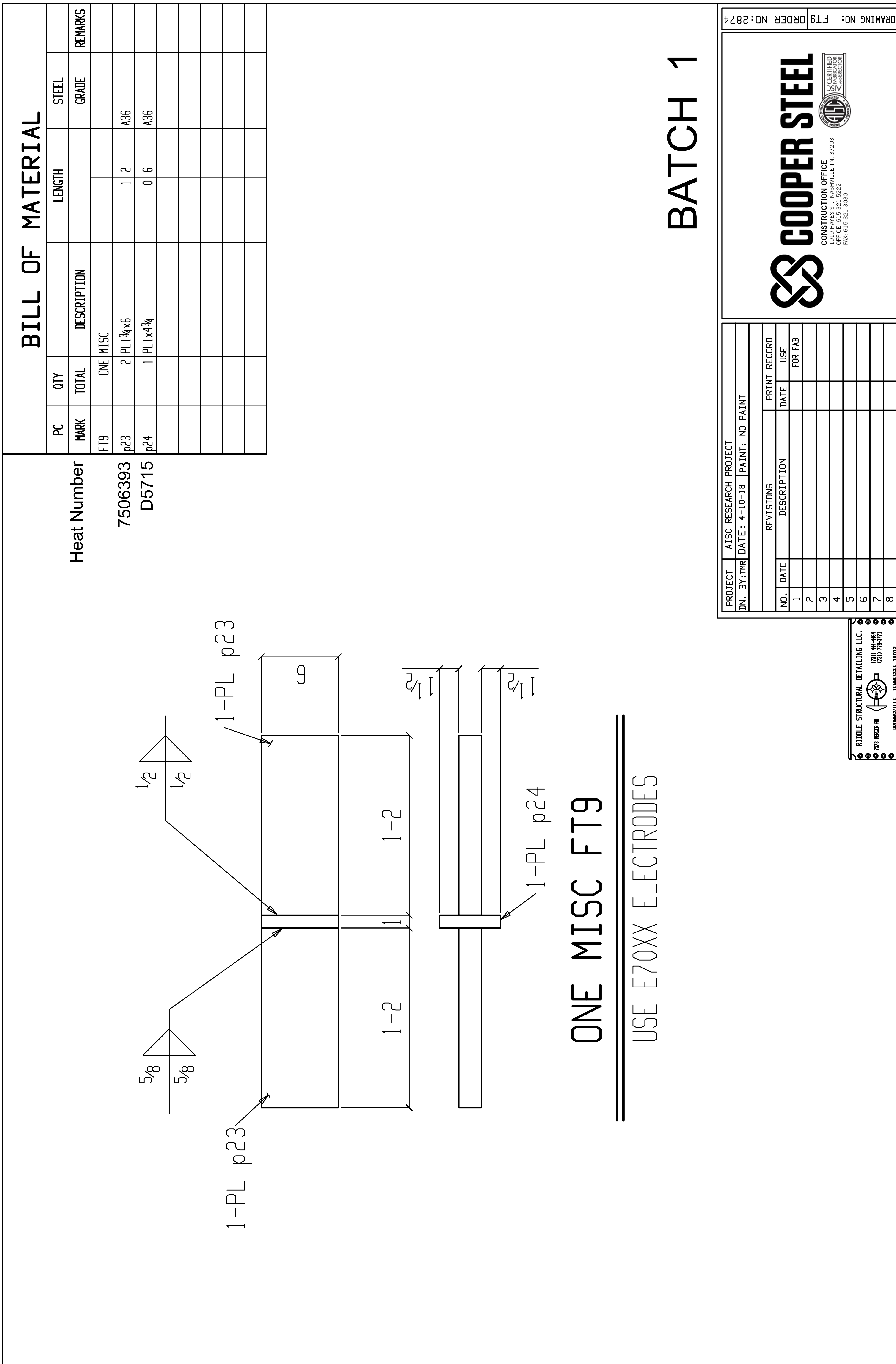
BILL OF MATERIAL
PC MARK | QTY TOTAL | DESCRIPTION | LENGTH | STEEL GRADE | REMARKS
FT9 | ONE | MISC
p23 | 2 | PL1¾x6 | 1 2 | A36
p24 | 1 | PL1x4¾ | 0 6 | A36
Heat Number
7506393
D5715
BATCH 1
DRAWING NO: FT9 ORDER NO:2874
COOPER STEEL
CONSTRUCTION OFFICE
1919 HAYES ST. NASHVILLE TN. 37203
OFFICE: 615-321-5222
FAX: 615-321-3030
CERTIFIED FABRICATOR and ERECTOR
PROJECT AISC RESEARCH PROJECT
DN. BY:TMR DATE: 4-10-18 PAINT: NO PAINT
REVISIONS
NO. DATE DESCRIPTION
PRINT RECORD
DATE USE
FOR FAB
1 2 3 4 5 6 7 8
RIDDLE STRUCTURAL DETAILING LLC.
7573 MERCER RD
BROWNSVILLE, TENNESSEE 38012
(731) 444-4464
(731) 779-3771
1-PL p23
6
1½
1½
½
½
1-2
1
1-PL p24
5/8
5/8
1-2
1-PL p23
ONE MISC FT9
USE E70XX ELECTRODES

BILL OF MATERIAL

Heat Number	PC MARK	QTY TOTAL	DESCRIPTION	LENGTH		STEEL GRADE	REMARKS
	FT10	ONE	MISC				
B7X6627	p140	2	PL1x6	1	2	A572-65	
B7X6627	p142	1	PL1x4	0	6	A572-65	

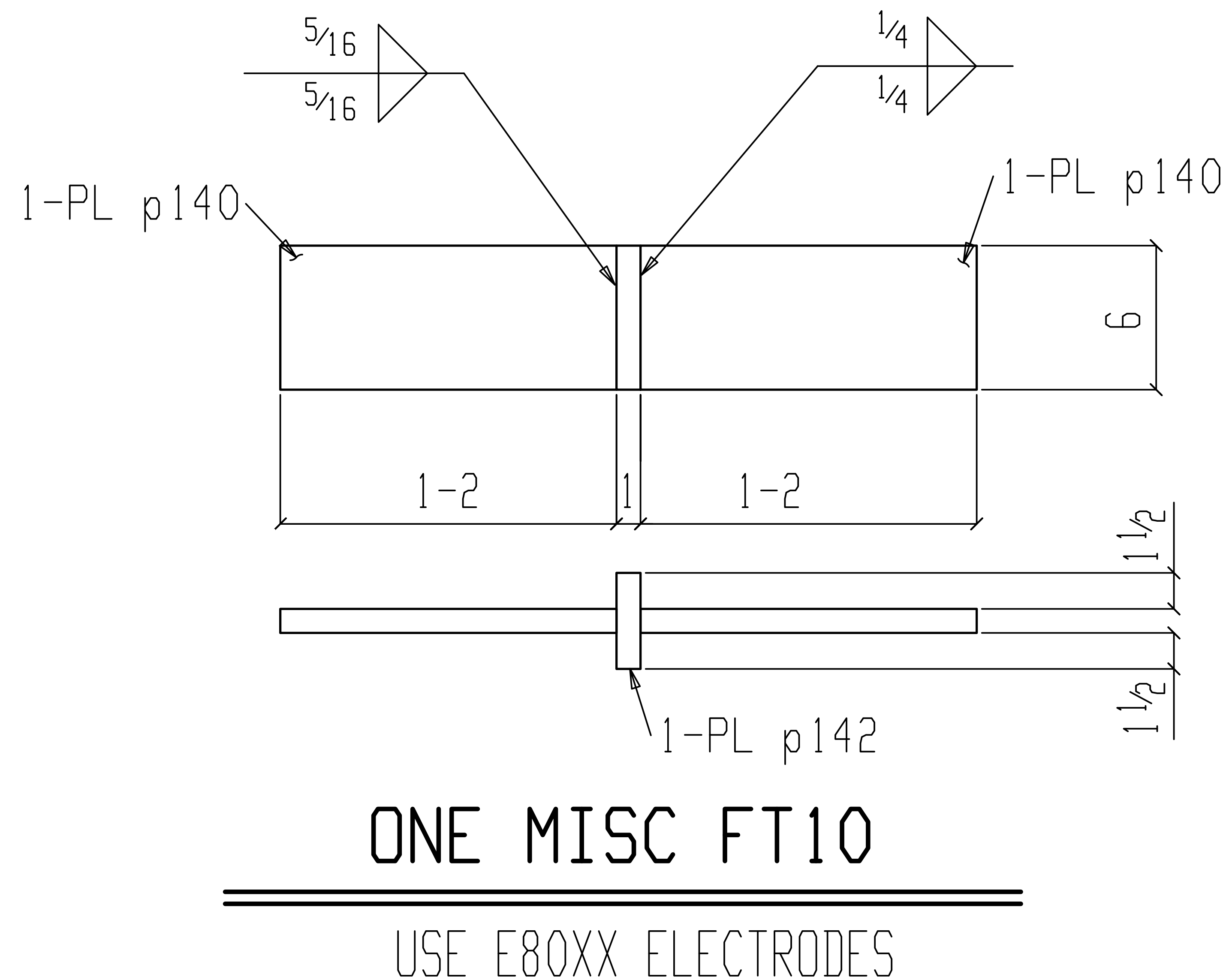

BATCH 1

PROJECT	AISC RESEARCH PROJECT	
DN. BY:TMR	DATE: 4-10-18	PAINT: NO PAINT

REVISIONS			PRINT RECORD	
NO.	DATE	DESCRIPTION	DATE	USE
1				FOR FAB
2				
3				
4				
5				
6				
7				
8				

COOPER STEEL
CONSTRUCTION OFFICE
1919 HAYES ST. NASHVILLE TN, 37203
OFFICE: 615-321-5222
FAX: 615-321-3030
AISC CERTIFIED FABRICATOR AND ERECTOR

DRAWING NO: FT10 ORDER NO:2874

RIDDLE STRUCTURAL DETAILING LLC.
7573 MERCER RD
(731) 444-4464
(731) 779-3771
BROWNSVILLE, TENNESSEE 38012

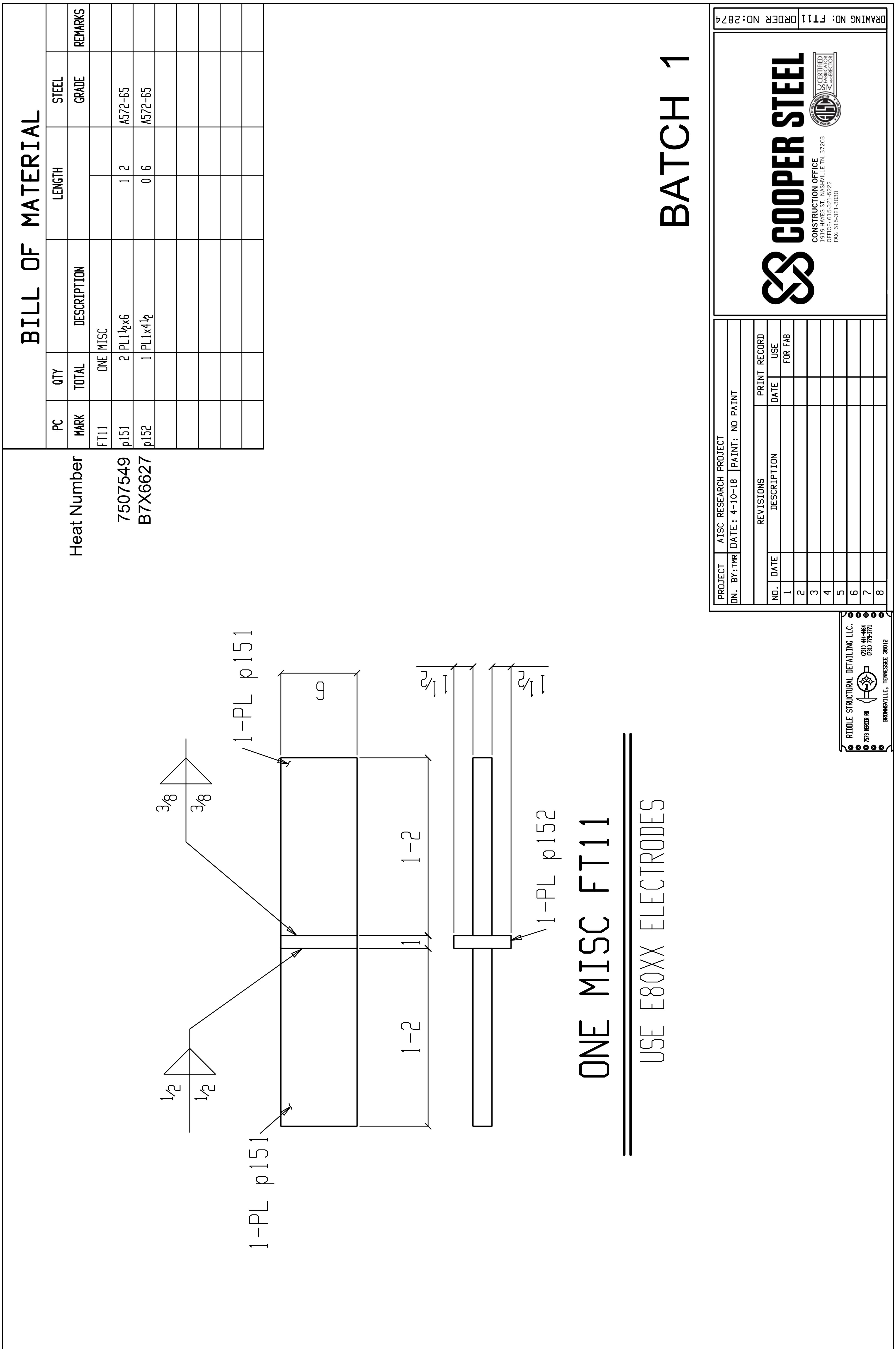
BILL OF MATERIAL
PC MARK | QTY TOTAL | DESCRIPTION | LENGTH | STEEL GRADE | REMARKS
FT11 | ONE | MISC
p151 | 2 | PL1½x6 | 1 2 | A572-65
p152 | 1 | PL1x4½ | 0 6 | A572-65
Heat Number
7507549
B7X6627
BATCH 1
1-PL p151
1-PL p152
3/8 3/8
1/2 1/2
6
1-2
1
1 1/2
ONE MISC FT11
USE E80XX ELECTRODES
DRAWING NO: FT11
ORDER NO:2874
COOPER STEEL
CONSTRUCTION OFFICE
1919 HAYES ST. NASHVILLE TN, 37203
OFFICE: 615-321-5222
FAX: 615-321-3030
CERTIFIED FABRICATOR and ERECTOR
PROJECT AISC RESEARCH PROJECT
DN. BY:TMR DATE: 4-10-18 PAINT: NO PAINT
REVISIONS
PRINT RECORD
NO. DATE DESCRIPTION DATE USE
FOR FAB
1 2 3 4 5 6 7 8
RIDDLE STRUCTURAL DETAILING LLC.
7573 MERCER RD
BROWNSVILLE, TENNESSEE 38012
(731) 444-4464
(731) 779-3771

BILL OF MATERIAL

Heat Number	PC MARK	QTY TOTAL	DESCRIPTION	LENGTH		STEEL GRADE	REMARKS
	FT12	ONE	MISC				
D2290	p143	2	PL2x4	1	2	A572-65	
B7X6627	p144	1	PL1x4	0	5	A572-65	

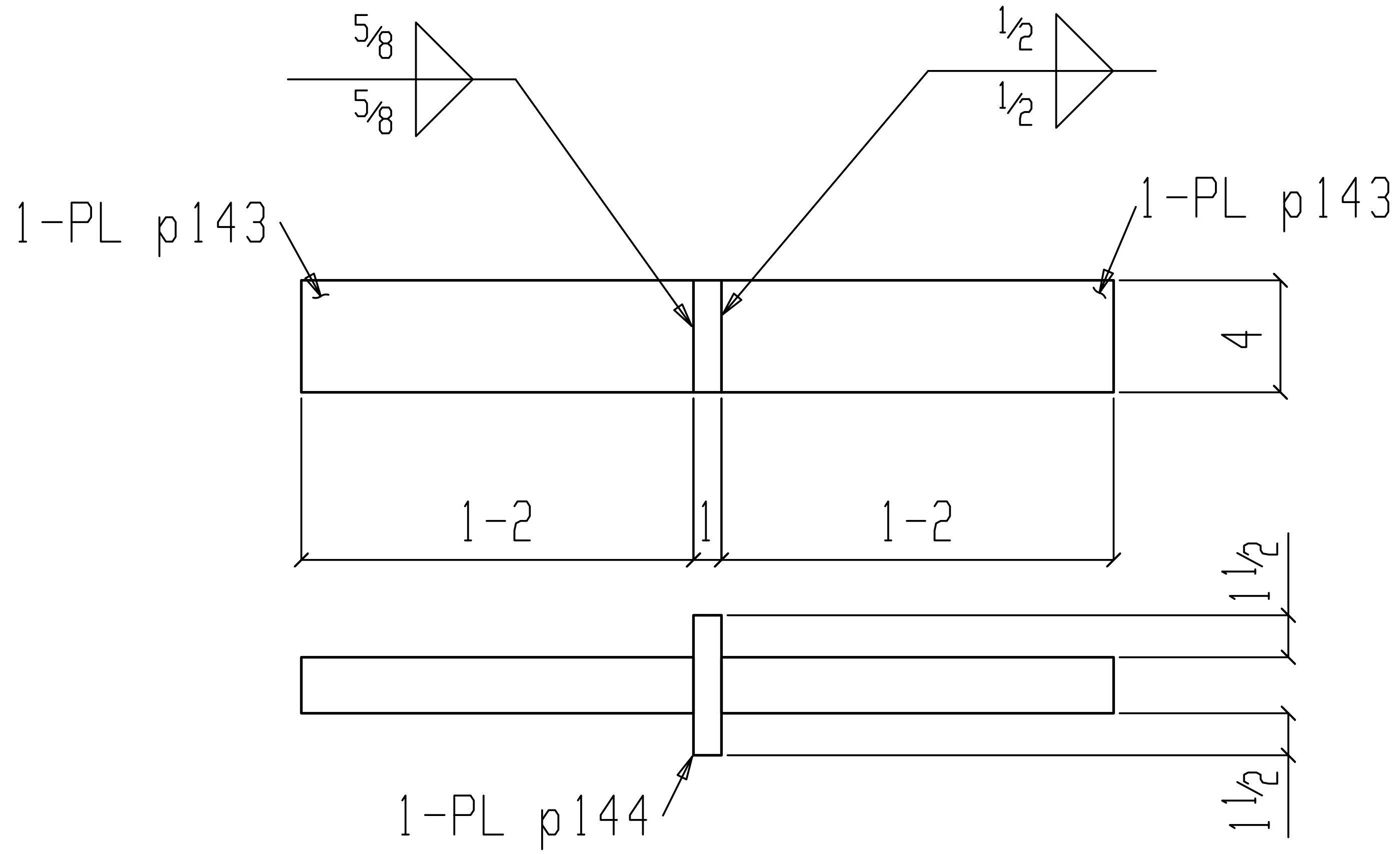

ONE MISC FT12

USE E80XX ELECTRODES

BATCH 1

PROJECT	AISC RESEARCH PROJECT			
DN. BY:TMR	DATE: 4-10-18	PAINT: NO PAINT		
	REVISIONS		PRINT RECORD	
NO.	DATE	DESCRIPTION	DATE	USE
1				FOR FAB
2				
3				
4				
5				
6				
7				
8				

RIDDLE STRUCTURAL DETAILING LLC.
7573 MERCER RD (731) 444-4464 (731) 779-3771
BROWNSVILLE, TENNESSEE 38012

COOPER STEEL
CONSTRUCTION OFFICE
1919 HAYES ST. NASHVILLE TN, 37203
OFFICE: 615-321-5222
FAX: 615-321-3030
AISC CERTIFIED FABRICATOR AND ERECTOR

DRAWING NO: FT12 | ORDER NO:2874

BILL OF MATERIAL

Heat Number	PC MARK	QTY TOTAL	DESCRIPTION	LENGTH		STEEL GRADE	REMARKS
	FT13	ONE	MISC				
W7H748	p153	2	PL1¼x2	1	2	A572-65	
B7X6627	p154	1	PL1x2	0	4¼	A572-65	

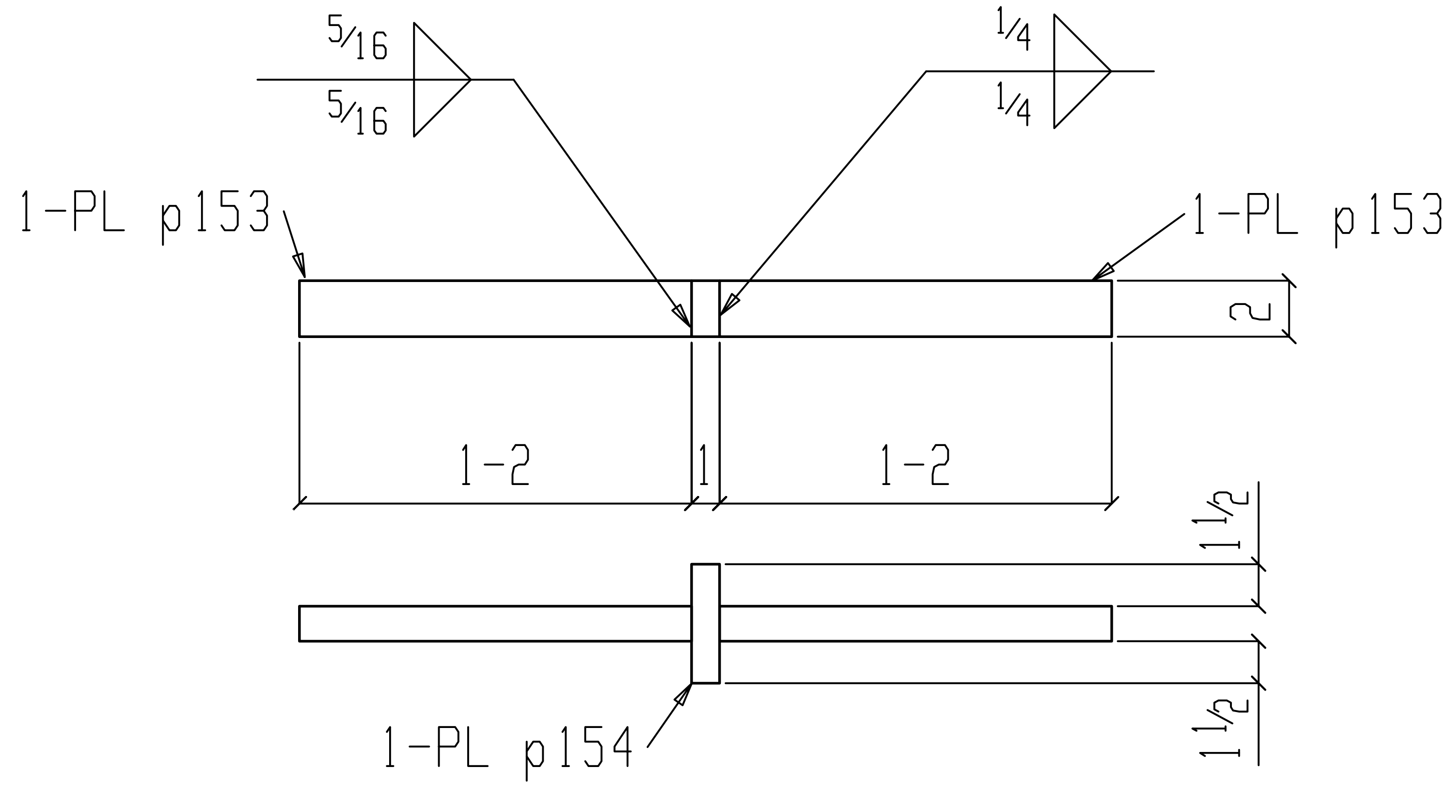

ONE MISC FT13

USE E100XX ELECTRODES

BATCH 1

PROJECT	AISC RESEARCH PROJECT		
DN. BY:TMR	DATE: 4-10-18	PAINT: NO PAINT	

REVISIONS			PRINT RECORD	
NO.	DATE	DESCRIPTION	DATE	USE
1				FOR FAB
2				
3				
4				
5				
6				
7				
8				

COOPER STEEL
CONSTRUCTION OFFICE
1919 HAYES ST. NASHVILLE TN, 37203
OFFICE: 615-321-5222
FAX: 615-321-3030
AISC CERTIFIED FABRICATOR AND ERECTOR

DRAWING NO: FT13 ORDER NO:2874

RIDDLE STRUCTURAL DETAILING LLC.
7573 MERCER RD (731) 444-4464 (731) 779-3771
BROWNSVILLE, TENNESSEE 38012

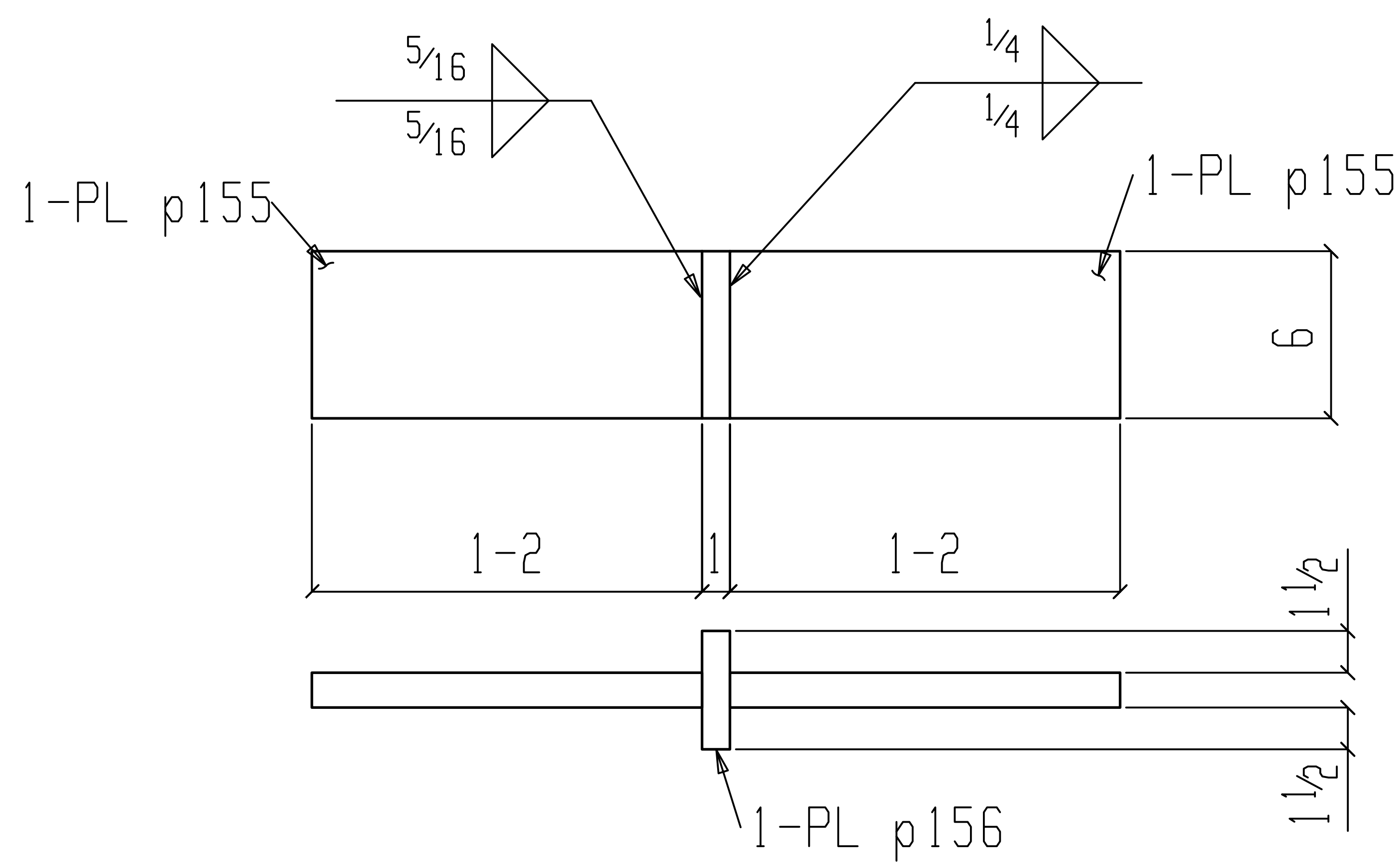

BILL OF MATERIAL

Heat Number	PC MARK	QTY TOTAL	DESCRIPTION	LENGTH		STEEL GRADE	REMARKS
	FT14	ONE	MISC				
W7H748	p155	2	PL1¼x6	1	2	A572-65	
B7X6627	p156	1	PL1x4¼	0	6	A572-65	

ONE MISC FT14

USE E100XX ELECTRODES

BATCH 1

RIDDLE STRUCTURAL DETAILING LLC.
7573 MERCER RD (731) 444-4464 (731) 779-3771
BROWNSVILLE, TENNESSEE 38012

PROJECT	AISC RESEARCH PROJECT			
DN. BY:TMR	DATE: 4-10-18	PAINT: NO PAINT		

REVISIONS			PRINT RECORD	
NO.	DATE	DESCRIPTION	DATE	USE
1				FOR FAB
2				
3				
4				
5				
6				
7				
8				

COOPER STEEL
CONSTRUCTION OFFICE
1919 HAYES ST. NASHVILLE TN, 37203
OFFICE: 615-321-5222
FAX: 615-321-3030
AISC CERTIFIED FABRICATOR AND ERECTOR

DRAWING NO: FT14 ORDER NO:2874

BILL OF MATERIAL

Heat Number	PC MARK	QTY TOTAL	DESCRIPTION	LENGTH		STEEL GRADE	REMARKS
	FT15	ONE	MISC				
D2044	p157	2	PL1¾x2	1	2	A572-65	
B7X6627	p158	1	PL1x2	0	4¾	A572-65	

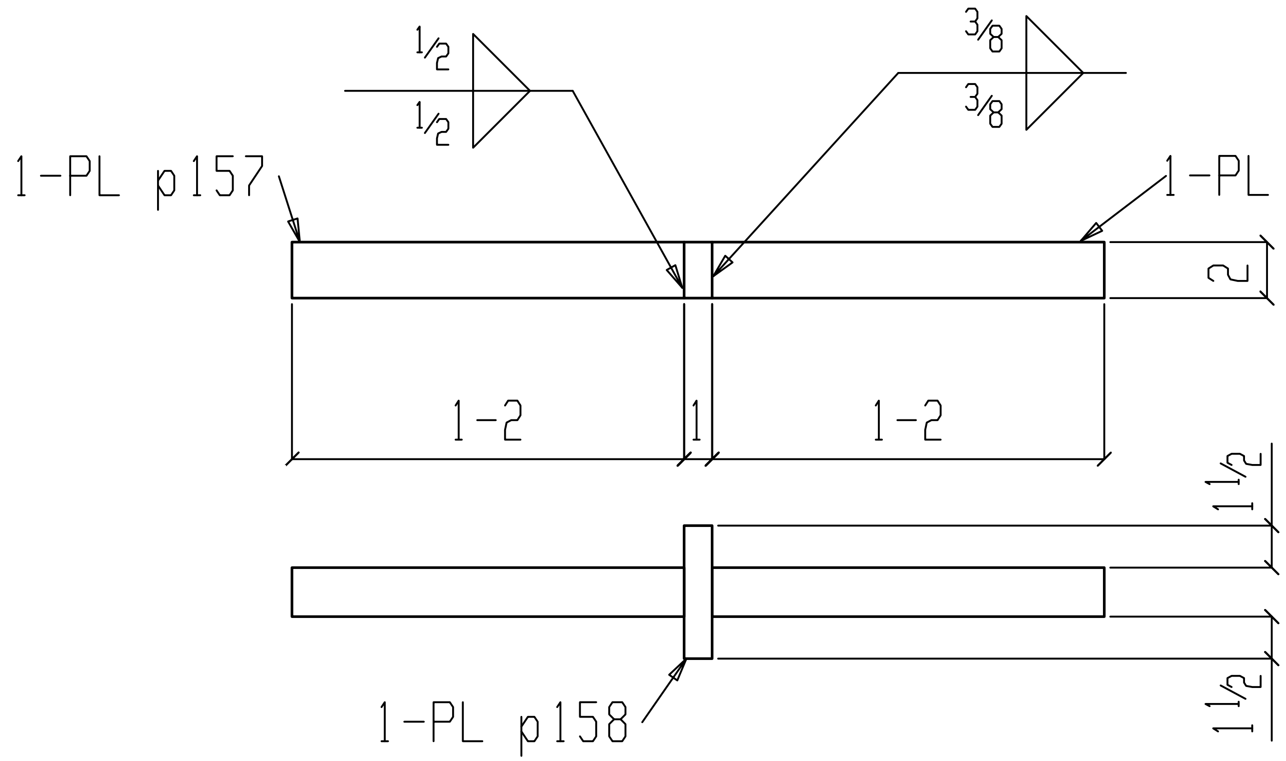

ONE MISC FT15

USE E100XX ELECTRODES

BATCH 1

RIDDLE STRUCTURAL DETAILING LLC.
7573 MERCER RD (731) 444-4464 (731) 779-3771
BROWNSVILLE, TENNESSEE 38012

PROJECT	AISC RESEARCH PROJECT	
DN. BY:TMR	DATE: 4-10-18	PAINT: NO PAINT

REVISIONS			PRINT RECORD	
NO.	DATE	DESCRIPTION	DATE	USE
1				FOR FAB
2				
3				
4				
5				
6				
7				
8				

COOPER STEEL
CONSTRUCTION OFFICE
1919 HAYES ST. NASHVILLE TN, 37203
OFFICE: 615-321-5222
FAX: 615-321-3030
AISC CERTIFIED FABRICATOR AND ERECTOR

DRAWING NO: FT15 ORDER NO:2874

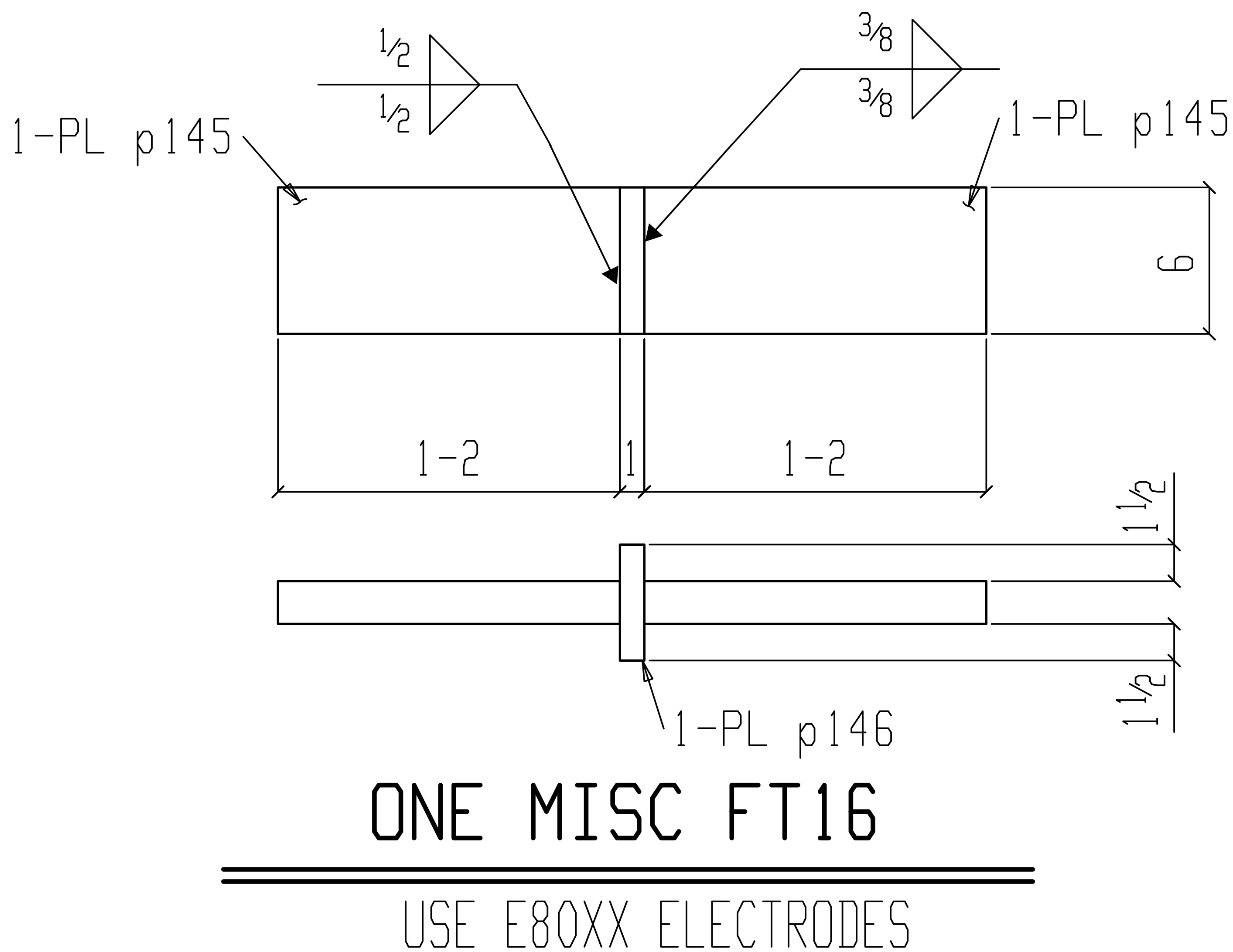

BILL OF MATERIAL

Heat Number	PC MARK	QTY TOTAL	DESCRIPTION	LENGTH		STEEL GRADE	REMARKS
	FT16	ONE	MISC				
D2044	p145	2	PL1¾x6	1	2	A572-65	
B7X6627	p146	1	PL1x4¾	0	6	A572-65	

BATCH 1

PROJECT	AISC RESEARCH PROJECT	
DN. BY:TMR	DATE: 4-10-18	PAINT: NO PAINT

REVISIONS			PRINT RECORD	
NO.	DATE	DESCRIPTION	DATE	USE
1				FOR FAB
2				
3				
4				
5				
6				
7				
8				

RIDDLE STRUCTURAL DETAILING LLC.
7573 MERCER RD
(731) 444-4464
(731) 779-3771
BROWNSVILLE, TENNESSEE 38012

COOPER STEEL
CONSTRUCTION OFFICE
1919 HAYES ST. NASHVILLE TN, 37203
OFFICE: 615-321-5222
FAX: 615-321-3030
AISC CERTIFIED FABRICATOR AND ERECTOR

DRAWING NO: FT16 ORDER NO:2874

BILL OF MATERIAL

Heat Number	PC MARK	QTY TOTAL	DESCRIPTION	LENGTH		STEEL GRADE	REMARKS
	FT17	ONE	MISC				
D2290	p159	2	PL2x2	1	2	A572-65	
B7X6627	p160	1	PL1x2	0	5	A572-65	

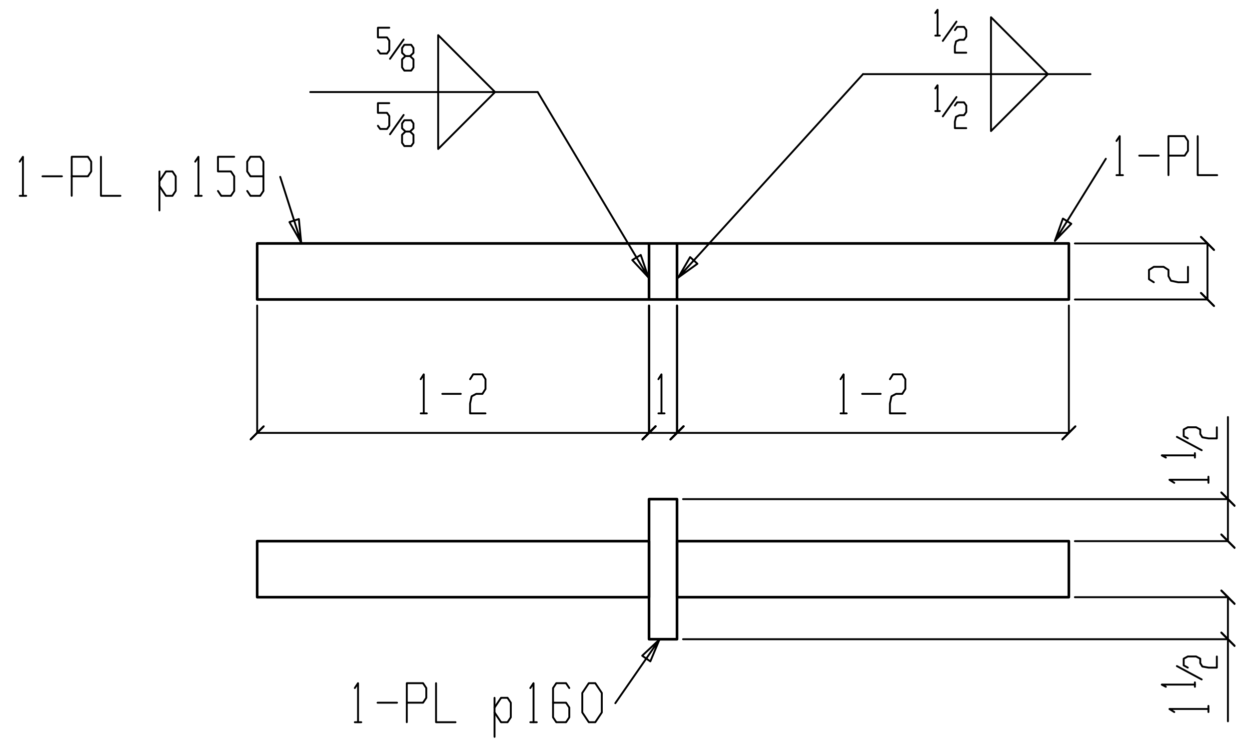

ONE MISC FT17

USE E100XX ELECTRODES

BATCH 1

PROJECT	AISC RESEARCH PROJECT	
DN. BY:TMR	DATE: 4-10-18	PAINT: NO PAINT

REVISIONS			PRINT RECORD	
NO.	DATE	DESCRIPTION	DATE	USE
1				FOR FAB
2				
3				
4				
5				
6				
7				
8				

RIDDLE STRUCTURAL DETAILING LLC.
7573 MERCER RD (731) 444-4464 (731) 779-3771
BROWNSVILLE, TENNESSEE 38012

COOPER STEEL
CONSTRUCTION OFFICE
1919 HAYES ST. NASHVILLE TN, 37203
OFFICE: 615-321-5222
FAX: 615-321-3030
AISC CERTIFIED FABRICATOR AND ERECTOR

DRAWING NO: FT17 ORDER NO:2874

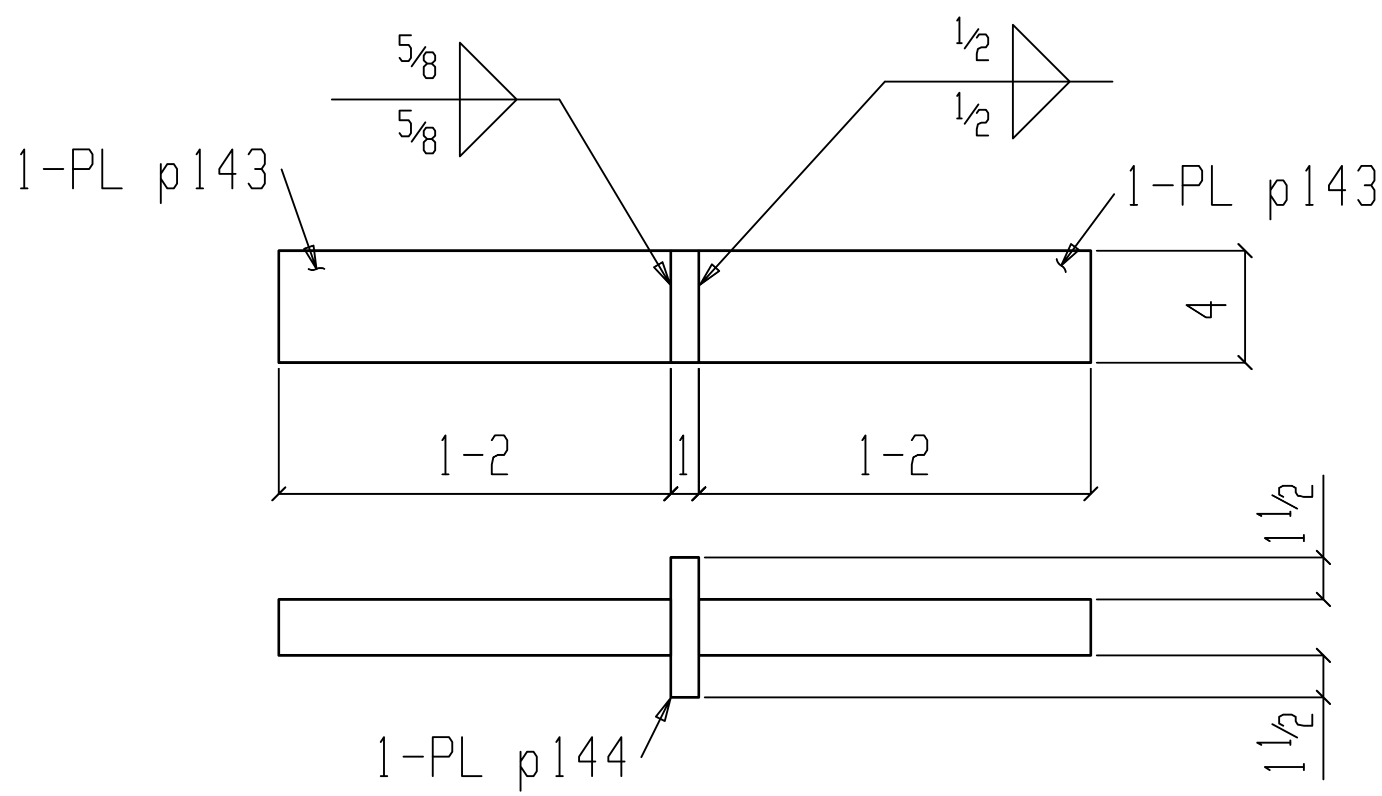

ONE MISC FT18

USE E100XX ELECTRODES

BILL OF MATERIAL

Heat Number	PC MARK	QTY TOTAL	DESCRIPTION	LENGTH		STEEL GRADE	REMARKS
	FT18	ONE	MISC				
D2290	FT18	1	PL2x4	1	2	A572-65	
D2290	p143	1	PL2x4	1	2	A572-65	
B7X6627	p144	1	PL1x4	0	5	A572-65	

BATCH 1

PROJECT	AISC RESEARCH PROJECT	
DN. BY:TMR	DATE: 4-10-18	PAINT: NO PAINT

REVISIONS			PRINT RECORD	
NO.	DATE	DESCRIPTION	DATE	USE
1				FOR FAB
2				
3				
4				
5				
6				
7				
8				

RIDDLE STRUCTURAL DETAILING LLC.
7573 MERCER RD (731) 444-4464 (731) 779-3771
BROWNSVILLE, TENNESSEE 38012

COOPER STEEL
CONSTRUCTION OFFICE
1919 HAYES ST. NASHVILLE TN, 37203
OFFICE: 615-321-5222
FAX: 615-321-3030
AISC CERTIFIED FABRICATOR AND ERECTOR

DRAWING NO: FT18 ORDER NO:2874

BILL OF MATERIAL

Heat Number	PC MARK	QTY TOTAL	DESCRIPTION	LENGTH		STEEL GRADE	REMARKS
	PL1	ONE	MISC				
8501452	PL1	1	PL1½x4	1	5	A36	
8501452	p79	1	PL1½x4	1	5	A36	
8502026	p81	2	PL¾x4	0	10	A36	

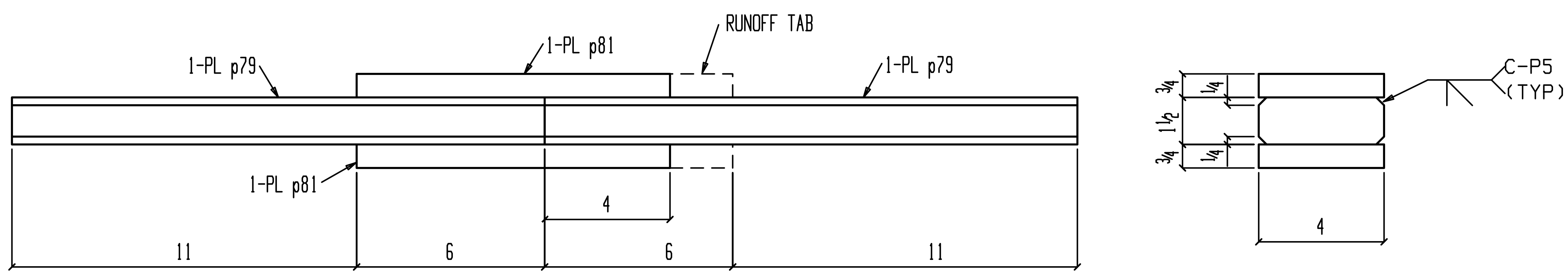

ONE MISC PL1

USE E70XX ELECTRODES

BATCH 1

PROJECT	AISC RESEARCH PROJECT	
DN. BY:TMR	DATE: 4-10-18	PAINT: NO PAINT

REVISIONS			PRINT RECORD	
NO.	DATE	DESCRIPTION	DATE	USE
1				FOR FAB
2				
3				
4				
5				
6				
7				
8				

COOPER STEEL
CONSTRUCTION OFFICE
1919 HAYES ST. NASHVILLE TN, 37203
OFFICE: 615-321-5222
FAX: 615-321-3030

DRAWING NO: PL1 ORDER NO:2874

RIDDLE STRUCTURAL DETAILING LLC.
7573 MERCER RD (731) 444-4464 (731) 779-3771
BROWNSVILLE, TENNESSEE 38012

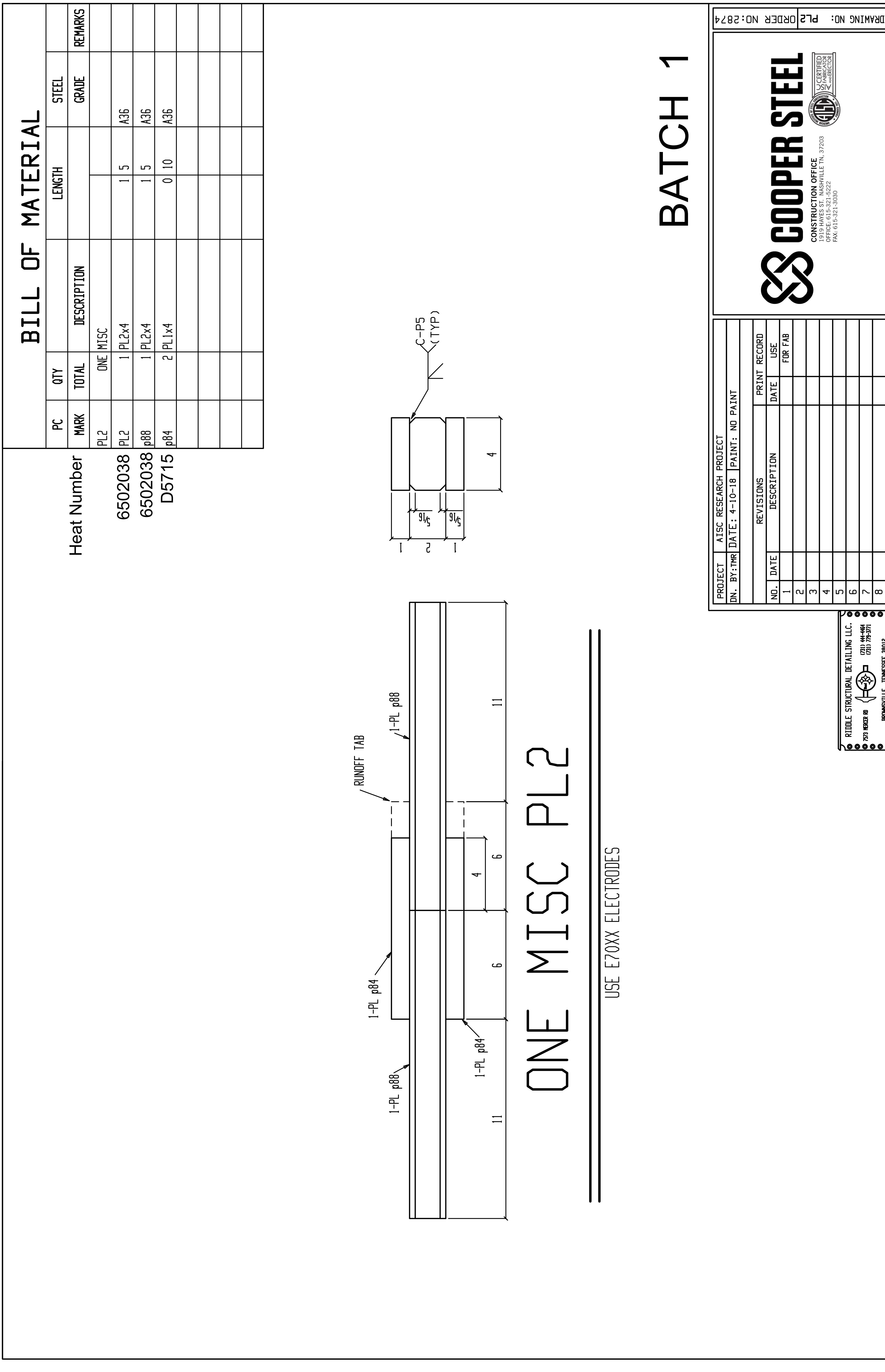

PC MARK	QTY TOTAL	DESCRIPTION	LENGTH		STEEL GRADE	REMARKS	Heat Number
PL2	ONE	MISC					
PL2	1	PL2x4	1	5	A36		6502038
p88	1	PL2x4	1	5	A36		6502038
p84	2	PL1x4	0	10	A36		D5715

BILL OF MATERIAL

Heat Number	PC MARK	QTY TOTAL	DESCRIPTION	LENGTH		STEEL GRADE	REMARKS
	PL3	ONE	MISC				
8500710	PL3	1	PL2½x4	1	5	A36	
8500710	p95	1	PL2½x4	1	5	A36	
7506515	p91	2	PL1¼x4	0	10	A36	

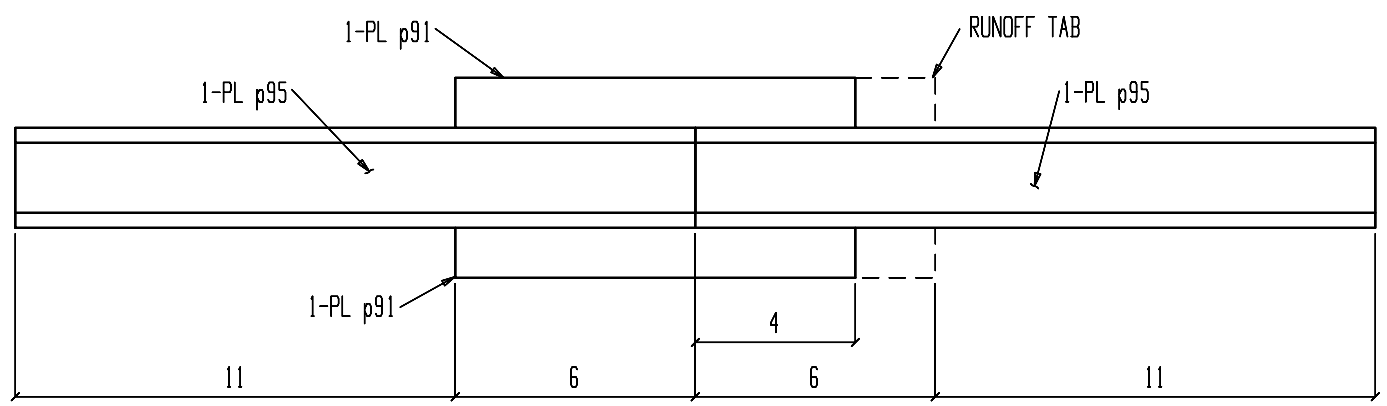

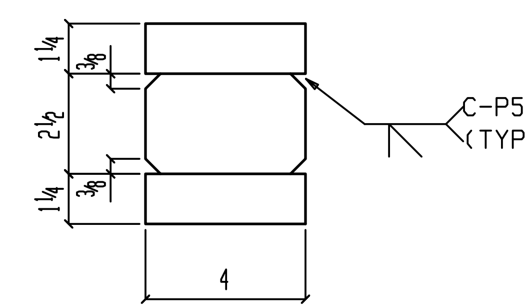

ONE MISC PL3

USE E70XX ELECTRODES

BATCH 1

PROJECT	AISC RESEARCH PROJECT			
DN. BY:TMR	DATE: 4-10-18	PAINT: NO PAINT		
REVISIONS			PRINT RECORD	
NO.	DATE	DESCRIPTION	DATE	USE
1				FOR FAB
2				
3				
4				
5				
6				
7				
8				

RIDDLE STRUCTURAL DETAILING LLC.
7573 MERCER RD (731) 444-4464 (731) 779-3771
BROWNSVILLE, TENNESSEE 38012

COOPER STEEL
CONSTRUCTION OFFICE
1919 HAYES ST. NASHVILLE TN, 37203
OFFICE: 615-321-5222
FAX: 615-321-3030
AISC CERTIFIED FABRICATOR AND ERECTOR

DRAWING NO: PL3 ORDER NO:2874

BILL OF MATERIAL

Heat Number	PC MARK	QTY TOTAL	DESCRIPTION	LENGTH		STEEL GRADE	REMARKS
	PL4	ONE	MISC				
8500710	PL4	1	PL2½x4	1	5	A36	
8500710	p99	1	PL2½x4	1	5	A36	
7506515	p91	2	PL1¼x4	0	10	A36	

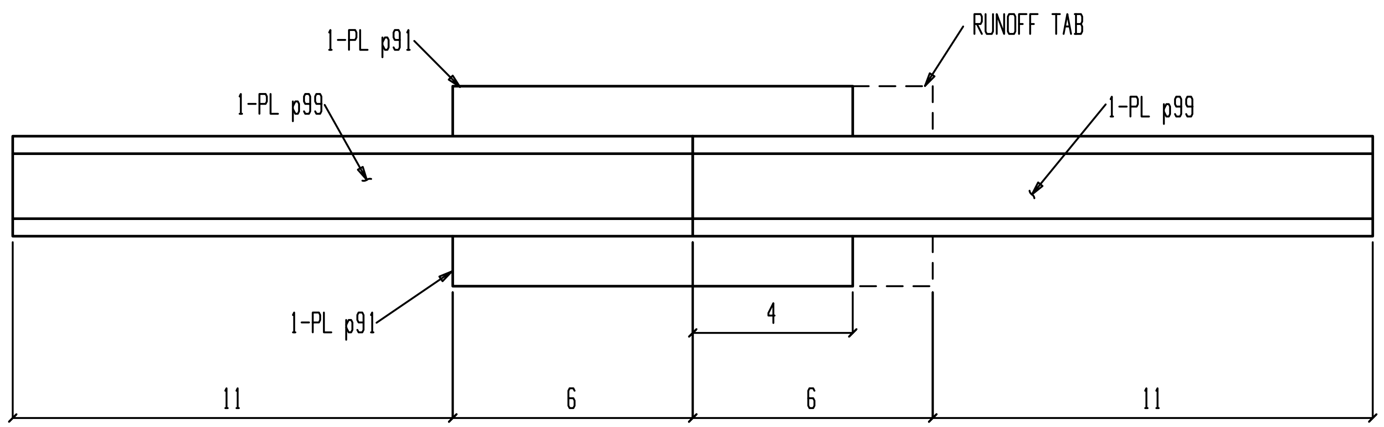

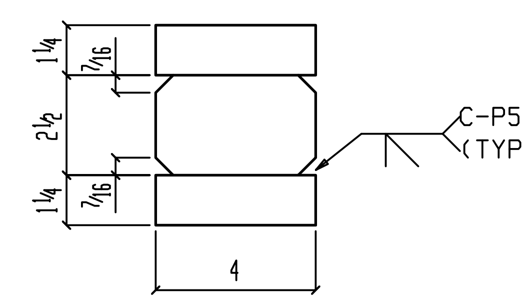

ONE MISC PL4

USE E70XX ELECTRODES

BATCH 1

PROJECT	AISC RESEARCH PROJECT	
DN. BY:TMR	DATE: 4-10-18	PAINT: NO PAINT

REVISIONS			PRINT RECORD	
NO.	DATE	DESCRIPTION	DATE	USE
1				FOR FAB
2				
3				
4				
5				
6				
7				
8				

RIDDLE STRUCTURAL DETAILING LLC.
7573 MERCER RD (731) 444-4464 (731) 779-3771
BROWNSVILLE, TENNESSEE 38012

COOPER STEEL
CONSTRUCTION OFFICE
1919 HAYES ST. NASHVILLE TN, 37203
OFFICE: 615-321-5222
FAX: 615-321-3030
AISC CERTIFIED FABRICATOR AND ERECTOR

DRAWING NO: PL4 ORDER NO:2874

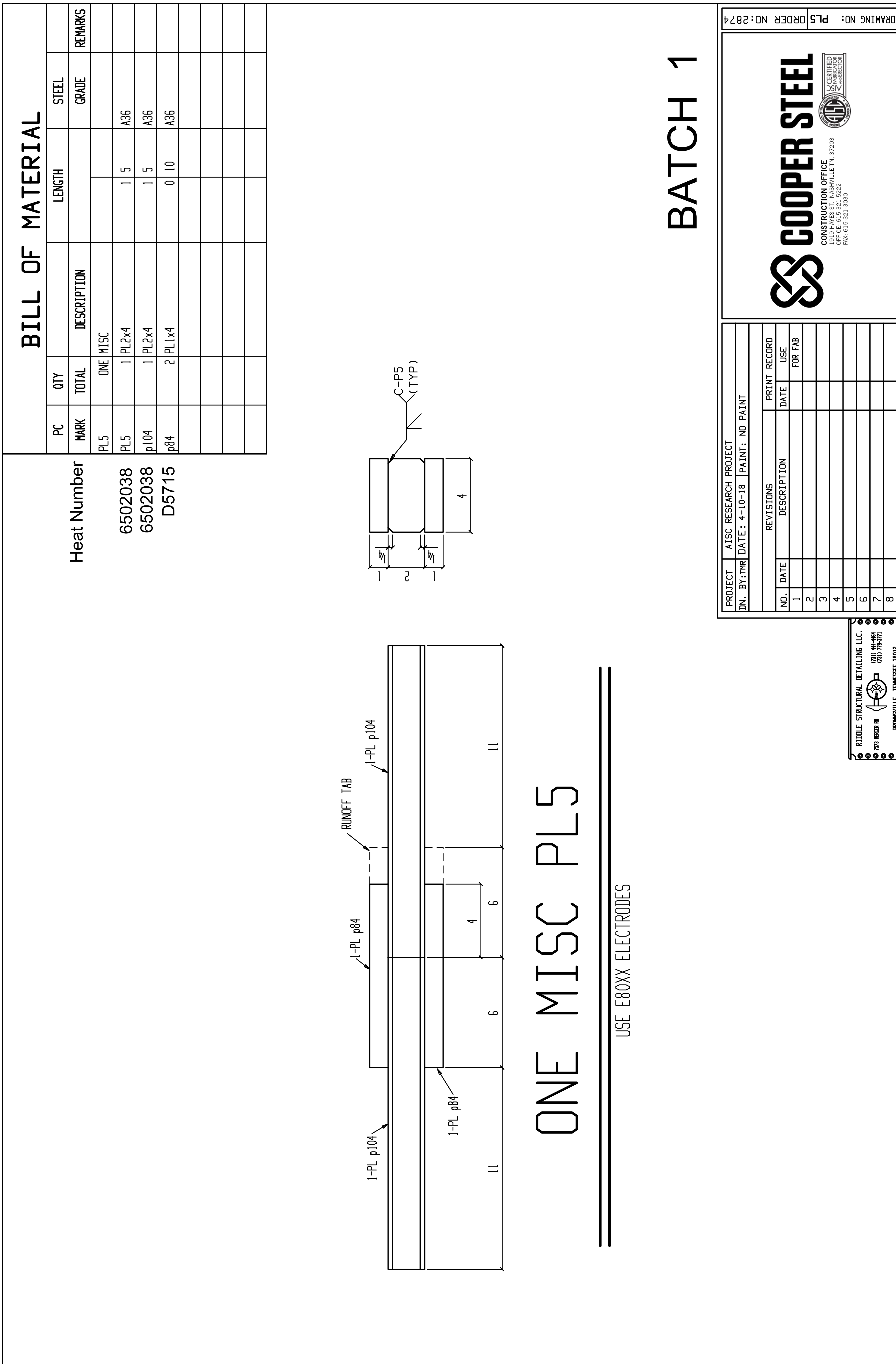
BILL OF MATERIAL
PC MARK | QTY TOTAL | DESCRIPTION | LENGTH | STEEL GRADE | REMARKS
PL5 | ONE | MISC
PL5 | 1 | PL2x4 | 1 5 | A36
p104 | 1 | PL2x4 | 1 5 | A36
p84 | 2 | PL1x4 | 0 10 | A36
Heat Number
6502038
6502038
D5715
BATCH 1
C-P5 (TYP)
4
1/4
1
2
1
RUNOFF TAB
1-PL p104
1-PL p84
11
6
4
6
11
ONE MISC PL5
USE E80XX ELECTRODES
DRAWING NO: PL5
ORDER NO: 2874
COOPER STEEL
CONSTRUCTION OFFICE
1919 HAYES ST. NASHVILLE TN, 37203
OFFICE: 615-321-5222
FAX: 615-321-3030
CERTIFIED FABRICATOR AND ERECTOR
PROJECT AISC RESEARCH PROJECT
DN. BY:TMR DATE: 4-10-18 PAINT: NO PAINT
REVISIONS
NO. DATE DESCRIPTION
PRINT RECORD
DATE USE
FOR FAB
1 2 3 4 5 6 7 8
RIDDLE STRUCTURAL DETAILING LLC.
7573 MERCER RD
(731) 444-4464
(731) 779-3771
BROWNSVILLE, TENNESSEE 38012

BILL OF MATERIAL

Heat Number	PC MARK	QTY TOTAL	DESCRIPTION	LENGTH		STEEL GRADE	REMARKS
	PL6	ONE	MISC				
8500710	PL6	1	PL2½x4	1	5	A36	
8500710	p95	1	PL2½x4	1	5	A36	
7506515	p91	2	PL1¼x4	0	10	A36	

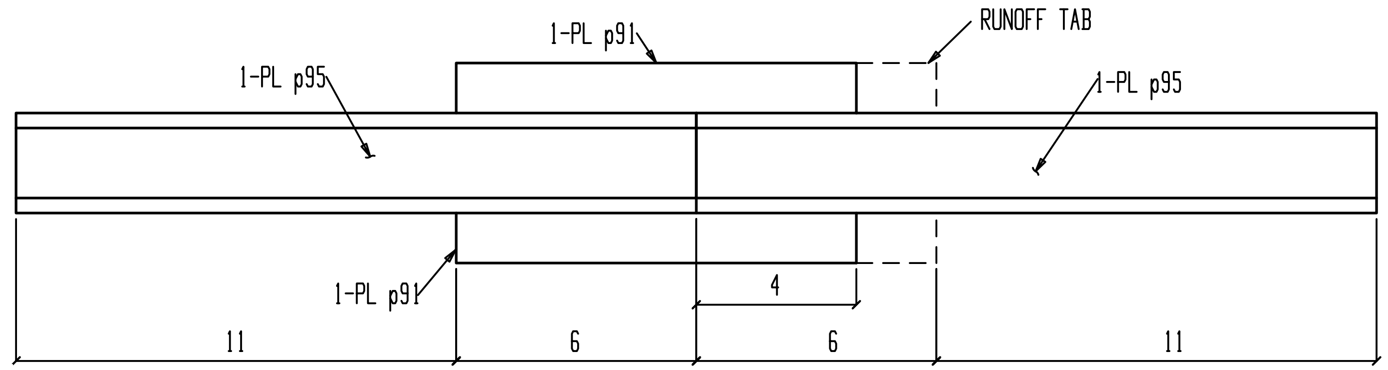

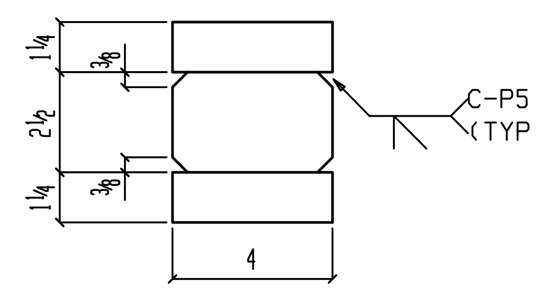

ONE MISC PL6

USE E80XX ELECTRODES

BATCH 1

PROJECT	AISC RESEARCH PROJECT	
DN. BY:TMR	DATE: 4-10-18	PAINT: NO PAINT

NO.	DATE	DESCRIPTION	DATE	USE
	REVISIONS		PRINT RECORD	
1				FOR FAB
2				
3				
4				
5				
6				
7				
8				

COOPER STEEL
CONSTRUCTION OFFICE
1919 HAYES ST. NASHVILLE TN, 37203
OFFICE: 615-321-5222
FAX: 615-321-3030
AISC CERTIFIED FABRICATOR AND ERECTOR

DRAWING NO: PL6 ORDER NO:2874

RIDDLE STRUCTURAL DETAILING LLC.
7573 MERCER RD
(731) 444-4464
(731) 779-3771
BROWNSVILLE, TENNESSEE 38012

BILL OF MATERIAL

Heat Number	PC MARK	QTY TOTAL	DESCRIPTION	LENGTH		STEEL GRADE	REMARKS
	PL7	ONE	MISC				
6502038	PL7	1	PL2x4	1	5	A36	
6502038	p104	1	PL2x4	1	5	A36	
D5715	p84	2	PL1x4	0	10	A36	

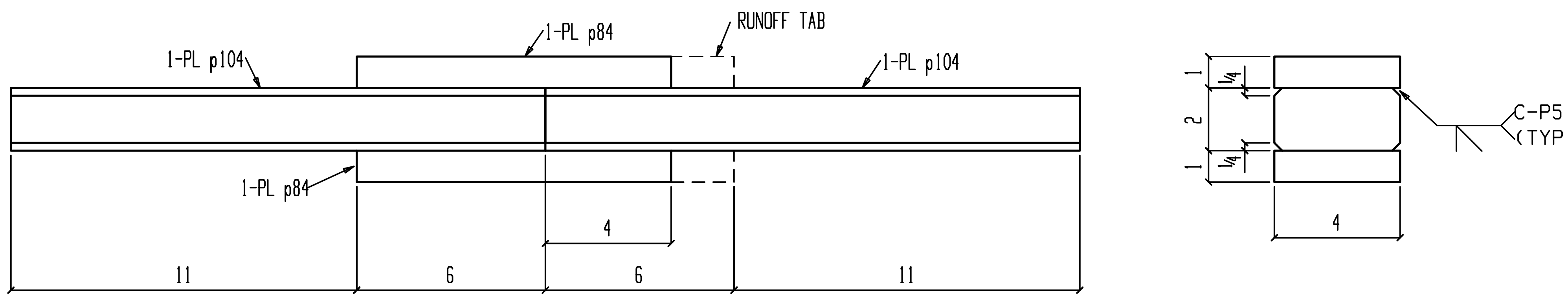

ONE MISC PL7

USE E100XX ELECTRODES

BATCH 1

PROJECT	AISC RESEARCH PROJECT	
DN. BY:TMR	DATE: 4-10-18	PAINT: NO PAINT

REVISIONS			PRINT RECORD	
NO.	DATE	DESCRIPTION	DATE	USE
1				FOR FAB
2				
3				
4				
5				
6				
7				
8				

COOPER STEEL
CONSTRUCTION OFFICE
1919 HAYES ST. NASHVILLE TN, 37203
OFFICE: 615-321-5222
FAX: 615-321-3030

AISC CERTIFIED FABRICATOR AND ERECTOR

DRAWING NO: PL7 ORDER NO:2874

RIDDLE STRUCTURAL DETAILING LLC.
7573 MERCER RD (731) 444-4464 (731) 779-3771
BROWNSVILLE, TENNESSEE 38012

BILL OF MATERIAL

PC MARK	QTY TOTAL	DESCRIPTION	LENGTH	STEEL GRADE	REMARKS	Heat Number
PL8	ONE	MISC				
PL8	1	PL2½x4	1 5	A36		8500710
p108	1	PL2½x4	1 5	A36		8500710
p91	2	PL1¼x4	0 10	A36		7506515

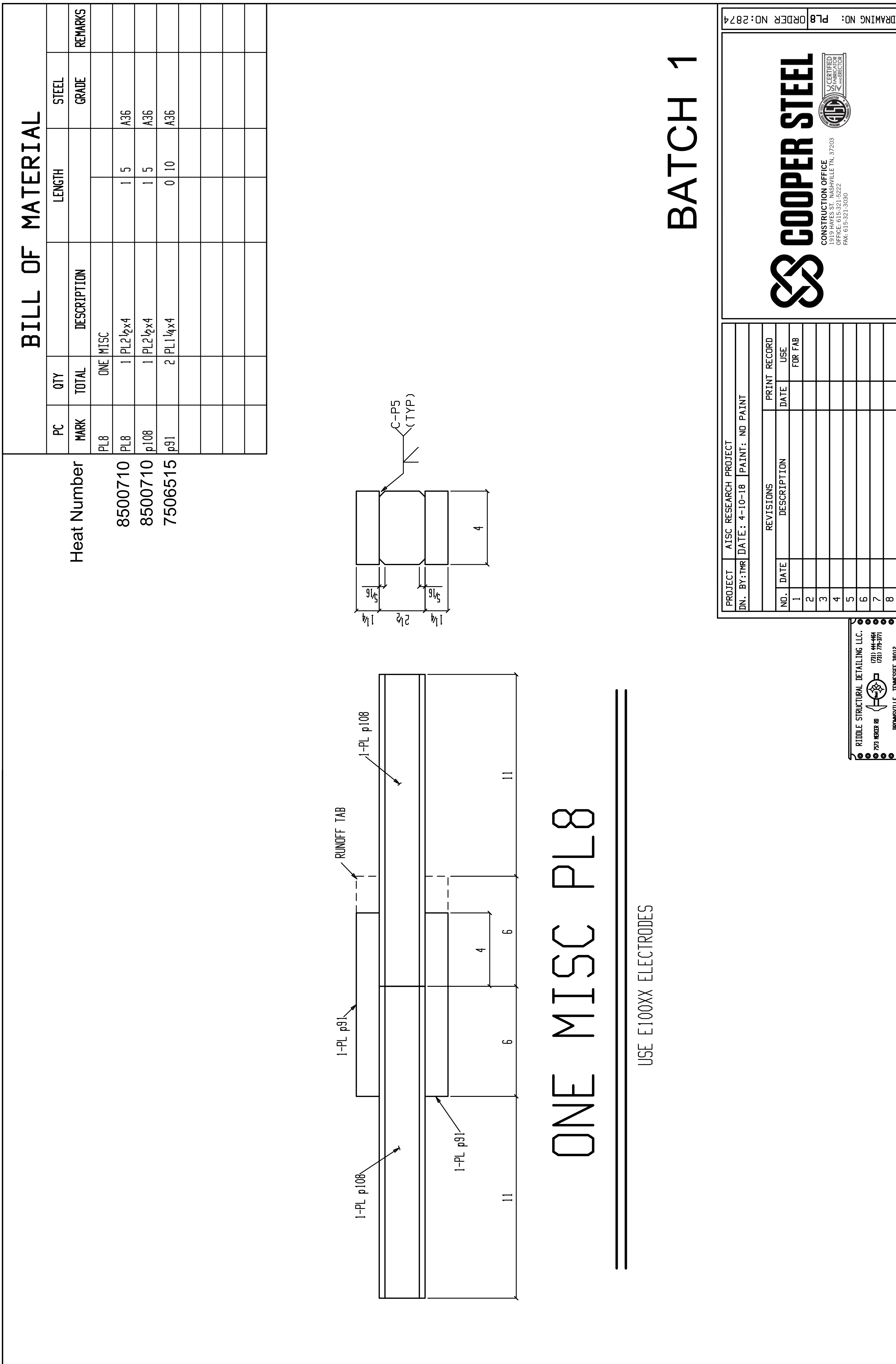

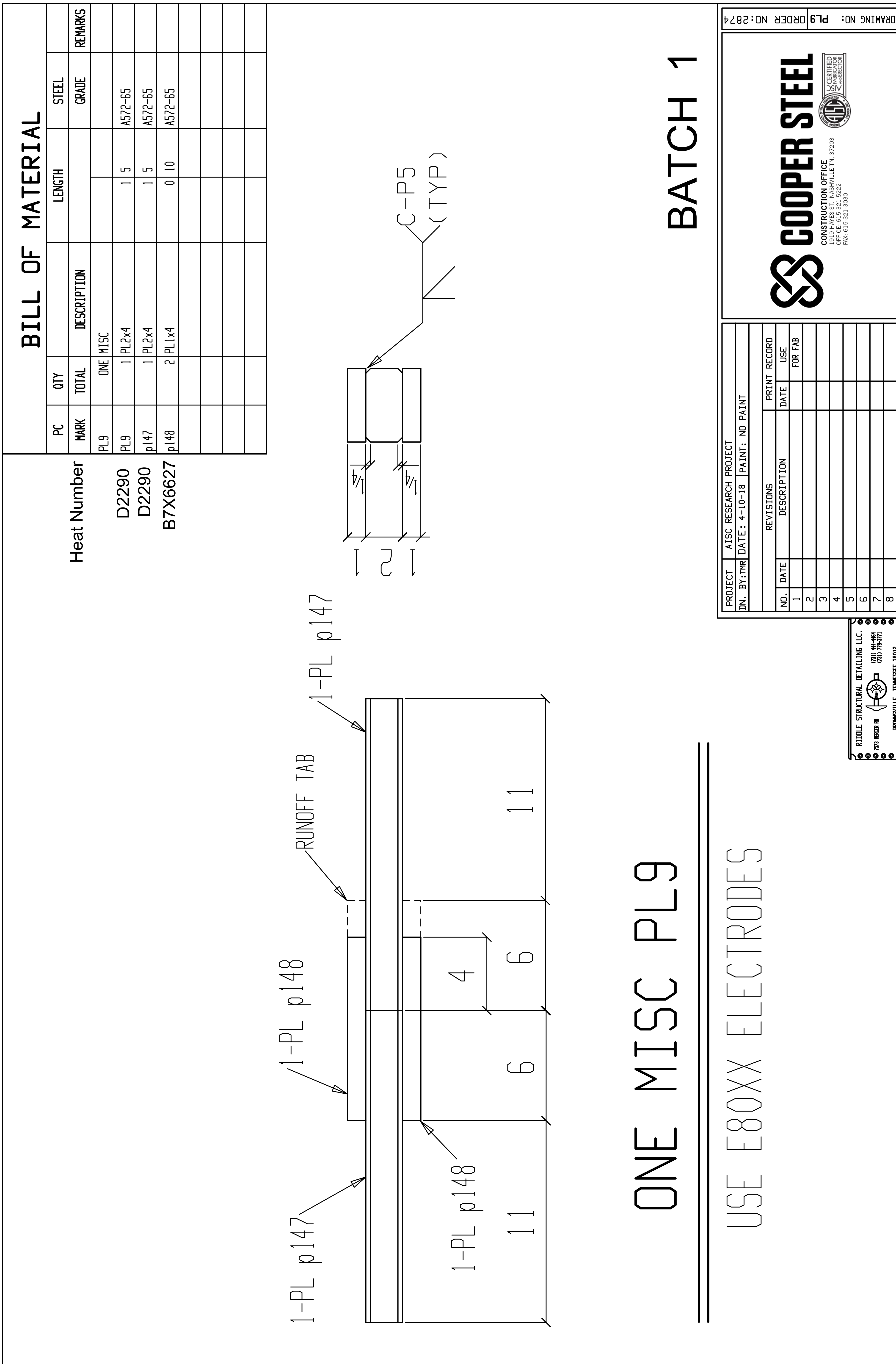

BILL OF MATERIAL

PC MARK	QTY TOTAL	DESCRIPTION	LENGTH	STEEL GRADE	REMARKS
PL9	ONE	MISC			
PL9	1	PL2x4	1 5	A572-65	
p147	1	PL2x4	1 5	A572-65	
p148	2	PL1x4	0 10	A572-65	

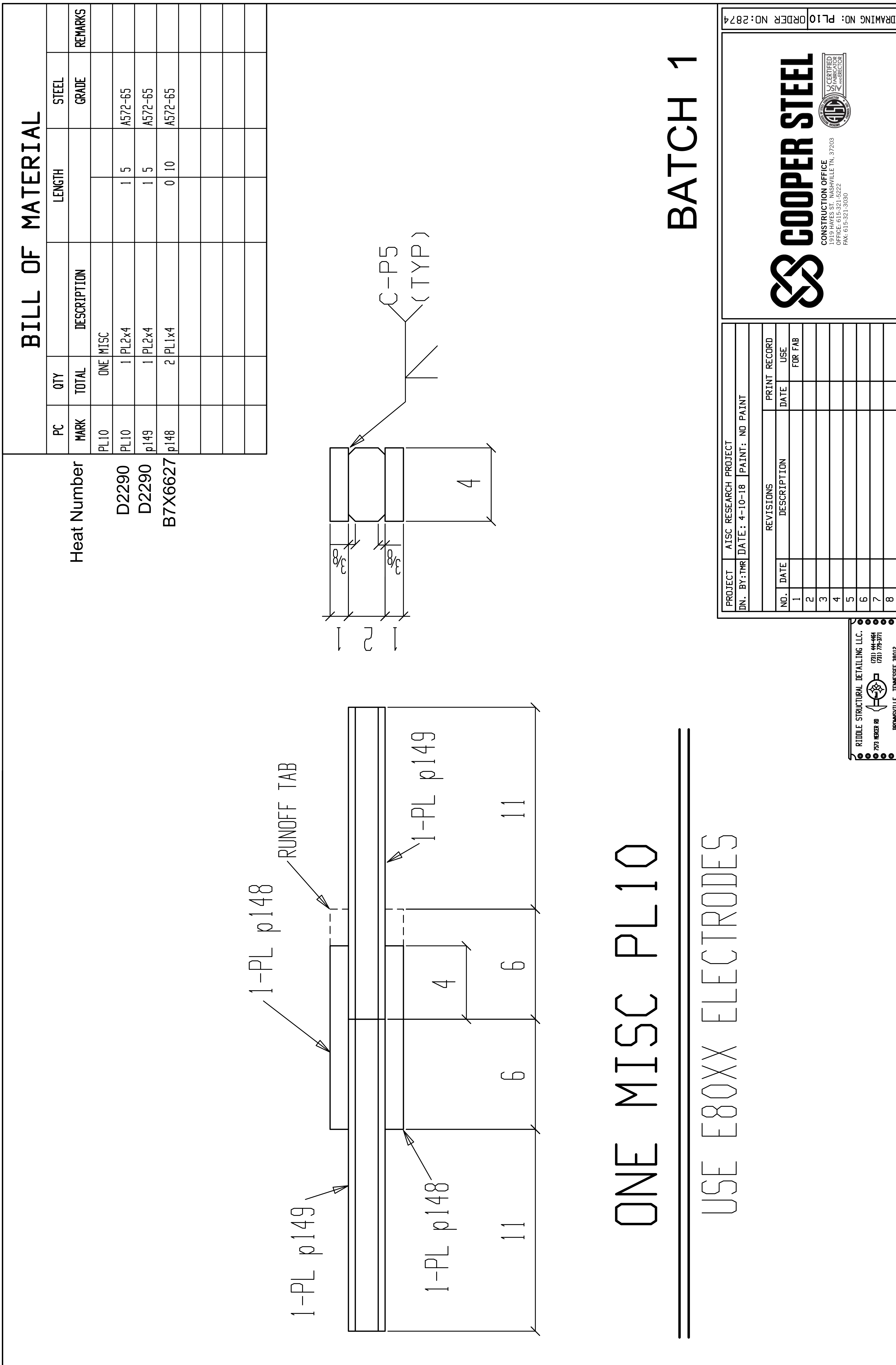
BILL OF MATERIAL
PC MARK | QTY TOTAL | DESCRIPTION | LENGTH | STEEL GRADE | REMARKS
PL10 | ONE | MISC
PL10 | 1 | PL2x4 | 1 5 | A572-65
p149 | 1 | PL2x4 | 1 5 | A572-65
p148 | 2 | PL1x4 | 0 10 | A572-65
Heat Number
D2290
D2290
B7X6627
BATCH 1
C-P5
(TYP)
4
3/8
3/8
1
2
1
1-PL p148
RUNOFF TAB
1-PL p149
1-PL p149
1-PL p148
4
11
6
6
11
ONE MISC PL10
USE E80XX ELECTRODES
PROJECT AISC RESEARCH PROJECT
DN. BY:TMR DATE: 4-10-18 PAINT: NO PAINT
REVISIONS
NO. DATE DESCRIPTION
PRINT RECORD
DATE USE
FOR FAB
1 2 3 4 5 6 7 8
DRAWING NO: PL10 ORDER NO:2874
COOPER STEEL
CONSTRUCTION OFFICE
1919 HAYES ST. NASHVILLE TN. 37203
OFFICE: 615-321-5222
FAX: 615-321-3030
CERTIFIED FABRICATOR and ERECTOR
RIDDLE STRUCTURAL DETAILING LLC.
7573 MERCER RD
BROWNSVILLE, TENNESSEE 38012

BILL OF MATERIAL

Heat Number	PC MARK	QTY TOTAL	DESCRIPTION	LENGTH		STEEL GRADE	REMARKS
	PL11	ONE	MISC				
D2290	PL11	1	PL2x4	1	5	A572-65	
D2290	p147	1	PL2x4	1	5	A572-65	
B7X6627	p148	2	PL1x4	0	10	A572-65	

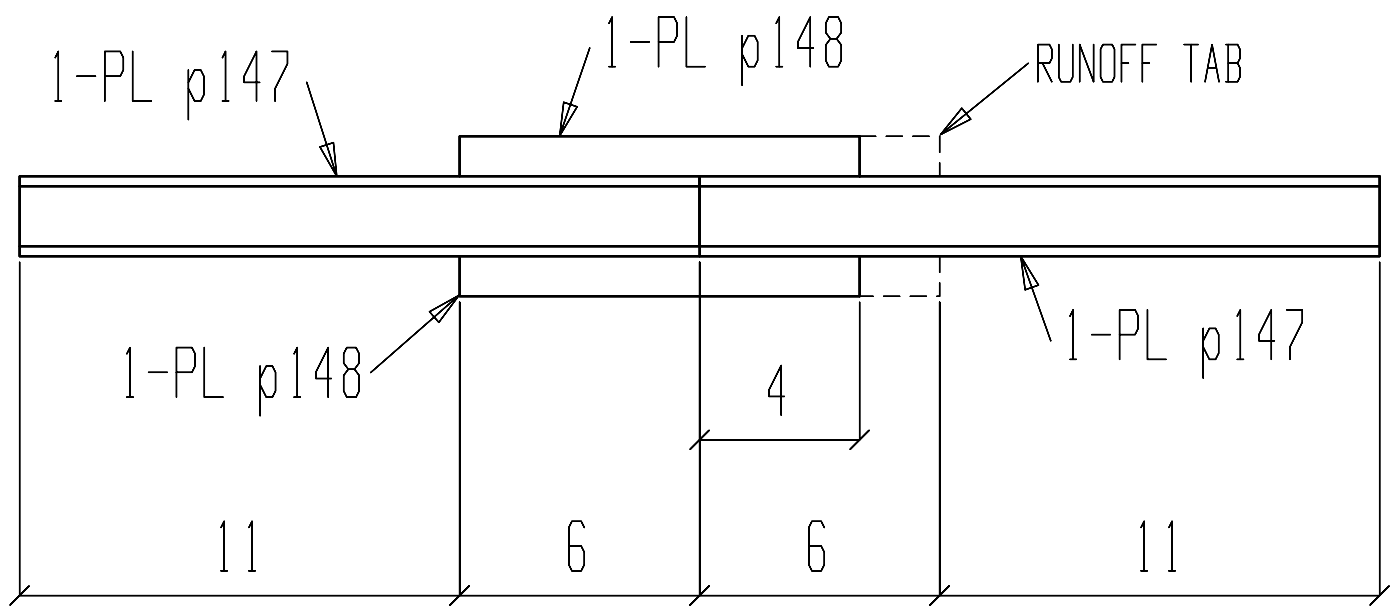

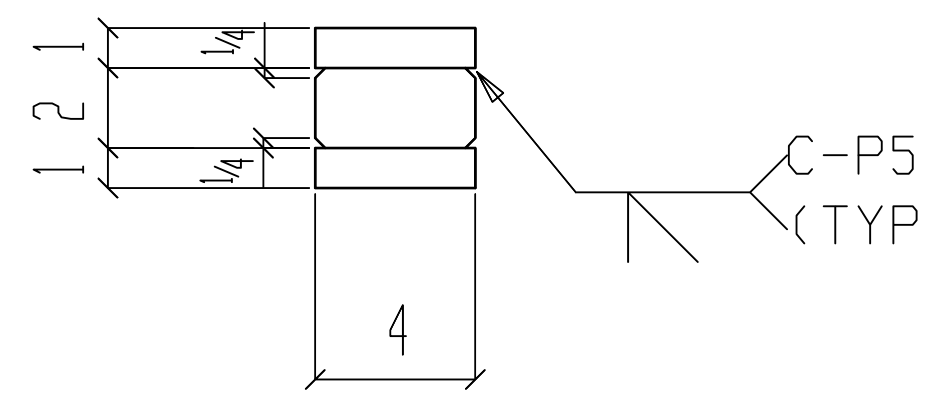

ONE MISC PL11

USE E100XX ELECTRODES

BATCH 1

RIDDLE STRUCTURAL DETAILING LLC.
7573 MERCER RD (731) 444-4464 (731) 779-3771
BROWNSVILLE, TENNESSEE 38012

PROJECT	AISC RESEARCH PROJECT			
DN. BY:TMR	DATE: 4-10-18	PAINT: NO PAINT		

REVISIONS			PRINT RECORD	
NO.	DATE	DESCRIPTION	DATE	USE
1				FOR FAB
2				
3				
4				
5				
6				
7				
8				

COOPER STEEL
CONSTRUCTION OFFICE
1919 HAYES ST. NASHVILLE TN, 37203
OFFICE: 615-321-5222
FAX: 615-321-3030
AISC CERTIFIED FABRICATOR and ERECTOR

DRAWING NO: PL11 | ORDER NO:2874

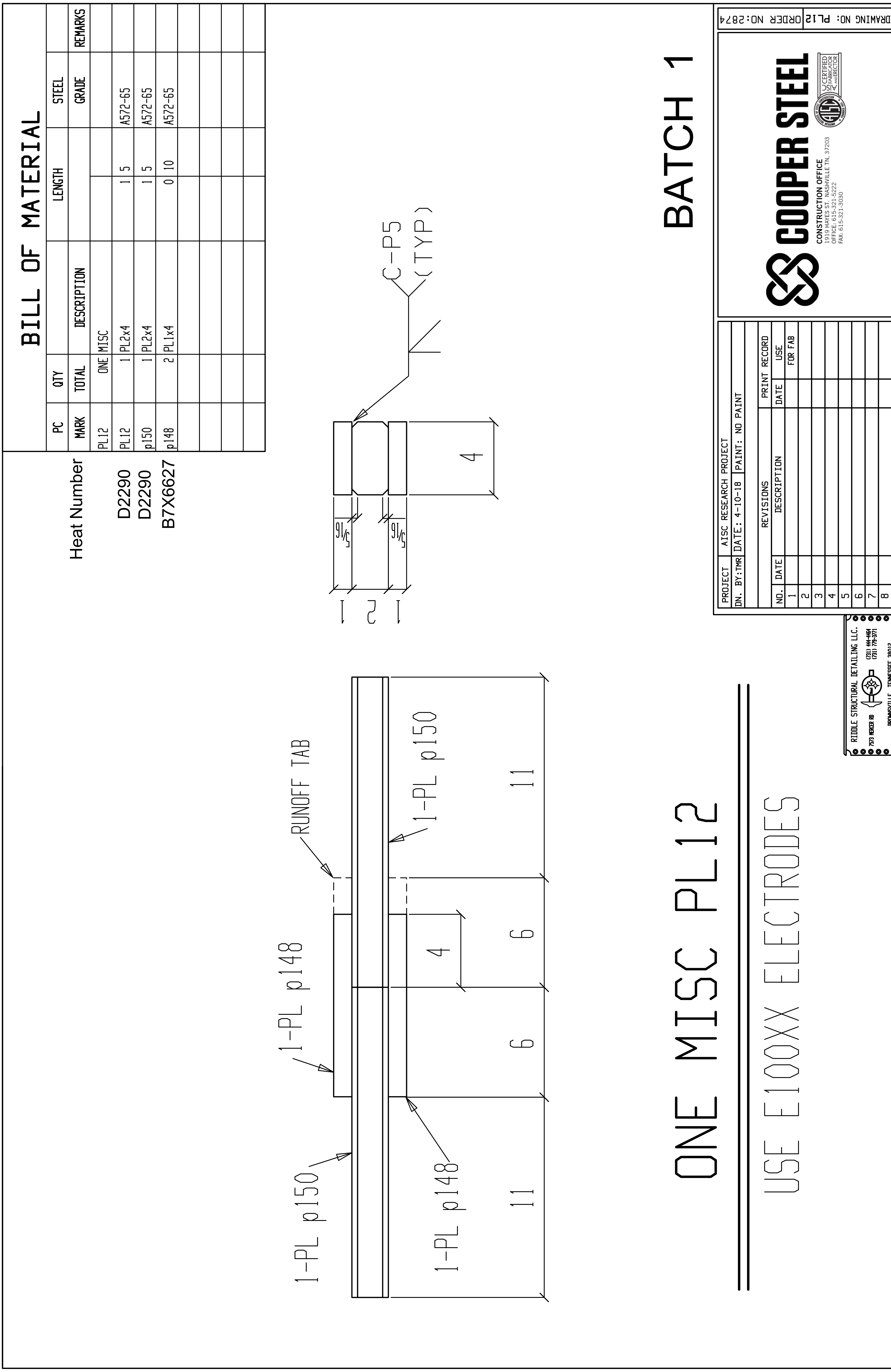
BILL OF MATERIAL
PC MARK | QTY TOTAL | DESCRIPTION | LENGTH | STEEL GRADE | REMARKS
PL12 | ONE | MISC
PL12 | 1 | PL2x4 | 1 5 | A572-65
p150 | 1 | PL2x4 | 1 5 | A572-65
p148 | 2 | PL1x4 | 0 10 | A572-65
Heat Number
D2290
D2290
B7X6627
C-P5
(TYP)
4
5/16
5/16
1
2
1
RUNOFF TAB
1-PL p150
1-PL p148
1-PL p150
1-PL p148
4
11
6
6
11
BATCH 1
ONE MISC PL12
USE E100XX ELECTRODES
DRAWING NO: PL12 ORDER NO:2874
COOPER STEEL
CONSTRUCTION OFFICE
1919 HAYES ST. NASHVILLE TN. 37203
OFFICE: 615-321-5222
FAX: 615-321-3030
CERTIFIED FABRICATOR and ERECTOR
PROJECT AISC RESEARCH PROJECT
DN. BY:TMR DATE: 4-10-18 PAINT: NO PAINT
REVISIONS
NO. DATE DESCRIPTION
PRINT RECORD
DATE USE
FOR FAB
1
2
3
4
5
6
7
8
RIDDLE STRUCTURAL DETAILING LLC.
7573 MERCER RD
BROWNSVILLE, TENNESSEE 38012
(731) 444-4464
(731) 779-3771

BILL OF MATERIAL

Heat Number	PC MARK	QTY TOTAL	DESCRIPTION	LENGTH		STEEL GRADE	REMARKS
	PL13	ONE	MISC				
8500710	PL13	1	PL2½x4	1	5	A36	
8500710	p95	1	PL2½x4	1	5	A36	
D5715	p114	2	PL1x6	0	10	A36	

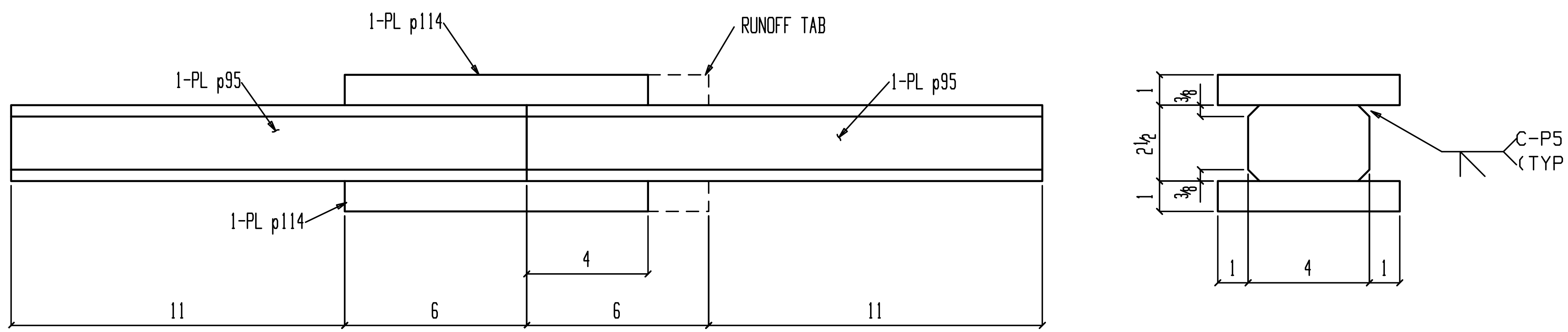

ONE MISC PL13

USE E70XX ELECTRODES

BATCH 1

PROJECT	AISC RESEARCH PROJECT			
DN. BY:TMR	DATE: 4-10-18	PAINT: NO PAINT		

REVISIONS			PRINT RECORD	
NO.	DATE	DESCRIPTION	DATE	USE
1				FOR FAB
2				
3				
4				
5				
6				
7				
8				

RIDDLE STRUCTURAL DETAILING LLC.
7573 MERCER RD (731) 444-4464 (731) 779-3771
BROWNSVILLE, TENNESSEE 38012

COOPER STEEL
CONSTRUCTION OFFICE
1919 HAYES ST. NASHVILLE TN, 37203
OFFICE: 615-321-5222
FAX: 615-321-3030
AISC CERTIFIED FABRICATOR AND ERECTOR

DRAWING NO: PL13 ORDER NO:2874

BILL OF MATERIAL

Heat Number	PC MARK	QTY TOTAL	DESCRIPTION	LENGTH		STEEL GRADE	REMARKS
	PL14	ONE	MISC				
8500710	PL14	1	PL2½x4	1	5	A36	
8500710	p95	1	PL2½x4	1	5	A36	
D5715	p114	2	PL1x6	0	10	A36	

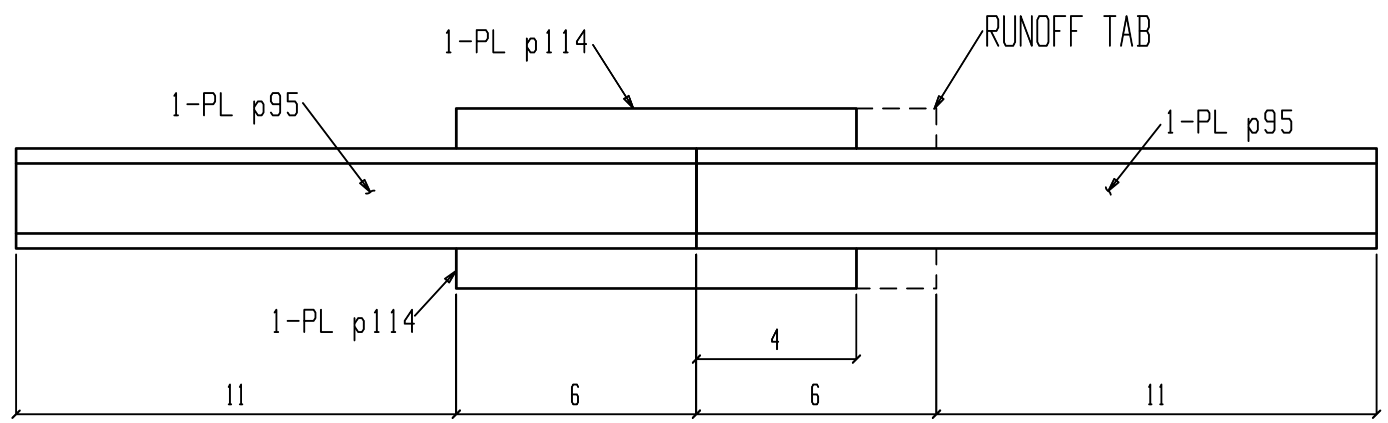

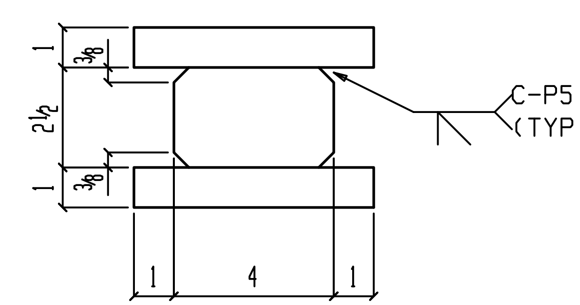

ONE MISC PL14

USE E80XX ELECTRODES

BATCH 1

PROJECT	AISC RESEARCH PROJECT	
DN. BY:TMR	DATE: 4-10-18	PAINT: NO PAINT

REVISIONS			PRINT RECORD	
NO.	DATE	DESCRIPTION	DATE	USE
1				FOR FAB
2				
3				
4				
5				
6				
7				
8				

COOPER STEEL
CONSTRUCTION OFFICE
1919 HAYES ST. NASHVILLE TN, 37203
OFFICE: 615-321-5222
FAX: 615-321-3030

AISC CERTIFIED FABRICATOR AND ERECTOR

DRAWING NO: PL14 ORDER NO:2874

RIDDLE STRUCTURAL DETAILING LLC.
7573 MERCER RD
(731) 444-4464
(731) 779-3771
BROWNSVILLE, TENNESSEE 38012

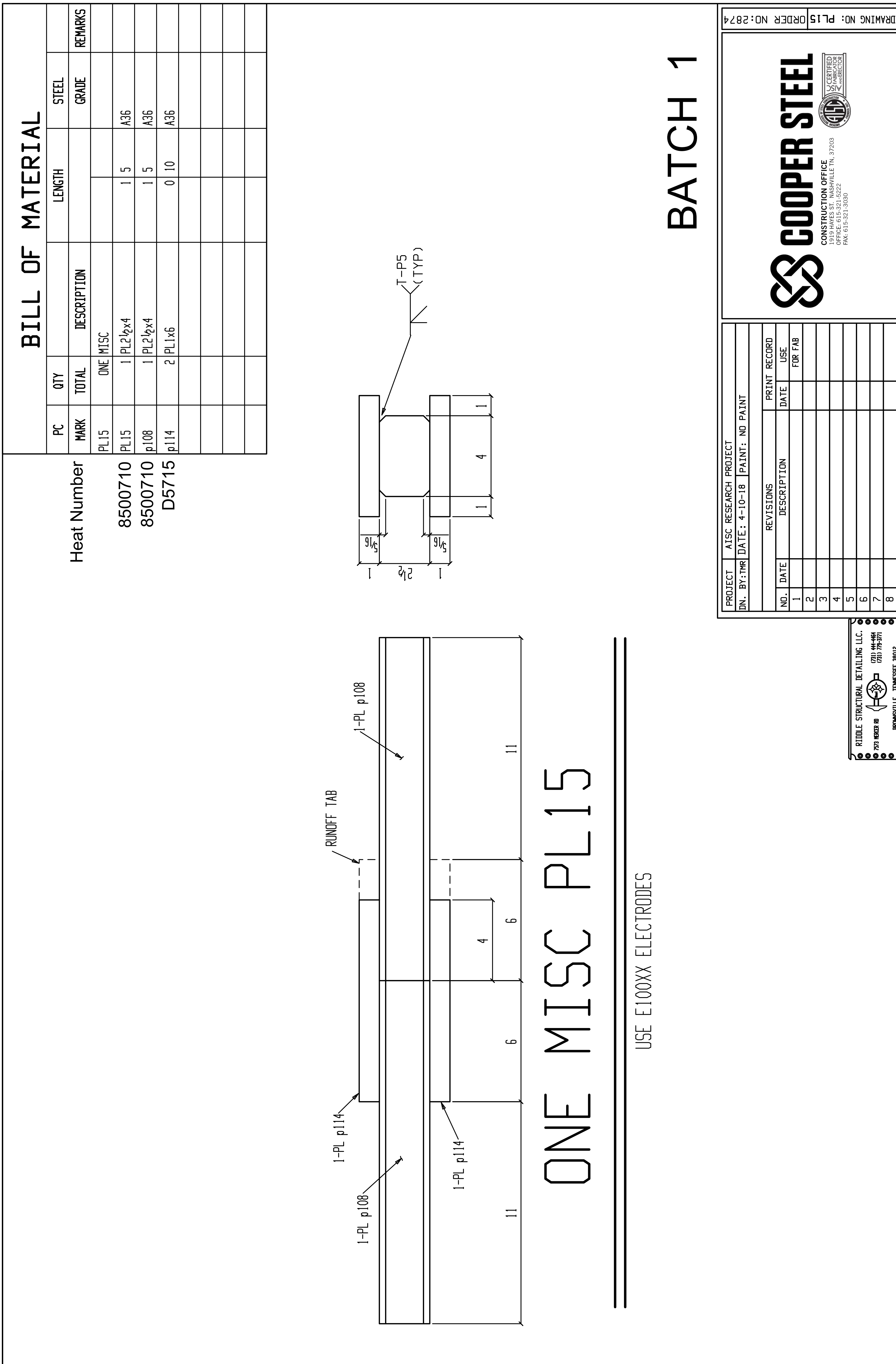

BILL OF MATERIAL

PC MARK	QTY TOTAL	DESCRIPTION	LENGTH	STEEL GRADE	REMARKS	Heat Number
PL15	ONE	MISC				
PL15	1	PL2½x4	1 5	A36		8500710
p108	1	PL2½x4	1 5	A36		8500710
p114	2	PL1x6	0 10	A36		D5715

BILL OF MATERIAL

Heat Number	PC MARK	QTY TOTAL	DESCRIPTION	LENGTH		STEEL GRADE	REMARKS
	PS1	ONE	MISC				
8502026	PS1	1	PL$\frac{3}{4}$x4	1	6	A36	
8502026	p121	1	PL$\frac{3}{4}$x4	1	6	A36	

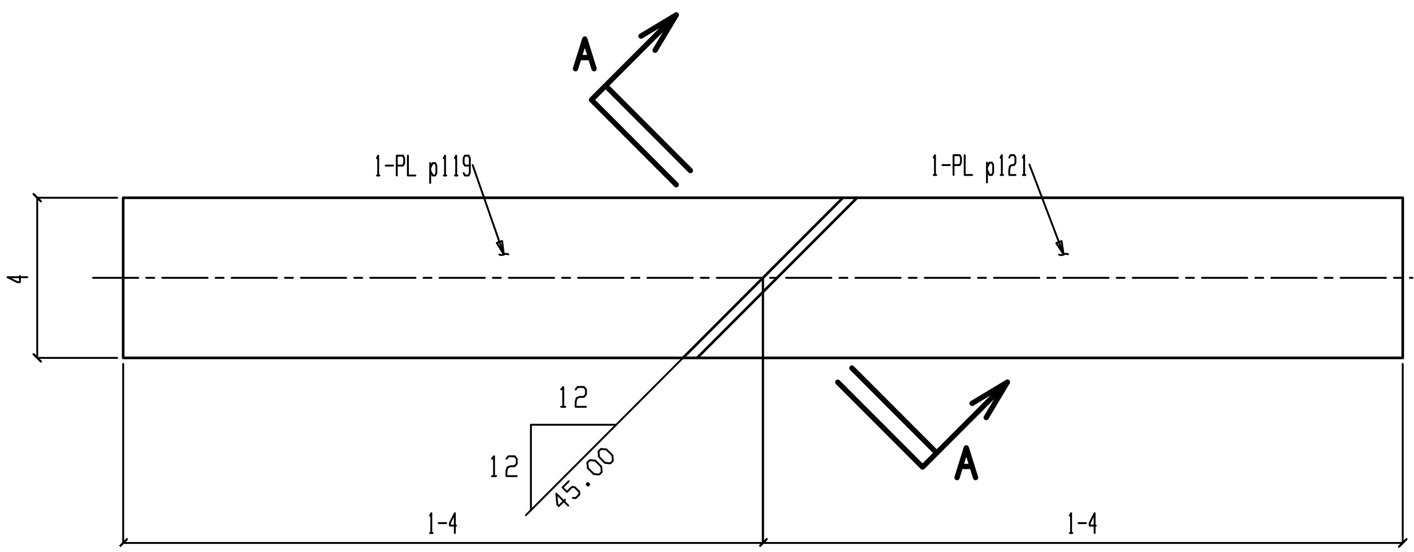

ONE MISC PS1

USE E70XX ELECTRODES

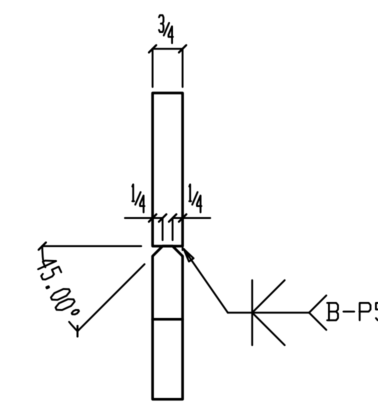

Section A-A

PS1

BATCH 1

PROJECT	AISC RESEARCH PROJECT			
DN. BY:TMR	DATE: 4-10-18	PAINT: NO PAINT		
	REVISIONS		PRINT RECORD	
NO.	DATE	DESCRIPTION	DATE	USE
1				FOR FAB
2				
3				
4				
5				
6				
7				
8				

COOPER STEEL
CONSTRUCTION OFFICE
1919 HAYES ST. NASHVILLE TN, 37203
OFFICE: 615-321-5222
FAX: 615-321-3030

AISC CERTIFIED FABRICATOR AND ERECTOR

DRAWING NO: PS1 ORDER NO:2874

RIDDLE STRUCTURAL DETAILING LLC.
7573 MERCER RD
(731) 444-4464
(731) 779-3771
BROWNSVILLE, TENNESSEE 38012

BILL OF MATERIAL

Heat Number	PC MARK	QTY TOTAL	DESCRIPTION	LENGTH		STEEL GRADE	REMARKS
	PS2	ONE	MISC				
8501452	PS2	1	PL1½x4	1	6	A36	
8501452	p125	1	PL1½x4	1	6	A36	

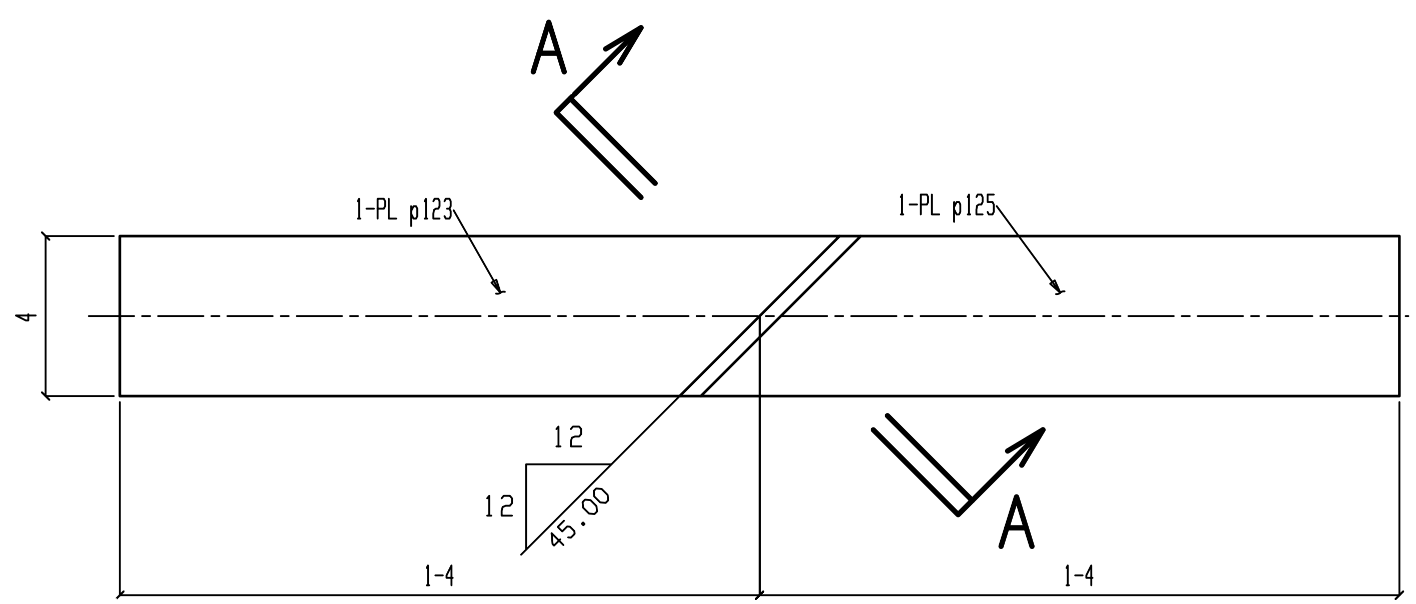

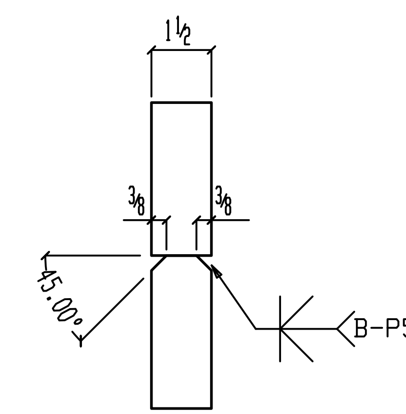

Section A-A

PS2

ONE MISC PS2

USE E70XX ELECTRODES

BATCH 1

PROJECT	AISC RESEARCH PROJECT	
DN. BY:TMR	DATE: 4-10-18	PAINT: NO PAINT

NO.	DATE	REVISIONS DESCRIPTION	PRINT RECORD DATE	USE
1				FOR FAB
2				
3				
4				
5				
6				
7				
8				

COOPER STEEL
CONSTRUCTION OFFICE
1919 HAYES ST. NASHVILLE TN, 37203
OFFICE: 615-321-5222
FAX: 615-321-3030
AISC CERTIFIED FABRICATOR AND ERECTOR

DRAWING NO: PS2 ORDER NO:2874

RIDDLE STRUCTURAL DETAILING LLC.
7573 MERCER RD
(731) 444-4464
(731) 779-3771
BROWNSVILLE, TENNESSEE 38012

BILL OF MATERIAL

Heat Number	PC MARK	QTY TOTAL	DESCRIPTION	LENGTH		STEEL GRADE	REMARKS
	PS3	ONE	MISC				
8501452	PS3	1	PL1½x4	1	6	A36	
8501452	p127	1	PL1½x4	1	6	A36	

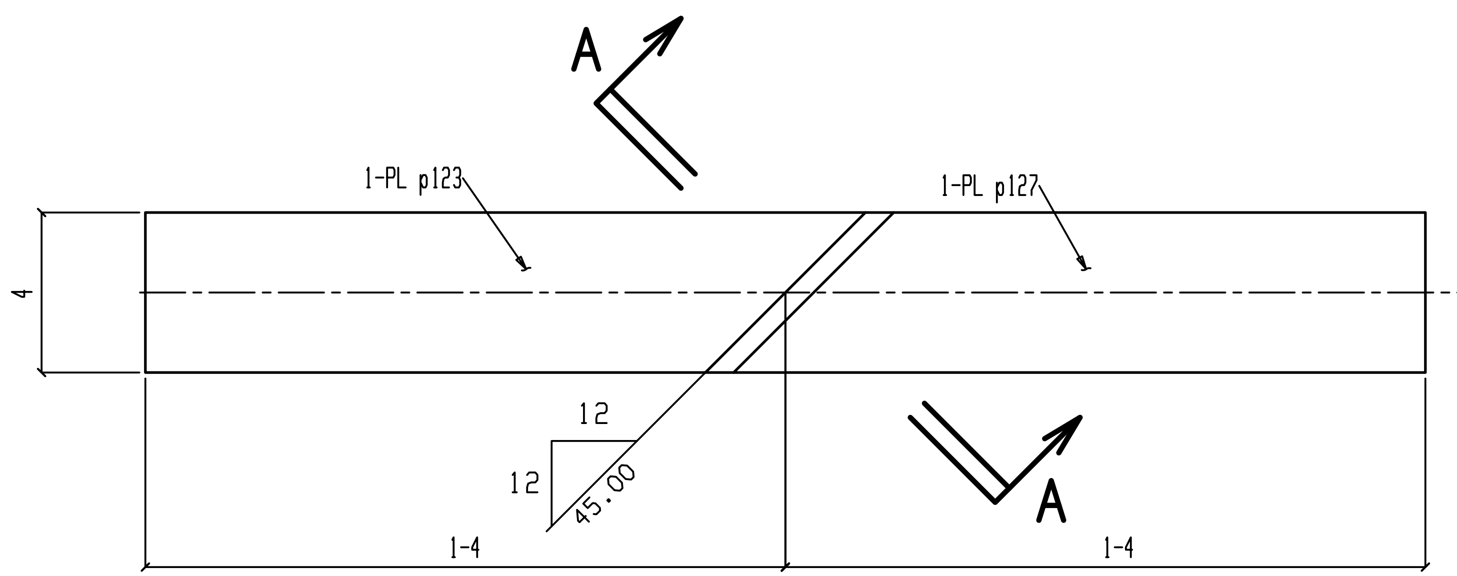

ONE MISC PS3

USE E70XX ELECTRODES

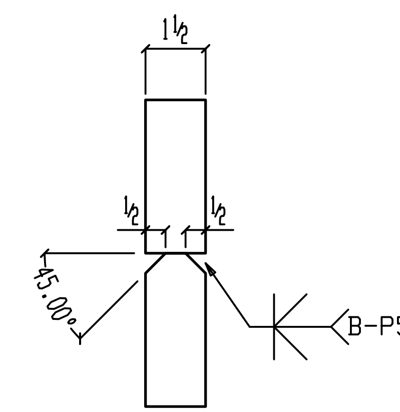

Section A-A

PS3

BATCH 1

PROJECT	AISC RESEARCH PROJECT	
DN. BY:TMR	DATE: 4-10-18	PAINT: NO PAINT

REVISIONS			PRINT RECORD	
NO.	DATE	DESCRIPTION	DATE	USE
1				FOR FAB
2				
3				
4				
5				
6				
7				
8				

RIDDLE STRUCTURAL DETAILING LLC.
7573 MERCER RD (731) 444-4464 (731) 779-3771
BROWNSVILLE, TENNESSEE 38012

COOPER STEEL
CONSTRUCTION OFFICE
1919 HAYES ST. NASHVILLE TN, 37203
OFFICE: 615-321-5222
FAX: 615-321-3030
AISC CERTIFIED FABRICATOR AND ERECTOR

DRAWING NO: PS3 ORDER NO:2874

BILL OF MATERIAL

Heat Number	PC MARK	QTY TOTAL	DESCRIPTION	LENGTH		STEEL GRADE	REMARKS
	PS4	ONE	MISC				
8502026	PS4	1	PL¾x4	1	6	A36	
8502026	p121	1	PL¾x4	1	6	A36	

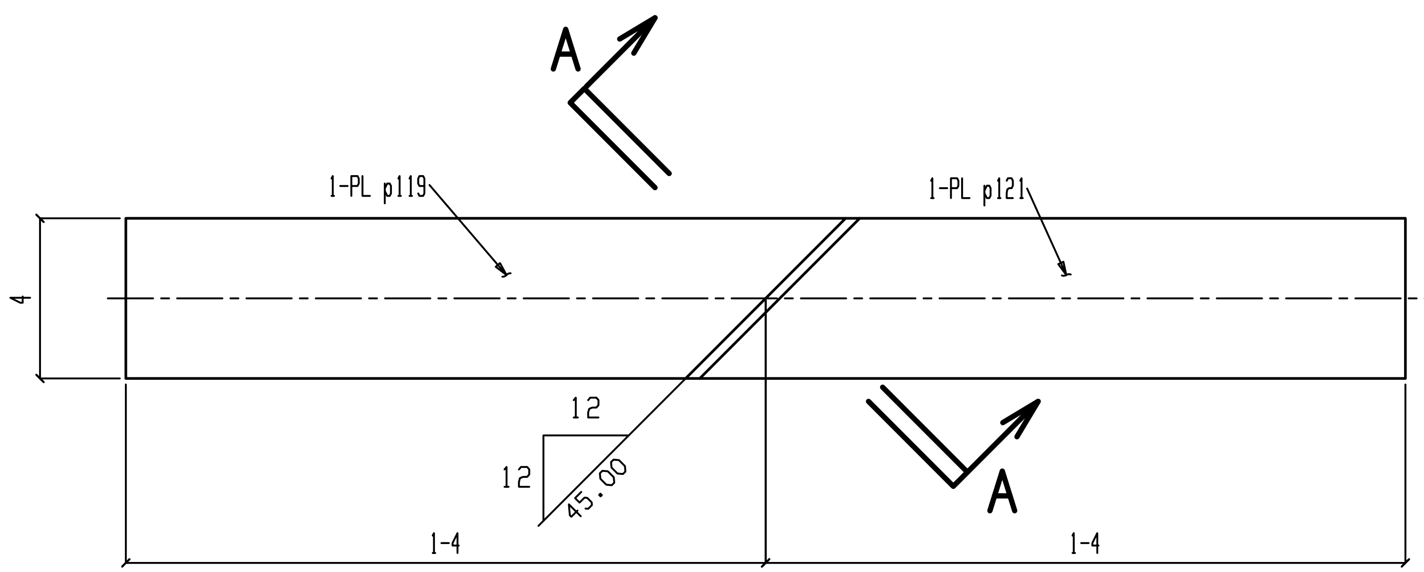

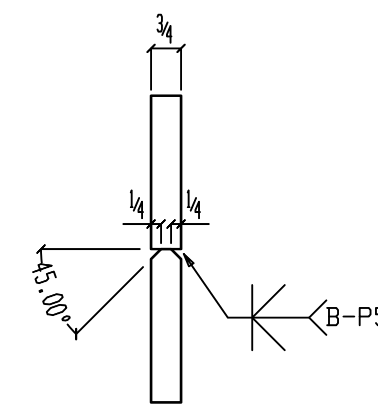

Section A-A

PS4

ONE MISC PS4

USE E100XX ELECTRODES

BATCH 1

PROJECT	AISC RESEARCH PROJECT	
DN. BY:TMR	DATE: 4-10-18	PAINT: NO PAINT

REVISIONS			PRINT RECORD	
NO.	DATE	DESCRIPTION	DATE	USE
1				FOR FAB
2				
3				
4				
5				
6				
7				
8				

RIDDLE STRUCTURAL DETAILING LLC.
7573 MERCER RD (731) 444-4464 (731) 779-3771
BROWNSVILLE, TENNESSEE 38012

COOPER STEEL
CONSTRUCTION OFFICE
1919 HAYES ST. NASHVILLE TN, 37203
OFFICE: 615-321-5222
FAX: 615-321-3030
AISC CERTIFIED FABRICATOR AND ERECTOR

DRAWING NO: PS4 ORDER NO:2874

BILL OF MATERIAL

Heat Number	PC MARK	QTY TOTAL	DESCRIPTION	LENGTH		STEEL GRADE	REMARKS
	PS5	ONE	MISC				
8501452	PS5	1	PL1½x4	1	6	A36	
8501452	p125	1	PL1½x4	1	6	A36	

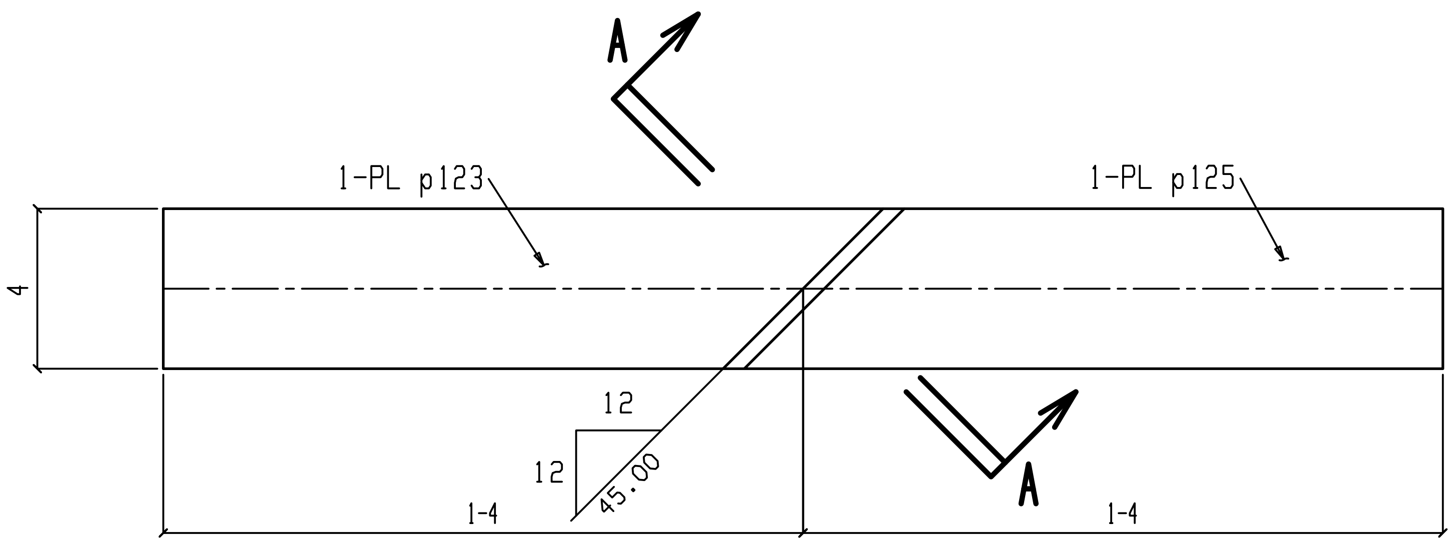

ONE MISC PS5

USE E100XX ELECTRODES

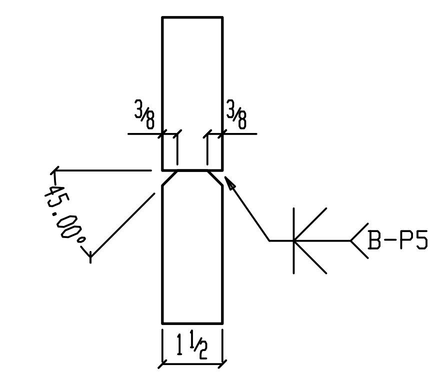

Section A-A

PS5

BATCH 1

PROJECT	AISC RESEARCH PROJECT	
DN. BY:TMR	DATE: 4-10-18	PAINT: NO PAINT

REVISIONS			PRINT RECORD	
NO.	DATE	DESCRIPTION	DATE	USE
1				FOR FAB
2				
3				
4				
5				
6				
7				
8				

COOPER STEEL
CONSTRUCTION OFFICE
1919 HAYES ST. NASHVILLE TN, 37203
OFFICE: 615-321-5222
FAX: 615-321-3030

AISC CERTIFIED FABRICATOR AND ERECTOR

DRAWING NO: PS5 ORDER NO:2874

RIDDLE STRUCTURAL DETAILING LLC.
7573 MERCER RD (731) 444-4464 (731) 779-3771
BROWNSVILLE, TENNESSEE 38012

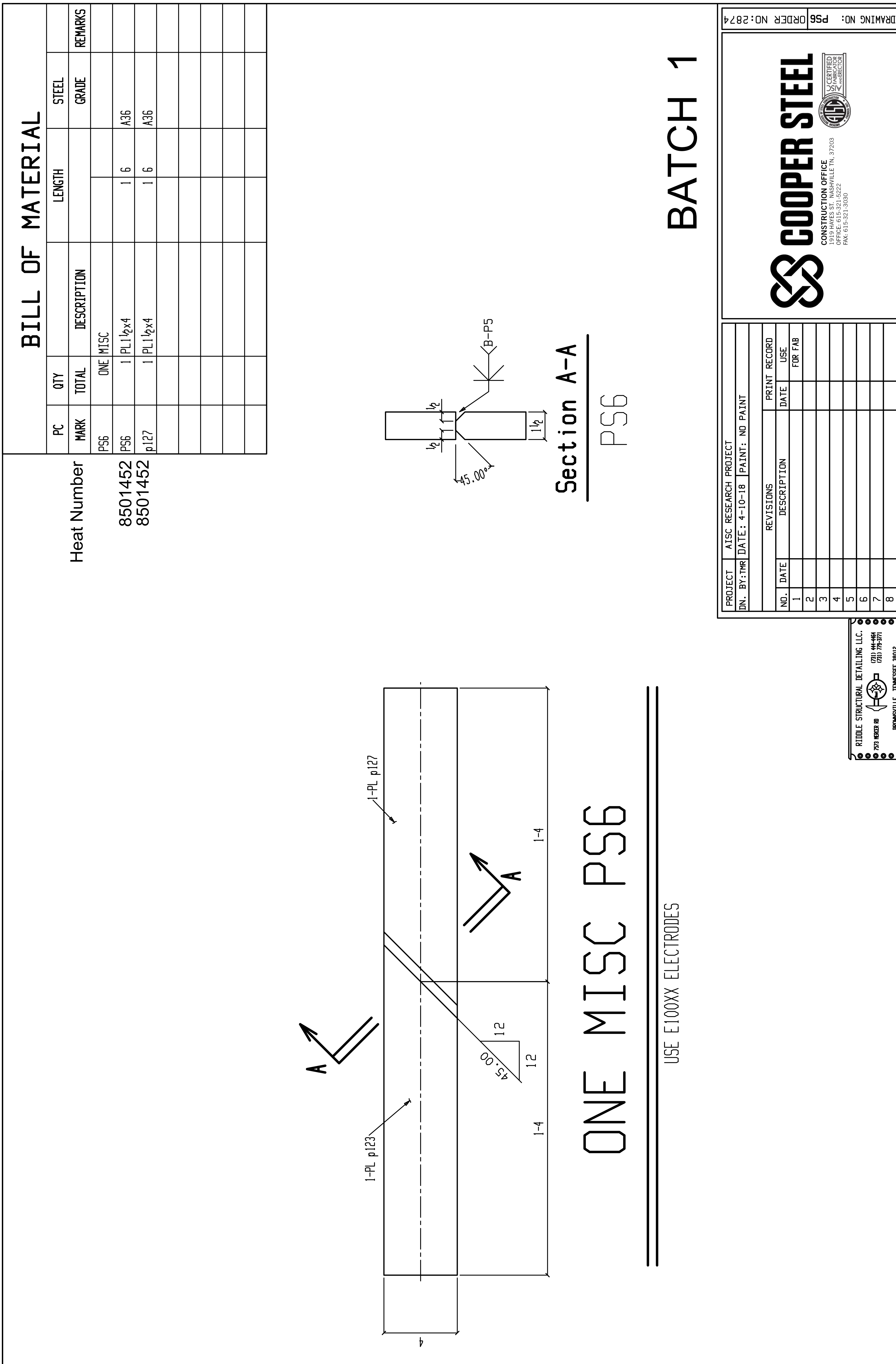
BILL OF MATERIAL
PC MARK | QTY TOTAL | DESCRIPTION | LENGTH | STEEL GRADE | REMARKS
P56 | ONE | MISC
P56 | 1 | PL1½x4 | 1 6 | A36
p127 | 1 | PL1½x4 | 1 6 | A36
Heat Number
8501452
8501452
BATCH 1
DRAWING NO: P56 ORDER NO: 2874
COOPER STEEL
CONSTRUCTION OFFICE
1919 HAYES ST. NASHVILLE TN, 37203
OFFICE: 615-321-5222
FAX: 615-321-3030
PROJECT AISC RESEARCH PROJECT
DN. BY: TMR DATE: 4-10-18 PAINT: NO PAINT
REVISIONS
NO. DATE DESCRIPTION
PRINT RECORD
DATE USE
FOR FAB
RIDDLE STRUCTURAL DETAILING LLC.
BROWNSVILLE, TENNESSEE 38012
B-P5
½
½
1½
45.00°
Section A-A
P56
1-PL p127
1-PL p123
1-4
1-4
12
12
45.00
4
A
A
ONE MISC P56
USE E100XX ELECTRODES

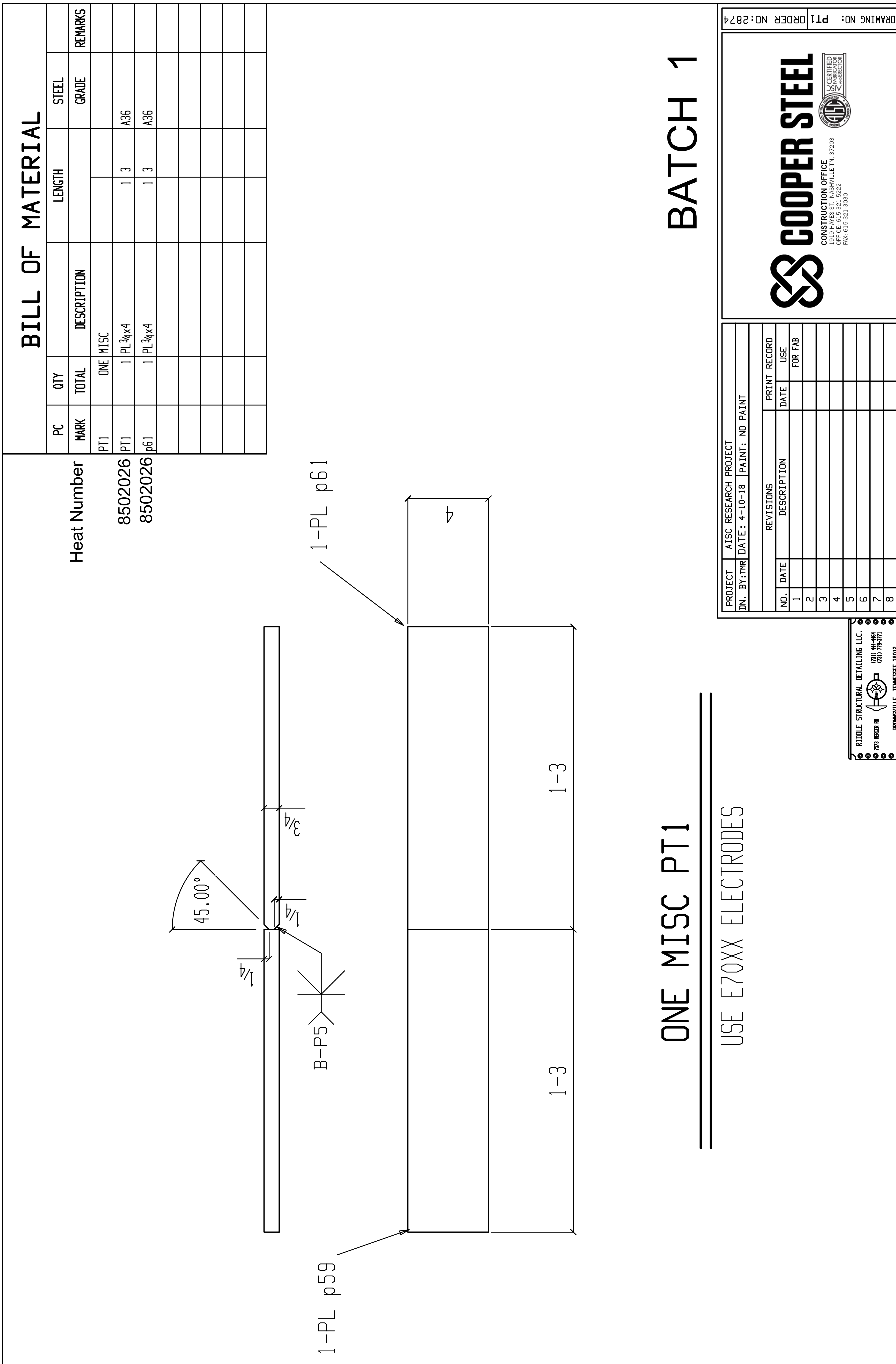
BILL OF MATERIAL
PC MARK
QTY TOTAL
DESCRIPTION
LENGTH
STEEL GRADE
REMARKS
Heat Number
PT1 ONE MISC
8502026 PT1 1 PL3/4x4 1 3 A36
8502026 p61 1 PL3/4x4 1 3 A36
45.00°
1/4
1/4
3/4
B-P5
1-PL p59
1-PL p61
4
1-3
1-3
ONE MISC PT1
USE E70XX ELECTRODES
BATCH 1
PROJECT AISC RESEARCH PROJECT
DN. BY:TMR DATE: 4-10-18 PAINT: NO PAINT
REVISIONS
PRINT RECORD
NO. DATE DESCRIPTION DATE USE
1 FOR FAB
2
3
4
5
6
7
8
COOPER STEEL
CONSTRUCTION OFFICE
1919 HAYES ST. NASHVILLE TN, 37203
OFFICE: 615-321-5222
FAX: 615-321-3030
AISC CERTIFIED FABRICATOR AND ERECTOR
DRAWING NO: PT1
ORDER NO:2874
RIDDLE STRUCTURAL DETAILING LLC.
7573 MERCER RD
(731) 444-4464
(731) 779-3771
BROWNSVILLE, TENNESSEE 38012

BILL OF MATERIAL

Heat Number	PC MARK	QTY TOTAL	DESCRIPTION	LENGTH		STEEL GRADE	REMARKS
	PT2	ONE	MISC				
D5715	PT2	1	PL1x4	1	3	A36	
D5715	p65	1	PL1x4	1	3	A36	

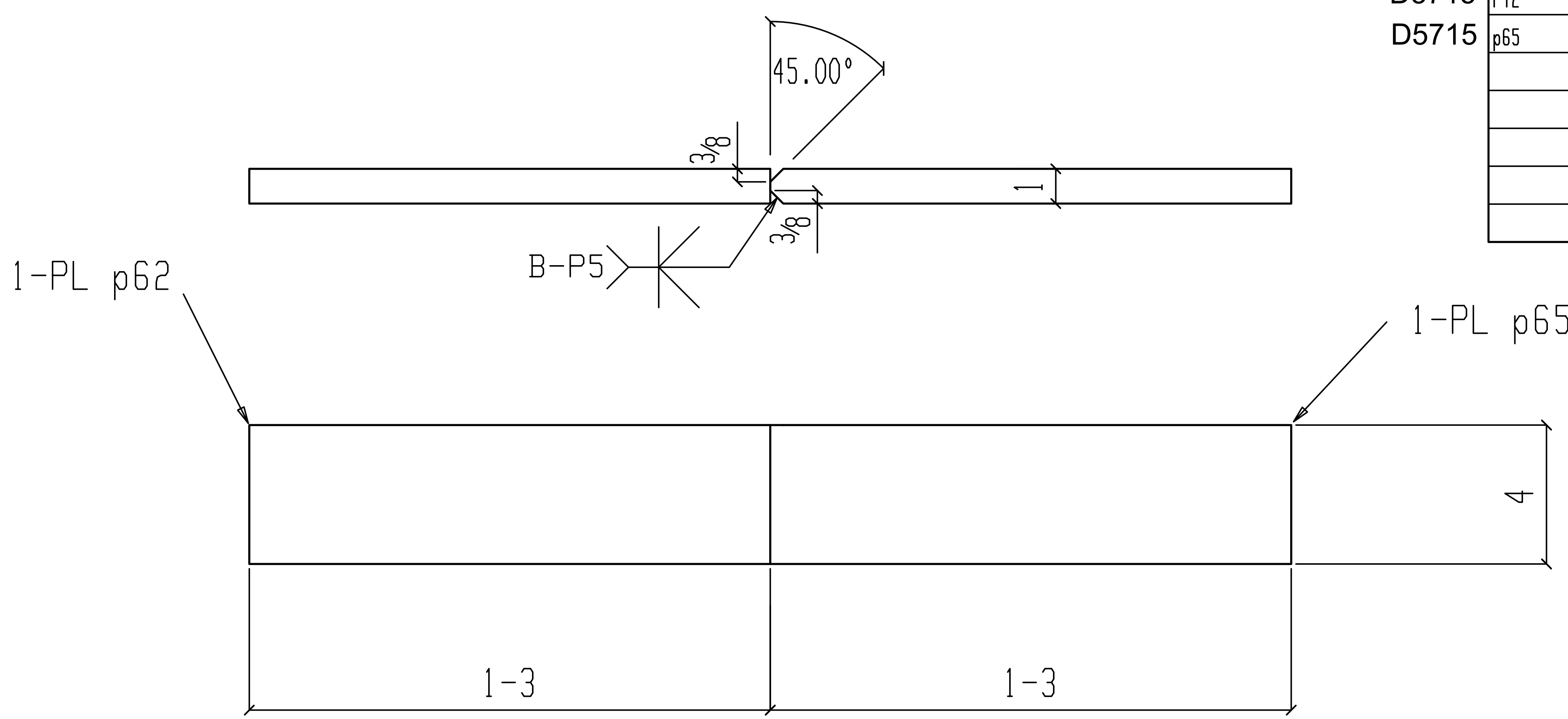

BATCH 1

ONE MISC PT2

USE E70XX ELECTRODES

PROJECT	AISC RESEARCH PROJECT		
DN. BY:TMR	DATE: 4-10-18	PAINT: NO PAINT	

NO.	DATE	REVISIONS DESCRIPTION	PRINT RECORD DATE	USE
1				FOR FAB
2				
3				
4				
5				
6				
7				
8				

RIDDLE STRUCTURAL DETAILING LLC.
7573 MERCER RD (731) 444-4464 (731) 779-3771
BROWNSVILLE, TENNESSEE 38012

COOPER STEEL
CONSTRUCTION OFFICE
1919 HAYES ST. NASHVILLE TN, 37203
OFFICE: 615-321-5222
FAX: 615-321-3030
AISC CERTIFIED FABRICATOR AND ERECTOR

DRAWING NO: PT2 ORDER NO:2874

BILL OF MATERIAL

Heat Number	PC MARK	QTY TOTAL	DESCRIPTION	LENGTH		STEEL GRADE	REMARKS
	PT3	ONE	MISC				
8501452	PT3	1	PL1½x4	1	3	A36	
8501452	p69	1	PL1½x4	1	3	A36	

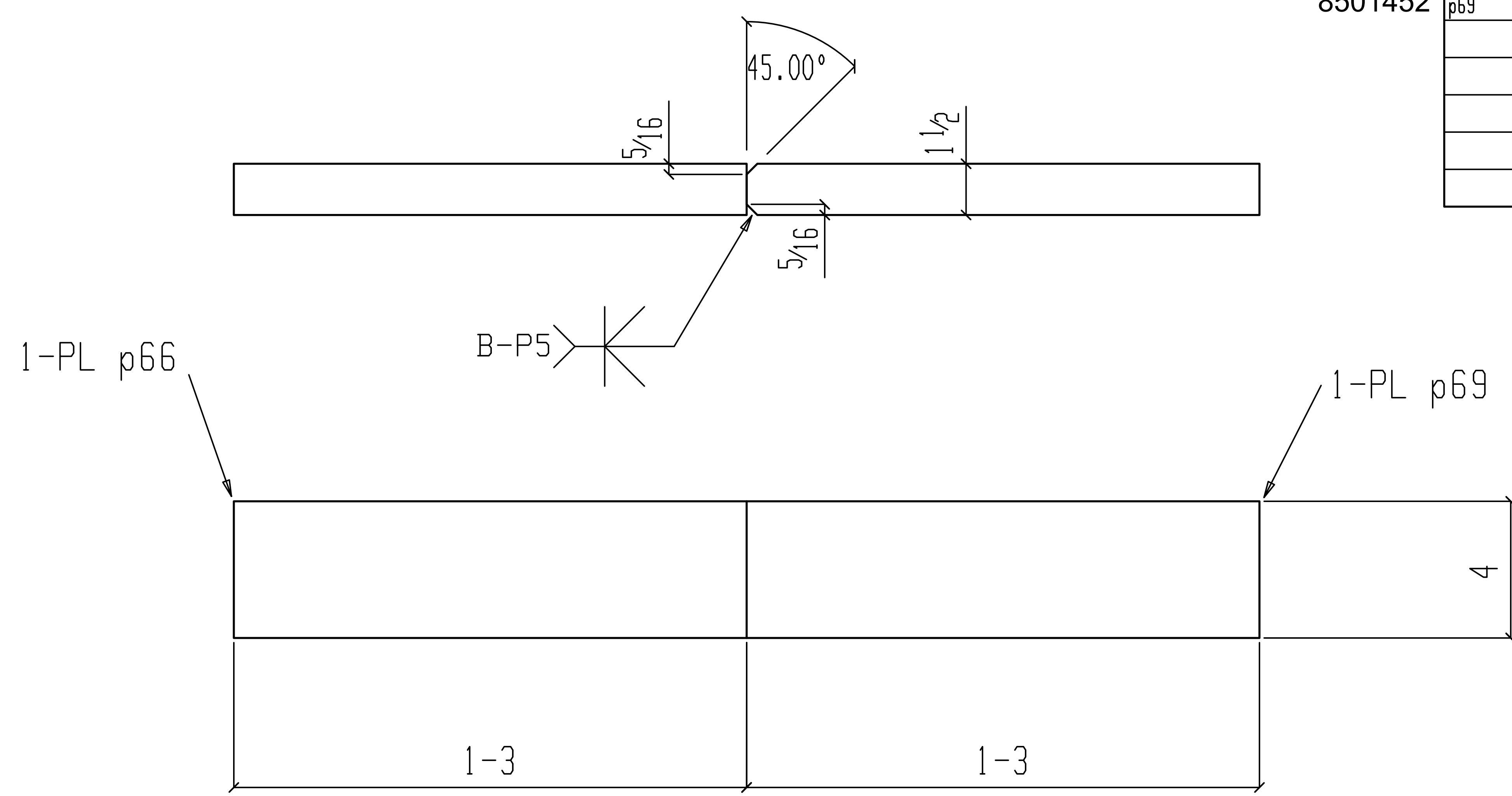

BATCH 1

ONE MISC PT3

USE E70XX ELECTRODES

PROJECT	AISC RESEARCH PROJECT				
DN. BY:TMR	DATE: 4-10-18	PAINT: NO PAINT			
		REVISIONS		PRINT RECORD	
NO.	DATE	DESCRIPTION		DATE	USE
1					FOR FAB
2					
3					
4					
5					
6					
7					
8					

COOPER STEEL
CONSTRUCTION OFFICE
1919 HAYES ST. NASHVILLE TN, 37203
OFFICE: 615-321-5222
FAX: 615-321-3030

AISC CERTIFIED FABRICATOR AND ERECTOR

DRAWING NO: PT3 ORDER NO:2874

RIDDLE STRUCTURAL DETAILING LLC.
7573 MERCER RD
(731) 444-4464
(731) 779-3771
BROWNSVILLE, TENNESSEE 38012

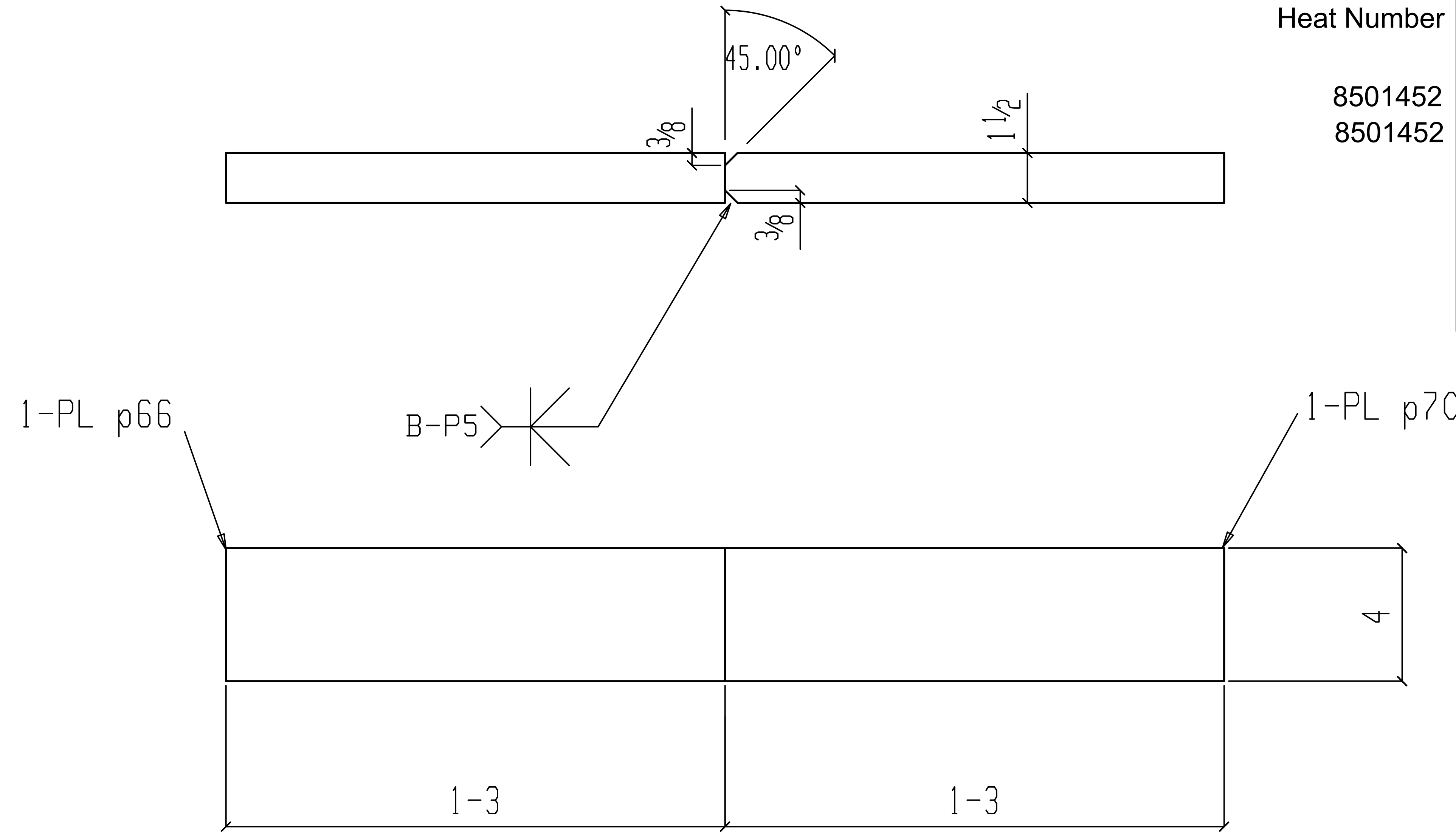

BILL OF MATERIAL

Heat Number	PC MARK	QTY TOTAL	DESCRIPTION	LENGTH		STEEL GRADE	REMARKS
	PT4	ONE	MISC				
8501452	PT4	1	PL1½x4	1	3	A36	
8501452	p70	1	PL1½x4	1	3	A36	

BATCH 1

ONE MISC PT4

USE E70XX ELECTRODES

RIDDLE STRUCTURAL DETAILING LLC.
7573 MERCER RD
(731) 444-4464
(731) 779-3771
BROWNSVILLE, TENNESSEE 38012

PROJECT	AISC RESEARCH PROJECT	
DN. BY:TMR	DATE: 4-10-18	PAINT: NO PAINT

REVISIONS			PRINT RECORD	
NO.	DATE	DESCRIPTION	DATE	USE
1				FOR FAB
2				
3				
4				
5				
6				
7				
8				

COOPER STEEL
CONSTRUCTION OFFICE
1919 HAYES ST. NASHVILLE TN, 37203
OFFICE: 615-321-5222
FAX: 615-321-3030
AISC CERTIFIED FABRICATOR AND ERECTOR

DRAWING NO: PT4 ORDER NO:2874

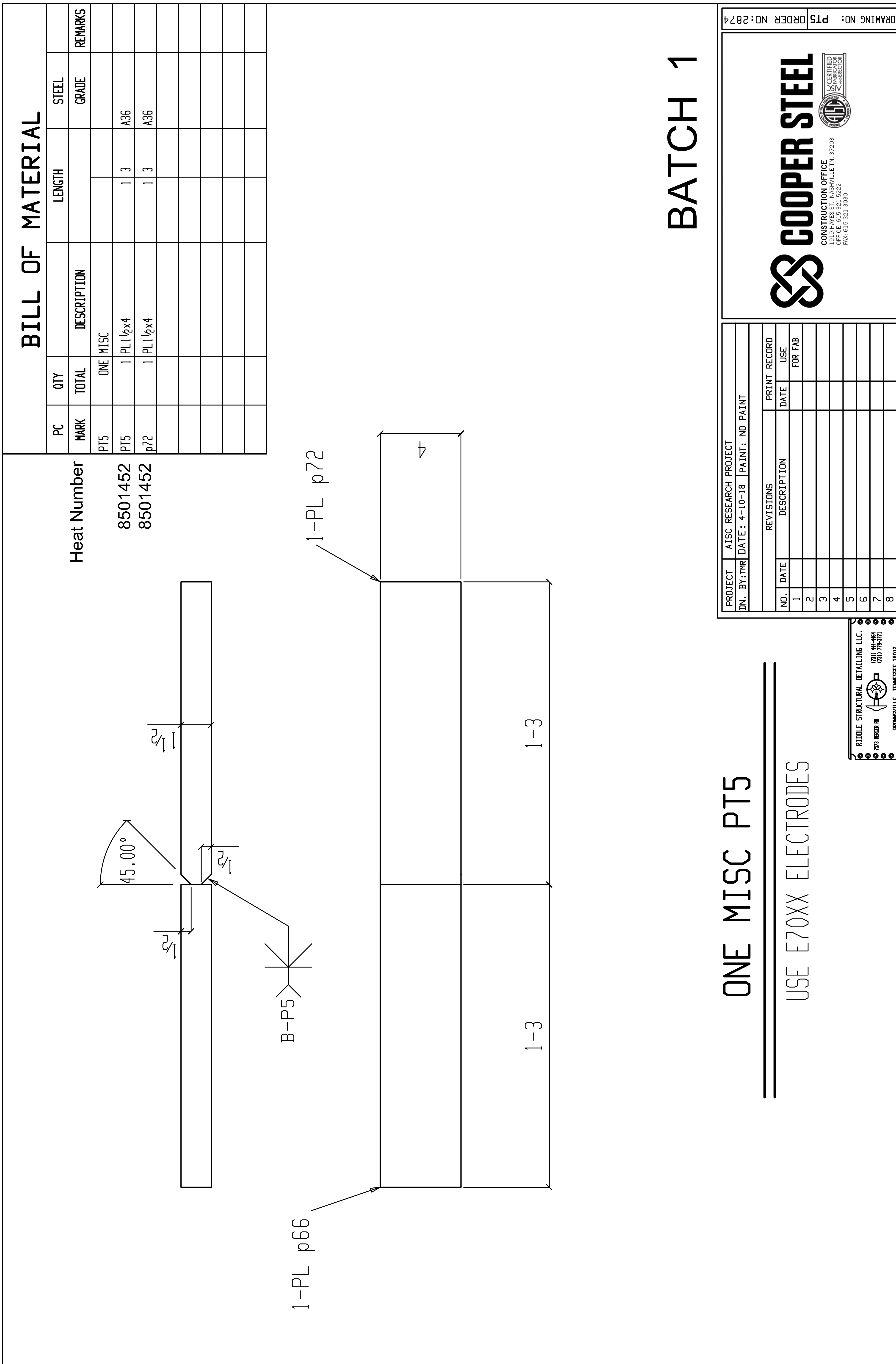

PC MARK	QTY TOTAL	DESCRIPTION	LENGTH	STEEL GRADE	REMARKS
PT5	ONE	MISC			
PT5	1	PL1½x4	1 3	A36	
p72	1	PL1½x4	1 3	A36	

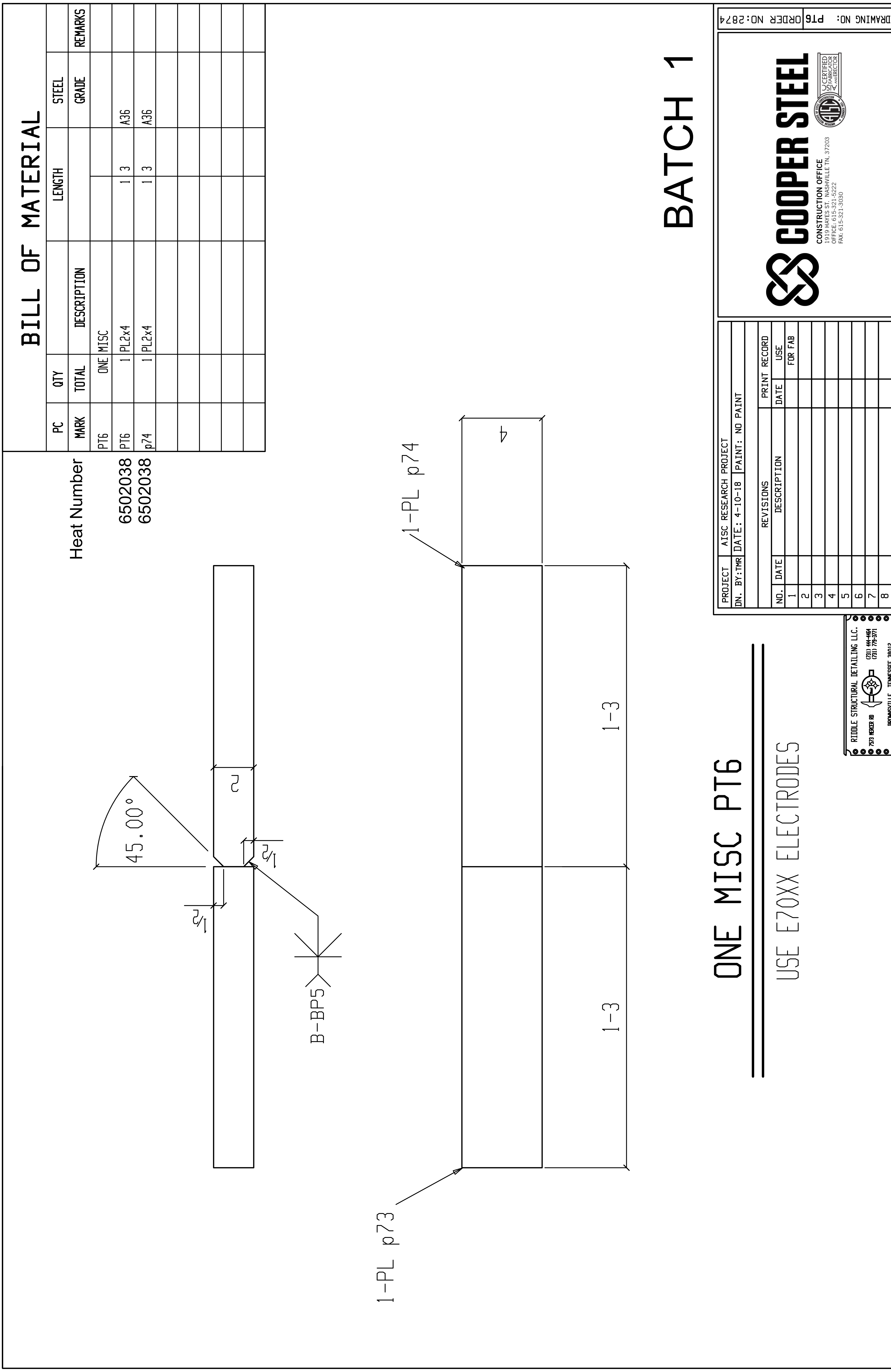
BILL OF MATERIAL
PC MARK | QTY TOTAL | DESCRIPTION | LENGTH | STEEL GRADE | REMARKS
PT6 | ONE | MISC
PT6 | 1 | PL2x4 | 1 3 | A36
p74 | 1 | PL2x4 | 1 3 | A36
Heat Number
6502038
6502038
BATCH 1
COOPER STEEL
CONSTRUCTION OFFICE
1919 HAYES ST. NASHVILLE TN. 37203
OFFICE: 615-321-5222
FAX: 615-321-3030
DRAWING NO: PT6 ORDER NO:2874
PROJECT AISC RESEARCH PROJECT
DN. BY:TMR DATE: 4-10-18 PAINT: NO PAINT
REVISIONS
NO. DATE DESCRIPTION
PRINT RECORD
DATE USE
FOR FAB
RIDDLE STRUCTURAL DETAILING LLC.
BROWNSVILLE, TENNESSEE 38012
ONE MISC PT6
USE E70XX ELECTRODES
1-PL p74
1-PL p73
4
1-3
1-3
2
45.00°
1/2
1/2
B-BP5

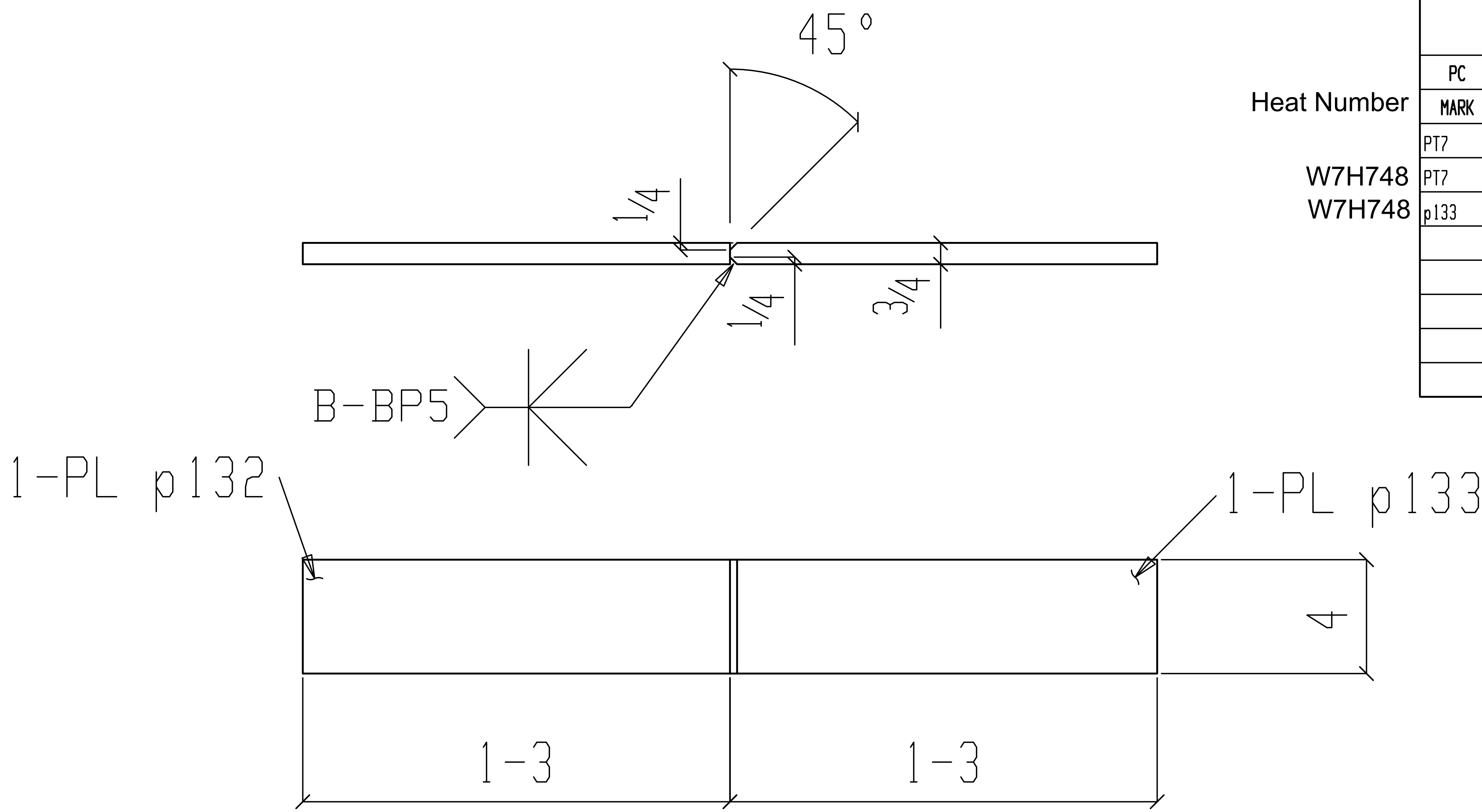

BILL OF MATERIAL

Heat Number	PC MARK	QTY TOTAL	DESCRIPTION	LENGTH		STEEL GRADE	REMARKS
	PT7	ONE	MISC				
W7H748	PT7	1	PL¾x4	1	3	A572-65	
W7H748	p133	1	PL¾x4	1	3	A572-65	

ONE MISC PT7

USE E70XX ELECTRODES

BATCH 1

PROJECT	AISC RESEARCH PROJECT			
DN. BY:TMR	DATE: 4-10-18	PAINT: NO PAINT		

REVISIONS			PRINT RECORD	
NO.	DATE	DESCRIPTION	DATE	USE
1				FOR FAB
2				
3				
4				
5				
6				
7				
8				

RIDDLE STRUCTURAL DETAILING LLC.
7573 MERCER RD (731) 444-4464 (731) 779-3771
BROWNSVILLE, TENNESSEE 38012

COOPER STEEL
CONSTRUCTION OFFICE
1919 HAYES ST. NASHVILLE TN, 37203
OFFICE: 615-321-5222
FAX: 615-321-3030
AISC CERTIFIED FABRICATOR AND ERECTOR

DRAWING NO: PT7 ORDER NO:2874

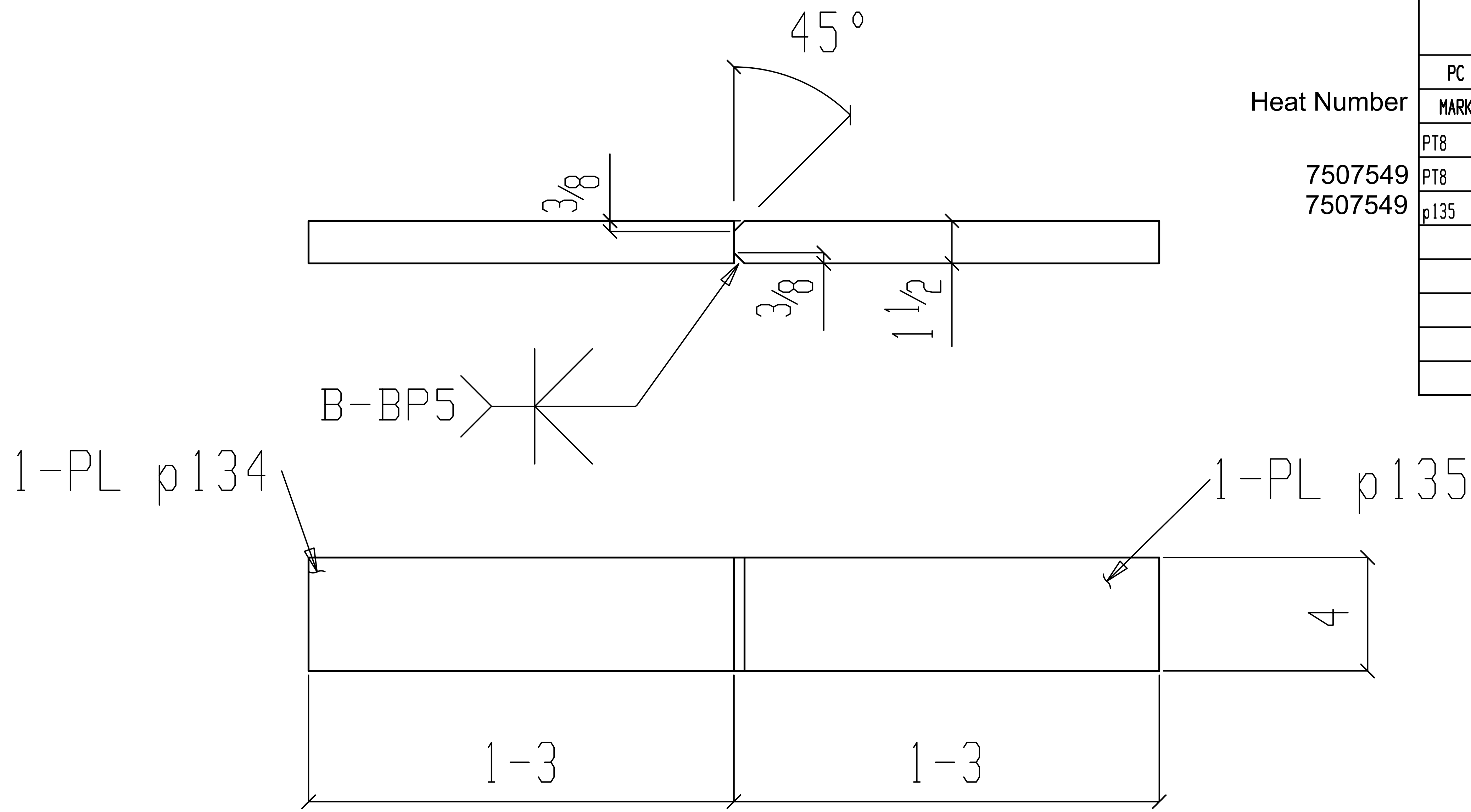

BILL OF MATERIAL

Heat Number	PC MARK	QTY TOTAL	DESCRIPTION	LENGTH		STEEL GRADE	REMARKS
	PT8	ONE	MISC				
7507549	PT8	1	PL1½x4	1	3	A572-65	
7507549	p135	1	PL1½x4	1	3	A572-65	

ONE MISC PT8

USE E70XX ELECTRODES

BATCH 1

PROJECT	AISC RESEARCH PROJECT		
DN. BY:TMR	DATE: 4-10-18	PAINT: NO PAINT	

NO.	DATE	DESCRIPTION	DATE	USE
	REVISIONS		PRINT RECORD	
1				FOR FAB
2				
3				
4				
5				
6				
7				
8				

RIDDLE STRUCTURAL DETAILING LLC.
7573 MERCER RD (731) 444-4464 (731) 779-3771
BROWNSVILLE, TENNESSEE 38012

COOPER STEEL
CONSTRUCTION OFFICE
1919 HAYES ST. NASHVILLE TN, 37203
OFFICE: 615-321-5222
FAX: 615-321-3030
AISC CERTIFIED FABRICATOR AND ERECTOR

DRAWING NO: PT8 ORDER NO:2874

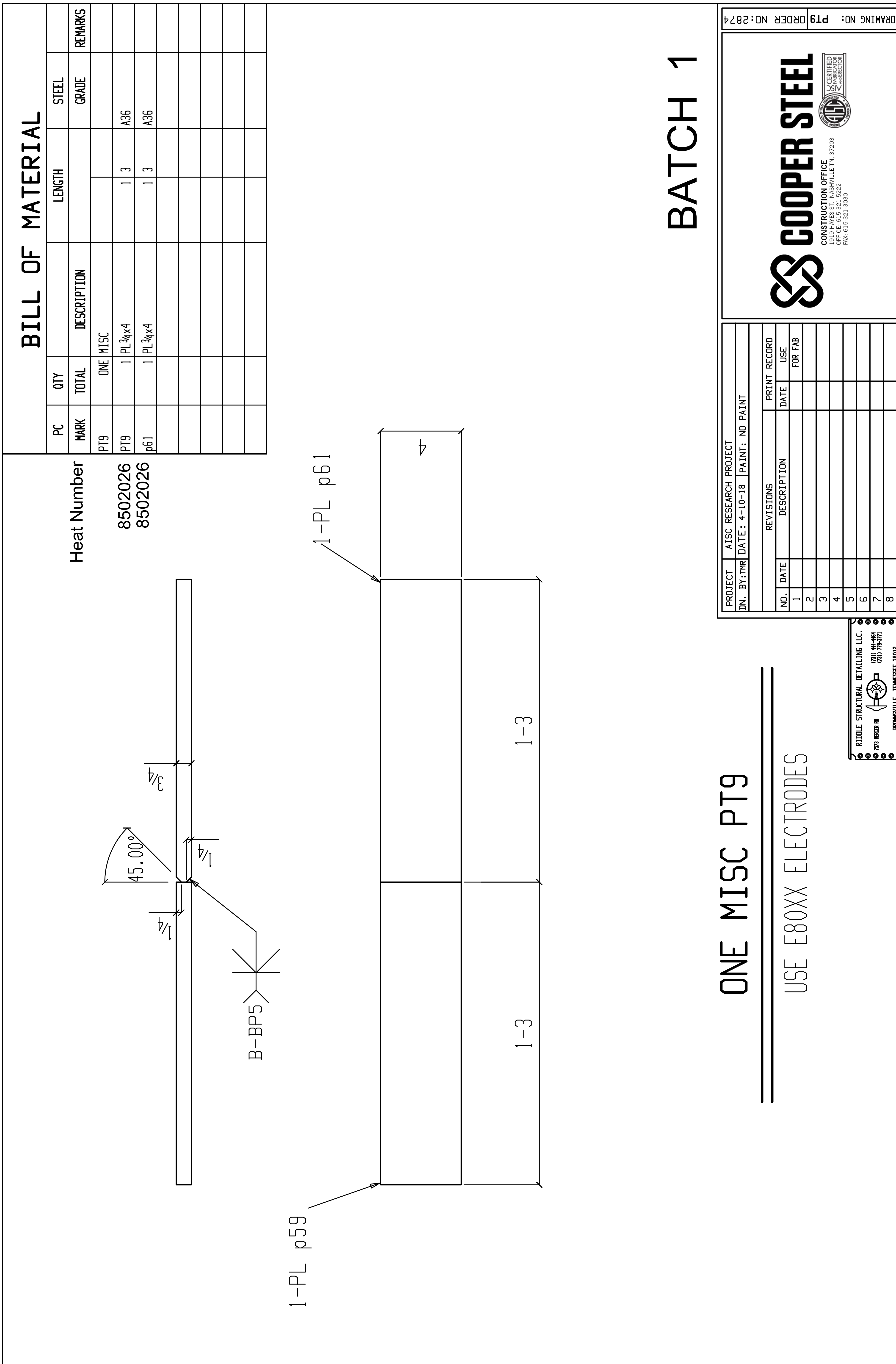

PC MARK	QTY TOTAL	DESCRIPTION	LENGTH	STEEL GRADE	REMARKS
PT9	ONE	MISC			
PT9	1	PL3/4x4	1 3	A36	
p61	1	PL3/4x4	1 3	A36	

BILL OF MATERIAL

Heat Number	PC MARK	QTY TOTAL	DESCRIPTION	LENGTH		STEEL GRADE	REMARKS
	PT10	ONE	MISC				
8501452	PT10	1	PL1½x4	1	3	A36	
8501452	p70	1	PL1½x4	1	3	A36	

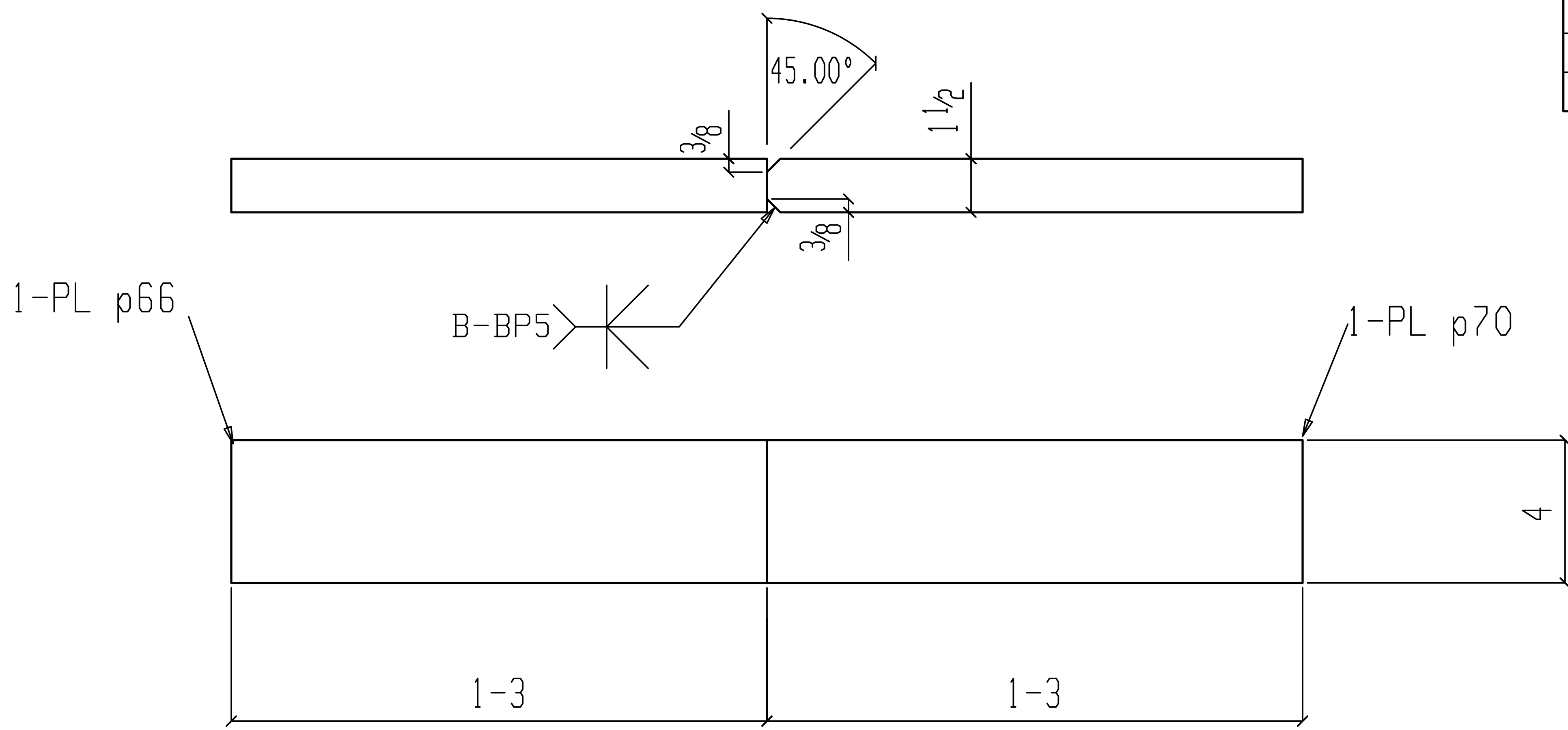

ONE MISC PT10

USE E80XX ELECTRODES

BATCH 1

PROJECT	AISC RESEARCH PROJECT	
DN. BY:TMR	DATE: 4-10-18	PAINT: NO PAINT

NO.	DATE	REVISIONS DESCRIPTION	PRINT RECORD DATE	USE
1				FOR FAB
2				
3				
4				
5				
6				
7				
8				

RIDDLE STRUCTURAL DETAILING LLC.
7573 MERCER RD (731) 444-4464 (731) 779-3771
BROWNSVILLE, TENNESSEE 38012

COOPER STEEL
CONSTRUCTION OFFICE
1919 HAYES ST. NASHVILLE TN, 37203
OFFICE: 615-321-5222
FAX: 615-321-3030
AISC CERTIFIED FABRICATOR AND ERECTOR

DRAWING NO: PT10 ORDER NO:2874

BILL OF MATERIAL

Heat Number	PC MARK	QTY TOTAL	DESCRIPTION	LENGTH		STEEL GRADE	REMARKS
	PT11	ONE	MISC				
8501452	PT11	1	PL1½x4	1	3	A36	
8501452	p72	1	PL1½x4	1	3	A36	

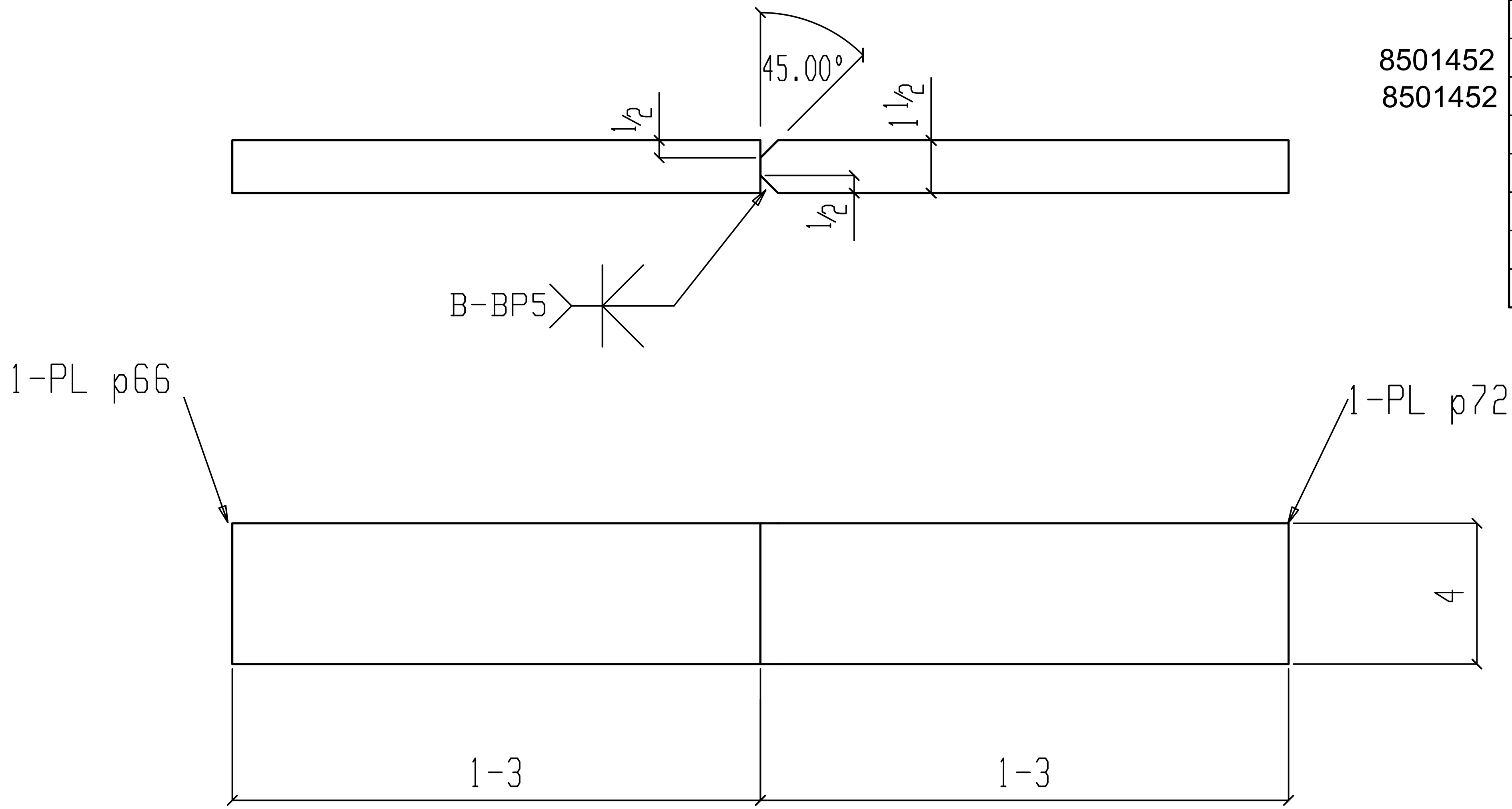

BATCH 1

ONE MISC PT11

USE E80XX ELECTRODES

RIDDLE STRUCTURAL DETAILING LLC.
7573 MERCER RD (731) 444-4464 (731) 779-3771
BROWNSVILLE, TENNESSEE 38012

PROJECT	AISC RESEARCH PROJECT			
DN. BY:TMR	DATE: 4-10-18	PAINT: NO PAINT		

REVISIONS			PRINT RECORD	
NO.	DATE	DESCRIPTION	DATE	USE
1				FOR FAB
2				
3				
4				
5				
6				
7				
8				

COOPER STEEL
CONSTRUCTION OFFICE
1919 HAYES ST. NASHVILLE TN, 37203
OFFICE: 615-321-5222
FAX: 615-321-3030
AISC CERTIFIED FABRICATOR AND ERECTOR

DRAWING NO: PT11 ORDER NO:2874

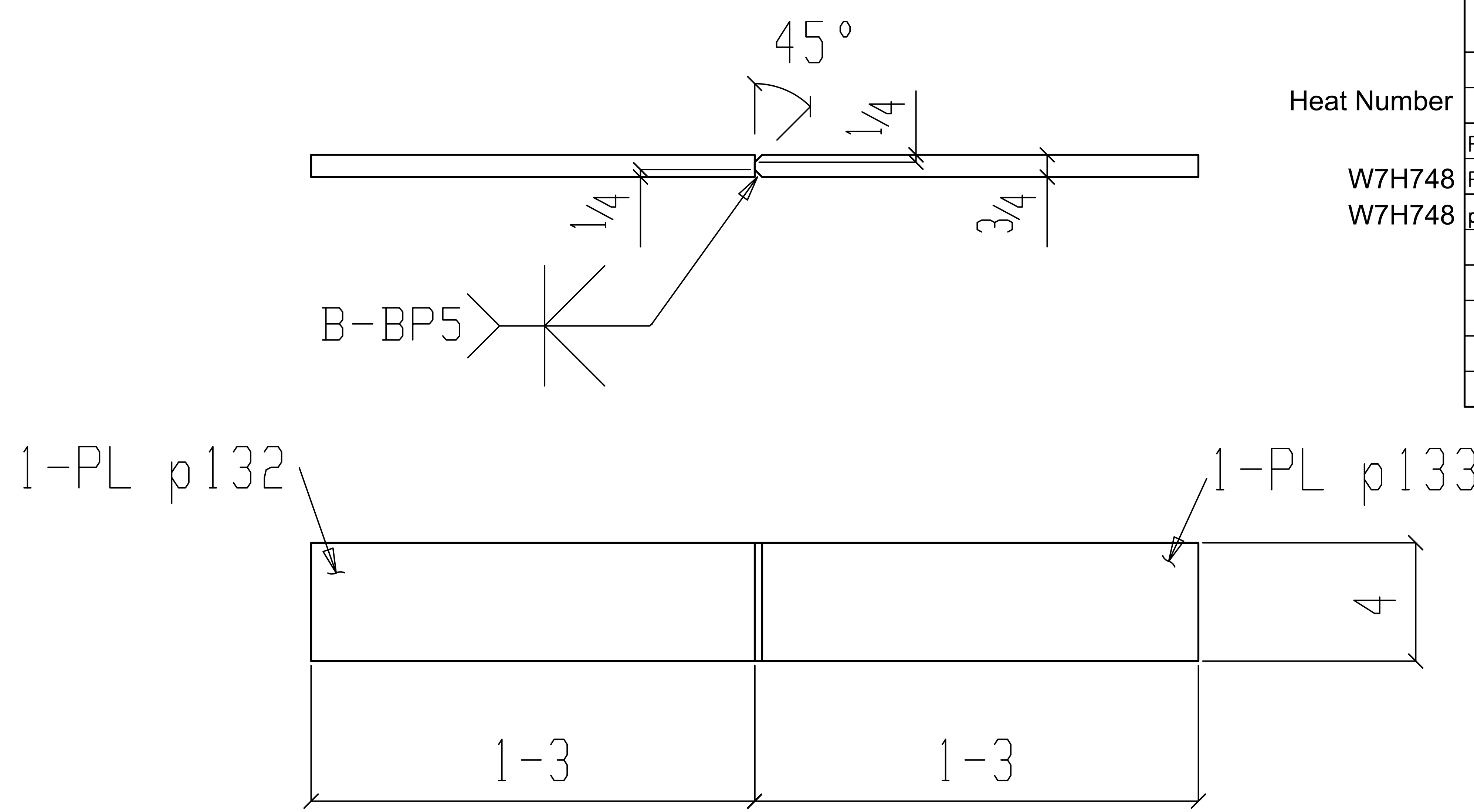

BILL OF MATERIAL

Heat Number	PC MARK	QTY TOTAL	DESCRIPTION	LENGTH		STEEL GRADE	REMARKS
	PT12	ONE	MISC				
W7H748	PT12	1	PL¾x4	1	3	A572-65	
W7H748	p133	1	PL¾x4	1	3	A572-65	

ONE MISC PT12

USE E80XX ELECTRODES

BATCH 1

PROJECT	AISC RESEARCH PROJECT	
DN. BY:TMR	DATE: 4-10-18	PAINT: NO PAINT

REVISIONS			PRINT RECORD	
NO.	DATE	DESCRIPTION	DATE	USE
1				FOR FAB
2				
3				
4				
5				
6				
7				
8				

RIDDLE STRUCTURAL DETAILING LLC.
7573 MERCER RD (731) 444-4464 (731) 779-3771
BROWNSVILLE, TENNESSEE 38012

COOPER STEEL
CONSTRUCTION OFFICE
1919 HAYES ST. NASHVILLE TN, 37203
OFFICE: 615-321-5222
FAX: 615-321-3030
AISC CERTIFIED FABRICATOR AND ERECTOR

DRAWING NO: PT12 ORDER NO:2874

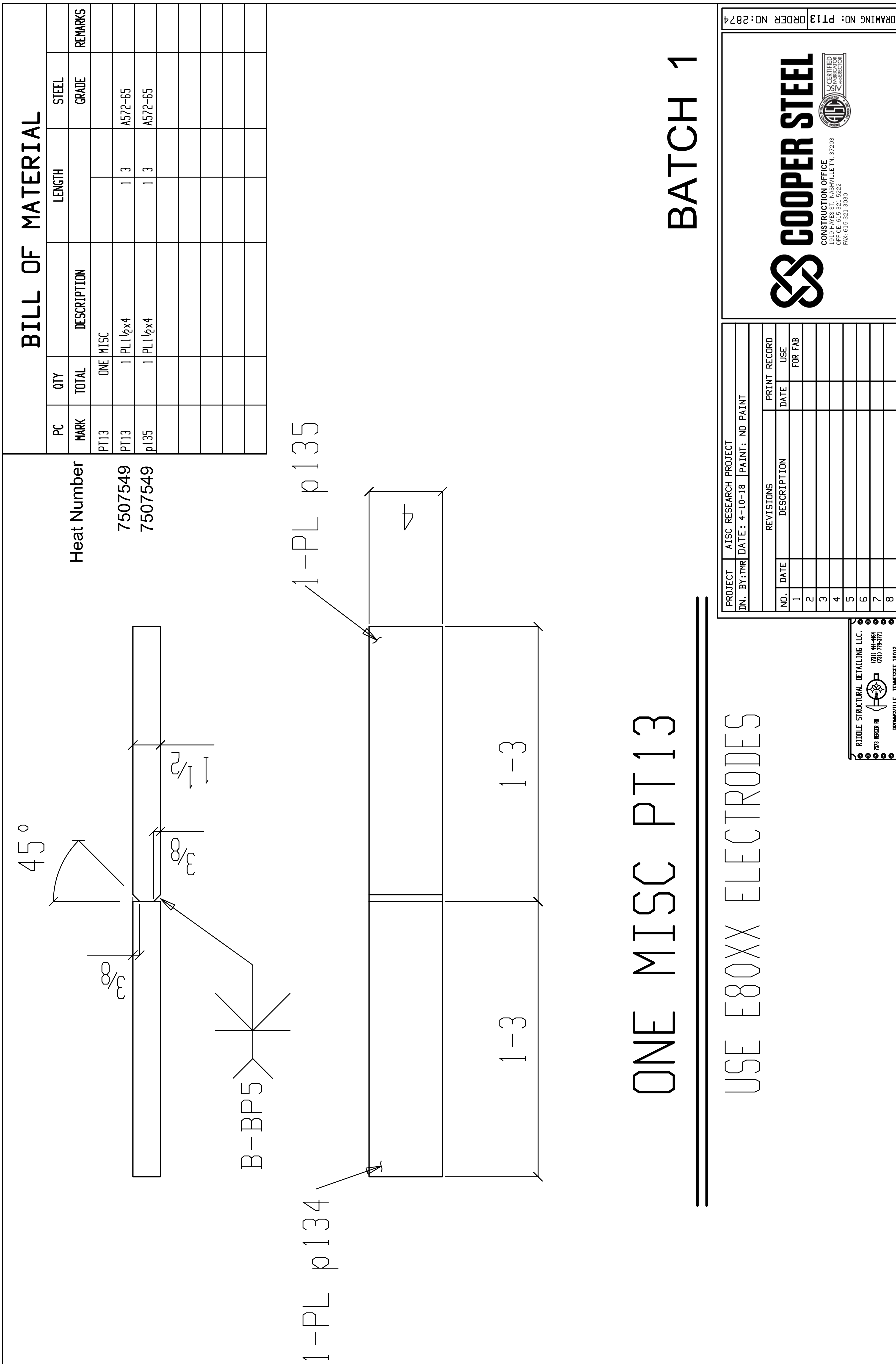
BILL OF MATERIAL
PC MARK
QTY TOTAL
DESCRIPTION
LENGTH
STEEL GRADE
REMARKS
PT13 ONE MISC
PT13 1 PL1½x4 1 3 A572-65
p135 1 PL1½x4 1 3 A572-65
Heat Number
7507549
7507549
BATCH 1
DRAWING NO: PT13
ORDER NO:2874
COOPER STEEL
CONSTRUCTION OFFICE
1919 HAYES ST. NASHVILLE TN, 37203
OFFICE: 615-321-5222
FAX: 615-321-3030
CERTIFIED FABRICATOR and ERECTOR
PROJECT AISC RESEARCH PROJECT
DN. BY:TMR DATE: 4-10-18 PAINT: NO PAINT
REVISIONS
NO. DATE DESCRIPTION
1 2 3 4 5 6 7 8
PRINT RECORD
DATE USE
FOR FAB
RIDDLE STRUCTURAL DETAILING LLC.
7573 MERCER RD
BROWNSVILLE, TENNESSEE 38012
45°
1/2
3/8
3/8
B-BP5
1-PL p134
1-PL p135
4
1-3
1-3
ONE MISC PT13
USE E80XX ELECTRODES

BILL OF MATERIAL

Heat Number	PC MARK	QTY TOTAL	DESCRIPTION	LENGTH		STEEL GRADE	REMARKS
	PT14	ONE	MISC				
8502026	PT14	1	PL¾x4	1	3	A36	
8502026	p61	1	PL¾x4	1	3	A36	

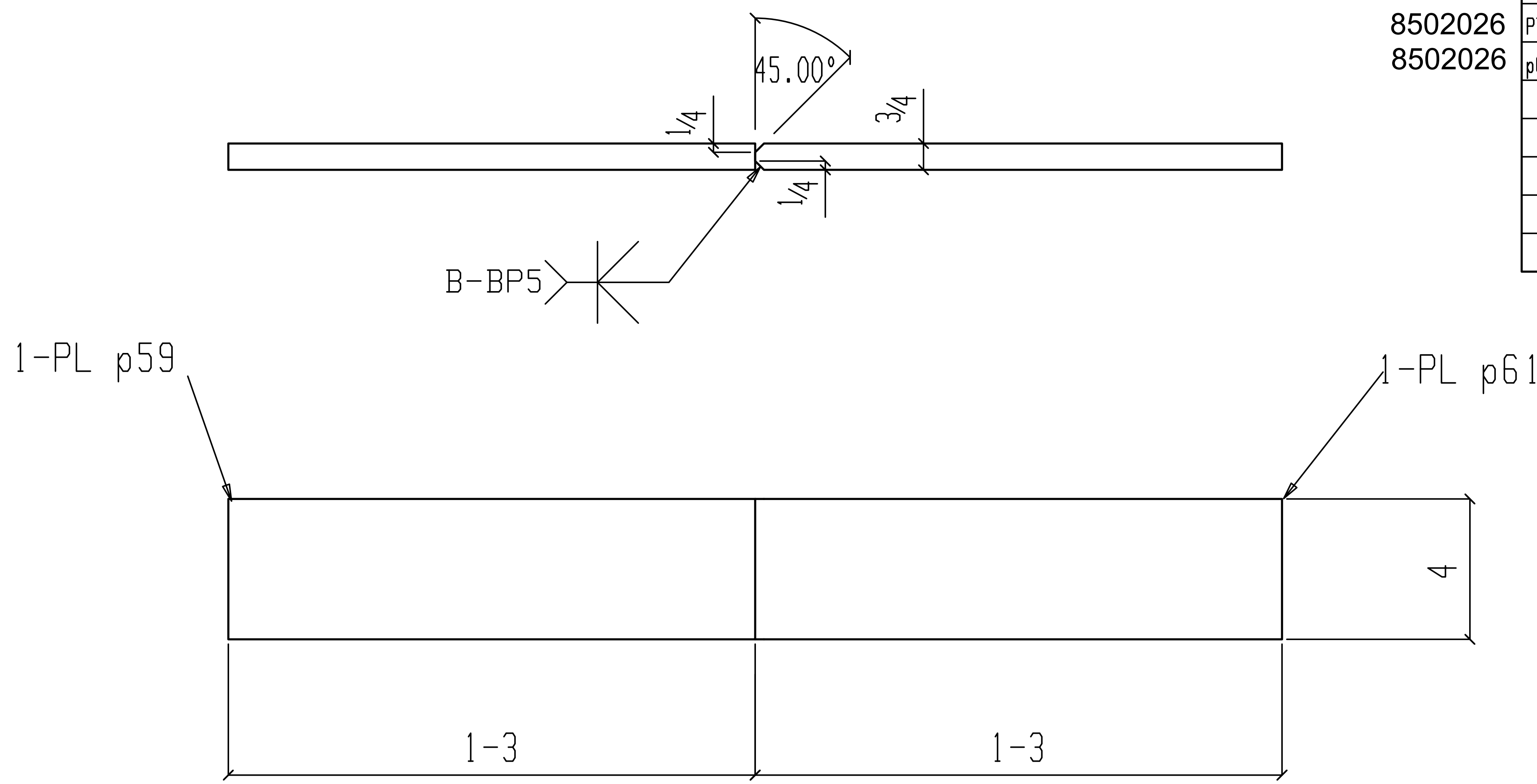

BATCH 1

ONE MISC PT14

USE E100XX ELECTRODES

RIDDLE STRUCTURAL DETAILING LLC.
7573 MERCER RD (731) 444-4464 (731) 779-3771
BROWNSVILLE, TENNESSEE 38012

PROJECT	AISC RESEARCH PROJECT	
DN. BY:TMR	DATE: 4-10-18	PAINT: NO PAINT

REVISIONS			PRINT RECORD	
NO.	DATE	DESCRIPTION	DATE	USE
1				FOR FAB
2				
3				
4				
5				
6				
7				
8				

COOPER STEEL
CONSTRUCTION OFFICE
1919 HAYES ST. NASHVILLE TN, 37203
OFFICE: 615-321-5222
FAX: 615-321-3030
AISC CERTIFIED FABRICATOR AND ERECTOR

DRAWING NO: PT14 ORDER NO:2874

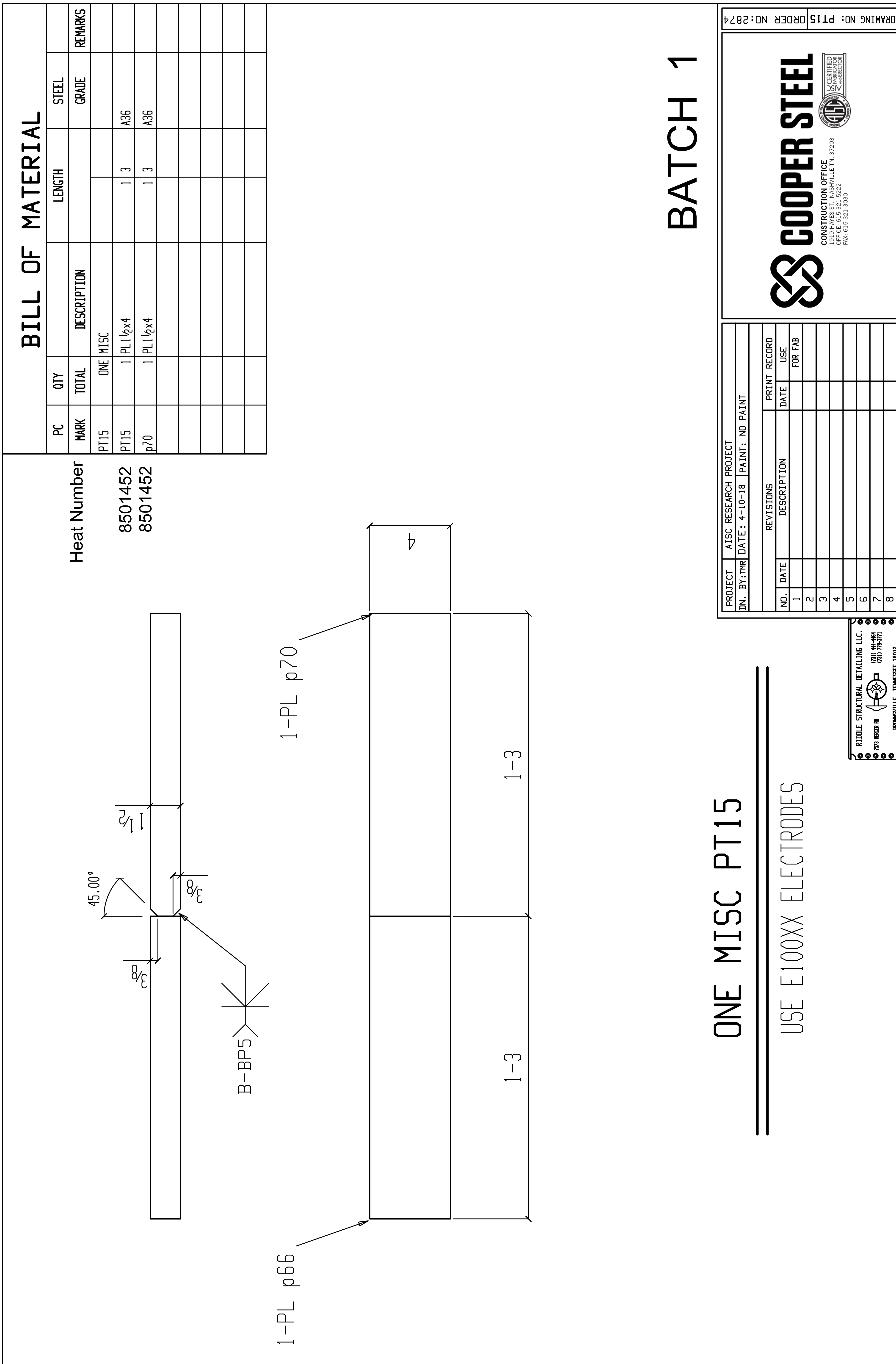

PC MARK	QTY TOTAL	DESCRIPTION	LENGTH		STEEL GRADE	REMARKS
PT15	ONE	MISC				
PT15	1	PL1½x4	1	3	A36	
p70	1	PL1½x4	1	3	A36	

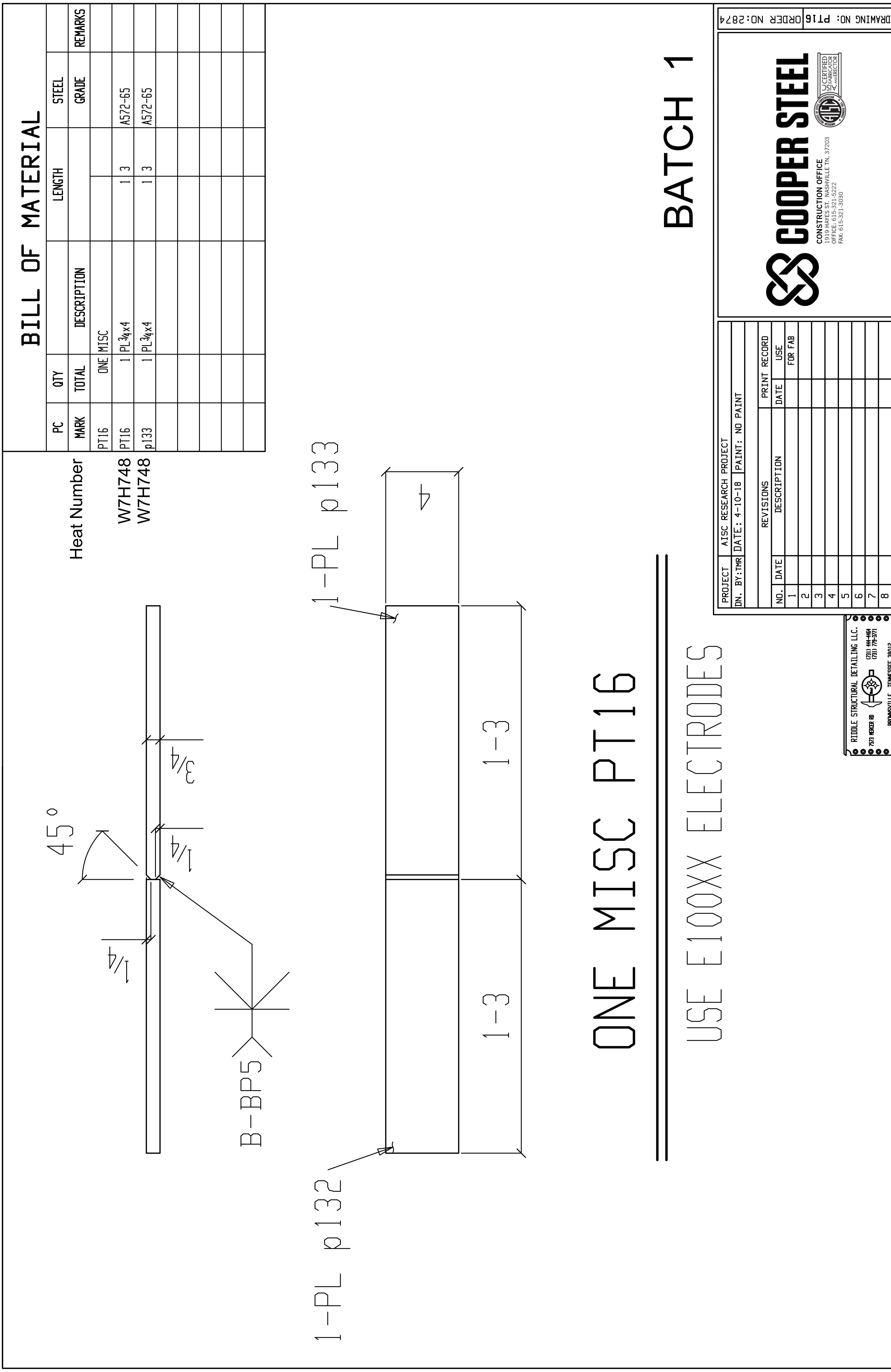
BILL OF MATERIAL
PC MARK | QTY TOTAL | DESCRIPTION | LENGTH | STEEL GRADE | REMARKS
PT16 | ONE | MISC
PT16 | 1 | PL¾x4 | 1 3 | A572-65
p133 | 1 | PL¾x4 | 1 3 | A572-65
Heat Number
W7H748
W7H748
45°
3/4
1/4
1/4
B-BP5
1-PL p133
1-PL p132
4
1-3
1-3
ONE MISC PT16
USE E100XX ELECTRODES
BATCH 1
DRAWING NO: PT16 ORDER NO:2874
COOPER STEEL
CONSTRUCTION OFFICE
1919 HAYES ST. NASHVILLE TN, 37203
OFFICE: 615-321-5222
FAX: 615-321-3030
PROJECT AISC RESEARCH PROJECT
DN. BY:TMR DATE: 4-10-18 PAINT: NO PAINT
REVISIONS
NO. DATE DESCRIPTION
PRINT RECORD
DATE USE
FOR FAB
1
2
3
4
5
6
7
8
RIDDLE STRUCTURAL DETAILING LLC.
7573 MERCER RD
BROWNSVILLE, TENNESSEE 38012
(731) 444-4464
(731) 779-3771

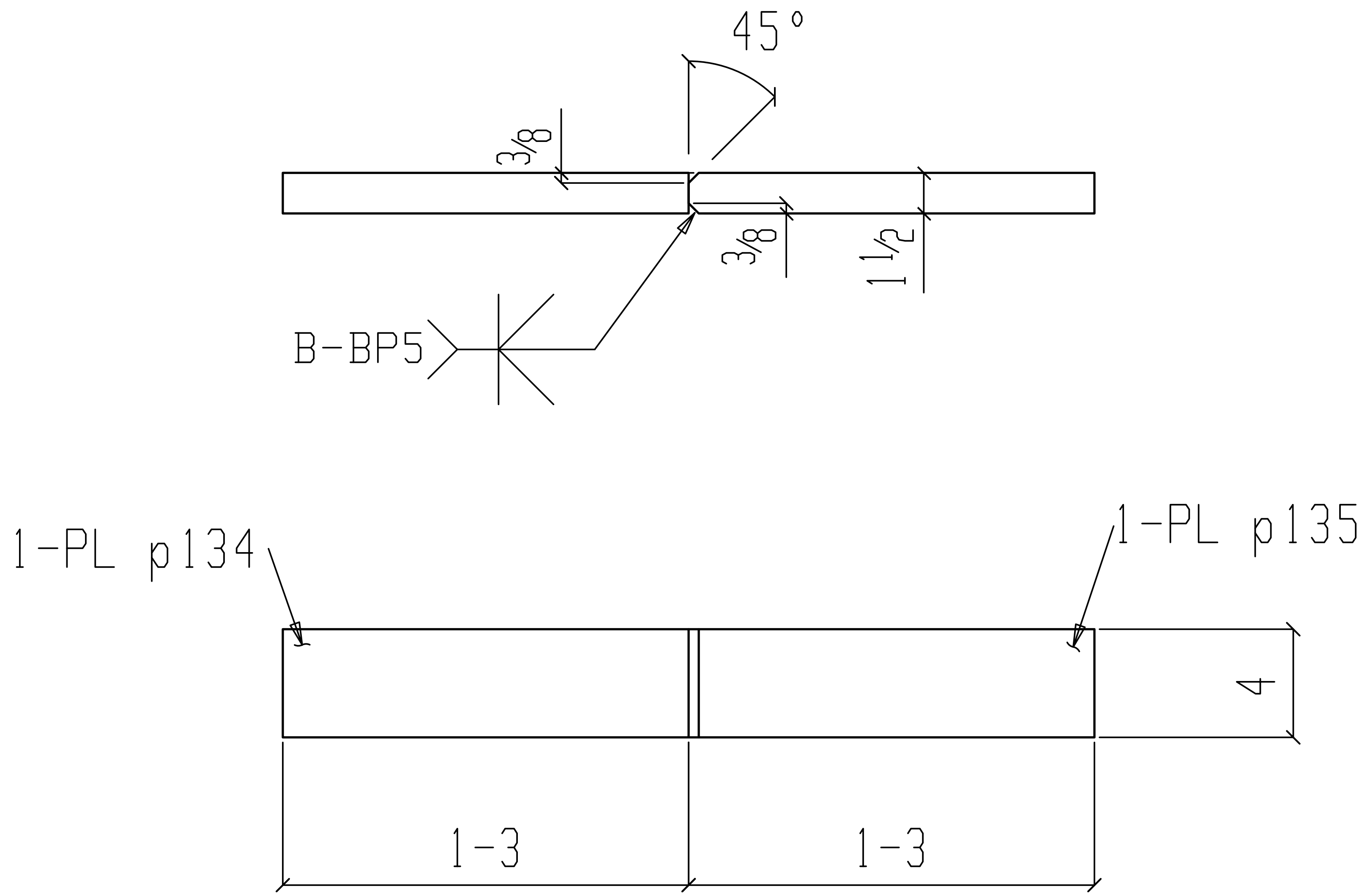

ONE MISC PT17

USE E100XX ELECTRODES

BILL OF MATERIAL

Heat Number	PC MARK	QTY TOTAL	DESCRIPTION	LENGTH		STEEL GRADE	REMARKS
	PT17	ONE	MISC				
7507549	PT17	1	PL1½x4	1	3	A572-65	
7507549	p135	1	PL1½x4	1	3	A572-65	

BATCH 1

PROJECT	AISC RESEARCH PROJECT	
DN. BY:TMR	DATE: 4-10-18	PAINT: NO PAINT

REVISIONS			PRINT RECORD	
NO.	DATE	DESCRIPTION	DATE	USE
1				FOR FAB
2				
3				
4				
5				
6				
7				
8				

COOPER STEEL
CONSTRUCTION OFFICE
1919 HAYES ST. NASHVILLE TN, 37203
OFFICE: 615-321-5222
FAX: 615-321-3030
AISC CERTIFIED FABRICATOR AND ERECTOR

DRAWING NO: PT17 ORDER NO:2874

RIDDLE STRUCTURAL DETAILING LLC.
7573 MERCER RD (731) 444-4464 (731) 779-3771
BROWNSVILLE, TENNESSEE 38012

APPENDIX B

PLATE MILL TEST REPORTS

ARCELORMITTAL PLATE LLC

TEST CERTIFICATE

SHIP TO:
KLOECKNER METALS CORP
500 MANCHESTER CT
CUSTOMER TRUCK
YORK PA 17408-7614

PAGE NO: 01 OF 02
FILE NO: 4385-15-49
MILL ORDER NO: 16053-002
MELT NO: D5715
DATE: 03/22/19

SOLD TO:
KLOECKNER METALS CORPORATION
STOCK
500 MANCHESTER CT
YORK PA 17406

SEND TO:
TEST REPORT WITH SHIPMENT

FOR BOL # 44974

STEEL PLATE DIMENSIONS / DESCRIPTION

TOTAL QTY	GAUGE	WIDTH	LENGTH	DESCRIPTION	PIECE WEIGHT
	1"	96"	240"	RECTANGLE	6534#

CUSTOMER INFORMATION

CUSTOMER PO: YOR-7360338

PART NO. PO LINE ITEM 10

SPECIFICATION(S)

THIS MATERIAL HAS BEEN MANUFACTURED AND TESTED IN ACCORDANCE WITH PURCHASE ORDER REQUIREMENTS AND SPECIFICATION(S).

AASHT M270-GR36 YR 15
DUAL CERT: ASTM A709 YR:18 GR:36 ASTM A36 YR:14.
ASME SA36 17ED
THE MANAGEMENT SYSTEMS FOR MANUFACTURE OF THIS PRODUCT ARE CERTIFIED TO ISO 9001:2015 (CERTIFICATE NO. 30130) AND ISO 14001:2015 (CERTIFICATE NO. 49009).

CHEMICAL COMPOSITION (WT%) FOR ALL ELEMENTS EXCEPT H (PPM)

	C	MN	P	S	CU	SI	NI	CR	MO
MELT:D5715	.16	.91	.014	.017	.27	.22	.29	.25	.09

	V	AL	CB
MELT:D5715	.004	.003	.001

TENSILE PROPERTIES

LOC	DIR	YIELD STRENGTH PSI X 1000	TENSILE STRENGTH PSI X 1000	ELONGATION AFTER FRACTURE GAGE LGTH	%
BOT.	TRANS.	48	77	8.00"	20.0
BOT.	TRANS.	49	77	8.00"	18.0

WE HEREBY CERTIFY THAT THE ABOVE INFORMATION IS CORRECT:

ARCELORMITTAL PLATE LLC
QUALITY ASSURANCE LABORATORY
139 MODENA ROAD
COATESVILLE, PA 19320

SUPERVISOR - TEST REPORTING
LOC V. TRAN

NUCOR
NUCOR STEEL TUSCALOOSA, INC.

MILL TEST CERTIFICATE

1700 HOLT RD N.E.
Tuscaloosa, AL 35404-1000
800 800-8204
customerservice@nucortusk.com

Load Number	Tally	Mill Order Number	PO NO | Line NO	Part Number	Certificate Number	Prepared
T168209	00000000756437	N-158673-003	BIR-7187778 3		S75643701-1	11/16/2017 15:46

Grade	Customer:
Order Description: Hot Roll Plate A57265T3, 1.0000 IN x 96.000 IN x 480.000 IN **Quality Plan Description:** A572-65 .50 CEV: ASTM A572-65 T3-07	**Sold TO:** KLOECKNER METALS Bessemer AL **Ship TO:** KLOECKNER METALS BESSEMER AL **Sent TO:**

Shipped Item	Heat/Slab Number	Certified By	C	Mn	P	S	Si	Cu	Ni	Cr	Mo	Cb	V	Al	Ti	N2	B	Ca	Sn	CEV	ACI
7J2826AA	B7X6627-03 ***	B7X6627	0.21	1.40	0.013	0.004	0.03	0.18	0.05	0.06	0.023	0.037	0.054	0.028	0.002	0.007	0.0002	0.0015		0.48	

Shipped Item	Certified By	Heat/Slab Number	Yield ksi	Tensile ksi	Y/T %	ELONGATION %		Bend OK?	Hard HB	Charpy Impacts (ft-lbs)					Shear %				Test Temp
						2"	8"			Size mm	1	2	3	Avg	1	2	3	Avg	
7J2826AA	S7J2826FTT	B7X6627-03 ***	74.2	94.1	78.9	31.9													

Items: 1 **PCS:** 1 **Weight:** 13068 LBS

Mercury has not come in contact with this product during the manufacturing process nor has any mercury been used by the manufacturing process. Certified in accordance with EN 10204 3.1. No weld repair has been performed on this material.
Manufactured to a fully killed fine grain practice.
ISO 9001:2015 Registered, PED Certified

"***" indicates Heats melted and Manufactured in the U.S.A.

We hereby certify that the product described above passed all of the tests required by the specifications.

Quilin Yu

Dr. Quilin Yu - Metallurgist

NUCOR
PLATE MILL

P.O.Box 279
Winton, NC 27986
(252) 356-3700

Mill Test Report
Page 3

1505 River Rd
Cofield, NC 27922
(252) 356-3700

NUCOR *It's Our Nature*

Issuing Date : 04/05/2018 **B/L No. :** 499189 **Load No. :** 507095 **Our Order No. :** 155034/3 **Cust. Order No. :** DVW6545

Vehicle No: 8294

Sold To: CHATHAM STEEL
2702 CHEEK RD
DURHAM,NC 27704

Ship To: CHATHAM STEEL
2702 CHEEK RD
DURHAM,NC 27704

Specification: 1.5000" x 96.000" x 240.000"
ASTM A36-14/ASTM A709 Grade 36-17/AASHTO M270Grade 36/ASME
SA36 2015/2017 AASHTO M270-2017 36

Marking :

Heat No	C	Mn	P	S	Si	Cu	Ni	Cr	Mo	Al(tot)	V	Nb	Ti	N	Ca	B	Sn	Ceq	Pcm
8501452	0.18	0.83	0.008	0.000	0.21	0.21	0.20	0.07	0.04	0.020	0.004	0.001	0.002		0.0040	0.0000	0.008	0.37	0.25

Plate Serial No	Pieces	Tons	Tensile Test Dir.	(psi) Yield	(psi) Tensile	Elong. % in 2"	Elong. % in 8"
8501452-01	1	4.90	T	47,800	72,900		21.5
			T	41,200	70,900		25.2

PRODUCED IN ACCORDANCE WITH NUCOR-HERTFORD QA MANUAL REV. 17 JUNE 23, 2015

Manufactured to fully killed fine grain practice by Electric Arc Furnace. Welding or weld repair was not performed on this material. Mercury has not been used in the direct manufacturing of this material. Produced as continuous cast discrete plate as-rolled, unless otherwise noted in Specification. For Mexico shipments:nhc-SalesMX@Nucor.com
Yield by 0.5EUL method unless otherwise specified. Ceq = C+(Mn/6)+((Cr+Mo+V)/5)+((Cu+Ni)/15).
Pcm = C+(Si/30)+(Mn/20)+(Cu/20)+(Ni/60)+(Cr/20)+(Mo/15)+(V/10)+5B
Melted and Manufactured in the USA. ISO 9001:2008 certified (#010940) by SRI Quality System Registrar (#0985-09). PED 97/23/EC 7/2 Annex 1, Para. 4.3 Compliant. DIN 50049 3.1.B/EN 10204 3.1B(2004), DIN EN 10204 3.1(2005) compliant. For ABS grades only, Quality Assurance certificate 14-MMPQA-723

We hereby certify that the contents of this report are accurate and correct. All test results and operations performed by the material manufacturer are in compliance with the applicable specifications, including customer specifications.

T. A. Depretis

T. A. Depretis, Metallurgist

4/5/2018 11:26:26 AM

NUCOR PLATE MILL
P.O.Box 279
Winton, NC 27986
(252) 356-3700

Mill Test Report
Page 19

1505 River Rd
Cofield, NC 27922
(252) 356-3700
NUCOR It's Our Nature.

Issuing Date : 12/30/2017 **B/L No. :** 490835 **Load No. :** 500766 **Our Order No. :** 152967/2 **Cust. Order No. :** 4500184525

Vehicle No: LW 62097

Sold To: HIGH STEEL STRUCTURES INC
PO BOX 10008
LANCASTER,PA 17605

Ship To: HIGH STEEL STRUCTURES
LANCASTER PLANT
144 GREENFIELD RD
LANCASTER,PA 17602

Specification: 1.5000" x 96.000" x 244.000" / 38.1mm x 2438.4mm x 6197.6mm
AASHTO M270-2017 HPS 70W/485W ASTM A709-17 HPS 70W/485W
T1T2T3 Q+T

Marking : 1170066F-15327 4500184525

Heat No	C	Mn	P	S	Si	Cu	Ni	Cr	Mo	Al(tot)	V	Nb	Ti	N	Ca	B	Sn	Ceq	Pcm
7507549	0.09	1.28	0.013	0.001	0.41	0.28	0.28	0.47	0.02	0.030	0.077	0.002	0.003	0.0077	0.0054	0.0000	0.011	0.45	0.22

			Tensile Test					Heat Treat			
Plate Serial No	Pieces	Tons	Dir.	Yield (psi)	Tensile (psi)	Elong. % in 2"	Elong. % in 8"	Quench (°F)	Time (min)	Temper (°F)	Time (min)
7507549-06-3	2	9.96	H-T	82,000	99,000	55.3		1665	58	1100	74

			Charpy Impacts																		
				Absorbed Energy (Ft-lbs)					Lateral Expansion (in.)					Shear (%)							
Plate Serial No	Pieces	Tons	Dir.	(ft-lbs) 1	(ft-lbs) 2	(ft-lbs) 3	(ft-lbs) Ave	Min	(in.) 1	(in.) 2	(in.) 3	(in.) Ave	(in.) Min	(%) 1	(%) 2	(%) 3	(%) Ave	Min	Temp (°F)	Size
7507549-06-3	2	9.96	H-L	146.1	149.8	142.0	146.0	25											-25	10mm

Metric Results			Tensile Test					Heat Treat			
Plate Serial No	Pieces	Tons	Dir.	Yield (MPa)	Tensile (MPa)	Elong. % in 2"	Elong. % in 8"	Quench (°C)	Time (min)	Temper (°C)	Time (min)
7507549-06-3	2	9.03	H-T	565	683	55.3		907	58	593	74

Metric Results			Charpy Impacts																	
				Absorbed Energy (J)					Lateral Expansion (mm)					Shear (%)						
			Dir.	(J) 1	(J) 2	(J) 3	(J) Ave	Min	(mm) 1	(mm) 2	(mm) 3	(mm) Ave	(mm) Min	(%) 1	(%) 2	(%) 3	(%) Ave	Min	Temp (°C)	Size
7507549-06-3	2	9.03	H-L	198.2	203.1	192.7	198.0	34											-32	10mm

NFCM, T1, T2, T3, 25ft-lbs @ -10 F (34J @ -23 C), P frequency. Temperature reduced by 15 F for each 10 ksi over 85 ksi ;

Manufactured to fully killed fine grain practice by Electric Arc Furnace. Welding or weld repair was not performed on this material. Mercury has not been used in the direct manufacturing of this material. Produced as continuous cast discrete plate on rectangular specimens, unless otherwise noted in Specification. For Mexico shipments:nhc-SalesMX@Nucor.com
Yield by 0.5EUL method unless otherwise specified. Ceq = C+(Mn/6)+((Cr+Mo+V)/5)+((Cu+Ni)/15)
Pcm = C+(Si/30)+(Mn/20)+(Cu/20)+(Ni/60)+(Cr/20)+(Mo/15)+(V/10)+5B
Melted and Manufactured in the USA. ISO 9001:2008 certified (#010940) by SRI Quality System Registrar (#0985-09). PED 97/23/EC 7/2 Annex 1, Para. 4.3 Compliant.
DIN 50049 3.1.B/EN 10204 3.1B(2004), DIN EN 10204 3.1(2005) compliant. For ABS grades only, Quality Assurance certificate 14-MMPQA-723

We hereby certify that the contents of this report are accurate and correct. All test results and operations performed by the material manufacturer are in compliance with the applicable specifications, including customer specifications.

T. A. Depretis

T. A. Depretis, Metallurgist

12/30/2017 1:16:46 PM

NUCOR PLATE MILL

P.O.Box 279
Winton, NC 27986
(252) 356-3700

Mill Test Report

Page 2

1505 River Rd
Cofield, NC 27922
(252) 356-3700

NUCOR It's Our Nature.

Issuing Date : 10/18/2017 B/L No. : 485050 Load No. : 494060 Our Order No. : 151424/1 Cust. Order No. : DVW6008

Vehicle No: Deloatch D3

Sold To: CHATHAM STEEL
2702 CHEEK RD
DURHAM,NC 27704

Ship To: CHATHAM STEEL
2702 CHEEK RD
DURHAM,NC 27704

Specification: 1.2500" x 72.000" x 240.000"
ASTM A36-14/ASTM A709 Grade 36-16a/AASHTO M270Grade 36/ASME SA36 2013/2015 AASHTO M270-2017 36

Marking : 35693

Heat No	C	Mn	P	S	Si	Cu	Ni	Cr	Mo	Al(tot)	V	Nb	Ti	N	Ca	B	Sn	Ceq	Pcm
7506515	0.19	0.84	0.009	0.002	0.18	0.25	0.12	0.10	0.03	0.022	0.004	0.002	0.002		0.0027	0.0001	0.011	0.38	0.26

Plate Serial No	Pieces	Tons	Tensile Test Dir.	(psi) Yield	(psi) Tensile	Elong. % in 2"	Elong. % in 8"
7506515-02	2	6.12	T	43,500	70,600		20.6
			T	40,800	70,300		25.3

PRODUCED IN ACCORDANCE WITH NUCOR-HERTFORD QA MANUAL REV. 17 JUNE 23, 2015

Manufactured to fully killed fine grain practice by Electric Arc Furnace. Welding or weld repair was not performed on this material. Mercury has not been used in the direct manufacturing of this material. Produced as continuous cast discrete plate as-rolled, unless otherwise noted in Specification. For Mexico shipments:nhc-SalesMX@Nucor.com
Yield by 0.5EUL method unless otherwise specified. Ceq = C+(Mn/6)+((Cr+Mo+V)/5)+((Cu+Ni)/15)
Pcm = C+(Si/30)+(Mn/20)+(Cu/20)+(Ni/60)+(Cr/20)+(Mo/15)+(V/10)+5B
Melted and Manufactured in the USA. ISO 9001:2008 certified (#010940) by SRI Quality System Registrar (#0985-09). PED 97/23/EC 7/2 Annex 1, Para. 4.3 Compliant. DIN 50049 3.1.B/EN 10204 3.1B(2004), DIN EN 10204 3.1(2005) compliant. For ABS grades only, Quality Assurance certificate 14-MMPQA-723

We hereby certify that the contents of this report are accurate and correct. All test results and operations performed by the material manufacturer are in compliance with the applicable specifications, including customer specifications.

T. A. Depretis

T. A. Depretis, Metallurgist

10/18/2017 1:11:48 PM

SSAB

12400 Highway 43 North, Axis, Alabama 36505, US

Test Certificate

Form TC1: Revision 2: Date 23 Apr 2014

Customer: KLOECKNER METALS CORPORATION 500 COLONIAL CENTER PARKWAY SUITE 500 ROSWELL GA 30076	**Customer P.O.No.:** CLT-7190228	**Mill Order No.** 41-514254-01	**Shipping Manifest:** AT249421	
	Product Description: ASTM A572(15) 65/M450		**Ship Date:** 06 Sep 17 **Cert Date:** 06 Sep 17	**Cert No:** 081621784 (Page 1 of 1)
	Size: 1.250 X 96.00 X 480.0 (IN)			

Tested Pieces:				Tensiles:							Charpy Impact Tests												
Heat Id	Piece Id	Tested Thickness	Tst Loc	YS (KSI)	UTS (KSI)	%RA	Elong % 2in	Elong % 8in	Tst Dir	Hardness	Abs. Energy(FTLB) 1	2	3	Avg	% Shear 1	2	3	Avg	Tst Tmp	Tst Dir	Tst Siz (mm)	BDWTT Tmp %Shr
W7H748	C03	1.249 (DISCRT)	L	71	91			14	T													
			T	70	92			16	T													

Chemical Analysis

Heat Id	C	Mn	P	S	Si	Tot Al	Cu	Ni	Cr	Mo	Cb	V	Ti	B	N	ORGN
W7H748	.16	1.55	.011	.005	.04	.038	.27	.16	.17	.04	.047	.094	.006	.0001	.0093	USA

KILLED STEEL
MERCURY IS NOT A METALLURGICAL COMPONENT OF THE STEEL AND NO MERCURY WAS INTENTIONALLY ADDED DURING THE MANUFACTURE OF THIS PRODUCT.
MTR EN 10204:2004 INSPECTION CERTIFICATE 3.1 COMPLIANT
100% MELTED AND MANUFACTURED IN THE USA.
WELD REPAIRING HAS NOT BEEN PERFORMED
PRODUCTS SHIPPED:
W7H748 C03 PCES: 2, LBS: 32670

(P) Cust Part #:

WE HEREBY CERTIFY THAT THIS MATERIAL WAS TESTED IN ACCORDANCE WITH, AND MEETS THE REQUIREMENTS OF, THE APPROPRIATE SPECIFICATION

Justin Ward
SENIOR METALLURGIST - PRODUCT

NUCOR PLATE MILL

P.O.Box 279
Winton, NC 27986
(252) 356-3700

Mill Test Report

Page 1

1505 River Rd
Cofield, NC 27922
(252) 356-3700

NUCOR It's Our Nature

Issuing Date : 11/28/2017 **B/L No. :** 488589 **Load No. :** 498289 **Our Order No. :** 152825/4 **Cust. Order No.** DVW6307

Vehicle No: DELOATCH D3

Sold To: CHATHAM STEEL
2702 CHEEK RD
DURHAM,NC 27704

Ship To: CHATHAM STEEL
2702 CHEEK RD
DURHAM,NC 27704

Specification: 1.7500" x 96.000" x 240.000"
ASTM A36-14/ASTM A709 Grade 36-17/AASHTO M270Grade 36/ASME SA36 2013/2015 AASHTO M270-2017 36

Marking : 36477

Heat No	C	Mn	P	S	Si	Cu	Ni	Cr	Mo	Al(tot)	V	Nb	Ti	N	Ca	B	Sn	Ceq	Pcm
7506393	0.23	1.10	0.009	0.003	0.20	0.19	0.09	0.06	0.01	0.035	0.004	0.002	0.003		0.0040	0.0001	0.010	0.44	0.30

Plate Serial No	Pieces	Tons	Tensile Test Dir.	(psi) Yield	(psi) Tensile	Elong. % in 2"	Elong. % in 8"
7506393-05	3	17.15	T	37,200	66,900		26.9

PRODUCED IN ACCORDANCE WITH NUCOR-HERTFORD QA MANUAL REV. 17 JUNE 23, 2015

Manufactured to fully killed fine grain practice by Electric Arc Furnace. Welding or weld repair was not performed on this material. Mercury has not been used in the direct manufacturing of this material. Produced as continuous cast discrete plate as-rolled, unless otherwise noted in Specification. For Mexico shipments:nhc-SalesMX@Nucor.com
Yield by 0.5EUL method unless otherwise specified. Ceq = C+(Mn/6)+((Cr+Mo+V)/5)+((Cu+Ni)/15)
Pcm = C+(Si/30)+(Mn/20)+(Cu/20)+(Ni/60)+(Cr/20)+(Mo/15)+(V/10)+5B
Melted and Manufactured in the USA. ISO 9001:2008 certified (#010940) by SRI Quality System Registrar (#0985-09). PED 97/23/EC 7/2 Annex 1, Para. 4.3 Compliant.
DIN 50049 3.1.B/EN 10204 3.1B(2004), DIN EN 10204 3.1(2005) compliant. For ABS grades only, Quality Assurance certificate 14-MMPQA-723

We hereby certify that the contents of this report are accurate and correct. All test results and operations performed by the material manufacturer are in compliance with the applicable specifications, including customer specifications.

T. A. Depretis

T. A. Depretis, Metallurgist

11/28/2017 12:47:59 PM

ArcelorMittal

T E S T C E R T I F I C A T E

ARCELORMITTAL PLATE LLC

PAGE NO: 01 OF 02
FILE NO: 3571-01-01
MILL ORDER NO: 84534-005
MELT NO: D2044
SLAB NO: 12
DATE: 10/18/17

SHIP TO:
HIGH STEEL STRUCTURES LLC
144 GREENFIELD ROAD
LANCASTER PA 17602

SOLD TO:
HIGH STEEL STRUCTURES LLC
PO BOX 10008
LANCASTER PA 17605-0008

SEND TO:

01-C

S T E E L P L A T E D I M E N S I O N S / D E S C R I P T I O N

TOTAL QTY	GAUGE	WIDTH	LENGTH	DESCRIPTION	PIECE WEIGHT
1	1-3/4"	96"	240"	RECTANGLE	11435#

C U S T O M E R I N F O R M A T I O N

CUSTOMER PO: 4500178787

-3

CUSTOMER ITEM NO. 0110

PART NO. 1170066F-06028

S P E C I F I C A T I O N (S)

THIS MATERIAL HAS BEEN MANUFACTURED AND TESTED IN ACCORDANCE WITH PURCHASE ORDER REQUIREMENTS AND SPECIFICATION(S).

AASHT M270-HPS70WF3 YR 15
SILICON KILLED & FINE GRAIN PRACTICE NEW YORK CON
MANUAL 3RD ED SECT 9 10/7/13 GR HPS70W & ASTM A709
HPS 16A GRADE 70WF3
THE MANAGEMENT SYSTEMS FOR MANUFACTURE OF THIS PRODUCT ARE CERTIFIED TO ISO 9001:2008 (CERTIFICATE NO. 30130) AND ISO 14001:2004 (CERTIFICATE NO. 49009).

CHEMICAL COMPOSITION (WT%) FOR ALL ELEMENTS EXCEPT H (PPM)

	C	MN	P	S	CU	SI	NI	CR	MO
MELT:D2044	.09	1.23	.006	.004	.31	.41	.32	.56	.07

	V	AL	CB	N
MELT:D2044	.050	.019	.002	.0097

M A N U F A C T U R E

FINELINE - VACUUM DEGASSED - FINE GRAIN PRACTICE

H E A T T R E A T C O N D I T I O N

MATL OR TEST	HEAT TREAT DESCRIPTION	NOM TEMP	HOLD MINS	COOL MTHD
PL/TEST	HARDEN	1675F	51	W.QUENCH
PL/TEST	TEMPER	1180F	99	W.QUENCH

WE HEREBY CERTIFY THE ABOVE INFORMATION IS CORRECT:

ARCELORMITTAL PLATE LLC
QUALITY ASSURANCE LABORATORY
139 MODENA ROAD
COATESVILLE, PA 19320

Loc Tran

SUPERVISOR – TEST REPORTING
LOC TRAN

TEST CERTIFICATE

PAGE NO: 02 OF 02
FILE NO: 3571-01-01
MILL ORDER NO: 84534-005
MELT NO: D2044
SLAB NO: 12
DATE: 10/18/17

TENSILE PROPERTIES

SLAB NO.	LOC	DIR	YIELD STRENGTH PSI X 1000	TENSILE STRENGTH PSI X 1000	ELONGATION AFTER FRACTURE GAGE LGTH	%
12	BOT.	TRANS.	80	93	2.00"	26.0

CHARPY V-NOTCH IMPACT RESULTS

SLAB	LOC	DIR	TEMP	SIZE	FT. LBS.	NO BREAK
12	BOT.	LONG.	-10F	FULL	141 146 185	NB
12	TOP	LONG.	-10F	FULL	132 135 137	

STRIKER RADIUS 8MM

GENERAL INFORMATION

ALL STEEL HAS BEEN MELTED AND MANUFACTURED IN THE U.S.A.
NO WELD REPAIR PERFORMED BY ARCELORMITTAL PLATE LLC.
MATERIAL HAS BEEN VACUUM DEGASSED AND CALCIUM TREATED
FOR SULFIDE SHAPE CONTROL.
FINELINE MOD FOR SULPHUR
ALL STEEL HAS BEEN MANUFACTURED IN THE U.S.A.
MFST:NYDOT D263452 PHASE 2 REPL
OF KOSCIUSZKO BR OVER NEWTOWN
CREEK KIGNS & QUEENS COS NY
ACID SOLUBLE ALUMINUM
FOR MORE INFORMATION AND PROCESSING GUIDELINES, REFER TO
WWW.USA.ARCELORMITTAL.COM/PLATE

B/L #23294 PYLE TRANSPORT

WE HEREBY CERTIFY THE ABOVE
INFORMATION IS CORRECT:

ARCELORMITTAL PLATE LLC
QUALITY ASSURANCE LABORATORY
139 MODENA ROAD
COATESVILLE, PA 19320

Loc Tran

SUPERVISOR – TEST REPORTING
LOC TRAN

NUCOR PLATE MILL

P.O.Box 279
Winton, NC 27986
(252) 356-3700

Mill Test Report

Page 1

1505 River Rd
Cofield, NC 27922
(252) 356-3700

NUCOR It's Our Nature.

Issuing Date : 05/03/2016 **B/L No. :** 443096 **Load No. :** 448408 **Our Order No. :** 136121/1 **Cust. Order No. :** DVW3563

Vehicle No: CHATHAM 5813

Sold To: CHATHAM STEEL
2702 CHEEK RD
DURHAM,NC 27704

Ship To: CHATHAM STEEL
2702 CHEEK RD
DURHAM,NC 27704

Specification: 2.0000" x 96.000" x 240.000"
ASTM A36-14/ASTM A709 Grade 36-13a/AASHTO M270Grade 36/ASME
SA36 2013/2015 AASHTO M270 36

Marking : 36740

Heat No	C	Mn	P	S	Si	Cu	Ni	Cr	Mo	Al(tot)	V	Nb	Ti	N	Ca	B	Sn	Ceq	Pcm
6502038	0.17	0.86	0.015	0.003	0.20	0.25	0.09	0.11	0.02	0.014	0.006	0.002	0.002		0.0014	0.0003	0.012	0.37	0.25

Plate Serial No	Pieces	Tons	Tensile Test Dir.	(psi) Yield	(psi) Tensile	Elongation % in 2"	Elongation % in 8"	Charpy Impacts Dir.	1	(%) shear	2	(%) shear	3	(%) shear	Ave.	(%) shear	Size	Temp	Min Ave.
6502038-02	1	6.53	T	42,100	70,900		18.4												
			T	42,000	70,000		21.2												

Manufactured to fully killed practice by Electric Arc Furnace. Welding or weld repair was not performed on this material. Mercury has not been used in the direct manufacturing of this material. Produced as continuous cast discrete plate as-rolled, unless otherwise noted in Specification. For Mexico shipments: nhc-SalesMX@Nucor.com
Yield by 0.5EUL method unless otherwise specified. Ceq = C+(Mn/6)+((Cr+Mo+V)/5)+((Cu+Ni)/15)
Pcm = C+(Si/30)+(Mn/20)+(Cu/20)+(Ni/60)+(Cr/20)+(Mo/15)+(V/10)+5B
Melted and Manufactured in the USA. ISO 9001:2008 certified (#010940) by SRI Quality System Registrar (#0985-09). PED 97/23/EC 7/2 Annex 1, Para. 4.3 Compliant.
DIN 50049 3.1.B/EN 10204 3.1B(2004), DIN EN 10204 3.1(2005) compliant. For ABS grades only, Quality Assurance certificate 14-MMPQA-723

We hereby certify that the contents of this report are accurate and correct. All test results and operations performed by the material manufacturer are in compliance with the applicable specifications, including customer specifications.

T. A. Depretis

T. A. Depretis, Metallurgist

5/3/2016 1:01:49 PM

ArcelorMittal

TEST CERTIFICATE

ARCELORMITTAL PLATE LLC

PAGE NO: 01 OF 02
FILE NO: 3571-01-01
MILL ORDER NO: 90954-001
MELT NO: D2290
SLAB NO: 7A
DATE: 01/19/18

SHIP TO:
HIGH STEEL STRUCTURES LLC
144 GREENFIELD ROAD
LANCASTER PA 17602

SOLD TO:
HIGH STEEL STRUCTURES LLC
PO BOX 10008
LANCASTER PA 17605-0008

SEND TO:

01-C

STEEL PLATE DIMENSIONS / DESCRIPTION

TOTAL QTY	GAUGE	WIDTH	LENGTH	DESCRIPTION	PIECE WEIGHT
2	2"	88"	240"	RECTANGLE	11979#

CUSTOMER INFORMATION

CUSTOMER PO: 4500183382

3

CUSTOMER ITEM NO. 0030 PART NO. 1170066F-15253

SPECIFICATION(S)

THIS MATERIAL HAS BEEN MANUFACTURED AND TESTED IN ACCORDANCE WITH PURCHASE ORDER REQUIREMENTS AND SPECIFICATION(S).

AASHT M270-HPS70WF3 YR 15
SILICON KILLED & FINE GRAIN PRACTICE ASTM A709 HPS
17 GRADE 70WF3 & NEW YORK CON MANUAL 3RD ED
SECTION 9 DTD 10/7/13 GR HPS70W
THE MANAGEMENT SYSTEMS FOR MANUFACTURE OF THIS PRODUCT ARE CERTIFIED TO ISO 9001:2008 (CERTIFICATE NO. 30130) AND ISO 14001:2004 (CERTIFICATE NO. 49009).

CHEMICAL COMPOSITION (WT%) FOR ALL ELEMENTS EXCEPT H (PPM)

	C	MN	P	S	CU	SI	NI	CR	MO
MELT:D2290	.10	1.22	.009	.002	.32	.39	.33	.55	.06

	V	AL	CB	N
MELT:D2290	.048	.024	.001	.0064

MANUFACTURE

FINELINE - VACUUM DEGASSED - FINE GRAIN PRACTICE

HEAT TREAT CONDITION

MATL OR TEST	HEAT TREAT DESCRIPTION	NOM TEMP	HOLD MINS	COOL MTHD
PL/TEST	HARDEN	1675F	50	W.QUENCH
PL/TEST	TEMPER	1160F	106	W.QUENCH

WE HEREBY CERTIFY THE ABOVE INFORMATION IS CORRECT:

ARCELORMITTAL PLATE LLC
QUALITY ASSURANCE LABORATORY
139 MODENA ROAD
COATESVILLE, PA 19320

Loc Tran

SUPERVISOR - TEST REPORTING
LOC TRAN

TEST CERTIFICATE

PAGE NO: 02 OF 02
FILE NO: 3571-01-01
MILL ORDER NO: 90954-001
MELT NO: D2290
SLAB NO: 7A
DATE: 01/19/18

TENSILE PROPERTIES

SLAB NO.	LOC	DIR	YIELD STRENGTH PSI X 1000	TENSILE STRENGTH PSI X 1000	ELONGATION AFTER FRACTURE GAGE LGTH	%
7A	BOT.	TRANS.	82	95	2.00"	24.0

CHARPY V-NOTCH IMPACT RESULTS

SLAB	LOC	DIR	TEMP	SIZE	FT. LBS.	NO BREAK
7A	BOT.	LONG.	-10F	FULL	168 168 177	NB NB NB
7A	TOP	LONG.	-10F	FULL	173 185 189	NB NB NB

STRIKER RADIUS 8MM

GENERAL INFORMATION

ALL STEEL HAS BEEN MELTED AND MANUFACTURED IN THE U.S.A.
NO WELD REPAIR PERFORMED BY ARCELORMITTAL PLATE LLC.
NO WELD REPAIR PERFORMED BY ARCELORMITTAL PLATE LLC.
MATERIAL HAS BEEN VACUUM DEGASSED AND CALCIUM TREATED
FOR SULFIDE SHAPE CONTROL.
FINELINE MOD FOR SULPHUR
ALL STEEL HAS BEEN MANUFACTURED IN THE U.S.A.
MFST:NYDOT D263452 PHASE 2 REPL
OF KOSCIUSZKO BR OVER NEWTOWN
CREEK KIGNS & QUEENS COS NY
ACID SOLUBLE ALUMINUM
FOR MORE INFORMATION AND PROCESSING GUIDELINES, REFER TO
WWW.USA.ARCELORMITTAL.COM/PLATE

B/L #27555 PYLE TRANSPORT

WE HEREBY CERTIFY THE ABOVE INFORMATION IS CORRECT:

ARCELORMITTAL PLATE LLC
QUALITY ASSURANCE LABORATORY
139 MODENA ROAD
COATESVILLE, PA 19320

Loc Tran

SUPERVISOR – TEST REPORTING
LOC TRAN

NUCOR PLATE MILL
P.O.Box 279
Winton, NC 27986
(252) 356-3700

Mill Test Report
Page 1

1505 River Rd
Cofield, NC 27922
(252) 356-3700
NUCOR It's Our Nature.

Issuing Date : 02/09/2018 B/L No. : 494177 Load No. : 504207 Our Order No. : 154463/10 Cust. Order No. : DVW6476

Vehicle No: DELOATCH D3

Sold To: CHATHAM STEEL, 2702 CHEEK RD, DURHAM,NC 27704

Ship To: CHATHAM STEEL, 2702 CHEEK RD, DURHAM,NC 27704

Specification: 2.5000" x 96.000" x 240.000"
ASTM A36-14/ASTM A709 Grade 36-17/AASHTO M270Grade 36/ASME SA36 2015/2017 AASHTO M270-2017 36

Marking : 37053

Heat No	C	Mn	P	S	Si	Cu	Ni	Cr	Mo	Al(tot)	V	Nb	Ti	N	Ca	B	Sn	Ceq	Pcm
8500710	0.18	0.89	0.010	0.001	0.18	0.16	0.06	0.11	0.01	0.016	0.005	0.002	0.002		0.0036	0.0002	0.008	0.37	0.25

			Tensile Test				
Plate Serial No	Pieces	Tons	Dir.	(psi) Yield	(psi) Tensile	Elong. % in 2"	Elong. % in 8"
8500710-05	2	16.33	T	42,000	72,000	26.4	
			T	42,000	72,000	30.9	

RODUCED IN ACCORDANCE WITH NUCOR-HERTFORD QA MANUAL REV. 17 JUNE 23, 2015

Ianufactured to fully killed practice by Electric Arc Furnace. Welding or weld repair was not performed on this material.
lercury has not been used in the direct manufacturing of this material. Produced as continuous cast discrete plate as-rolled, unless
therwise noted in Specification. For Mexico shipments:nhc-SalesMX@Nucor.com
ield by 0.5EUL method unless otherwise specified. Ceq = C+(Mn/6)+((Cr+Mo+V)/5)+((Cu+Ni)/15)
cm = C+(Si/30)+(Mn/20)+(Cu/20)+(Ni/60)+(Cr/20)+(Mo/15)+(V/10)+5B
elted and Manufactured in the USA. ISO 9001:2008 certified (#010940) by SRI Quality System Registrar (#0985-09). PED 97/23/EC 7/2 Annex 1, Para. 4.3 Compliant.
IN-50049 3.1.B/EN-10204 3.1B(2004), DIN EN 10204 3.1(2005) compliant. For ABS grades only, Quality Assurance certificate 14-MMPQA-723

We hereby certify that the contents of this report are accurate and correct. All test results and operations performed by the material manufacturer are in compliance with the applicable specifications, including customer specifications.

T. A. Depretis

T. A. Depretis, Metallurgist

2/9/2018 12:34:53 PM

NUCOR
PLATE MILL

P.O.Box 279
Winton, NC 27986
(252) 356-3700

Mill Test Report

Page 2

1505 River Rd
Cofield, NC 27922
(252) 356-3700

NUCOR
It's Our Nature

Issuing Date : 04/10/2018 **B/L No. :** 499524 **Load No. :** 508879 **Our Order No. :** 155034/2 **Cust. Order No. :** DVW6545

Vehicle No: TSH 8294

Sold To: CHATHAM STEEL
2702 CHEEK RD
DURHAM,NC 27704

Ship To: CHATHAM STEEL
2702 CHEEK RD
DURHAM,NC 27704

Specification: 0.7500" x 96.000" x 240.000"
ASTM A36-14/ASTM A709 Grade 36-17/AASHTO M270Grade 36/ASME
SA36 2015/2017 AASHTO M270-2017 36

Marking : DVW6545

Heat No	C	Mn	P	S	Si	Cu	Ni	Cr	Mo	Al(tot)	V	Nb	Ti	N	Ca	B	Sn	Ceq	Pcm
8502026	0.17	0.86	0.007	0.001	0.18	0.27	0.10	0.09	0.02	0.026	0.004	0.002	0.002		0.0026	0.0001	0.011	0.36	0.24

			Tensile Test				
Plate Serial No	Pieces	Tons	Dir.	(psi) Yield	(psi) Tensile	Elong. % in 2"	Elong. % in 8"
8502026-02	4	9.80	T	43,200	70,500		29.9
			T	44,700	73,400		23.2

PRODUCED IN ACCORDANCE WITH NUCOR-HERTFORD QA MANUAL REV. 17 JUNE 23, 2015

Manufactured to fully killed fine grain practice by Electric Arc Furnace. Welding or weld repair was not performed on this material. Mercury has not been used in the direct manufacturing of this material. Produced as continuous cast discrete plate as-rolled, unless otherwise noted in Specification. For Mexico shipments:nhc-SalesMX@Nucor.com
Yield by 0.5EUL method unless otherwise specified. Ceq = C+(Mn/6)+((Cr+Mo+V)/5)+((Cu+Ni)/15)
Pcm = C+(Si/30)+(Mn/20)+(Cu/20)+(Ni/60)+(Cr/20)+(Mo/15)+(V/10)+5B
Melted and Manufactured in the USA. ISO 9001:2008 certified (#010940) by SRI Quality System Registrar (#0985-09). PED 97/23/EC 7/2 Annex 1, Para. 4.3 Compliant.
DIN 50049 3.1.B/EN 10204 3.1B(2004), DIN EN 10204 3.1(2005) compliant. For ABS grades only, Quality Assurance certificate 14-MMPQA-723

We hereby certify that the contents of this report are accurate and correct. All test results and operations performed by the material manufacturer are in compliance with the applicable specifications, including customer specifications.

T. A. Depretis

T. A. Depretis, Metallurgist

4/10/2018 3:13:59 PM

SSAB

Test Certificate

12400 Highway 43 North, Axis, Alabama 36505, US

Form TC1: Revision 2: Date 23 Apr 2014

Customer:	Customer P.O.No.: CLT-7190228	Mill Order No. 41-514254-02	Shipping Manifest: AT249421
KLOECKNER METALS CORPORATION 500 COLONIAL CENTER PARKWAY SUITE 500 ROSWELL GA 30076	Product Description: ASTM A572(15) 65/M450 Size: 0.750 X 96.00 X 480.0 (IN)	Ship Date: 06 Sep 17 Cert Date: 06 Sep 17	Cert No: 081621785 (Page 1 of 1)

Tested Pieces:				Tensiles:							Charpy Impact Tests						BDWTT
Heat Id	Piece Id	Tested Thickness	Tst Loc	YS (KSI)	UTS (KSI)	%RA	Elong % 2in	Elong % 8in	Tst Dir	Hardness	Abs. Energy(FTLB) 1 2 3 Avg	% Shear 1 2 3 Avg	Tst Tmp	Tst Dir	Tst Siz (mm)	Tmp %Shr
W7H748	C07	0.751 (DISCRT)	L	73	95			18	T							
			T	72	93			17	T							

Chemical Analysis

Heat Id	C	Mn	P	S	Si	Tot Al	Cu	Ni	Cr	Mo	Cb	V	Ti	B	N	ORGN
W7H748	.16	1.55	.011	.005	.04	.038	.27	.16	.17	.04	.047	.094	.006	.0001	.0093	USA

KILLED STEEL
MERCURY IS NOT A METALLURGICAL COMPONENT OF THE STEEL AND NO MERCURY WAS INTENTIONALLY ADDED DURING THE MANUFACTURE OF THIS PRODUCT.
MTR EN 10204:2004 INSPECTION CERTIFICATE 3.1 COMPLIANT
100% MELTED AND MANUFACTURED IN THE USA.
WELD REPAIRING HAS NOT BEEN PERFORMED
PRODUCTS SHIPPED:
W7H748 C07 PCES: 1, LBS: 9801

(P) Cust Part #:

WE HEREBY CERTIFY THAT THIS MATERIAL WAS TESTED IN ACCORDANCE WITH, AND MEETS THE REQUIREMENTS OF, THE APPROPRIATE SPECIFICATION

Justin Ward
SENIOR METALLURGIST - PRODUCT

APPENDIX C

WELDING PROCEDURE SPECIFICATIONS

Lynchburg Steel
& Specialty Company
275 Francis Avenue P.O. Box 158 Monroe, VA 24574 Phone: (434) 929-0951 Fax: (434) 929-2613
www.lynchburgsteel.com

AWS QC 1 JOHN D. WRIGHT 00040821 CWI

WELDING PROCEDURE SPECIFICATION (WPS) Yes ☑
PREQUALIFIED ☑ QUALIFIED BY TESTING ☐
or PROCEDURE QUALIFICATION RECORDS (PQR) Yes ☐

Identification # 2
Revision 2 Date 11/07/13 By JW
Authorized by John D. Wright Date 01/19/01
Type---Manual ☑ Semiautomatic ☑
Mechanized ☐ Automatic ☐

Company Name Lynchburg Steel and Specialty Co.
Welding Process(es) FCAW
Supporting PQR No.(s) N/A

JOINT DESIGN USED
Type: Fillet Weld
Single ☐ Double Weld ☐
Backing: Yes ☐ No ☐
Backing Material: N/A
Root Opening 0 - 3/16" Root Face Dimension N/A
Groove Angle N/A Radius (J-U) N/A
Back Gouging: Yes ☐ No ☐ Method

POSITION
Position of Groove: N/A Fillet: 1F, 2F
Vertical Progression: Up ☐ Down ☐

ELECTRICAL CHARACTERISTICS
Transfer Mode (GMAW) Short-Circuiting ☐
Globular ☐ Spray ☑
Current: AC ☐ DCEP ☑ DCEN ☐ Pulsed ☐
Power Source: CC ☐ CV ☑
Other
Tungsten Electrode (GTAW)
Size:
Type:

BASE METALS
Material Spec. Group I - II (see Table 1 on pages 6-8)
Type or Grade All grades listed in Table 1
Thickness: Groove N/A Fillet 1/8" - Unlimited
Diameter (Pipe) All diameters welding Pipe to Plate

FILLER METALS
AWS Specification AWS A5.20
AWS Classification E71T-1, E70T-1

SHIELDING
Flux N/A Gas CO2
Composition 100%
Electrode-Flux (Class) Flow Rate 40-45 CFH
Gas Cup Size N/A

TECHNIQUE
Stringer or Weave Bead: Stringer or Weave
Multi-Pass or Single Pass (per side) Single or Multi
Number of Electrodes 1
Electrode Spacing Longitudinal N/A
Lateral N/A
Angle N/A
Contact Tube to Work Distance 1"
Peening None
Interpass Cleaning: Remove slag, chip or brush

PREHEAT and INTERPASS TEMPERATURE
Min for Thicknesses 1/8" - 3/4" (included) 32°F see note*
Min for Thicknesses over 3/4" - 1 1/2" (included) 50°F
Min for Thicknesses 1 1/2" - 2 1/2" (included) 150°F
Min for Thicknesses over 2 1/2" 225°F
Max Interpass Temperature 550°F

* Note: When base metal is below 32*F, preheat to 70*F and maintain during welding.

POST WELD HEAT TREATMENT
Temperature N/A
Time N/A

WELDING PROCEDURE

Pass or Weld Layer(s)	Process	Filler Metals: Class	Filler Metals: Diameter	Current: Type & Polarity	Current: Amps or Wire Feed Speed	Volts	Travel Speed	Joint Details: Fillet Weld
1 - n	FCAW	E71T-1	1/16"	DC+	265a - 325a	26-30	11-15 ipm	
1 - n	FCAW	E70T-1	3/32"	DC+	360a - 440a	26-30	11-15 ipm	

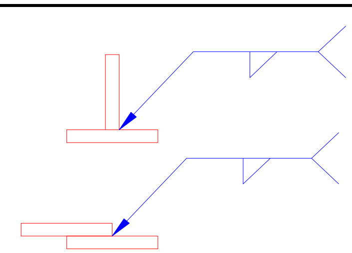

COOPER STEEL

275 Francis Avenue, Monroe Virginia 24574

WELDING PROCEDURE SPECIFICATION (WPS) Yes ☑
PREQUALIFIED ☐ QUALIFIED BY TESTING ☐
or PROCEDURE QUALIFICATION RECORDS (PQR) Yes ☐

Identification # 1/4 Fillet - E80T1
Revision 0 Date 05/24/19 By John D. Wright
Company Name Cooper Steel
Authorized by Andrew Anderson Date 05/24/19
Welding Process(es) FCAW
Type---Manual ☑ Semiautomatic ☑
Supporting PQR No.(s) N/A
Mechanized ☐ Automatic ☐

JOINT DESIGN USED
Type: Fillet Weld
Single ☐ Double Weld ☐
Backing: Yes ☐ No ☐
Backing Material: N/A
Root Opening 0 - 3/16" Root Face Dimension N/A
Groove Angle N/A Radius (J-U) N/A
Back Gouging: Yes ☐ No ☐ Method

POSITION
Position of Groove: N/A Fillet: 1F, 2F
Vertical Progression: Up ☐ Down ☐

ELECTRICAL CHARACTERISTICS
Transfer Mode (GMAW) Short-Circuiting ☐
Globular ☐ Spray ☑
Current: AC ☐ DCEP ☑ DCEN ☐ Pulsed ☐
Power Source: CC ☐ CV ☑
Other
Tungsten Electrode (GTAW)
Size:
Type:

BASE METALS
Material Spec.
Type or Grade
Thickness: Groove N/A Fillet 1/8" - Unlimited
Diameter (Pipe) N/A

FILLER METALS
AWS Specification AWS A5.29
AWS Classification E80T-1

SHIELDING
Flux N/A Gas CO_2
Composition 100%
Electrode-Flux (Class) Flow Rate 45 CFH
Gas Cup Size N/A

TECHNIQUE
Stringer or Weave Bead: Stringer or Weave
Multi-Pass or Single Pass (per side) Single or Multi
Number of Electrodes 1
Electrode Spacing Longitudinal N/A
Lateral N/A
Angle N/A
Contact Tube to Work Distance 1"
Peening None
Interpass Cleaning: Remove slag, chip or brush

PREHEAT and INTERPASS TEMPERATURE
Min for Thicknesses 1/8" - 3/4" (included) 32°F see note*
Min for Thicknesses over 3/4" - 1 1/2" (included) 50°F
Min for Thicknesses 1 1/2" - 2 1/2" (included) 150°F
Min for Thicknesses over 2 1/2" 225°F
Max Interpass Temperature 550°F

POST WELD HEAT TREATMENT
Temperature N/A
Time N/A

Calculated Heat Input (kJ/in) 47.67

* Note: When base metal is below 32*F, preheat to 70*F and maintain during welding.

ACTUAL WELDING PARAMETERS USED

Pass or Weld Layer(s)	Process	Filler Metals: Class	Filler Metals: Diameter	Current: Type & Polarity	Current: Amps or Wire Feed Speed	Volts	Travel Speed (IPM)	Joint Details
1	FCAW	E80T-1	1/16"	DC+	330	31.3	13	Fillet Weld
This WPS is only to show the welding parameters used - *NOT for PRODUCTION*								

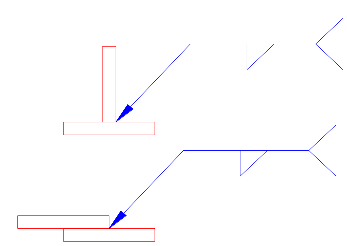

COOPER STEEL

275 Francis Avenue, Monroe Virginia 24574

WELDING PROCEDURE SPECIFICATION (WPS) Yes ☑
PREQUALIFIED ☐ QUALIFIED BY TESTING ☐
or PROCEDURE QUALIFICATION RECORDS (PQR) Yes ☐

Identification # 1/4 Fillet - E100T1
Revision 0 Date 05/24/19 By John D. Wright
Authorized by Andrew Anderson Date 05/24/19
Type---Manual ☑ Semiautomatic ☑
Mechanized ☐ Automatic ☐

Company Name Cooper Steel
Welding Process(es) FCAW
Supporting PQR No.(s) N/A

JOINT DESIGN USED
Type: Fillet Weld
Single ☐ Double Weld ☐
Backing: Yes ☐ No ☐
Backing Material: N/A
Root Opening 0 - 3/16" Root Face Dimension N/A
Groove Angle N/A Radius (J-U) N/A
Back Gouging: Yes ☐ No ☐ Method

POSITION
Position of Groove: N/A Fillet: 1F, 2F
Vertical Progression: Up ☐ Down ☐

ELECTRICAL CHARACTERISTICS
Transfer Mode (GMAW) Short-Circuiting ☐
Globular ☐ Spray ☑
Current: AC ☐ DCEP ☑ DCEN ☐ Pulsed ☐
Power Source: CC ☐ CV ☑
Other
Tungsten Electrode (GTAW)
Size:
Type:

BASE METALS
Material Spec.
Type or Grade
Thickness: Groove N/A Fillet 1/8" - Unlimited
Diameter (Pipe) N/A

FILLER METALS
AWS Specification AWS A5.29
AWS Classification E100T-1

TECHNIQUE
Stringer or Weave Bead: Stringer or Weave
Multi-Pass or Single Pass (per side) Single or Multi
Number of Electrodes 1
Electrode Spacing Longitudinal N/A
Lateral N/A
Angle N/A
Contact Tube to Work Distance 1"
Peening None
Interpass Cleaning: Remove slag, chip or brush

SHIELDING
Flux N/A Gas CO_2
Composition 100%
Electrode-Flux (Class) Flow Rate 45 CFH
Gas Cup Size N/A

PREHEAT and INTERPASS TEMPERATURE
Min for Thicknesses 1/8" - 3/4" (included) 32°F see note*
Min for Thicknesses over 3/4" - 1 1/2" (included) 50°F
Min for Thicknesses 1 1/2" - 2 1/2" (included) 150°F
Min for Thicknesses over 2 1/2" 225°F
Max Interpass Temperature 550°F

POST WELD HEAT TREATMENT
Temperature N/A
Time N/A

Calculated Heat Input (kJ/in) 44.22

* Note: When base metal is below 32*F, preheat to 70*F and maintain during welding.

ACTUAL WELDING PARAMETERS USED

Pass or Weld Layer(s)	Process	Filler Metals: Class	Filler Metals: Diameter	Current: Type & Polarity	Current: Amps or Wire Feed Speed	Volts	Travel Speed (IPM)	Joint Details
1	FCAW	E100T-1	1/16"	DC+	327	29.3	13	Fillet Weld
This WPS is only to show the welding parameters used - *NOT for PRODUCTION*								

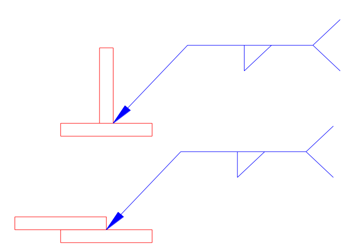

APPENDIX D

WELD WIRE MILL TEST REPORTS

SELECT ARC INC.

Manufactured In The USA

600 Enterprise Drive
PO Box 259
Fort Loramie, OH 45845
800.341.5215

Shipped Production Numbers:

6212D901A1401, 6211D901A1402

Diameter: 1/16

Certificate of Conformance

This is to certify that the product stated below is of the same classification, manufacturing process, and material requirements as the electrode used for the testing on the date stated. All tests required by the specifications for classification were performed and the material met all requirements. It was manufactured and supplied according to the quality management system of Select-Arc, Inc., which meets the requirements of ISO 9001 and other applicable specifications. This certificate complies with the requirements of EN 10204, Type 2.2.

Product: Encore

Diameter(s): .045 - 1/16

Specifications: AWS A5.20:2005

Classification: E71T-1C-H4, E71T-1M-H4, E71T-9C-H4, E71T-9M-H4

Test Completion Date: 2/19/2014

Lot Numbers: (1/16) 8549

Chemical Analysis (*wt%*)

Diameter			1/16	
Shielding Gas			75% Ar / 25% CO2	CO2
	Max	**Min**	**Results**	**Results**
C	0.12	-	0.07	0.05
Si	0.90	-	0.32	0.25
P	0.03	-	0.011	0.007
Mn	1.75	-	1.13	0.99
S	0.03	-	0.009	0.012

Weld Parameters

Electrode Diameter:	1/16	
Shielding Gas	75% Ar / 25% CO2	CO2
Amperage:	261	255
Arc Voltage:	28.0	28.5
Current Polarity:	DCEP	DCEP
CTWD (in):	3/4	1
No. of Passes/Layers:	17/9	14/7
Preheat Temperature(°F):	70	70
Interpass Temperature(°F):	300	300

Radiographic Test: **Met Requirement**

Fillet Weld Test: **Met Requirement**

Weld Metal Diffusible Hydrogen (ml/100g) per AWS A4.3-93

Diameter:	1/16
Shielding Gas	CO2
Requirements	Results
4	3.8

Mechanical Properties

Electrode Diameter:		1/16	
Shielding Gas		75% Ar / 25% CO2	CO2
Requirements		**Results**	**Results**
Test Condition:	As-Welded	As-Welded	As-Welded
PWHT Temperature:	-	-	-
Tensile Strength (psi):	70000 - 90000	82000	71000
Yield Strength (psi):	58000 min	72000	62000
Elongation (%):	22 min	37	33
Charpy V-Notch Impacts:		33, 41, 45	62, 53, 74
ft-lb f @ -20°F	20 avg.	40 avg	63 avg

The undersigned certifies that the product supplied will meet the requirements of the applicable AWS Filler Metal Specification when tested in accordance with that specification.

Signed By: Martin L. Caruso

Martin L. Caruso, Director of Technology

SELECT ARC INC.

Manufactured In The USA

600 Enterprise Drive
PO Box 259
Fort Loramie, OH 45845
800.341.5215

Diameter: 1/16

Certificate of Conformance

This is to certify that the product stated below is of the same classification, manufacturing process, and material requirements as the electrode used for the testing on the date stated. All tests required by the specifications for classification were performed and the material met all requirements. It was manufactured and supplied according to the quality management system of Select-Arc, Inc., which meets the requirements of ISO 9001 and other applicable specifications. This certificate complies with the requirements of EN 10204, Type 2.2.

Product: Select 101-K3C
Diameter(s): .045 - 1/16
Specifications: AWS A5.29: 2010
Classification: E101T1-K3C

Test Completion Date: 8/18/2017
Lot Numbers: (1/16) 6366

Chemical Analysis (*wt%*)

Diameter			1/16
Shielding Gas			CO2
	Max	**Min**	**Results**
Ni	2.60	1.25	1.78
Cr	0.15	-	0.03
Si	0.80	-	0.31
C	0.15	-	0.05
P	0.030	-	0.007
Mn	2.25	0.75	1.43
Mo	0.65	0.25	0.39
S	0.030	-	0.010
V	0.05	-	0.02

Radiographic Test: **Met Requirement**
Fillet Weld Test: **Met Requirement**

Weld Parameters

Electrode Diameter:	1/16
Shielding Gas	CO2
Amperage:	317
Arc Voltage:	28.0
Current Polarity:	DCEP
CTWD (in):	3/4
No. of Passes/Layers:	13/6
Preheat Temperature(°F):	300
Interpass Temperature(°F):	300

Mechanical Properties

Electrode Diameter:		1/16
Shielding Gas		CO2
Requirements		**Results**
Test Condition:	As-Welded	As-Welded
PWHT Temperature:	-	-
Tensile Strength (psi):	100000 - 120000	107000
Yield Strength (psi):	88000 min	99000
Elongation (%):	16 min	19
Charpy V-Notch Impacts:		65, 69, 65
ft-lb f @ 0°F	20 avg.	66 avg

The undersigned certifies that the product supplied will meet the requirements of the applicable AWS Filler Metal Specification when tested in accordance with that specification.

Signed By: Martin L. Caruso

Martin L. Caruso, Director of Technology

SELECT ARC INC.

Manufactured In The USA

600 Enterprise Drive
PO Box 259
Fort Loramie, OH 45845
800.341.5215

Diameter: 1/16

Certificate of Conformance

This is to certify that the product stated below is of the same classification, manufacturing process, and material requirements as the electrode used for the testing on the date stated. All tests required by the specifications for classification were performed and the material met all requirements. It was manufactured and supplied according to the quality management system of Select-Arc, Inc., which meets the requirements of ISO 9001 and other applicable specifications. This certificate complies with the requirements of EN 10204, Type 2.2.

Product: Select 820-Ni1

Diameter(s): .045 - 1/16

Specifications: AWS A5.29:2010, AWS A5.36:2016

Classification: E81T1-Ni1CJ-H4, E81T1-Ni1MJ-H4, E81T1-M21A4-Ni1-H4, E81T1-C1A4-Ni1-H4

Test Completion Date: 5/13/2019

Lot Numbers: (1/16) 1919

Chemical Analysis (*wt%*)

Diameter			1/16	
Shielding Gas			75% Ar / 25% CO2	CO2
	Max	**Min**	**Results**	**Results**
Ni	1.10	0.80	0.95	1.03
C	0.12	-	0.04	0.03
Si	0.80	-	0.53	0.41
Cr	0.15	-	0.06	0.06
P	0.030	-	0.010	0.010
Mn	1.50	-	1.49	1.21
Mo	0.35	-	0.01	0.01
S	0.030	-	0.009	0.010
V	0.05	-	0.02	0.03

Radiographic Test: **Met Requirement**

Fillet Weld Test: **Met Requirement**

Weld Metal Diffusible Hydrogen (ml/100g) per AWS A4.3-93

Diameter:	1/16	
Shielding Gas	75% Ar / 25% CO2	CO2
Requirements	Results	Results
4	3.8	2.5

Weld Parameters

Electrode Diameter:	1/16	
Shielding Gas	75% Ar / 25% CO2	CO2
Amperage:	286	274
Arc Voltage:	27.0	28.0
Current Polarity:	DCEP	DCEP
CTWD (in):	1	1
No. of Passes/Layers:	12/6	12/6
Preheat Temperature(°F):	300	300
Interpass Temperature(°F):	300	300

Mechanical Properties

	Electrode Diameter:	1/16	
	Shielding Gas	75% Ar / 25% CO2	CO2
Requirements		**Results**	**Results**
Test Condition:	As-Welded	As-Welded	As-Welded
PWHT Temperature:	-	-	-
Tensile Strength (psi):	80000 - 100000	91000	82000
Yield Strength (psi):	68000 min	80000	72000
Elongation (%):	22 min	27	29
Charpy V-Notch Impacts:		65, 81, 52	55, 68, 64
ft-lb f @ -20°F	20 avg.	66 avg	62 avg
Charpy V-Notch Impacts:		43, 44, 51	38, 21, 24
ft-lb f @ -40°F	20 avg.	46 avg	28 avg

The undersigned certifies that the product supplied will meet the requirements of the applicable AWS Filler Metal Specification when tested in accordance with that specification.

Signed By: Martin L. Caruso

Martin L. Caruso, Director of Technology

APPENDIX E

ALL-WELD-METAL TENSION TEST REPORTS

MATERIALS TECHNOLOGY INCORPORATED
www.TestMetal.com
213 Lyon Lane
Birmingham, AL 35211
205.940.9480

REPORT OF ANALYSIS

ARC International, LLC
Attention: Bo Dowswell
Suite 116
300 Cahaba Park Circle
Birmingham, AL 35242

Test Date:	08/01/2019
Report Date:	08/01/2019
Lab Number:	192488
P. O. Number:	

Sample Identification: (9) 3/4" Thick Welded Plates (Groove Welds)

		SPECIMEN IDENTIFICATION					
		AT1			**AT2**		
Properties	**Unit**	**Specimen #1**	**Specimen #2**	**Specimen #3**	**Specimen #1**	**Specimen #2**	**Specimen #3**
Tensile Properties							
Tensile Strength	psi	75,900	76,300	75,100	79,700	82,700	79,900
Yield Strength (0.2 % offset)	psi	62,500	64,700	61,100	69,000	72,000	68,200
Elongation (Gage=4D)	%	32	30	31	30	28	30
Reduction in Area	%	70	69	69	70	70	70

		AT3		
		Specimen #1	**Specimen #2**	**Specimen #3**
Tensile Properties				
Tensile Strength	psi	101,000	100,600	98,300
Yield Strength (0.2 % offset)	psi	69,300	66,300	81,700
Elongation (Gage=4D)	%	23	24	23
Reduction in Area	%	59	61	60

Test Method(s): AWS B4.0

Respectfully Submitted,
Materials Technology, Inc.

Quality Assurance Representative

Tests and analysis performed in accordance with procedures derived from methods described and approved by the ASTM and other accepted industry practices. This report shall not be reproduced, except in full, without the prior written approval of Materials Technology, Inc.

Testing efforts were in accordance with MTI QA Program, Rev. 7 – March 16, 2017.

APPENDIX F

SPECIMEN PHOTOGRAPHS

TRANSVERSE FILLET WELD SPECIMENS

Specimen FT1

Specimen FT4

Specimen FT9

Specimen FT10

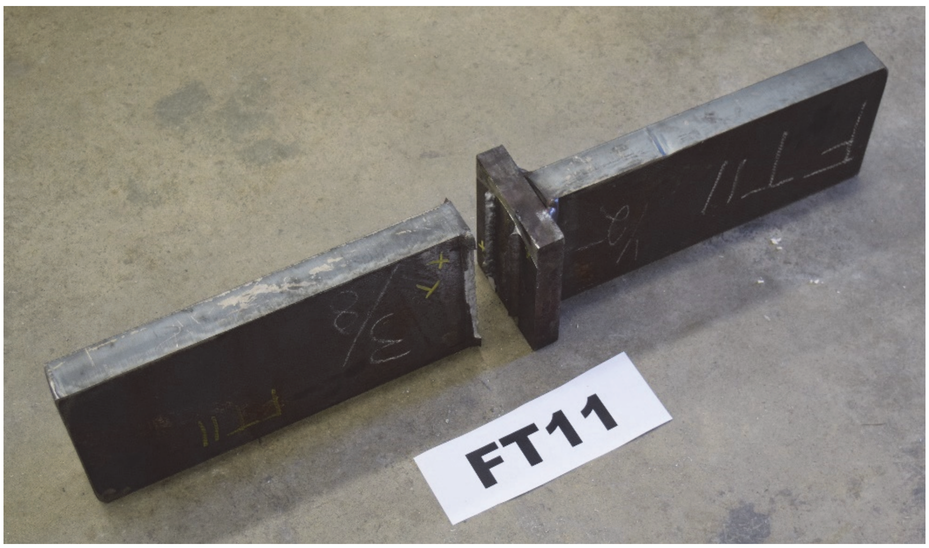

Specimen FT11

Specimen FT14

LONGITUDINAL FILLET WELD SPECIMENS

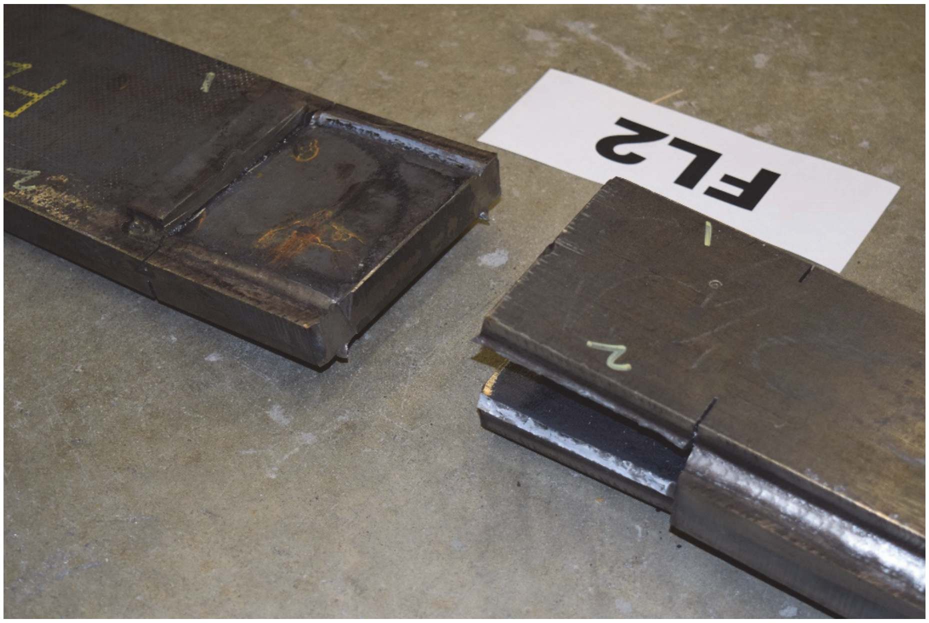

Specimen FL2

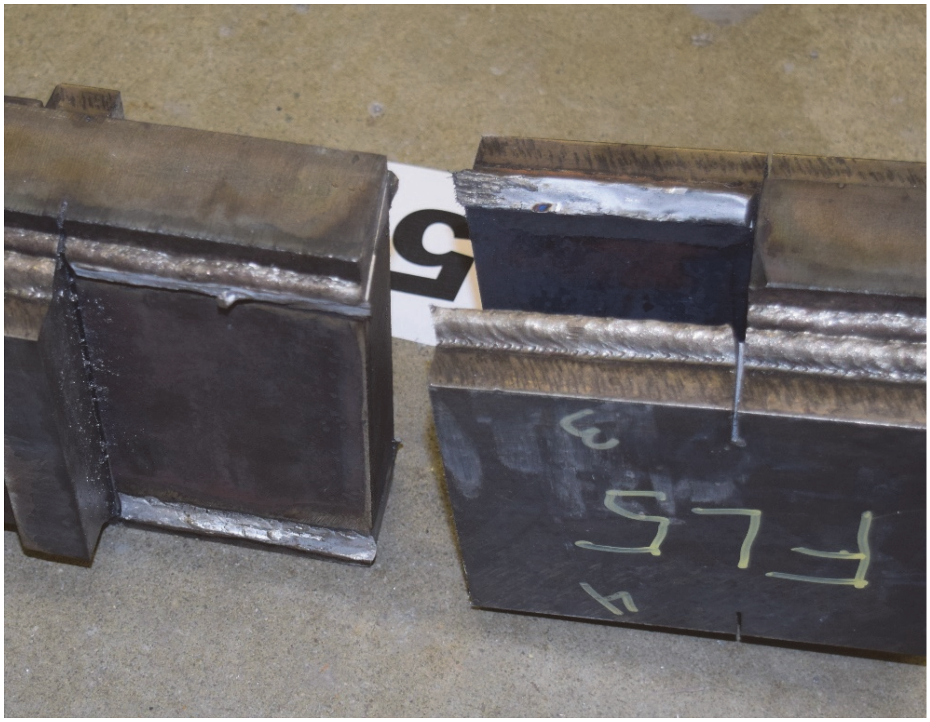

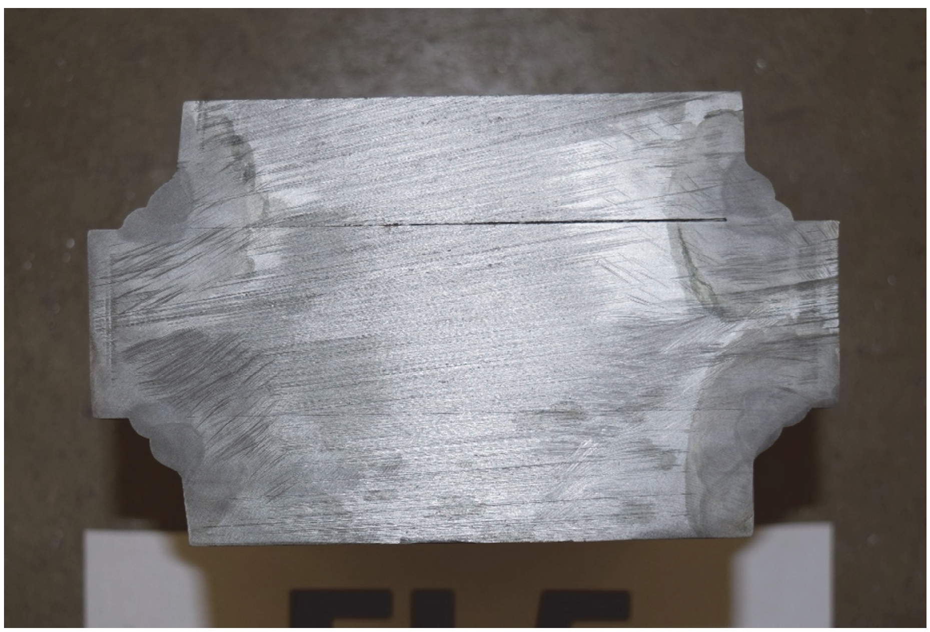

Specimen FL5

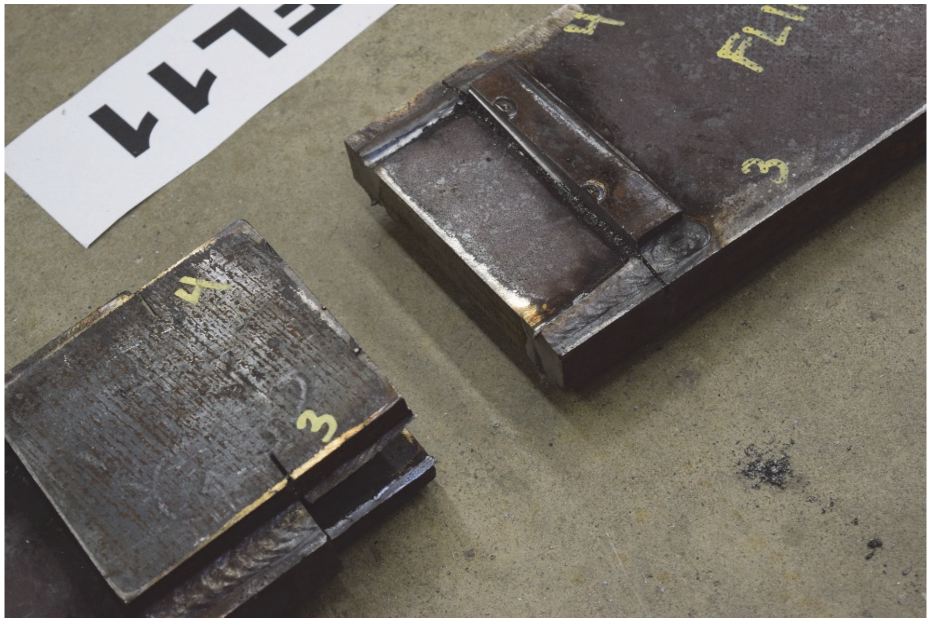

Specimen FL11

Specimen FL13

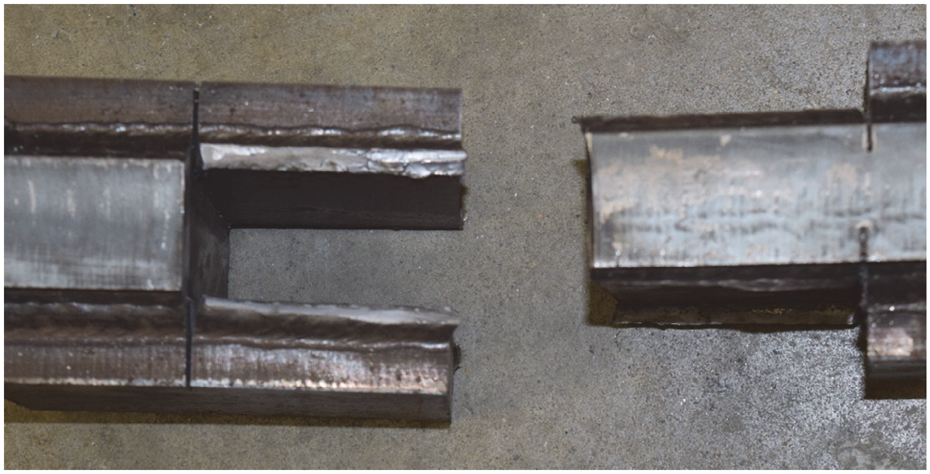

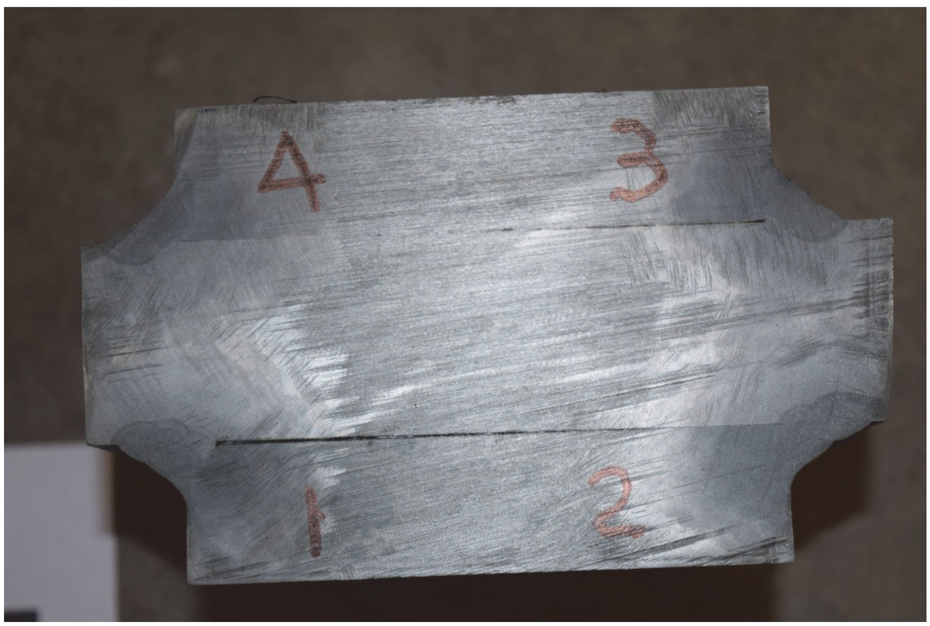

Specimen FL14

TRANSVERSE PJP WELD SPECIMENS

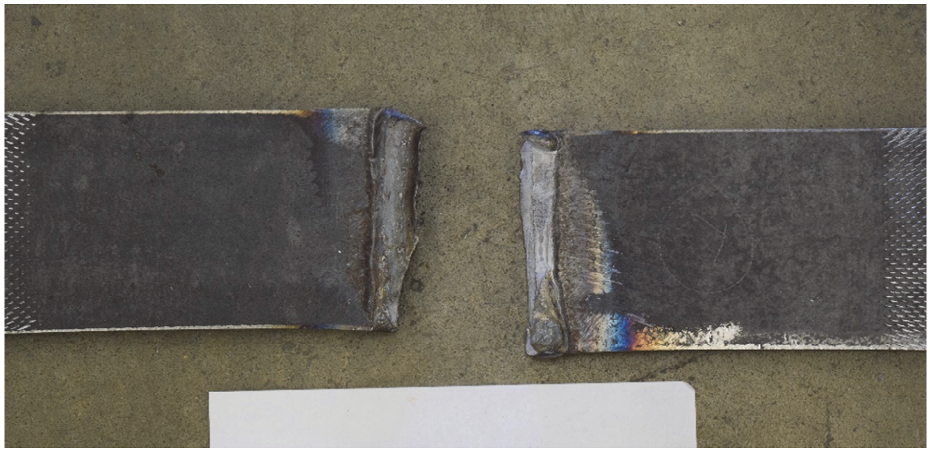

Specimen PT1

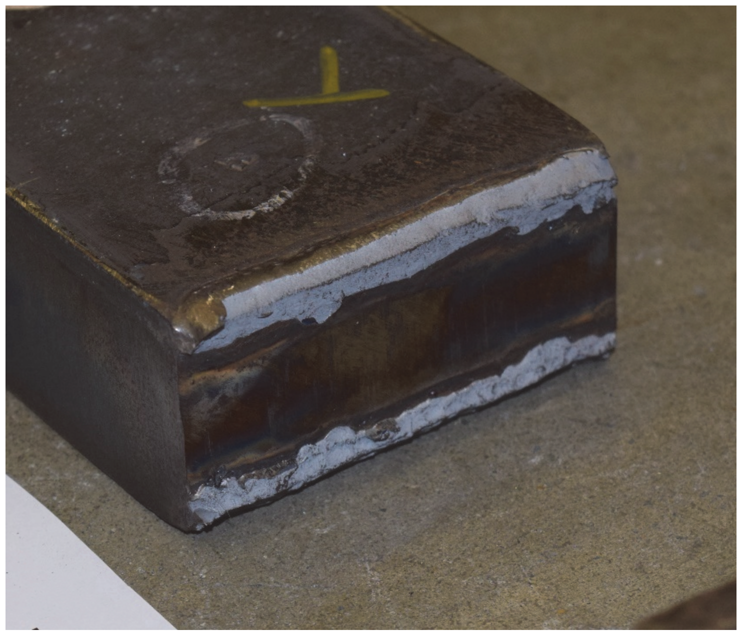

Specimen PT6

Specimen PT15

Specimen PT16

LONGITUDINAL PJP WELD SPECIMENS

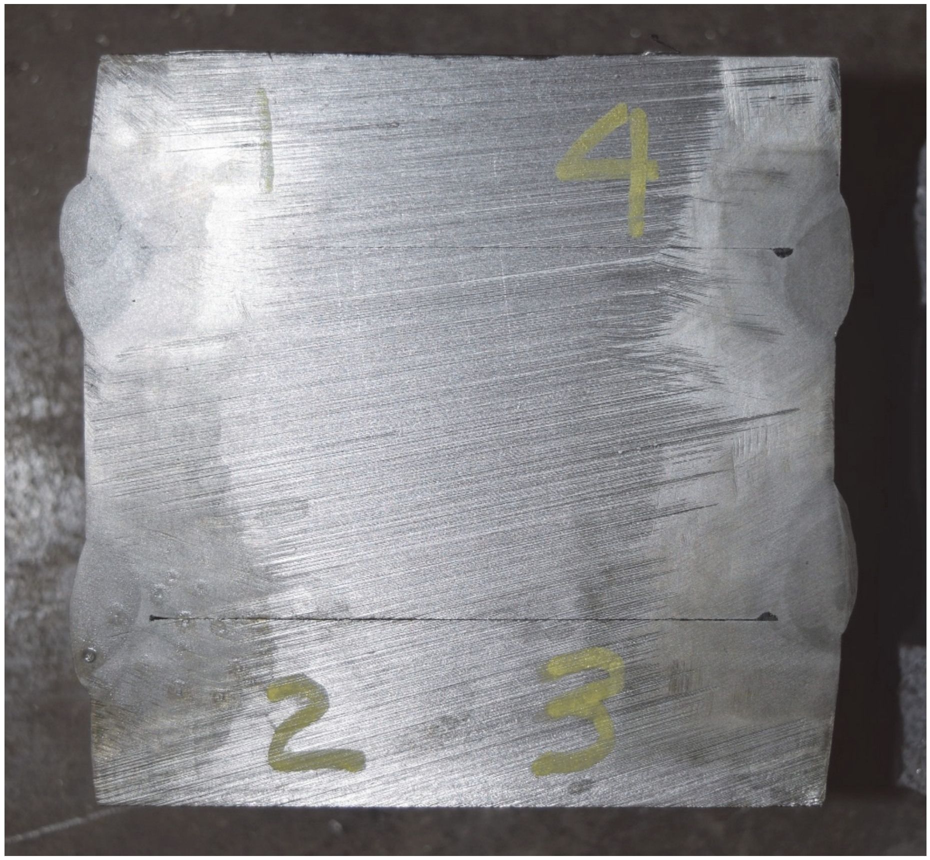

Specimen PL2 (etched)

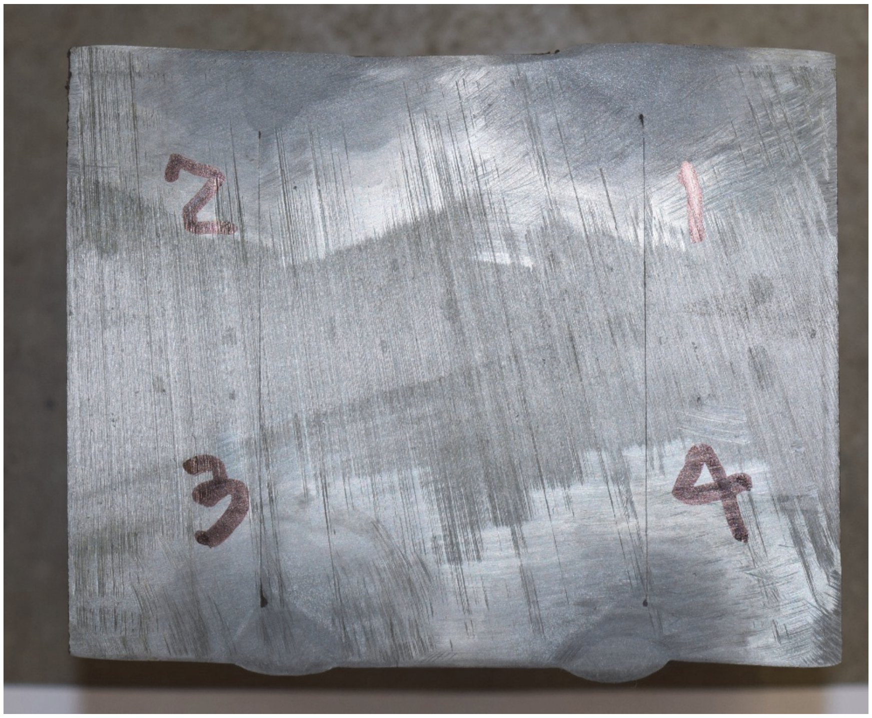

Weld 1

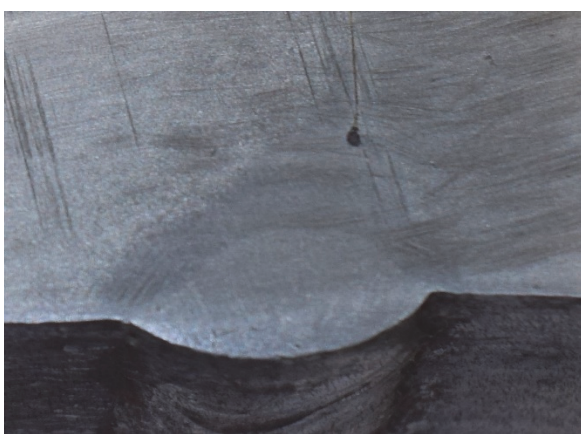

Weld 4

Specimen PL4 (etched)

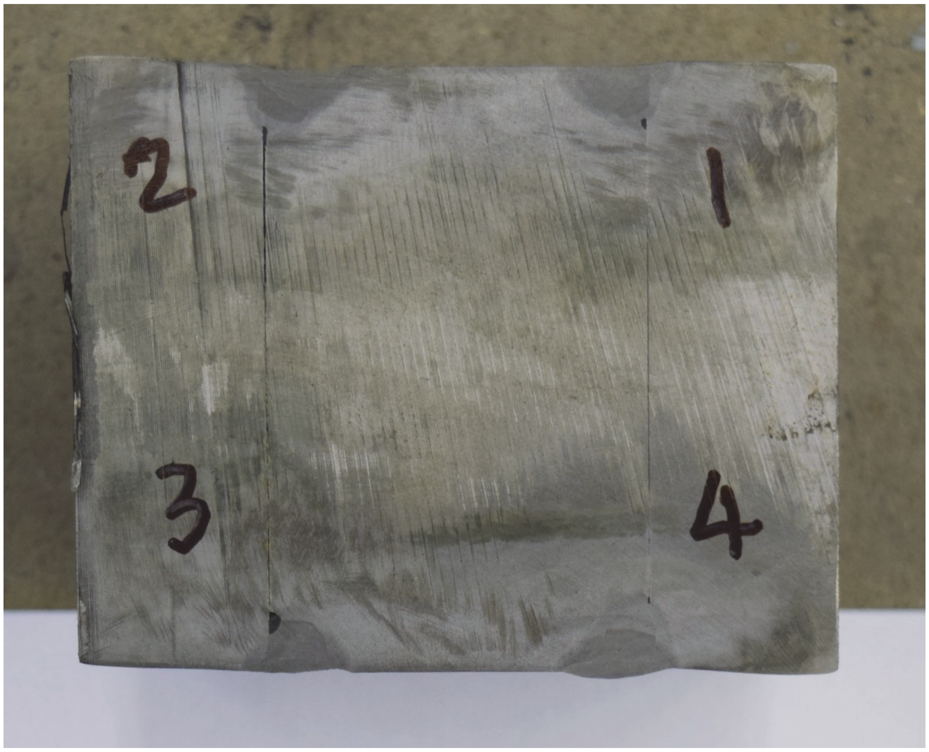

Specimen PL8 (etched)

Specimen PL11

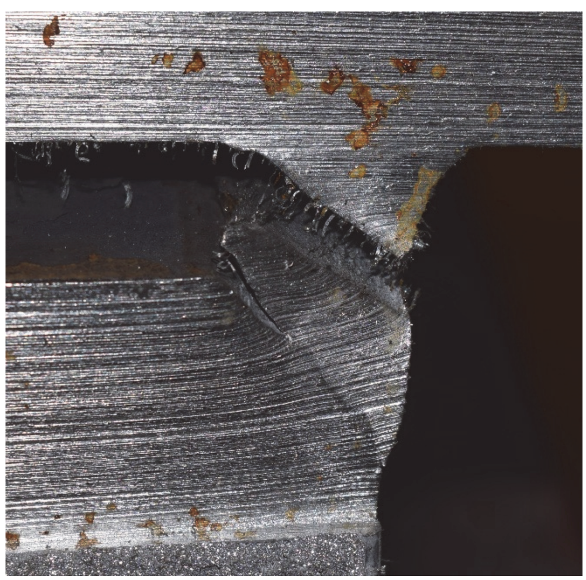

Specimen PL13

Specimen PL13 (etched)

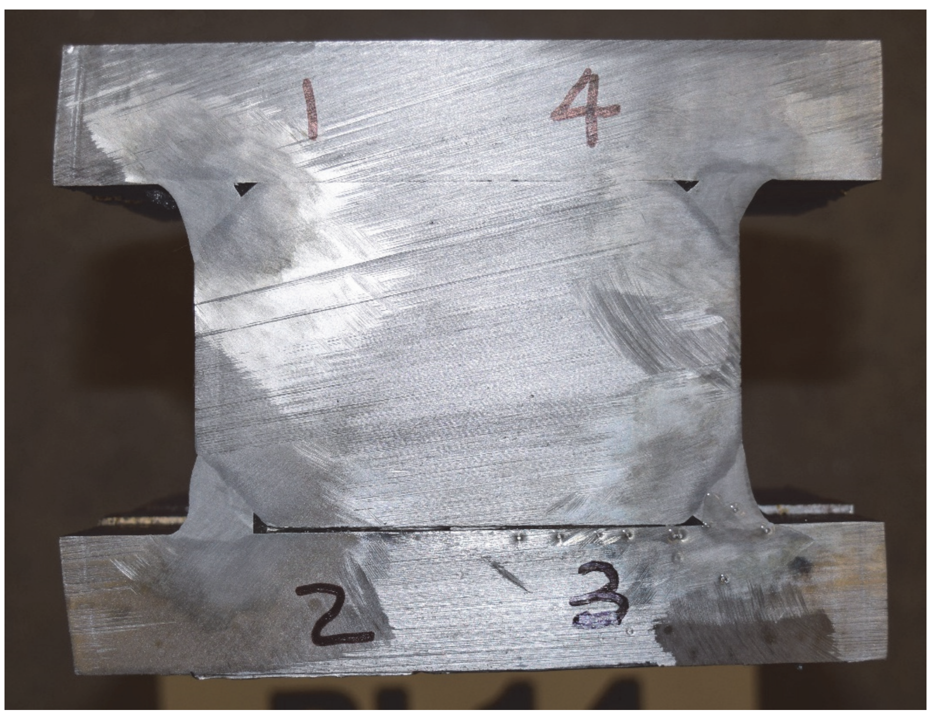

Specimen PL14 (etched)

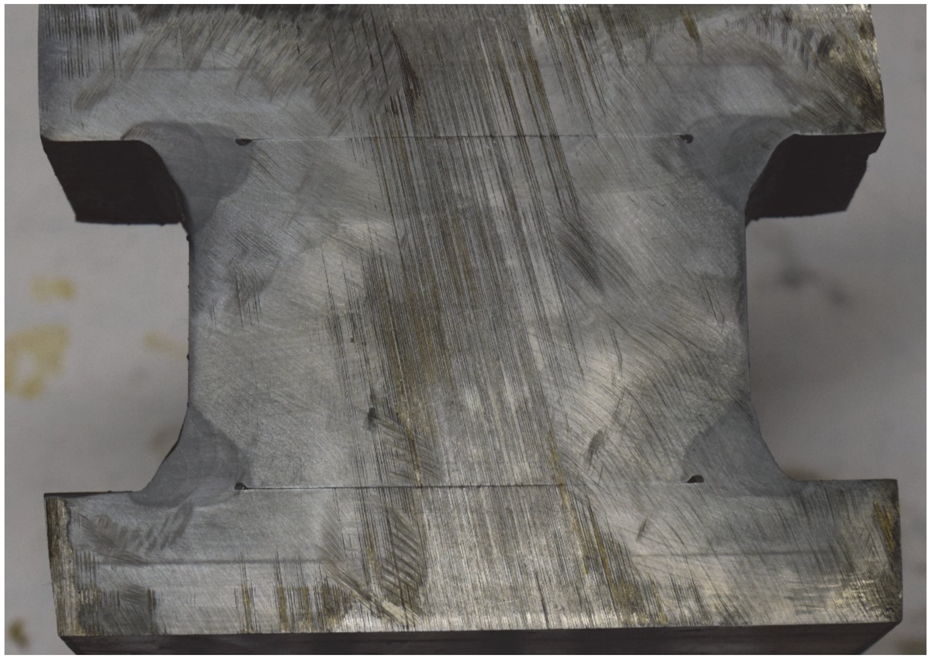

Specimen PL15 (etched)

SKEWED PJP WELD SPECIMENS

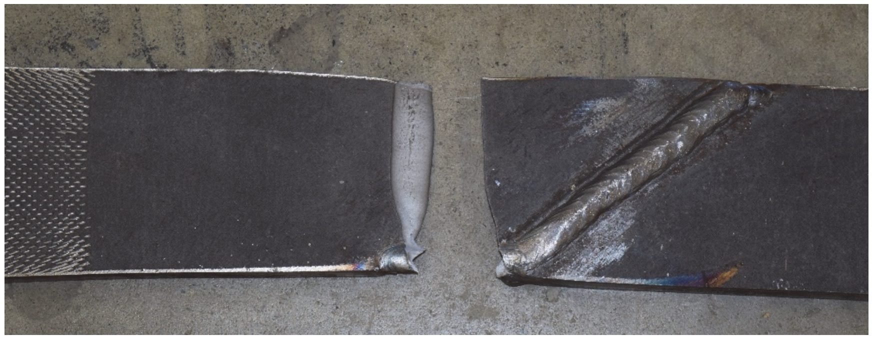

Specimen PS1

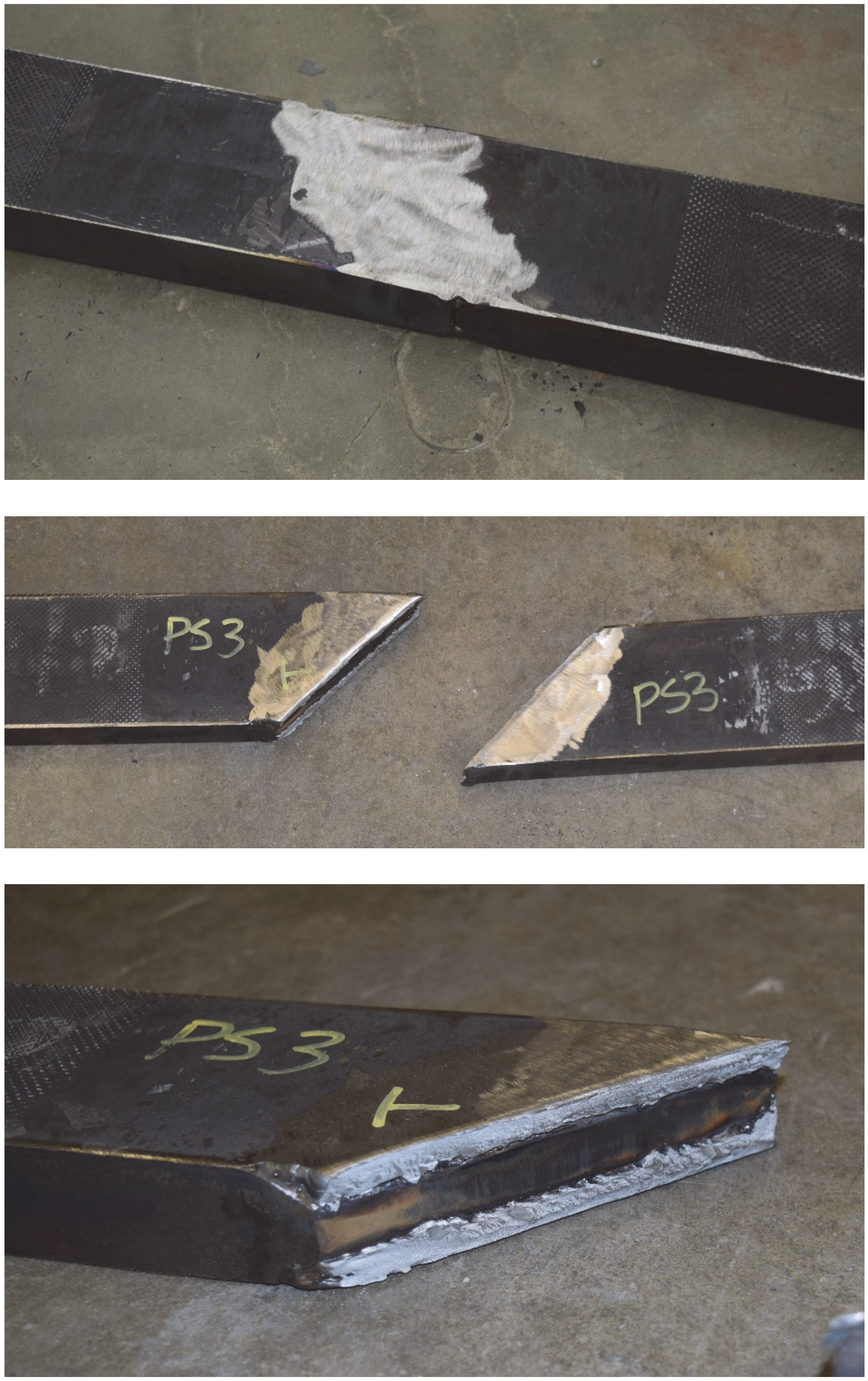

Specimen PS3

Specimen PS4

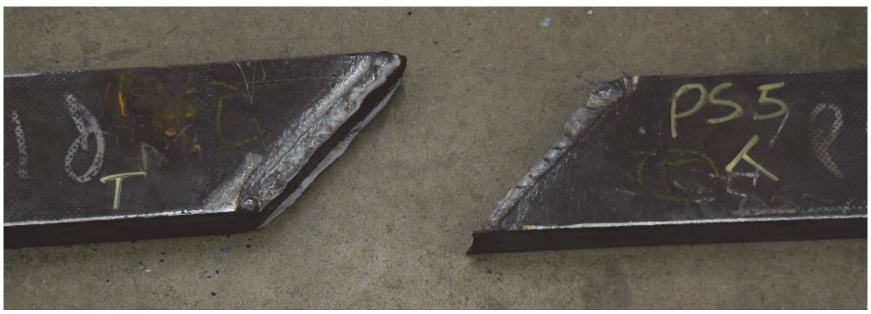

Specimen PS5

APPENDIX G

SPECIMEN DATA

TRANSVERSE FILLET WELD SPECIMENS

Table G1a. Transverse fillet weld specimens: pre-test measurements.

Specimen Number	w_{T1}	w_{T2}	w_{B1}	w_{B2}	L_T	L_B
	in.	in.	in.	in.	in.	in.
FT1	0.319	0.315	0.326	0.337	1.74	1.74
FT2	0.256	0.303	0.324	0.343	3.46	3.77
FT3	0.248	0.349	0.260	0.255	5.76	5.70
FT4	0.457	0.489	0.452	0.511	1.78	1.73
FT5	0.402	0.435	0.440	0.444	3.69	3.73
FT6	0.420	0.441	0.372	0.443	5.59	5.60
FT7	0.534	0.592	0.484	0.518	1.81	1.92
FT8	0.460	0.482	0.462	0.489	3.74	3.79
FT9	0.503	0.496	0.478	0.512	4.80	4.62
FT10	0.283	0.308	0.258	0.284	5.82	5.78
FT11	0.368	0.419	0.398	0.424	4.71	4.39
FT12	0.494	0.489	0.473	0.518	3.81	3.77
FT13	0.263	0.385	0.306	0.426	1.79	1.83
FT14	0.299	0.396	0.291	0.354	5.71	5.75
FT15	0.448	0.513	0.461	0.485	1.84	1.79
FT16	0.404	0.414	0.390	0.475	4.76	4.78
FT17	0.424	0.607	0.441	0.667	1.76	1.79
FT18	0.395	0.545	0.561	0.598	3.80	3.76

Table G1b. Transverse fillet weld specimens: post-test measurements.

Specimen Number	E_{r1}	E_{r2}	γ_1	γ_2
	in.	in.	degrees	degrees
FT1	0.394	0.363	70	86
FT2	0.320	0.310	85	72
FT3	0.358	0.382	52	88
FT4	0.518	0.571	48	89
FT5	0.524	0.457	76	64
FT6	0.427	0.398	80	50
FT7	0.428	0.437	67	52
FT8	0.414	0.380	85	78
FT9	0.528	0.571	78	88
FT10	0.291	0.261	82	76
FT11	0.370	0.361	84	82
FT12	0.435	0.432	81	64
FT13	0.259	0.242	65	70
FT14	0.270	0.266	72	72
FT15	0.340	0.350	63	89
FT16	0.381	0.312	88	59
FT17	0.449	0.457	84	58
FT18	0.370	0.380	73	61

Table G1c. Transverse fillet weld specimens: experimental results.

Specimen Number	P_e	P_n	P_c	f_r	P_e / P_n	P_e / P_c	f_r / σ_{uw}	Comments
	kips	kips	kips	ksi				
FT1	85.0	38.8	54.4	60.7	2.19	1.56	0.801	Fusion face rupture in the bottom weld only
FT2	174	80.5	107	72.7	2.15	1.63	0.959	Fusion face rupture in the top weld only
FT3	288	128	150	65.7	2.26	1.92	0.867	
FT4	116	58.6	80.5	56.1	1.97	1.44	0.740	Fusion face rupture in the bottom weld only
FT5	225	124	154	61.3	1.82	1.46	0.809	
FT6	331	187	225	71.6	1.77	1.47	0.945	
FT7	119	83.0	95.2	74.5	1.44	1.25	0.982	
FT8	239	167	171	80.9	1.43	1.39	1.07	Fusion face rupture in the top weld and partially at the bottom weld
FT9	324	210	226	62.3	1.54	1.44	0.823	Welds cut to ≈ 5 in. long before testing. Fusion face rupture in the bottom weld only.
FT10	253	148	168	78.8	1.71	1.50	0.975	
FT11	279	174	188	83.5	1.60	1.49	1.03	No failure in initial test. Re-test after cutting welds. Fusion face rupture in both welds.
FT12	245	193	192	75.3	1.27	1.28	0.931	
FT13	76.4	57.7	76.1	82.5	1.32	1.00	0.825	
FT14	238	182	239	77.3	1.30	1.00	0.773	
FT15	111	87	110	89.5	1.27	1.01	0.895	
FT16	300	228	253	90.0	1.32	1.18	0.900	Welds cut to ≈ 5 in. long before testing
FT17	118	113	114	76.7	1.04	1.03	0.767	
FT18	281	240	248	98.4	1.17	1.13	0.984	

LONGITUDINAL FILLET WELD SPECIMENS

Table G2a. Longitudinal fillet weld specimens-pre-test measurements.

Specimen Number	w_{T1}	w_{T2}	w_{T3}	w_{T4}	w_{L1}	w_{L2}	w_{L3}	w_{L4}	L_1	L_2	L_3	L_4
	in.	in.	in.	in.	in.	in.	in.	in.	in.	in.	in.	in.
FL1	0.307	0.262	0.258	0.275	0.301	0.291	0.341	0.291	2.17	2.12	2.16	2.12
FL2	0.297	0.289	0.332	0.288	0.335	0.291	0.322	0.243	4.06	4.03	4.03	4.03
FL3	0.232	0.307	0.267	0.292	0.384	0.380	0.386	0.393	2.94	2.92	3.07	3.02
FL4	0.463	0.417	0.439	0.405	0.497	0.427	0.424	0.402	1.97	2.09	2.03	1.91
FL5	0.506	0.457	0.509	0.464	0.489	0.426	0.448	0.481	3.25	3.22	3.16	3.16
FL6	0.472	0.456	0.471	0.440	0.478	0.429	0.381	0.434	2.92	2.98	2.97	2.99
FL7	0.461	0.481	0.582	0.521	0.445	0.552	0.413	0.492	2.05	2.03	2.08	2.04
FL8	0.750	0.528	0.590	0.510	0.637	0.484	0.545	0.490	2.97	2.94	2.90	2.86
FL9	0.296	0.237	0.289	0.218	0.227	0.330	0.275	0.264	3.39	3.39	3.63	3.60
FL10	0.417	0.405	0.394	0.406	0.389	0.383	0.383	0.431	3.37	3.31	3.41	3.42
FL11	0.250	0.281	0.264	0.277	0.359	0.462	0.442	0.365	2.03	2.03	2.06	2.02
FL12	0.299	0.260	0.293	0.243	0.349	0.397	0.328	0.292	4.46	4.53	4.43	4.27
FL13	0.403	0.380	0.398	0.361	0.508	0.509	0.440	0.486	2.01	2.03	2.08	2.09
FL14	0.443	0.448	0.435	0.458	0.470	0.611	0.452	0.496	3.05	3.09	3.07	2.95
FL15	0.486	0.491	0.484	0.474	0.525	0.479	0.535	0.452	1.72	1.77	1.62	1.63

Table G2b. Longitudinal fillet weld specimens-post-test measurements.								
Specimen Number	E_{r1}	E_{r2}	E_{r3}	E_{r4}	γ_1	γ_2	γ_3	γ_4
	in.	in.	in.	in.	degrees	degrees	degrees	degrees
FL1	0.273	0.276	0.232	0.283	56	56	68	57
FL2	0.278	0.246	0.240	0.277	69	63	60	53
FL3	0.227	0.294	0.210	0.244	64	59	62	64
FL4	0.340	0.349	0.353	0.300	60	51	49	48
FL5	0.319	0.380	0.379	0.315	40	43	25	42
FL6	0.324	0.343	0.366	0.369	48	41	37	46
FL7	0.409	0.371	0.410	0.405	39	41	44	50
FL8	0.470	0.428	0.404	0.397	32	43	39	39
FL9	0.202	0.202	0.214	0.206	54	61	48	55
FL10	0.314	0.337	0.321	0.296	35	50	43	43
FL11	0.158	0.233	0.180	0.248	63	64	61	64
FL12	0.157	0.190	0.168	0.204	45	35	52	45
FL13	0.329	0.301	0.289	0.337	50	50	53	40
FL14	0.298	0.301	0.312	0.311	60	59	66	52
FL15	0.330	0.373	0.336	0.382	44	53	35	42

Table G2c. Longitudinal fillet weld specimens-experimental results.

Specimen Number	P_e	P_n	P_c	f_r	P_e / P_n	P_e / P_c	f_r/σ_{uw}	Comments
	kips	kips	kips	ksi				
FL1	150	63.6	79.4	64.4	2.35	1.89	0.849	
FL2	301	120	155	70.9	2.51	1.94	0.935	
FL3	193	88.7	121	66.2	2.18	1.59	0.873	Test was terminated at 330 kips. Welds were cut to ≈ 3 in. long and the specimen was re-tested.
FL4	178	89.2	112	64.9	2.00	1.60	0.856	
FL5	297	142	194	66.6	2.09	1.53	0.878	Welds were cut shorter by ≈ 3/4 in. before testing
FL6	284	132	169	66.2	2.15	1.68	0.874	Welds were cut to ≈ 3 in. long before testing
FL7	197	122	128	58.6	1.62	1.53	0.773	
FL8	314	173	212	61.7	1.81	1.48	0.814	Welds were cut to ≈ 3 in. long before testing
FL9	244	119	125	84.0	2.05	1.94	1.04	Welds were cut to ≈ 3.5 in. long before testing
FL10	319	172	185	74.1	1.86	1.72	0.917	Welds were cut to ≈ 3.5 in. long before testing
FL11	126	86.4	109	75.2	1.46	1.15	0.752	
FL12	317	188	226	98.8	1.69	1.40	0.988	Welds were cut to ≈ 4.5 in. long before testing. Weld rupture and rupture at one lap plate.
FL13	182	131	148	70.9	1.39	1.23	0.709	
FL14	282	193	243	76.4	1.46	1.16	0.764	Welds were cut to ≈ 3 in. long before testing
FL15	173	143	140	63.3	1.21	1.24	0.633	

TRANSVERSE PJP WELD SPECIMENS

Table G3a. Transverse PJP weld specimens: pre-test measurements.				
Specimen Number	X_T	X_B	L_T	L_B
	in.	in.	in.	in.
PT1	0.0725	0.119	3.84	3.92
PT2	0.121	0.0540	3.72	3.71
PT3	0.0850	0.0670	3.75	3.82
PT4	0.0655	0.0360	3.75	3.73
PT5	0.0680	0.0385	3.75	3.77
PT6	0.0325	0.0390	3.81	3.84
PT7	0.0995	0.0955	3.98	3.81
PT8	0.0615	0.0675	3.76	3.77
PT9	-0.00500	0.0165	3.88	3.92
PT10	0.0300	0.0180	3.90	3.85
PT11	0.0290	-0.0130	3.87	3.83
PT12	0.0410	0.0510	3.99	4.00
PT13	0.0130	0.0260	3.72	3.72
PT14	0.0315	0.0285	3.89	3.95
PT15	0.0000	0.0000	3.83	3.81
PT16	-0.00700	0.0455	3.96	3.98
PT17	-0.0340	0.0360	3.83	3.83

Table G3b. Transverse PJP weld specimens: post-test measurements.				
Specimen Number	E_{rT}	E_{rB}	γ_T	γ_B
	in.	in.	degrees	degrees
PT1	0.382	0.344		
PT2	0.509	0.448	40	40
PT3	0.304	0.320	45	44
PT4	0.358	0.365	45	47
PT5	0.298	0.379	55	48
PT6	0.380	0.383	43	45
PT7	0.236	0.260	0	0
PT8	0.399	0.349	49	45
PT9	0.167	0.197		
PT10	0.206	0.259	53	43
PT11	0.327	0.289	40	52
PT12	0.218	0.201		
PT13	0.171	0.230	0	41
PT14	0.184	0.239	0	
PT15	0.331	0.339	43	39
PT16	0.207	0.189	0	0
PT17	0.283	0.268	36	38

Table G3c. Transverse PJP weld specimens: experimental results.

Specimen Number	P_e	P_n	P_c	f_r	P_e / P_n	P_e / P_c	f_r/σ_{uw}	Comments
	kips	kips	kips	ksi				
PT1	215	81.4	122	78.0	2.64	1.76	1.03	Mixed rupture at weld and fusion zone
PT2	296	117	156	83.4	2.53	1.89	1.10	
PT3	258	99.4	134	107	2.60	1.93	1.41	
PT4	269	118	145	95.8	2.28	1.86	1.26	
PT5	258	158	189	97.5	1.63	1.36	1.29	
PT6	308	161	186	104	1.92	1.65	1.37	
PT7	225	81.8	123	117	2.75	1.83	1.55	Rupture at fusion zone in non-prepared plate
PT8	269	119	151	93.0	2.27	1.79	1.23	
PT9	163	93.6	96.7	120	1.74	1.69	1.48	
PT10	267	140	150	148	1.91	1.78	1.83	
PT11	256	185	190	108	1.38	1.35	1.34	
PT12	190	95.9	115	117	1.98	1.66	1.44	
PT13	205	134	142	137	1.53	1.44	1.70	
PT14	203	118	132	124	1.73	1.54	1.24	Top weld: rupture at fusion zone in non-prepared plate. Bottom weld: rupture at weld metal.
PT15	243	172	172	94.9	1.41	1.41	0.949	
PT16	195	119	128	128	1.63	1.52	1.28	Rupture at fusion zone in non-prepared plate
PT17	255	172	173	121	1.48	1.48	1.21	

LONGITUDINAL PJP WELD SPECIMENS

Table G4a. Longitudinal PJP weld specimens: pre-test measurements.

Specimen Number	X_1	X_2	X_3	X_4	L_1	L_2	L_3	L_4
	in.	in.	in.	in.	in.	in.	in.	in.
PL1	0.0250	0.0525	0.0505	0.0845	4.00	4.00	4.11	3.99
PL2	0.131	0.118	0.131	0.100	3.73	3.85	3.88	3.74
PL3	0.108	0.0840	0.0655	0.0715	2.90	2.96	2.89	2.86
PL4	0.0555	0.0030	0.0690	0.0485	2.97	3.06	2.95	3.01
PL5								
PL6	0.0160	0.0470	0.0500	0.0435	2.99	3.02	2.92	3.06
PL7	0.0495	-0.0120	-0.0395	0.0080	2.95	3.01	3.09	3.00
PL8	-0.0240	-0.0660	-0.0180	0.0440	2.66	2.75	2.65	2.67
PL9	0.0545	0.0240	0.0620	0.0350	3.93	4.07	4.09	4.02
PL10	0.0055	-0.0165	0.0100	-0.00800	2.19	2.33	2.16	2.10
PL11	0.0775	-0.0320	0.0080	0.0555	3.94	4.07	4.17	4.05
PL12	0.0180	-0.00600	0.0260	0.0610	2.84	2.74	2.75	2.67
PL13	0.246	0.147	0.240	0.263	2.55	2.43	2.64	2.61
PL14	0.177	0.156	0.256	0.190	3.04	3.09	2.83	3.03
PL15	0.291	0.295	0.291	0.259	2.75	2.98	2.89	2.92

Table G4b. Longitudinal PJP weld specimens: post-test measurements.

Specimen Number	E_{r1}	E_{r2}	E_{r3}	E_{r4}	γ_1	γ_2	γ_3	γ_4
	in.	in.	in.	in.	degrees	degrees	degrees	degrees
PL1	0.229	0.226	0.248	0.182	12	30	26	15
PL2	0.405	0.417	0.368	0.309				
PL3	0.402	0.438	0.385	0.376	29	16	21	16
PL4	0.463	0.511	0.404	0.384	0			0
PL5								
PL6	0.384	0.367	0.402	0.375	19	8	9	5
PL7	0.256	0.360	0.226	0.290	8	6	20	4
PL8	0.389	0.346	0.312	0.363	27	14	19	34
PL9	0.198	0.191	0.168	0.202	9	4	4	11
PL10	0.289	0.281	0.176	0.287	2	0	15	0
PL11	0.241	0.256	0.257	0.256	18	3	8	7
PL12	0.219	0.281	0.212	0.270	6	3	2	7
PL13	0.434	0.411	0.560	0.417				
PL14	0.431	0.469	0.408	0.401				
PL15	0.500	0.522	0.490	0.484				

Table G4c. Longitudinal PJP weld specimens: experimental results.

Specimen Number	P_e	P_n	P_c	f_r	P_e / P_n	P_e / P_c	f_r/σ_{uw}	Comments
	kips	kips	kips	ksi				
PL1	237	169	222	66.4	1.40	1.07	0.876	
PL2	291	199	299	51.1	1.46	0.974	0.675	Rupture in plates after Weld 3 failed
PL3	269	183	241	56.8	1.47	1.11	0.749	Welds were cut to ≈ 3.5 in. long
PL4	285	220	262	54.0	1.29	1.09	0.712	Welds cut to ≈ 3 in. long. Rupture at Welds 1 and 4 followed by rupture at middle plate. Weld 4 ruptured at the
PL5								Specimen did not fail
PL6	272	216	241	57.8	1.26	1.13	0.715	
PL7	244	181	182	71.1	1.35	1.34	0.711	Welds were cut to ≈ 3 in. long.
PL8	244	201	191	63.7	1.21	1.28	0.637	
PL9	228	193	229	75.6	1.18	0.994	0.936	
PL10	120.6	158	159	52.7	0.763	0.760	0.652	Welds were cut to ≈ 2.25 in. long
PL11	319	244	270	78.1	1.31	1.18	0.781	
PL12	213	206	222	79.2	1.03	0.957	0.792	Welds were cut to ≈ 2.75 in. long
PL13	283	161	279	60.6	1.76	1.01	0.799	Welds were cut to ≈ 3 in. long. Complete rupture at Welds 1 and 2. Large deformation (≈ 0.10 in.) and partial
PL14	331	216	330	64.6	1.53	1.00	0.799	Welds were cut to ≈ 3 in. long. No failure, but weld rupture was imminent
PL15	334	216	413	58.0	1.54	0.809	0.580	The welds were cut to approximately 3 in. long. No rupture. Large deformation (»0.08 in.) in the welds.

SKEWED PJP WELD SPECIMENS

Table G5a. Skewed PJP weld specimens: pre-test measurements.				
Specimen Number	X_T	X_B	L_T	L_B
	in.	in.	in.	in.
PS1	0.0890	0.0940	5.35	5.29
PS2	0.122	0.0760	5.40	5.31
PS3	0.0610	0.0535	5.17	5.32
PS4	0.0065	0.0650	5.35	5.31
PS5	-0.0130	0.0350	5.12	5.20
PS6	-0.0190	-0.0225	5.30	5.31

Table G5b. Skewed PJP weld specimens: post-test measurements.				
Specimen Number	E_{rT}	E_{rB}	γ_T	γ_B
	in.	in.	degrees	degrees
PS1				
PS2	0.365	0.389	46	34
PS3	0.299	0.320	4	1
PS4				
PS5	0.242	0.275	45	41
PS6	0.287	0.349	25	34

Table G5c. Skewed PJP weld specimens: experimental results.

Specimen Number	P_e kips	P_n kips	P_c kips	f_r ksi	P_e / P_n	P_e / P_c	f_r/σ_{uw}	Comments
PS1	216	112	165		1.93	1.31		Rupture only in the plate
PS2	299	169	231	72.1	1.77	1.29	0.951	
PS3	284	193	236	83.1	1.47	1.20	1.10	Test was terminated at 330 kips. Weld reinforcement was ground flush and the specimen was re-tested.
PS4	208	160	183		1.30	1.14		Rupture only in the plate
PS5	272	232	239	96.1	1.17	1.14	0.961	
PS6	320	279	265	91.4	1.15	1.21	0.914	

APPENDIX H
MATHEMATICAL MODELS

In this Appendix, three different failure theories were considered in the derivations for the strength of skewed fillet welds: von-Mises, maximum normal stress and maximum shear stress (Tresca). The suggested models were based on the following assumptions:

- Failure occurs in the weld metal and not the base metal.
- The weld fracture surface is where the maximum stresses are generated.
- The weld material is homogeneous.
- No weld penetration.
- Stresses in the fracture surface are uniform.

For each model, the surface where maximum stresses are generated was determined for both longitudinal and transverse loading. The location of maximum stress is not necessarily located in the plane of minimum throat. The following calculations show the location of maximum stresses and so the location of failure surface in the weld.

Single Fillet Welds with Transverse Loading

According to the AISC *Specification* and AWS D1.1, the fillet weld design is mainly dependent on the allowable shear stress of the weld. Nevertheless, tensile stresses can be the controlling stresses for failure and not shear. This case is present in high obtuse dihedral of fillet weld. Consequently, the analysis due to transverse loading is conducted with respect to both allowable shear stress and allowable tensile stress of the weld and then both cases were combined to generalize the design of the fillet weld in skewed T-Joints. Figure H.1 shows the connection details in the case of transverse loading.

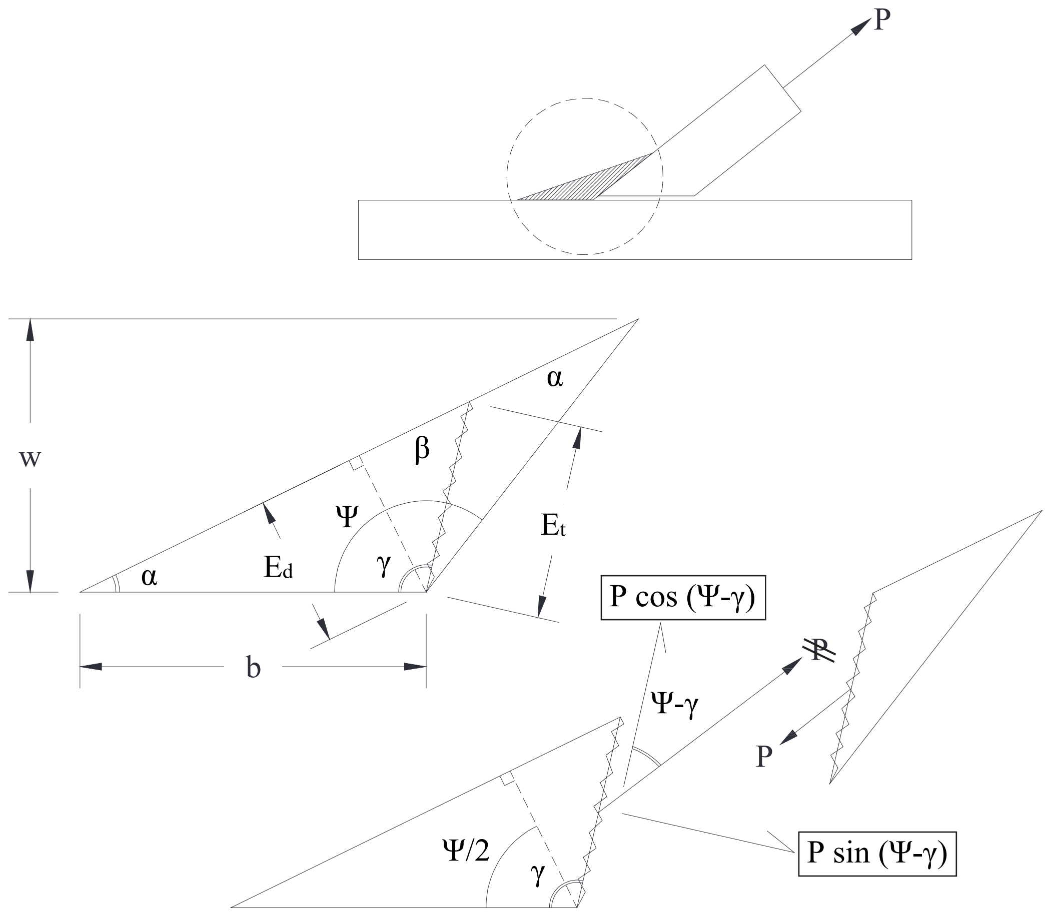

Fig. H.1. Skewed T-Joint with a single fillet weld.

$$w = b \sin \Psi$$

$$\alpha = \frac{180 - \Psi}{2} = 90 - \frac{\Psi}{2}$$

$$\beta = 180 - (\alpha + \gamma) = 180 - 90 + \frac{\Psi}{2} - \gamma = 90 - \left(\gamma - \frac{\Psi}{2}\right)$$

$$\frac{b}{\sin \beta} = \frac{E_t}{\sin \alpha}$$

$$E_t = \frac{b \ \sin \alpha}{\sin \beta} = \frac{w * \sin\left(90 - \frac{\Psi}{2}\right)}{\sin \Psi * \sin\left(90 - \left(\gamma - \frac{\Psi}{2}\right)\right)} = \frac{w * \cos\left(\frac{\Psi}{2}\right)}{2 * \sin\left(\frac{\Psi}{2}\right) * \cos\left(\frac{\Psi}{2}\right) * \cos\left(\gamma - \frac{\Psi}{2}\right)}$$

$$= \frac{w}{2 * \sin\left(\frac{\Psi}{2}\right) * \cos\left(\gamma - \frac{\Psi}{2}\right)}$$

$$E_t = \frac{E_d}{\cos\left(\gamma - \frac{\Psi}{2}\right)}$$

where,

E_d = design effective throat (shortest distance from the root to the face of the weld)
E_t = theoretical rupture plane width
P = force acting on the fillet weld
b = weld leg length
w = weld size
γ = angle of the fracture plane, measured from the horizontal surface of the base metal
Ψ = dihedral angle of the skewed joint

Maximum Shear Stress (Tresca)

The Tresca stress or maximum shear stress in the weld is expressed by τ.

$$\tau = \frac{P\cos(\Psi - \gamma)}{E_t\ .\ l}$$

where, l is the weld length. Assume the unit length for l.

$$\tau = \frac{P\cos(\Psi - \gamma)}{E_t} = \frac{P\cos(\Psi - \gamma)}{w} * 2 * \sin\left(\frac{\Psi}{2}\right) * \cos\left(\gamma - \frac{\Psi}{2}\right)$$
$$= \frac{2P}{w}\sin\left(\frac{\Psi}{2}\right) * \cos(\Psi - \gamma) * \cos\left(\gamma - \frac{\Psi}{2}\right)$$

To determine the angle of shear failure (γ), where maximum shear stress or Tresca stress is generated, the derivative of the shear stress with respect to the failure angle should be equal to zero.

$$\frac{d\tau}{d\gamma} = 0$$

$$\frac{2P}{w}\sin\left(\frac{\Psi}{2}\right) * \left[\left(\cos(\Psi - \gamma) * -\sin\left(\gamma - \frac{\Psi}{2}\right)\right) + \left(\cos\left(\gamma - \frac{\Psi}{2}\right) * \sin(\Psi - \gamma)\right)\right] = 0$$

$$\left(\cos(\Psi - \gamma) * -\sin\left(\gamma - \frac{\Psi}{2}\right)\right) + \left(\cos\left(\gamma - \frac{\Psi}{2}\right) * \sin(\Psi - \gamma)\right) = 0$$

$$\cos(\Psi - \gamma) * \sin\left(\gamma - \frac{\Psi}{2}\right) = \cos\left(\gamma - \frac{\Psi}{2}\right) * \sin(\Psi - \gamma)$$

$$\tan\left(\gamma - \frac{\Psi}{2}\right) = \tan(\Psi - \gamma)$$

$$\gamma - \frac{\Psi}{2} = \Psi - \gamma$$

$$\gamma = 0.75\Psi$$

$$\tau_{max} = \frac{2P}{w}\sin\left(\frac{\Psi}{2}\right) * \cos(\Psi - 0.75\Psi) * \cos\left(0.75\Psi - \frac{\Psi}{2}\right) = \frac{2P}{w}\sin\left(\frac{\Psi}{2}\right) * \cos\left(\frac{\Psi}{4}\right) * \cos\left(\frac{\Psi}{4}\right)$$
$$= \frac{2P}{w} * \sin\left(\frac{\Psi}{2}\right) * \cos^2\left(\frac{\Psi}{4}\right)$$

The allowable transverse joint load for the weld, P, can be calculated accordingly by substituting τ_{max} with the ultimate shear stress of the fillet weld material, τ_u (Miazga and Kennedy, 1989) even though the Tresca theory includes comparing the maximum shear stress with the tensile yield stress divided by 2 (Boresi, Schmidt, and Sidebottom, 1993).

$$P_{UT-S} = \frac{\tau_u . w}{2\sin\left(\frac{\Psi}{2}\right) * \cos^2\left(\frac{\Psi}{4}\right)}$$

P_{UT-S} is the ultimate transverse load that can be curried by the weld based on the predicted failure plane and not the weld throat based on the maximum shear stress (Tresca) criterion. The ultimate shear strength of fillet weld is equal to $1/\sqrt{3}$ of the ultimate tensile strength of the weld (Naka and Kato, 1966).

$$\tau_u = \frac{F_{EXX}}{\sqrt{3}} \approx 0.6F_{EXX}$$

$$P_{UT-S} = \frac{F_{EXX} . w}{2\sqrt{3}\sin\left(\frac{\Psi}{2}\right) * \cos^2\left(\frac{\Psi}{4}\right)}$$

If we assumed that the shear failure happens where minimum throat is ($\gamma = 0.5\Psi$), which is inaccurate, the nominal ultimate transverse joint load would be less conservative (higher) than the actual case ($\gamma = 0.75\Psi$).

$$\gamma = \frac{\Psi}{2} \quad and \quad E_d = E_t = \frac{w}{2 * \sin\left(\frac{\Psi}{2}\right)}$$

$$\tau = \frac{2P}{w}\sin\left(\frac{\Psi}{2}\right) * \cos(\Psi - \gamma) * \cos\left(\gamma - \frac{\Psi}{2}\right) = \frac{2P}{w}\sin\left(\frac{\Psi}{2}\right) * \cos\left(\frac{\Psi}{2}\right) = \frac{P}{w}\sin\Psi$$

$$P_{UTH-S} = \frac{\tau_u . w}{\sin\Psi}$$

P_{UTH-S} is the hypothetical ultimate transverse load carried by the weld based on the maximum shear stress (Tresca) criterion, assuming that the failure plane is at the throat section.

$$\frac{P_{UT-S}}{P_{UTH-S}} = \frac{\sin\Psi}{2\sin\left(\frac{\Psi}{2}\right) * \cos^2\left(\frac{\Psi}{4}\right)} = \frac{\cos\left(\frac{\Psi}{2}\right)}{\cos^2\left(\frac{\Psi}{4}\right)} = \frac{\cos^2\left(\frac{\Psi}{4}\right) - \sin^2\left(\frac{\Psi}{4}\right)}{\cos^2\left(\frac{\Psi}{4}\right)}$$
$$= 1 - \tan^2\left(\frac{\Psi}{4}\right) \quad \dots\dots\dots \ \mathit{Always\ less\ than}\ 1$$

Maximum Normal Stress

Depending on the skewness of the T-Joint the generated stresses in the fillet weld varies. For instance, the main generated stresses in the fillet weld of an acute angle is shear, while it is tension for the obtuse angle. In this section, the capacity of the fillet weld is determined based on comparing the maximum principal stress in the weld with the ultimate tensile strength of the weld material.

$$\sigma = \frac{P\sin(\Psi - \gamma)}{E_t\ .\ l}$$

where, l is the weld length. Assume the unit length for l.

$$\sigma = \frac{P\sin(\Psi - \gamma)}{E_t} = \frac{P\sin(\Psi - \gamma)}{w} * 2 * \sin\left(\frac{\Psi}{2}\right) * \cos\left(\gamma - \frac{\Psi}{2}\right)$$
$$= \frac{2P}{w}\sin\left(\frac{\Psi}{2}\right) * \sin(\Psi - \gamma) * \cos\left(\gamma - \frac{\Psi}{2}\right)$$

To determine the angle of tensile failure (γ), where maximum tensile stress is generated, the derivative of the tensile stress with respect to the failure angle should be equal to zero.

$$\frac{d\sigma}{d\gamma} = 0$$

$$\frac{2P}{w}\sin\left(\frac{\Psi}{2}\right) * \left[\left(-\sin(\Psi - \gamma) * \sin\left(\gamma - \frac{\Psi}{2}\right)\right) + \left(-\cos\left(\gamma - \frac{\Psi}{2}\right) * \cos(\Psi - \gamma)\right)\right] = 0$$

$$\left(\sin(\Psi - \gamma) * \sin\left(\gamma - \frac{\Psi}{2}\right)\right) + \left(\cos\left(\gamma - \frac{\Psi}{2}\right) * \cos(\Psi - \gamma)\right) = 0$$

$$\cos\left(\Psi - \gamma - \gamma + \frac{\Psi}{2}\right) = 0$$

$$1.5\Psi - 2\gamma = 90$$

$$\gamma = 0.75\Psi - 45$$

The above angle of failure (γ) equation is mathematically correct for dihedral angles, Ψ, ranging from 60º to 180º. Nevertheless, this should not be a problem and we should not be concerned about the applicability of maximum principal stress criterion to the case of dihedral angles less than 60º. As shown in the next section, for acute dihedral angles, shear forces in the weld were the ones controlling its failure.

$$\begin{aligned}
\sigma_{max} = \frac{2P}{w}\sin\left(\frac{\Psi}{2}\right) * \sin(\Psi - 0.75\Psi + 45) * \cos\left(0.75\Psi - 45 - \frac{\Psi}{2}\right) \\
= \frac{2P}{w}\sin\left(\frac{\Psi}{2}\right) * \sin\left(\frac{\Psi}{4} + 45\right) * \cos\left(\frac{\Psi}{4} - 45\right) \\
= \frac{2P}{w}\sin\left(\frac{\Psi}{2}\right) * \left(0.707\sin\left(\frac{\Psi}{4}\right) + 0.707\cos\left(\frac{\Psi}{4}\right)\right) \\
* \left(0.707\cos\left(\frac{\Psi}{4}\right) + 0.707\sin\left(\frac{\Psi}{4}\right)\right) \\
= \frac{P}{w}\sin\left(\frac{\Psi}{2}\right) * \left(\sin^2\left(\frac{\Psi}{4}\right) + \cos^2\left(\frac{\Psi}{4}\right) + 2\sin\left(\frac{\Psi}{4}\right)\cos\left(\frac{\Psi}{4}\right)\right) \\
= \frac{P}{w}\sin\left(\frac{\Psi}{2}\right) * \left(1 + \sin\left(\frac{\Psi}{2}\right)\right) = \frac{P}{w}\left(\sin\left(\frac{\Psi}{2}\right) + \sin^2\left(\frac{\Psi}{2}\right)\right)
\end{aligned}$$

The allowable transverse joint load for the weld, P, can be calculated accordingly by substituting σ_{max} with the ultimate tensile strength of the fillet weld, F_{EXX}.

$$P_{UT-P} = \frac{F_{EXX}.w}{\sin\left(\frac{\Psi}{2}\right) + \sin^2\left(\frac{\Psi}{2}\right)}$$

P_{UT-P} is the ultimate transverse load carried by the weld that is calculated based on the maximum principal stress criterion and the predicted failure plane. If we assumed that the tensile failure happens where minimum throat is ($\gamma = 0.5\Psi$), which is wrong, the allowable transverse joint load would be less conservative (higher) than the actual case ($\gamma = 0.75\Psi - 45$).

$$\gamma = \frac{\Psi}{2} \quad and \quad E_d = E_t = \frac{w}{2 * \sin\left(\frac{\Psi}{2}\right)}$$

$$\begin{aligned}
\sigma = \frac{2P}{w}\sin\left(\frac{\Psi}{2}\right) * \sin(\Psi - \gamma) * \cos\left(\gamma - \frac{\Psi}{2}\right) = \frac{2P}{w}\sin\left(\frac{\Psi}{2}\right) * \sin\left(\Psi - \frac{\Psi}{2}\right) * \cos\left(\frac{\Psi}{2} - \frac{\Psi}{2}\right) \\
= \frac{2P}{w}\sin^2\left(\frac{\Psi}{2}\right)
\end{aligned}$$

$$P_{UTH-P} = \frac{F_{EXX}.w}{2\sin^2\left(\frac{\Psi}{2}\right)}$$

P_{UTH-P} is the hypothetical ultimate transverse load carried by the weld and is calculated based on the maximum principal stress criterion assuming the failure plane is located at the throat section.

$$\frac{P_{UTH-P}}{P_{UT-P}} = \frac{\sin\left(\frac{\Psi}{2}\right) + \sin^2\left(\frac{\Psi}{2}\right)}{2\sin^2\left(\frac{\Psi}{2}\right)} = 0.5 + \frac{1}{2\sin\left(\frac{\Psi}{2}\right)}$$

For all values of Ψ between 0 and 180º, the above ratio will always be higher than 1.

Maximum Shear and Maximum Normal Stresses in Design

The allowable transverse load so that the maximum shear stress (Tresca) in the fillet weld will not exceed the ultimate shear strength of the weld material is:

$$P_{UT-S} = \frac{\tau_u . w}{2\sin\left(\frac{\Psi}{2}\right) * \cos^2\left(\frac{\Psi}{4}\right)}$$

The allowable transverse load so that the maximum principal stress in the fillet weld will not exceed the ultimate tensile strength of the weld is:

$$P_{UT-P} = \frac{F_{EXX} . w}{\sin\left(\frac{\Psi}{2}\right) + \sin^2\left(\frac{\Psi}{2}\right)}$$

$$\tau_u = \frac{F_{EXX}}{\sqrt{3}} \approx 0.6F_{EXX}$$

$$\frac{P_{UT-P}}{P_{UT-S}} = \frac{\dfrac{F_{EXX} . w}{\sin\left(\frac{\Psi}{2}\right) + \sin^2\left(\frac{\Psi}{2}\right)}}{\dfrac{\tau_u . w}{2\sin\left(\frac{\Psi}{2}\right) * \cos^2\left(\frac{\Psi}{4}\right)}} = \sqrt{3} * \frac{2\sin\left(\frac{\Psi}{2}\right) * \cos^2\left(\frac{\Psi}{4}\right)}{\sin\left(\frac{\Psi}{2}\right) + \sin^2\left(\frac{\Psi}{2}\right)} = \frac{2\sqrt{3}\sin\left(\frac{\Psi}{2}\right) * \cos^2\left(\frac{\Psi}{4}\right)}{\sin\left(\frac{\Psi}{2}\right) + \sin^2\left(\frac{\Psi}{2}\right)}$$

For design purposes, the less allowable transverse load from maximum principal stress criterion and Tresca criterion is the one controlling the weld design. Figure H.2 shows the ratio between both while varying the dihedral angle.

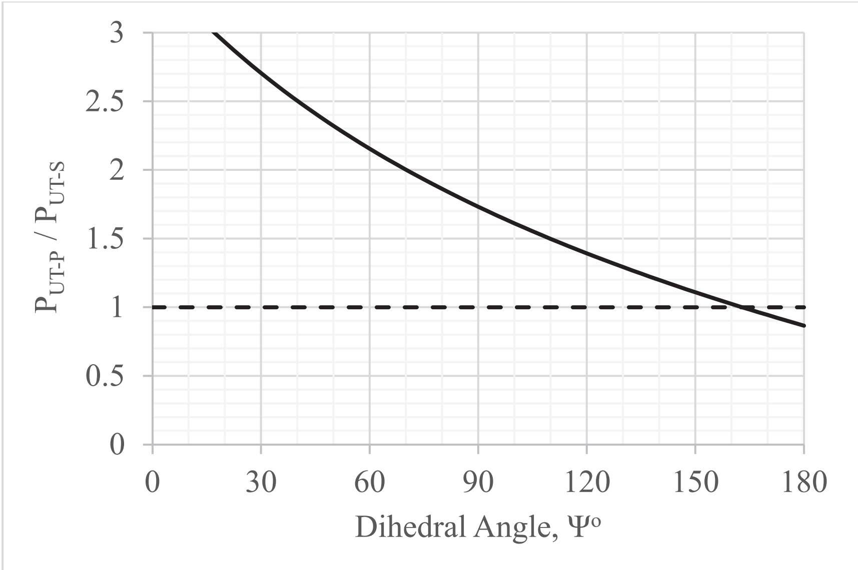

Fig. H.2. Fillet weld design criteria (tension or shear).

Assuming that the ultimate tensile to shear stress ratio is $\sqrt{3}$ and from Figure H.2, we can conclude that if the dihedral angle of the fillet weld is more than or equal to 162º, the fillet weld should be designed based on the maximum principal stress criterion. The surface of maximum principal stress (surface of failure) is 0.25 of the dihedral angle + 45º measured from the transverse force direction ($\gamma = 0.75\Psi - 45^o$). On the other hand, if the dihedral angle is less than 162º, the fillet weld should be designed based on the Tresca criterion. The surface of maximum shear stress (surface of failure) is 0.25 of the dihedral angle measured from the transverse force direction ($\gamma = 0.75\Psi$).

Maximum von-Mises Stress

In this case, the fracture surface is assumed to be generated in the fillet weld, where the maximum von-Mises effective stress, σ_e, is generated.

$$\sigma = \sigma_{xx} = \frac{2P}{w}\sin\left(\frac{\Psi}{2}\right) * \sin(\Psi - \gamma) * \cos\left(\gamma - \frac{\Psi}{2}\right)$$

$$\tau = \tau_{xy} = \frac{2P}{w}\sin\left(\frac{\Psi}{2}\right) * \cos(\Psi - \gamma) * \cos\left(\gamma - \frac{\Psi}{2}\right)$$

$$\sigma_e = \sqrt{\frac{1}{2}\left[\left(\sigma_{xx}-\sigma_{yy}\right)^2 + \left(\sigma_{yy}-\sigma_{zz}\right)^2 + \left(\sigma_{zz}-\sigma_{xx}\right)^2\right] + 3\left(\tau_{xy}^2+\tau_{yz}^2+\tau_{zx}^2\right)} = \sqrt{\sigma_{xx}^2 + 3\tau_{xy}^2}$$

$$= \sqrt{\frac{4P^2}{w^2}\sin^2\left(\frac{\Psi}{2}\right) * \sin^2(\Psi-\gamma) * \cos^2\left(\gamma-\frac{\Psi}{2}\right) + \frac{12P^2}{w^2}\sin^2\left(\frac{\Psi}{2}\right) * \cos^2(\Psi-\gamma) * \cos^2\left(\gamma-\frac{\Psi}{2}\right)}$$

$$= \sqrt{\frac{4P^2}{w^2}\sin^2\left(\frac{\Psi}{2}\right) * \cos^2\left(\gamma-\frac{\Psi}{2}\right)\left[\sin^2(\Psi-\gamma) + 3\cos^2(\Psi-\gamma)\right]}$$

$$= \frac{2P}{w}\sin\left(\frac{\Psi}{2}\right) * \cos\left(\gamma-\frac{\Psi}{2}\right)\sqrt{\left[1+2\cos^2(\Psi-\gamma)\right]}$$

$$= \frac{P}{w}\left[\sin\gamma + \sin(\Psi-\gamma)\right]\sqrt{\left[1+2\cos^2(\Psi-\gamma)\right]}$$

To determine the angle of fracture surface (γ), where maximum von-Mises stress is generated, the derivative of the von-Mises stress with respect to the failure angle should be equal to zero.

$$\frac{d\sigma_e}{d\gamma} = 0$$

$$\frac{d\sigma_e}{d\gamma} = \frac{P}{w}\left[\left(\frac{(\sin\gamma + \sin(\Psi-\gamma)) * 0.5}{\sqrt{\left[1+2\cos^2(\Psi-\gamma)\right]}} * 4 * \cos(\Psi-\gamma) * (-\sin(\Psi-\gamma)) * (-1)\right) + \left(\sqrt{\left[1+2\cos^2(\Psi-\gamma)\right]} * (\cos\gamma - \cos(\Psi-\gamma))\right)\right]$$

$$\frac{P}{w}\left[\left(\frac{2(\sin\gamma + \sin(\Psi-\gamma))}{\sqrt{\left[1+2\cos^2(\Psi-\gamma)\right]}} * \cos(\Psi-\gamma) * \sin(\Psi-\gamma)\right) + \left(\sqrt{\left[1+2\cos^2(\Psi-\gamma)\right]} * (\cos\gamma - \cos(\Psi-\gamma))\right)\right] = 0$$

$$\left(\frac{2(\sin\gamma + \sin(\Psi-\gamma))}{\sqrt{\left[1+2\cos^2(\Psi-\gamma)\right]}} * \cos(\Psi-\gamma) * \sin(\Psi-\gamma)\right) + \left(\sqrt{\left[1+2\cos^2(\Psi-\gamma)\right]} * (\cos\gamma - \cos(\Psi-\gamma))\right) = 0$$

The relation between γ and Ψ was drawn based on the above equation as shown in Figure H.3. A fitted line was drawn to reflect the mathematical relation between them.

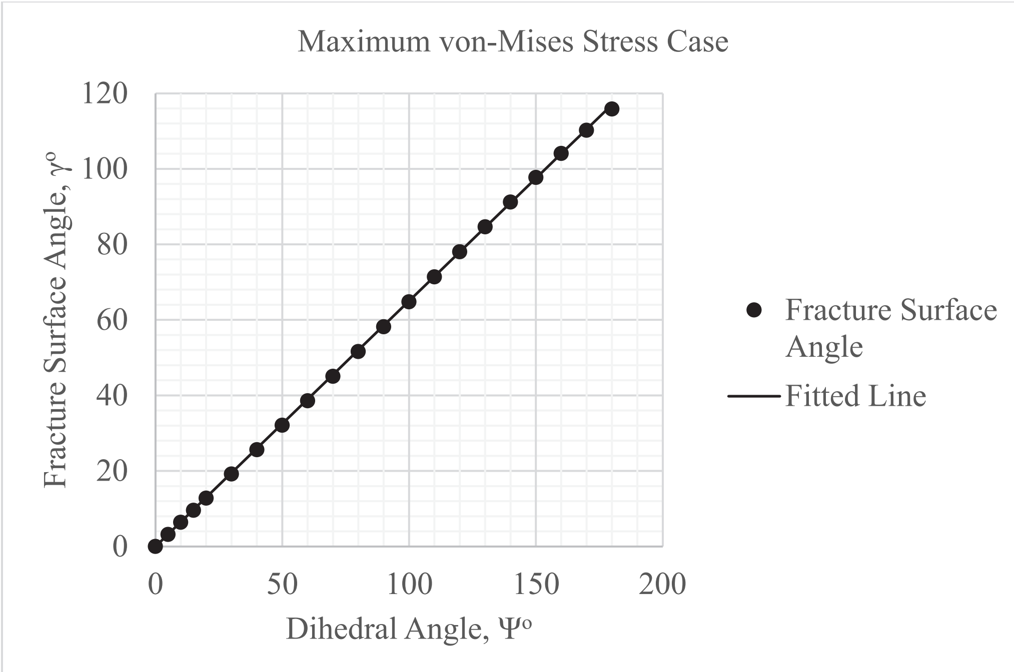

Fig. H.3. Fracture surface angle using von-Mises approach.

$\gamma \approx 0.68\Psi$

$$
\begin{aligned}
\sigma_{e-max} &= \frac{P}{w}[\sin\gamma + \sin(\Psi - \gamma)]\sqrt{[1 + 2\cos^2(\Psi - \gamma)]} \\
&= \frac{P}{w}[\sin(0.68\Psi) + \sin(\Psi - 0.68\Psi)]\sqrt{[1 + 2\cos^2(\Psi - 0.68\Psi)]} \\
&= \frac{P}{w}[\sin(0.68\Psi) + \sin(0.32\Psi)]\sqrt{[1 + 2\cos^2(0.32\Psi)]} \\
&= \frac{P}{w}[\sin(0.68\Psi) + \sin(0.32\Psi)]\sqrt{2 + \cos(0.64\Psi)}
\end{aligned}
$$

According to IIW (1976) and CEN (2005), the maximum calculated stresses based on von-Mises were compared to the ultimate tensile strength. Thus, to find the design load for the joint, P_{UT-V}, the maximum von-Mises stress is set equal to the nominal tensile strength of the weld metal, F_{EXX}.

$$\sigma_{e-max} = F_{EXX}$$

$$F_{EXX} = \frac{P_{UT-V}}{w}[\sin(0.68\Psi) + \sin(0.32\Psi)]\sqrt{2 + \cos(0.64\Psi)}$$

$$P_{UT-V} = \frac{w.F_{EXX}}{[\sin(0.68\Psi) + \sin(0.32\Psi)]\sqrt{2 + \cos(0.64\Psi)}}$$

P_{UT-V} is the ultimate transverse load carried by the weld based on the maximum von-Mises stress criterion at the predicted failure plane. If we assumed that the fracture happens where minimum throat is ($\gamma = 0.5\Psi$), which is wrong, the allowable transverse joint load, using von-Mises approach, would be less conservative (higher) than the actual case, where $\gamma = 0.68\Psi$.

$$\gamma = \frac{\Psi}{2} \quad and \quad E_d = E_t = \frac{w}{2 * \sin\left(\frac{\Psi}{2}\right)}$$

$$\sigma_{e-at\ throat} = \frac{P}{w}\left[\sin\frac{\Psi}{2} + \sin\left(\Psi - \frac{\Psi}{2}\right)\right]\sqrt{\left[1 + 2\cos^2\left(\Psi - \frac{\Psi}{2}\right)\right]} = \frac{2P}{w}\sin\frac{\Psi}{2}\sqrt{[2 + \cos\Psi]}$$

$$P_{UTH-V} = \frac{w.F_{EXX}}{2\sin\frac{\Psi}{2}\sqrt{[2 + \cos\Psi]}}$$

P_{UTH-V} is the hypothetical ultimate transverse carried by the weld using the von-Mises stress criterion and assuming the failure plane is at the throat section.

$$\frac{P_{UTH-V}}{P_{UT-V}} = \frac{[\sin(0.68\Psi) + \sin(0.32\Psi)]\sqrt{2 + \cos(0.64\Psi)}}{2\sin\frac{\Psi}{2}\sqrt{[2 + \cos\Psi]}} = \text{Range of } 1 - 1.15$$

Longitudinal Loading

The load is acting in the direction parallel to the axis of the fillet weld. The internal forces in the weld due to longitudinal loading are mainly shear forces. The maximum shear stresses are located in the weld plane where the weld throat is minimum and this is where the failure plane in the weld is located.

$$\gamma = \frac{\Psi}{2} \quad and \quad E_d = E_t$$

$$\tau_{max} = \frac{P}{E_d.l}$$

where, E_d is the minimum weld throat and l is the weld length. Assume the unit length for l.

$$\tau_{max} = \frac{P}{E_d.l} = \frac{2P * \sin\left(\frac{\Psi}{2}\right)}{w}$$

$$P_{UL} = \frac{\tau_u.w}{2\sin\left(\frac{\Psi}{2}\right)}$$

P_{UL} is the ultimate longitudinal load carried by the weld.

$$\tau_u = \frac{F_{EXX}}{\sqrt{3}} \approx 0.6F_{EXX}$$

$$P_{UL} = \frac{F_{EXX}.w}{2\sqrt{3}\sin\left(\frac{\Psi}{2}\right)}$$

Transverse versus Longitudinal Loading

Based on the above calculations, for the same nominal tensile strength of the fillet weld (F_{EXX}) and the same size (*w*), the load capacity of fillet weld is dependent on the skewness of the base plates (dihedral angle). Figure H.4 shows a comparison between the weld capacity in case of longitudinal and transverse loading for the same weld size depending on dihedral angle (Ψ).

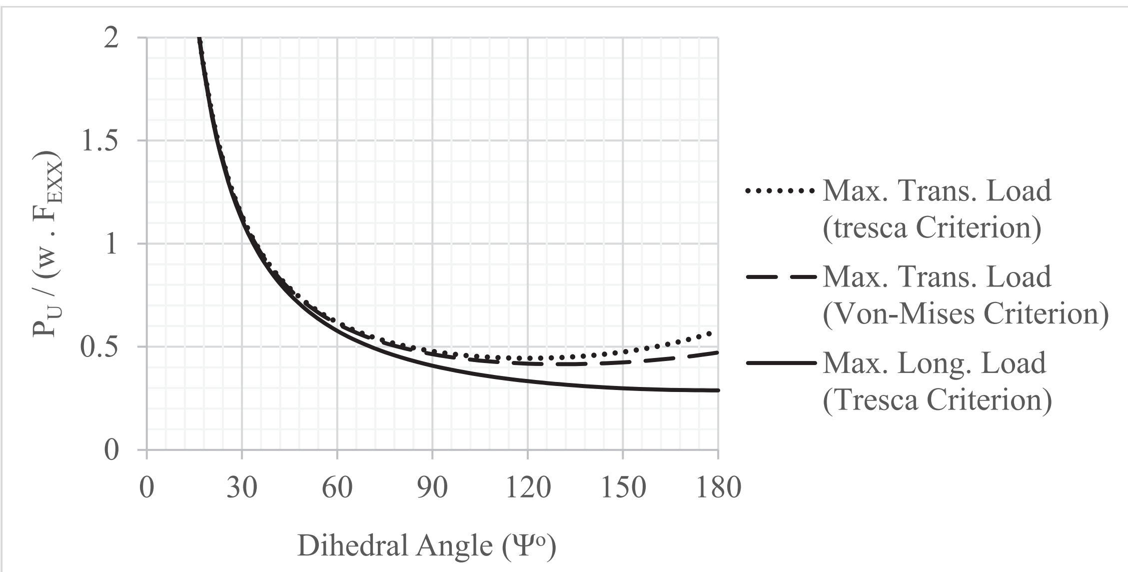

Fig. H.4. Capacity of fillet weld (same size).

The maximum normal stress approach was not presented in Figure H.4 because it was found that the maximum shear stress (Tresca) approach was more dominant in controlling the ultimate load, when the dihedral angle is less than 162°. If we considered the same minimum weld throat (E_d), the weld capacity equations will change as follows:

$$E_d = \frac{w}{2\sin\left(\frac{\Psi}{2}\right)}$$

$$P_{UT-S} = \frac{F_{EXX}.w}{2\sqrt{3}\sin\left(\frac{\Psi}{2}\right) * \cos^2\left(\frac{\Psi}{4}\right)} = \frac{F_{EXX}.E_d}{\sqrt{3} * \cos^2\left(\frac{\Psi}{4}\right)}$$

$$P_{UT-V} = \frac{F_{EXX}.w}{[\sin(0.68\Psi) + \sin(0.32\Psi)]\sqrt{2 + \cos(0.64\Psi)}} = \frac{F_{EXX}.E_d * 2\sin\left(\frac{\Psi}{2}\right)}{[\sin(0.68\Psi) + \sin(0.32\Psi)]\sqrt{2 + \cos(0.64\Psi)}}$$

$$P_{UL} = \frac{F_{EXX}.w}{2\sqrt{3}\sin\left(\frac{\Psi}{2}\right)} = \frac{F_{EXX}.E_d}{\sqrt{3}}$$

Accordingly, Figure H.4 can be represented as shown in Figure H.5, which shows a comparison between the weld capacity load in case of longitudinal and transverse loading for the same weld throat (E_d). The transverse loading curve in the same figure also represents the ratio between the fillet weld capacity in case of transverse loading and in case of longitudinal loading based on both Tresca stress criterion and maximum von-Mises stress criterion.

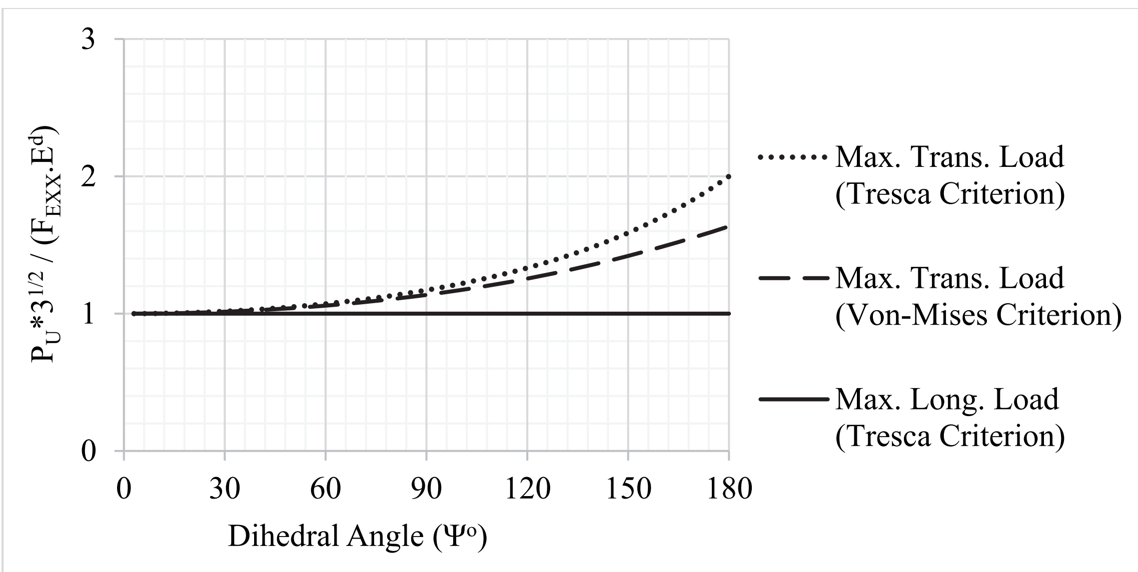

Fig. H.5. Capacity of fillet weld (same throat).

All the above calculations are for beveled plates where there is no gap between the plates. If the skewed plate in the skewed T-joint was square cut, a gap, R_n^*, will be created between this plate and the main plate. Similar steps as before should apply except that the gap should be subtracted from the weld size on the obtuse side. The weld throat, E_d, should be modified as shown.

$$w_{new} = w - R_n^*$$

$$R_n^* = t^{"}\sin(\Psi - 90)$$

$$E_d = \frac{w_{new}}{2\sin\left(\frac{\Psi}{2}\right)} = \frac{w - t^{"}\sin(\Psi - 90)}{2\sin\left(\frac{\Psi}{2}\right)}$$

where, $t^{"}$ is the thickness of the skewed plate. Figure H.5 is applicable to the square cut plate condition, if the weld throat, E_d, in the ordinate was modified to exclude the gap generated from dihedral angles above 90°. Similarly, Figure H.4 is applicable to the square cut plate condition, if the weld leg size, w, in the ordinate was replaced with the effective weld size, w_{new}, for dihedral angles above 90°.

Skewed Welds in Lap-Joints

Even though the restraining is different, the same mathematical derivations made for the skewed T-Joint are applicable to the fillet weld in double-lap spliced joints with skewed angles except for minor differences. The angles in the skewed T-Joints were measured from the based plate surface. The equations would have been exactly the same in the lap-splice joint as in the skewed T-joint if the angles were measured from the beveled surface in the lap-splice joints as shown in Figure H.6.

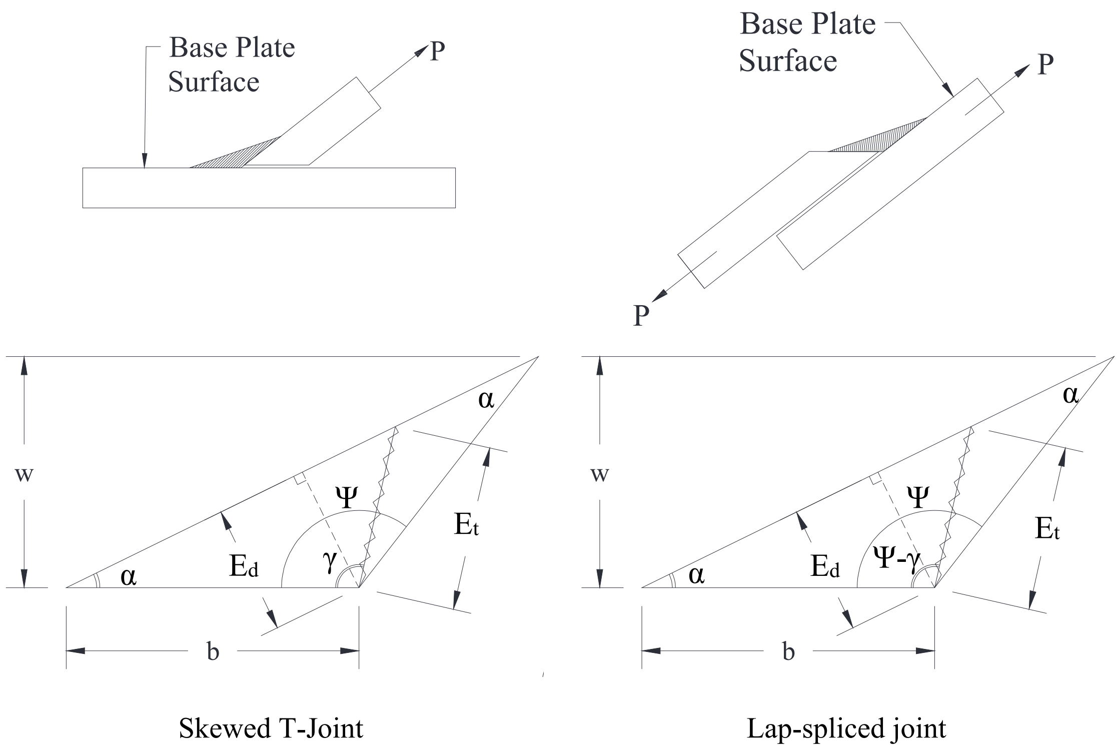

Fig. H. Fillet weld analysis for Skewed T-Joint versus beveled lap-splice joint.

Consequently, the same equation derived above shall apply, when the angle γ is replaced with $\Psi - \gamma$, where γ is the fracture angle of fillet weld measured from the base plate surface in the lap-splice joint.

Summary for Single Fillet Welds

Transverse Loading

- Tresca Stress

$$\tau = \frac{2P}{w}\sin\left(\frac{\Psi}{2}\right) * \cos(\gamma) * \cos\left(\frac{\Psi}{2} - \gamma\right)$$

$$\gamma = 0.25\Psi$$

$$\tau_{max} = \frac{2P}{w} * \sin\left(\frac{\Psi}{2}\right) * \cos^2\left(\frac{\Psi}{4}\right)$$

$$P_{UT-S} = \frac{F_{EXX}.w}{2\sqrt{3}\sin\left(\frac{\Psi}{2}\right) * \cos^2\left(\frac{\Psi}{4}\right)}$$

- Maximum Normal Stress

$$\sigma = \frac{2P}{w}\sin\left(\frac{\Psi}{2}\right) * \sin(\gamma) * \cos\left(\frac{\Psi}{2} - \gamma\right)$$

$$\gamma = 0.25\Psi + 45$$

$$\sigma_{max} = \frac{P}{w}\left(\sin\left(\frac{\Psi}{2}\right) + \sin^2\left(\frac{\Psi}{2}\right)\right)$$

$$P_{UT-P} = \frac{F_{EXX}.w}{\sin\left(\frac{\Psi}{2}\right) + \sin^2\left(\frac{\Psi}{2}\right)}$$

- Maximum von-Mises Stress

$$\sigma_e = \frac{P}{w}[\sin\gamma + \sin(\Psi - \gamma)]\sqrt{[1 + 2\cos^2(\gamma)]}$$

$$\gamma = 0.32\Psi$$

$$\sigma_{e-max} = \frac{P}{w}[\sin(0.32\Psi) + \sin(0.68\Psi)]\sqrt{2 + \cos(0.64\Psi)}$$

$$P_{UT-V} = \frac{w.F_{EXX}}{[\sin(0.68\Psi) + \sin(0.32\Psi)]\sqrt{2 + \cos(0.64\Psi)}}$$

Longitudinal Loading

$$\gamma = \frac{\Psi}{2}$$

$$\tau_{max} = \frac{2P * \sin\left(\frac{\Psi}{2}\right)}{w}$$

$$P_{UL} = \frac{F_{EXX}.w}{2\sqrt{3}\sin\left(\frac{\Psi}{2}\right)}$$

Double Fillet Welds with Transverse Loading

For this model an additional force was considered in the analysis. When a tensile load is applied to the plate, the plate tries to deform in the perpendicular direction. Because the weld restrains the plate, transverse internal forces are generated within the plate thickness, which provide an additional tensile load, *F*, on the weld as shown in Figure H.7. The resulting force, *F*, is a ratio, a, of the main load, *P*.

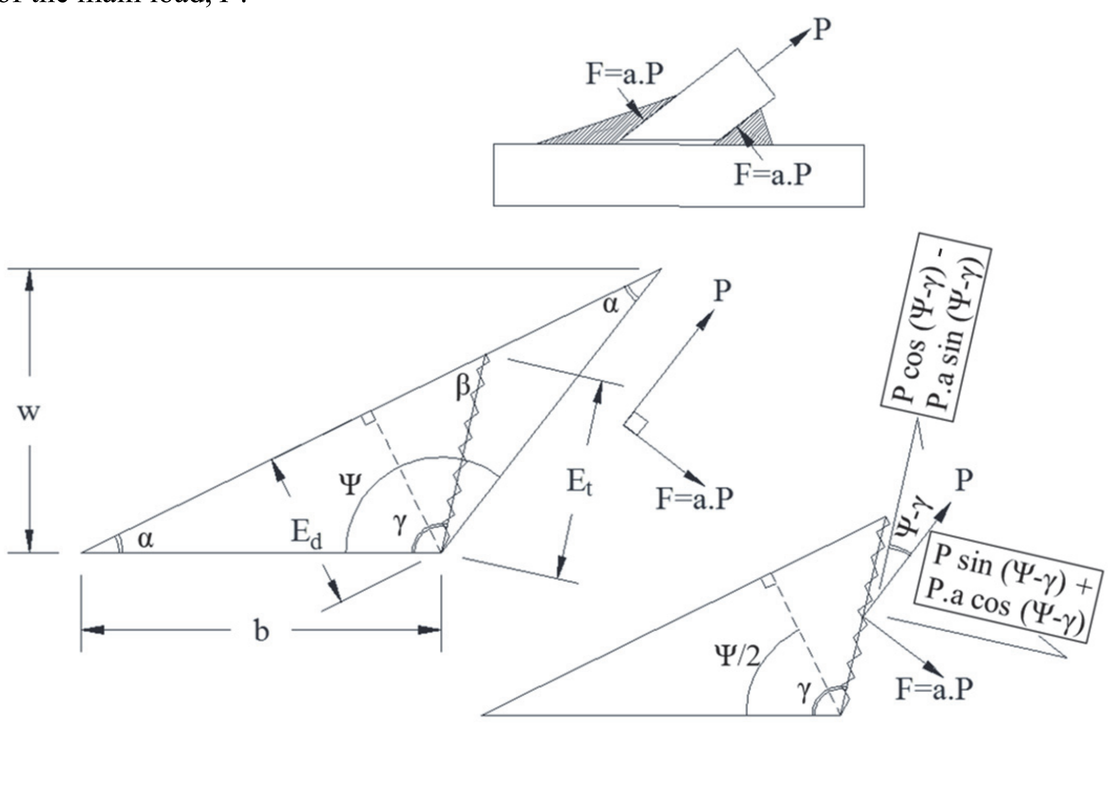

Fig. H.7. Skewed T-Joint with double fillet welds.

Maximum Shear Stress (Tresca) Criterion

$$\tau = \frac{P\cos(\Psi - \gamma) - P.a\sin(\Psi - \gamma)}{E_t\ .\ l}$$

where, l is the weld length. Assume the unit length for l.

$$\tau = \frac{P[\cos(\Psi - \gamma) - a\sin(\Psi - \gamma)]}{E_t}$$
$$= \frac{2P}{w} * [\cos(\Psi - \gamma) - a\sin(\Psi - \gamma)] * \sin\left(\frac{\Psi}{2}\right) * \cos\left(\gamma - \frac{\Psi}{2}\right)$$

To determine the angle of shear failure (γ), where maximum shear stress or Tresca stress is generated, the derivative of the shear stress with respect to the failure angle should be equal to zero.

$$\frac{d\tau}{d\gamma} = 0$$

$$\frac{-2P}{w}[\cos(\Psi - \gamma) - a\sin(\Psi - \gamma)] * \sin\left(\frac{\Psi}{2}\right) * \sin\left(\gamma - \frac{\Psi}{2}\right) + \frac{2P}{w}[\sin(\Psi - \gamma) + a\cos(\Psi - \gamma)] * \sin\left(\frac{\Psi}{2}\right) * \cos\left(\gamma - \frac{\Psi}{2}\right) = 0$$

$$-\cos(\Psi - \gamma)\sin\left(\gamma - \frac{\Psi}{2}\right) + a\sin(\Psi - \gamma)\sin\left(\gamma - \frac{\Psi}{2}\right) + \sin(\Psi - \gamma)\cos\left(\gamma - \frac{\Psi}{2}\right) + a\cos(\Psi - \gamma)\cos\left(\gamma - \frac{\Psi}{2}\right) = 0$$

$$\left[\sin(\Psi - \gamma)\cos\left(\gamma - \frac{\Psi}{2}\right) - \cos(\Psi - \gamma)\sin\left(\gamma - \frac{\Psi}{2}\right)\right] + a\left[\cos(\Psi - \gamma)\cos\left(\gamma - \frac{\Psi}{2}\right) + \sin(\Psi - \gamma)\sin\left(\gamma - \frac{\Psi}{2}\right)\right] = 0$$

$$\sin\left(\Psi - \gamma - \gamma + \frac{\Psi}{2}\right) + a.\cos\left(\Psi - \gamma - \gamma + \frac{\Psi}{2}\right) = 0$$

$$a = -\tan(1.5\Psi - 2\gamma)$$

$$1.5\Psi - 2\gamma = \tan^{-1}(-a)$$

$$\gamma = 0.75\Psi - 0.5\tan^{-1}(-a)$$

$$\gamma = 0.75\Psi + 0.5\tan^{-1}(a)$$

$$E_d = \frac{w}{2 * \sin\left(\frac{\Psi}{2}\right)}$$

$$\tau_{max} = \frac{2P[\cos(\Psi - 0.75\Psi - 0.5\tan^{-1}(a)) - a\sin(\Psi - 0.75\Psi - 0.5\tan^{-1}(a))]}{w} * \sin\left(\frac{\Psi}{2}\right) * \cos\left(0.75\Psi + 0.5\tan^{-1}(a) - \frac{\Psi}{2}\right)$$

$$= \frac{2P[\cos(0.25\Psi - 0.5\tan^{-1}(a)) - a\sin(0.25\Psi - 0.5\tan^{-1}(a))]}{w} * \sin\left(\frac{\Psi}{2}\right) * \cos(0.25\Psi + 0.5\tan^{-1}(a))$$

$$= \frac{2P[\cos(0.25\Psi - 0.5\tan^{-1}(a)) - a\sin(0.25\Psi - 0.5\tan^{-1}(a))]}{2E_d * \sin\left(\frac{\Psi}{2}\right)} * \sin\left(\frac{\Psi}{2}\right) * \cos(0.25\Psi + 0.5\tan^{-1}(a))$$

$$\tau_{max}(\text{transverse}) = \frac{P}{E_d} * [\cos(0.25\Psi - 0.5\tan^{-1}(a)) - a\sin(0.25\Psi - 0.5\tan^{-1}(a))] * \cos(0.25\Psi + 0.5\tan^{-1}(a))$$

For longitudinal loading, the failure angle will be in the center of the dihedral angle and the maximum shear stress is:

$$\tau_{max}(\text{longitudinal}) = \frac{2\mathrm{P}}{\mathrm{w}}\sin\left(\frac{\Psi}{2}\right) = \frac{P}{E_d}$$

$$\frac{P_{UT-S}}{P_{UL}} = \frac{1}{[\cos(0.25\Psi - 0.5\tan^{-1}(a)) - a\sin(0.25\Psi - 0.5\tan^{-1}(a))] * \cos(0.25\Psi + 0.5\tan^{-1}(a))}$$

For normal fillet weld, where Ψ is 90°,

$$\frac{P_{UT-S}}{P_{UL}} = \frac{1}{[\cos(22.5 - 0.5\tan^{-1}(a)) - a\sin(22.5 - 0.5\tan^{-1}(a))] * \cos(22.5 + 0.5\tan^{-1}(a))}$$

This relation can be drawn as shown in Figure H.8 and so it can be rewritten as:

$$\frac{P_{UT-S}}{P_{UL}} \approx -0.266\, a^2 + 0.508\, a + 1.171$$

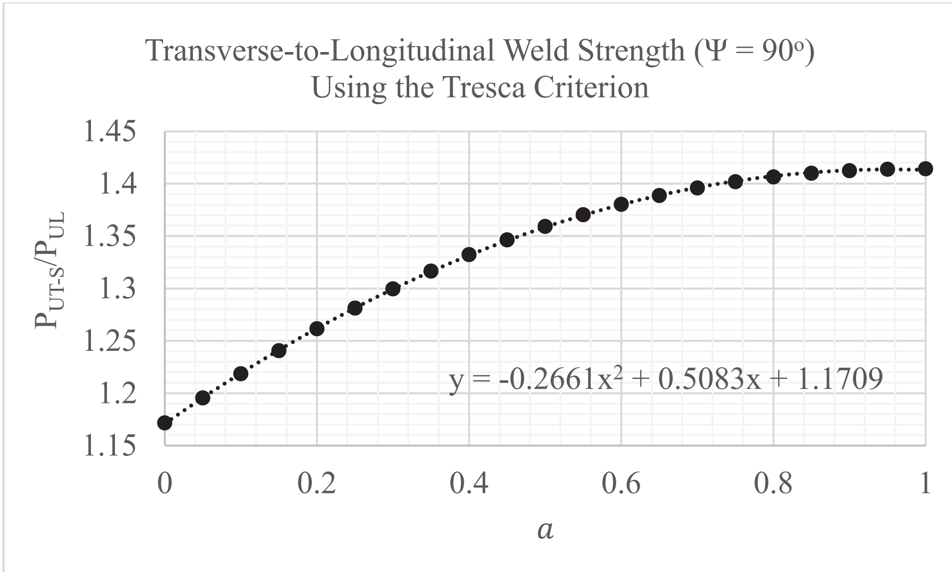

Fig. H.8. Transverse-to-longitudinal strength ratio using the Tresca criterion.

Maximum Principal Stress Criterion

$$\sigma = \frac{P\sin(\Psi-\gamma) + P.a\cos(\Psi-\gamma)}{E_t\ .\ l}$$

where, l is the weld length. Assume the unit length for l.

$$\sigma = \frac{P(\sin(\Psi-\gamma) + a\cos(\Psi-\gamma))}{E_t}$$
$$= \frac{P(\sin(\Psi-\gamma) + a\cos(\Psi-\gamma))}{w} * 2 * \sin\left(\frac{\Psi}{2}\right) * \cos\left(\gamma - \frac{\Psi}{2}\right)$$
$$= \frac{2P}{w} * (\sin(\Psi-\gamma) + a\cos(\Psi-\gamma)) * \sin\left(\frac{\Psi}{2}\right) * \cos\left(\gamma - \frac{\Psi}{2}\right)$$

To determine the angle of tensile failure (γ), where maximum tensile stress is generated, the derivative of the tensile stress with respect to the failure angle should be equal to zero.

$$\frac{d\sigma}{d\gamma} = 0$$

$$\frac{-2P}{w} * (\sin(\Psi-\gamma) + a\cos(\Psi-\gamma)) * \sin\left(\frac{\Psi}{2}\right) * \sin\left(\gamma - \frac{\Psi}{2}\right) + \frac{2P}{w} * (-\cos(\Psi-\gamma) + a\sin(\Psi-\gamma)) * \sin\left(\frac{\Psi}{2}\right) * \cos\left(\gamma - \frac{\Psi}{2}\right) = 0$$

$$-(\sin(\Psi-\gamma)+a\cos(\Psi-\gamma))*\sin\left(\gamma-\frac{\Psi}{2}\right)+(-\cos(\Psi-\gamma)+a\sin(\Psi-\gamma))*\cos\left(\gamma-\frac{\Psi}{2}\right)=0$$

$$-\sin(\Psi-\gamma)\sin\left(\gamma-\frac{\Psi}{2}\right)-a\cos(\Psi-\gamma)\sin\left(\gamma-\frac{\Psi}{2}\right)-\cos(\Psi-\gamma)\cos\left(\gamma-\frac{\Psi}{2}\right)+a\sin(\Psi-\gamma)\cos\left(\gamma-\frac{\Psi}{2}\right)=0$$

$$a\left\{\sin(\Psi-\gamma)\cos\left(\gamma-\frac{\Psi}{2}\right)-\cos(\Psi-\gamma)\sin\left(\gamma-\frac{\Psi}{2}\right)\right\}-\left\{\sin(\Psi-\gamma)\sin\left(\gamma-\frac{\Psi}{2}\right)+\cos(\Psi-\gamma)\cos\left(\gamma-\frac{\Psi}{2}\right)\right\}=0$$

$$a\sin\left(\Psi-\gamma-\gamma+\frac{\Psi}{2}\right)-\cos\left(\Psi-\gamma-\gamma+\frac{\Psi}{2}\right)=0$$

$$a=\frac{1}{\tan(1.5\Psi-2\gamma)}$$

$$1.5\Psi-2\gamma=\tan^{-1}\left(\frac{1}{a}\right)$$

$$\gamma=0.75\Psi-0.5\tan^{-1}\left(\frac{1}{a}\right)$$

$$\sigma_{max}=\frac{2P}{w}*\left(\sin\left(\Psi-0.75\Psi+0.5\tan^{-1}\left(\frac{1}{a}\right)\right)+a\cos\left(\Psi-0.75\Psi+0.5\tan^{-1}\left(\frac{1}{a}\right)\right)\right)*\sin\left(\frac{\Psi}{2}\right)*\cos\left(0.75\Psi-0.5\tan^{-1}\left(\frac{1}{a}\right)-\frac{\Psi}{2}\right)$$

$$\sigma_{max}=\frac{2P}{w}*\left(\sin\left(0.25\Psi+0.5\tan^{-1}\left(\frac{1}{a}\right)\right)+a\cos\left(0.25\Psi+0.5\tan^{-1}\left(\frac{1}{a}\right)\right)\right)*\sin\left(\frac{\Psi}{2}\right)*\cos\left(0.25\Psi-0.5\tan^{-1}\left(\frac{1}{a}\right)\right)$$
$$=\frac{P}{E_d}*\left(\sin\left(0.25\Psi+0.5\tan^{-1}\left(\frac{1}{a}\right)\right)+a\cos\left(0.25\Psi+0.5\tan^{-1}\left(\frac{1}{a}\right)\right)\right)*\cos\left(0.25\Psi-0.5\tan^{-1}\left(\frac{1}{a}\right)\right)$$

Maximum von-Mises Criterion

$$\sigma_e = \sqrt{\sigma^2 + 3\tau^2} = \sqrt{\begin{array}{c}\left(\frac{2P}{w}(\sin(\Psi-\gamma) + a\cos(\Psi-\gamma))\sin\left(\frac{\Psi}{2}\right)\cos\left(\gamma-\frac{\Psi}{2}\right)\right)^2 + \\ +3\left(\frac{2P}{w}[\cos(\Psi-\gamma) - a\sin(\Psi-\gamma)]\sin\left(\frac{\Psi}{2}\right) * \cos\left(\gamma-\frac{\Psi}{2}\right)\right)^2\end{array}}$$

$$= \frac{2P}{w}\sin\left(\frac{\Psi}{2}\right)\cos\left(\gamma-\frac{\Psi}{2}\right)\sqrt{\begin{array}{c}(\sin(\Psi-\gamma) + a\cos(\Psi-\gamma))^2 + \\ +3(\cos(\Psi-\gamma) - a\sin(\Psi-\gamma))^2\end{array}}$$

$$= \frac{2P}{w}\sin\left(\frac{\Psi}{2}\right)\cos\left(\gamma-\frac{\Psi}{2}\right)\sqrt{\begin{array}{c}\sin^2(\Psi-\gamma) + a^2\cos^2(\Psi-\gamma) + \\ 2a\sin(\Psi-\gamma)\cos(\Psi-\gamma) \\ +3\cos^2(\Psi-\gamma) + 3a^2\sin^2(\Psi-\gamma) \\ -6a\sin(\Psi-\gamma)\cos(\Psi-\gamma)\end{array}}$$

$$= \frac{2P}{w}\sin\left(\frac{\Psi}{2}\right)\cos\left(\gamma-\frac{\Psi}{2}\right)\sqrt{\begin{array}{c}(1+3a^2)\sin^2(\Psi-\gamma) \\ +(3+a^2)\cos^2(\Psi-\gamma) - 2a\sin(2\Psi-2\gamma)\end{array}}$$

To determine the angle of fracture surface (γ), where maximum von-Mises stress is generated, the derivative of the von-Mises stress with respect to the failure angle should be equal to zero.

$$\frac{d\sigma_e}{d\gamma} = 0$$

$$\frac{\frac{P}{w}\sin\left(\frac{\Psi}{2}\right)\cos\left(\gamma-\frac{\Psi}{2}\right)}{\sqrt{(1+3a^2)\sin^2(\Psi-\gamma) + (3+a^2)\cos^2(\Psi-\gamma) - 2a\sin(2\Psi-2\gamma)}} *$$
$$* \left\{\begin{array}{c}-2(1+3a^2)\sin(\Psi-\gamma)\cos(\Psi-\gamma) + \\ +2(3+a^2)\cos(\Psi-\gamma)\sin(\Psi-\gamma) + 4a\cos(2\Psi-2\gamma)\end{array}\right\}$$
$$- \frac{2P}{w}\sin\left(\frac{\Psi}{2}\right)\sin\left(\gamma-\frac{\Psi}{2}\right)\sqrt{\begin{array}{c}(1+3a^2)\sin^2(\Psi-\gamma) + \\ (3+a^2)\cos^2(\Psi-\gamma) - 2a\sin(2\Psi-2\gamma)\end{array}} = 0$$

$$\frac{\cos\left(\gamma-\frac{\Psi}{2}\right)}{\sqrt{(1+3a^2)\sin^2(\Psi-\gamma) + (3+a^2)\cos^2(\Psi-\gamma) - 2a\sin(2\Psi-2\gamma)}} *$$
$$* \left\{\begin{array}{c}-2(1+3a^2)\sin(\Psi-\gamma)\cos(\Psi-\gamma) + \\ +2(3+a^2)\cos(\Psi-\gamma)\sin(\Psi-\gamma) + 4a\cos(2\Psi-2\gamma)\end{array}\right\}$$
$$- 2\sin\left(\gamma-\frac{\Psi}{2}\right)\sqrt{\begin{array}{c}(1+3a^2)\sin^2(\Psi-\gamma) + \\ (3+a^2)\cos^2(\Psi-\gamma) - 2a\sin(2\Psi-2\gamma)\end{array}} = 0$$

$$\frac{\cos\left(\gamma-\frac{\Psi}{2}\right)}{\sqrt{(1+3a^2)\sin^2(\Psi-\gamma)+(3+a^2)\cos^2(\Psi-\gamma)-2a\sin(2\Psi-2\gamma)}}*$$
$$*\begin{Bmatrix}-2(1+3a^2)\sin(\Psi-\gamma)\cos(\Psi-\gamma)+\\+2(3+a^2)\cos(\Psi-\gamma)\sin(\Psi-\gamma)+4a\cos(2\Psi-2\gamma)\end{Bmatrix}$$
$$-2\sin\left(\gamma-\frac{\Psi}{2}\right)\sqrt{\begin{matrix}(1+3a^2)\sin^2(\Psi-\gamma)+\\(3+a^2)\cos^2(\Psi-\gamma)-2a\sin(2\Psi-2\gamma)\end{matrix}}=0$$

$$\frac{\cos\left(\gamma-\frac{\Psi}{2}\right)}{\sqrt{(1+3a^2)\sin^2(\Psi-\gamma)+(3+a^2)\cos^2(\Psi-\gamma)-2a\sin(2\Psi-2\gamma)}}*$$
$$*\begin{Bmatrix}-(1+3a^2)\sin(2\Psi-2\gamma)+\\+(3+a^2)\sin(2\Psi-2\gamma)+4a\cos(2\Psi-2\gamma)\end{Bmatrix}$$
$$-2\sin\left(\gamma-\frac{\Psi}{2}\right)\sqrt{\begin{matrix}(1+3a^2)\sin^2(\Psi-\gamma)+\\(3+a^2)\cos^2(\Psi-\gamma)-2a\sin(2\Psi-2\gamma)\end{matrix}}=0$$

$$\frac{\cos\left(\gamma-\frac{\Psi}{2}\right)*\{2(1-a^2)\sin(2\Psi-2\gamma)+4a\cos(2\Psi-2\gamma)\}}{\sqrt{(1+3a^2)\sin^2(\Psi-\gamma)+(3+a^2)\cos^2(\Psi-\gamma)-2a\sin(2\Psi-2\gamma)}}$$
$$-2\sin\left(\gamma-\frac{\Psi}{2}\right)\sqrt{\begin{matrix}(1+3a^2)\sin^2(\Psi-\gamma)+\\(3+a^2)\cos^2(\Psi-\gamma)-2a\sin(2\Psi-2\gamma)\end{matrix}}=0$$

The angle of failure is dependent on both factor a and the dihedral angle, Ψ. To simplify the above derivative equation, different a values were selected and accordingly a relation was drawn between the failure angle in the weld, γ, and the dihedral angle, Ψ. For instance, when $a = 0$ and $\Psi = 110^o$, the failure angle, γ, was 76.21^o as shown in Figure H.9. The failure angle was determined from the intersection of the curve with the horizontal axis (where the derivation is zero). Other cases resulted in multiple failure angles, as shown in Figure H.10. At $a = 0.2$ and $\Psi = 150^o$, the failure angle had three values: 45.4^o, 67.5^o, 104.8^o. Using the same concept, the failure angles for different values of factor a and different dihedral angles in the range between 30^o and 150^o are summarized in Table H.1.

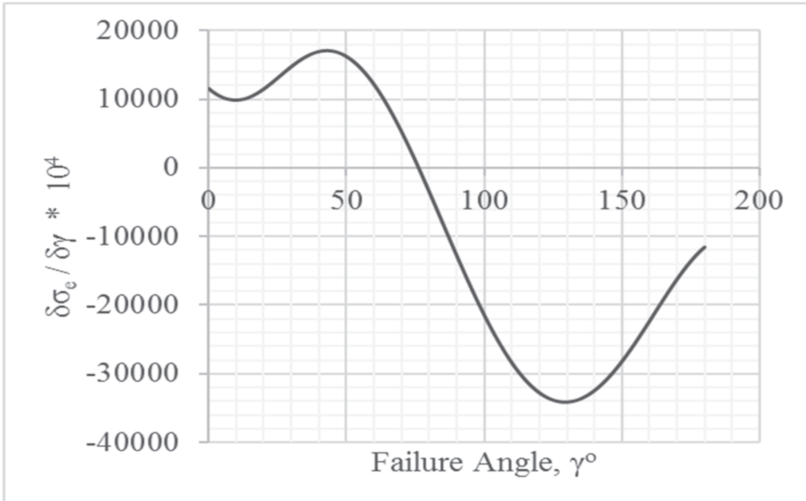

Fig. H.9. Determining the failure angle ($a = 0$ and Ψ = 110°).

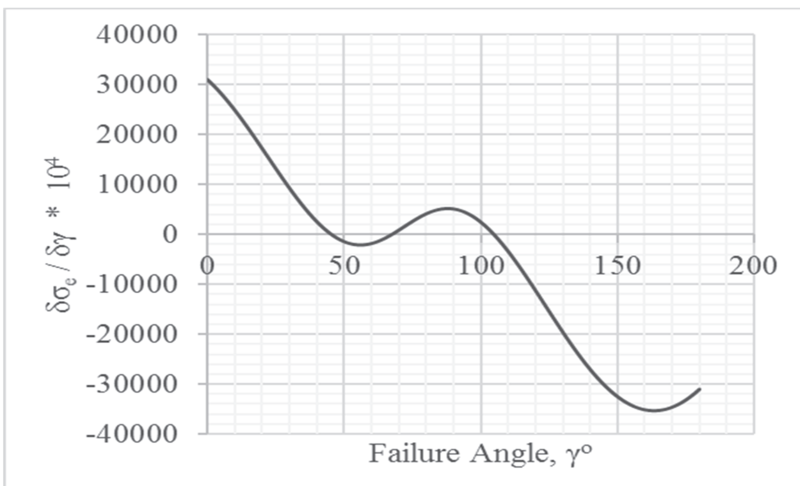

Fig. H.10. Determining the failure angle ($a = 0.2$ and Ψ = 150°).

Table H.1. Failure angle, γ, for different values of a and Ψ (degrees).

		a									
		0	**0.1**	**0.2**	**0.3**	**0.4**	**0.5**	**0.6**	**0.7**	**0.8**	**1.0**
Ψ	**30**	21.0	23.3	25.5	27.6	29.5	31.3	33.0	34.4	35.7	37.9
	40	28.0	30.2	32.4	34.5	36.4	38.2	39.8	41.2	42.5	44.6
	50	34.9	37.2	39.3	41.4	43.3	45.0	46.6	47.9	49.1	51.1
	60	41.9	44.1	46.2	48.2	50.1	51.8	53.3	54.6	55.7	57.5
	70	48.8	51.0	53.1	55.0	56.8	58.5	59.9	61.1	62.2	63.7
	80	55.7	57.9	59.9	61.8	63.5	65.1	66.4	67.5	68.4	10.8 29.6 69.6
	90	62.6	64.7	66.7	68.5	70.1	71.6	72.8	73.7	16.5 31.5 74.4	15.0 45.0 75.0
	100	69.4	71.5	73.4	75.1	76.6	77.9	78.9	20.8 39.6 79.6	20.0 47.4 80.0	20.4 60.4 79.2
	110	76.2	78.2	80.0	81.6	83.0	29.2 35.0 84.0	25.4 46.8 84.7	25.0 55.0 85.0	25.2 64.5 84.6	26.3
	120	82.9	84.8	86.5	87.9	33.5 41.0 89.1	30.4 53.0 89.8	30.0 61.9 90.0	30.4 70.3 89.2	31.0 81.4 85.0	32.5
	130	89.6	91.3	92.8	38.8 45.5 94.1	35.3 58.6 94.9	35.0 68.1 94.9	35.5 77.6 93.8	36.3	37.2	38.9
	140	96.1	97.7	45.2 48.8 100.0	40.3 63.3 99.8	40.1 73.6 99.9	40.7 84.1 98.4	41.5	42.5	43.5	45.4
	150	102.5	103.9	45.4 67.5 104.8	45.0 78.5 105.0	45.7 89.8 103.2	46.6	47.75	48.9	50.0	52.1

In order to exclude the multiple values of the failure angle that are present for some cases, the maximum von-Mises stress was calculated as a function of the external ultimate load, P, divided by the weld throat, E_d.

$$\sigma_e = \frac{2P}{w}\sin\left(\frac{\Psi}{2}\right)\cos\left(\gamma - \frac{\Psi}{2}\right)\sqrt{\begin{array}{c}(1+3a^2)\sin^2(\Psi-\gamma)\\ +(3+a^2)\cos^2(\Psi-\gamma) - 2a\sin(2\Psi-2\gamma)\end{array}}$$

$$= \frac{P}{E_d}\cos\left(\gamma - \frac{\Psi}{2}\right)\sqrt{\begin{array}{c}(1+3a^2)\sin^2(\Psi-\gamma)\\ +(3+a^2)\cos^2(\Psi-\gamma) - 2a\sin(2\Psi-2\gamma)\end{array}}$$

The failure angles that resulted in highest stress were the correct ones among the three values. The correct values are shaded in Table H.1. Only two conditions had two failure angles where the maximum von-Mises stress was the same. They are the cases for $a = 0.7$ and Ψ = 110° and for $a = 1.0$ and Ψ = 90°. The maximum von-Mises stress for the cases in Table H.1 are shown in Table H.2 in the form of factor $1/\eta$. The factor η is called herein after as the weld capacity factor.

Table H.2. Maximum von-Mises stress, 1/η, for different values of a and Ψ.											
		a									
		0	**0.1**	**0.2**	**0.3**	**0.4**	**0.5**	**0.6**	**0.7**	**0.8**	**1.0**
Ψ	**30**	1.708	1.696	1.693	1.701	1.717	1.742	1.775	1.814	1.859	1.964
	40	1.690	1.672	1.664	1.665	1.676	1.696	1.723	1.756	1.796	1.890
	50	1.667	1.643	1.630	1.626	1.631	1.645	1.667	1.695	1.729	1.813
	60	1.639	1.610	1.591	1.582	1.582	1.591	1.608	1.631	1.661	1.735
	70	1.607	1.573	1.549	1.535	1.530	1.534	1.546	1.565	1.590	1.656
	80	1.570	1.532	1.503	1.485	1.476	1.475	1.483	1.498	1.519	1.577
	90	1.530	1.487	1.454	1.431	1.418	1.414	1.418	1.429	1.447	1.500
	100	1.486	1.439	1.402	1.376	1.360	1.352	1.353	1.361	1.377	1.577
	110	1.439	1.388	1.348	1.319	1.300	1.290	1.288	1.295	1.409	1.656
	120	1.389	1.335	1.293	1.261	1.239	1.228	1.249	1.361	1.480	1.735
	130	1.336	1.281	1.236	1.203	1.180	1.205	1.313	1.429	1.552	1.813
	140	1.282	1.225	1.179	1.145	1.163	1.266	1.378	1.497	1.623	1.890
	150	1.227	1.169	1.123	1.126	1.223	1.329	1.443	1.565	1.693	1.964

According to the results shown in Table H.2, for the same effective throat of the weld, E_d and for the same failure stress ($\sigma_{e-max} = F_{EXX}$), increasing the dihedral angle increases the weld capacity, P. Additionally, having tensile forces on the shear face of the weld ($F = a.P$) affects the weld strength. The values in Table H.2 were used to draw the graph in Figure H.11. For the unit length of weld line ($l = 1$), the weld capacity, P, was calculated as a function of the ultimate von-Mises stress that can be carried by the weld, which was substituted with the ultimate tensile strength of the weld material, F_{EXX}, and weld's effective throat.

$$\frac{\sigma_{e-max}}{\left(\frac{P}{E_d}\right)} = \frac{F_{EXX}}{\left(\frac{P}{E_d}\right)} = \frac{1}{\eta}$$

$$P = \eta . F_{EXX} . E_d$$

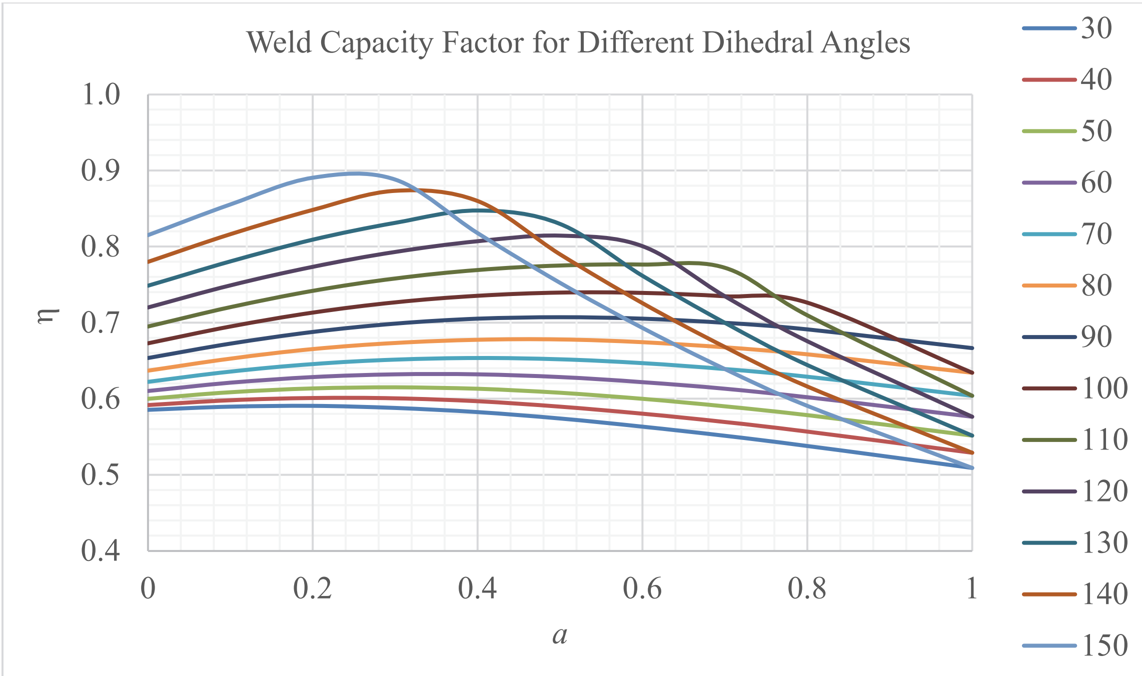

Fig. H.11. Weld capacity factor.

For the case of right dihedral angle ($\Psi = 90^o$), the weld capacity factor, η, is changing within a very small range of 0.65 to 0.71 for all values of factor a. Consequently, η can be a constant of 0.68. To compare the obtained results in Figure H.11 with the current AISC *Specification* equations, the weld capacity was modified as follows:

$$R_n = 0.60F_{EXX}(1.0 + 0.50\sin^{1.5}\theta) * A_{we} = 0.60F_{EXX}(1.0 + 0.50\sin^{1.5}90) * [E_d * (l = 1)]$$
$$= 0.60 * 1.5 * F_{EXX} * E_d = 0.90F_{EXX}E_d$$

To match the weld capacity of a normal T-Joint, using the von-Mises approach, with the weld capacity, using the *Specification*, the weld capacity factor should be modified from 0.68 to 0.90. Nevertheless, this can result in very conservative designs.

$$\eta^* = \frac{0.90}{0.68}\,\eta = 1.32\,\eta$$

where, η^* is the modified capacity factor.

$$P = \eta^*.F_{EXX}.E_d$$

The modified weld capacity factor, η^*, as a function of the factor a is shown in Figure H.12.

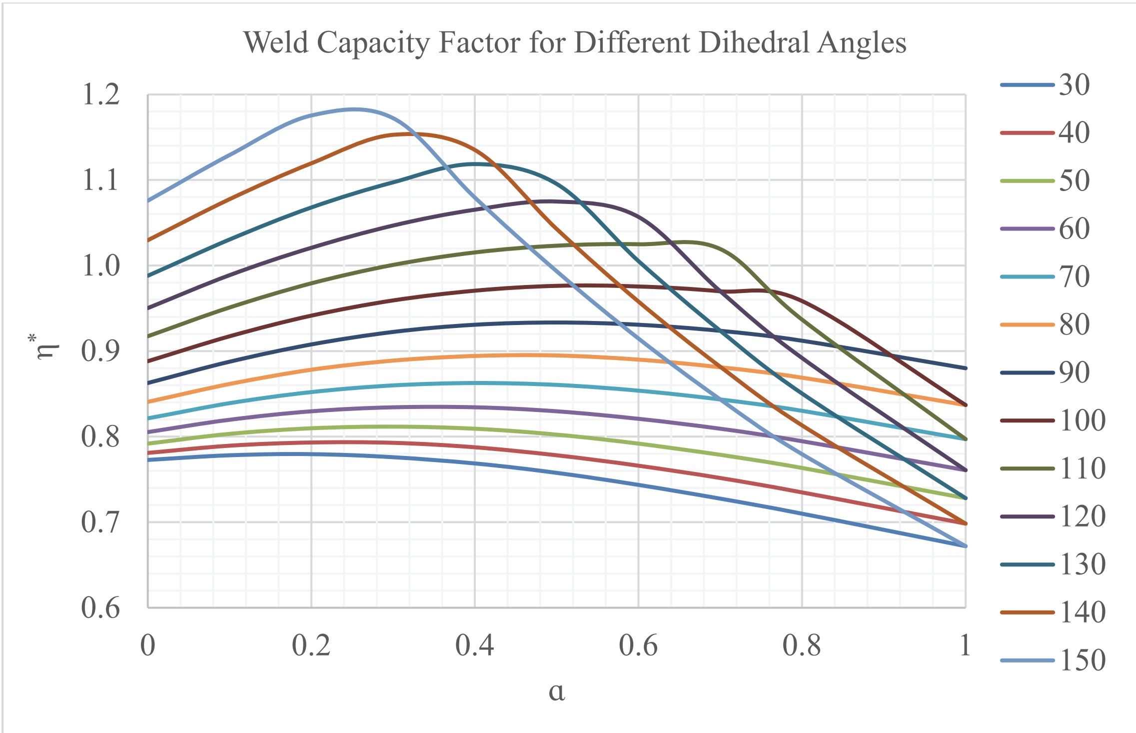

Fig. H.12. Modified weld capacity factor.

Further Analysis of the Maximum Shear Stress Model
For transversely-loaded fillet welds, the optimum mathematical model among those investigated is the maximum shear stress model. The maximum shear stress criterion is:

$$\tau_{max} = \frac{P}{E_d} * [\cos(0.25\Psi - 0.5\tan^{-1}(a)) - a\sin(0.25\Psi - 0.5\tan^{-1}(a))] * \cos(0.25\Psi + 0.5\tan^{-1}(a))$$

Theis equation can be rewritten as:

$$\frac{P}{A_w} = \frac{\tau_u}{[\cos(0.25\Psi - 0.5\tan^{-1}(a)) - a\sin(0.25\Psi - 0.5\tan^{-1}(a))]} * \frac{1}{\cos(0.25\Psi + 0.5\tan^{-1}(a))}$$

Where τ_u is the weld metal shear rupture strength. The nominal value in the AISC *Specification* is $0.6F_{EXX}$. However, for the maximum shear stress criterion to match the experimental results in Gallow (2019), the shear strength should be $0.8F_{EXX}$. Using $\tau_u = 0.8F_{EXX}$, results in:

$$\frac{P}{A_w} = \frac{0.8F_{EXX}}{[\cos(0.25\Psi - 0.5\tan^{-1}(a)) - a\sin(0.25\Psi - 0.5\tan^{-1}(a))]} * \frac{1}{\cos(0.25\Psi + 0.5\tan^{-1}(a))}$$

The plots of this equation in Figure H.13 show that a value of a = 0.21 provides results similar to the experimental values. With a = 0.21, the maximum difference between the proposed equation and the experimental results is less than 7%.

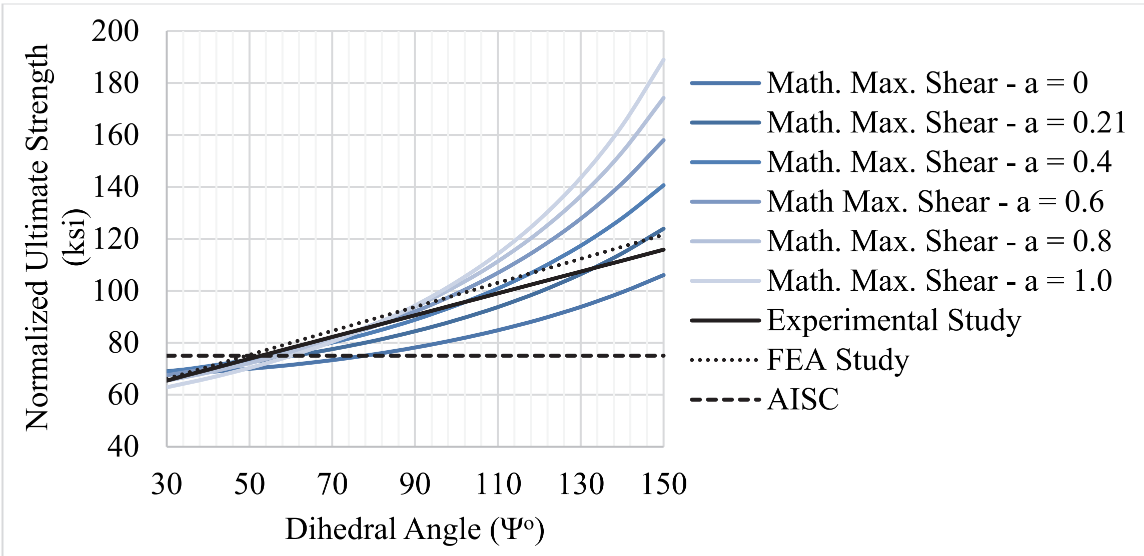

Fig. H.13. Maximum shear stress model versus FEA and experimental results.